Structure of amphiphilic block copolymer micelles in aqueous dispersions

Leslie, Stuart

Structure of Amphiphilic Block Copolymer Micelles in Aqueous Dispersions

2003

Stuart Leslie

Graduate Society

University of Durham

Supervisor:

Professor Randal W Richards

A thesis submitted to the University of Durham in partial fulfilment of the regulations for the degree of Doctor of Philosophy.

Abstract

Structure of Amphiphilic Block Copolymer Micelles in Aqueous Dispersions

Stuart Leslie

PhD Thesis University of Durham 2003

Two molecular weight series of Poly(butadiene)-Poly(ethylene oxide) diblock copolymers have been synthesised using anionic polymerisation techniques. The amphiphilic nature of the copolymers results in micelles being formed on dispersion in water. Dynamic light scattering was employed to ascertain the critical micelle concentration and micelle dimensions. Small-angle X-ray and neutron scattering were used to investigate high concentration dispersions providing micelle dimensions and an insight into the nature of the interactions between micelles from the structure factor, which develops at higher concentrations. The detailed model used polymer brush theory to fit the small-angle scattering data at low concentrations in the absence of interparticle interactions. Micelle dimensions determined by model fitting matched well with those predicted from theory. At higher concentrations when these interactions are dominant, a Yukawa potential between micelles was used to model the observed structure factor.

The unsaturation of the poly(butadiene) chains comprising the core of the micelle facilitated post-polymerisation cross-linking of the core using a redox-initiated free-radical polymerisation at room temperature. Dynamic light scattering was employed to determine the micelle dimensions, with small angle X-ray and neutron scattering used to investigate higher concentration dispersions. The micelle cores were seen to contract by circa 10-40% upon cross-linking in relation to the virgin micelles, resulting in the junction points of the coronal chains on the surface of the micelle core coming closer together. Interestingly the thickness of the corona decreased in relation to the virgin micelles, a phenomenon due to the presence of inorganic ions from the cross-linking reaction reducing the thermodynamic quality of the solvent for the poly(ethylene oxide) brush, causing it to partially collapse.

Acknowledgements

Firstly, I would like to thank my supervisor Professor Randal Richards for providing me with the opportunity to carry out this research and for his support and encouragement during it. Special thanks also go to Dr Nigel Clarke for his assistance and constructive comments following the departure of Professor Richards.

None of this work would have been possible without the guidance of many people, to whom I am greatly indebted. At Durham, Dr. Lian Hutchings for constructive discussions about the synthetic chemistry, Dr. Zaijun Lu for supplying the deuterated poly(butadiene), Doug for SEC, DSC and general encouragement, Alan, Ian and Catherine for NMR spectra, Jean, Anne and Irene for sorting out my various travel arrangements, Malcolm and Peter for constantly repairing the stream of broken glass and keeping me out of trouble! At Rutherford Appleton Laboratory, Steve King for help with the neutron scattering experiments and Richard Heenan for assistance with the data fitting and the use of his FISH analysis software. At Sheffield, Dr Patrick Fairclough for the use of his light scattering apparatus.

My time in Durham has been an interesting one and I would like to thank all members of the IRC both past and present, of which there are too many to mention, with whom I have had the pleasure of working alongside, the occupants of lab 1, and Gradsoc AFC.

I would like to thank my wife Wendy for putting up with me and for her love, support and encouragement. Without you none of this would have been possible, and my sanity would have suffered far more than it has!

Finally I would like to thank my parents and sister Donna for their love and support.

Declaration

The work reported in this thesis has been carried out at the Durham site of the Interdisciplinary Research Centre in Polymer Science and Technology, the Department of Chemistry, University of Sheffield and the Rutherford Appleton Laboratory, Chilton, Oxfordshire between October 2000 and September 2003. This work has not been submitted for any other degree either in Durham or elsewhere and is the original work of the author except where otherwise stated.

Statement of Copyright

Financial Support

The author gratefully acknowledges the provision of a maintenance grant by the EPSRC.

Contents

1. Introduction

1.1. Introduction

Block copolymers consist of two or more polymeric components covalently bonded together. They are an important class of material, not only from an academic standpoint, but also in terms of industrial applications. They find many uses from impact modifiers and compatibilisers in the solid state to solubilisers and dispersion agents in solution.[1] Recent work has also focussed on their use as organic dielectric band gap materials.[2] The reason for their importance is the interesting properties they possess. In the solid state they exhibit microphase separation into domains of colloidal dimensions.[3, 4] These domains give rise to very definite morphologies that exhibit considerable long-range order, and have been widely studied.[5] In a solvent selective for one of the blocks, micelle formation is observed.[4] In common with the solid phase domains, the micelles also have definite morphologies and exhibit long-range order at higher concentrations.

These two processes are due to the same phenomenon; i.e. self-assembly.

Self-assembly can be defined as the spontaneous formation of well-defined structures from the components of a system by non-covalent forces.[6, 7] As a result, the system becomes more ordered. This transition from a disordered to an ordered phase occurs when either the thermodynamic or field strength is changed, e.g. concentration, temperature or pressure. For ordered structures to be formed, both long-range repulsive and short-range attractive forces must exist simultaneously, shown schematically in figure 1.1.

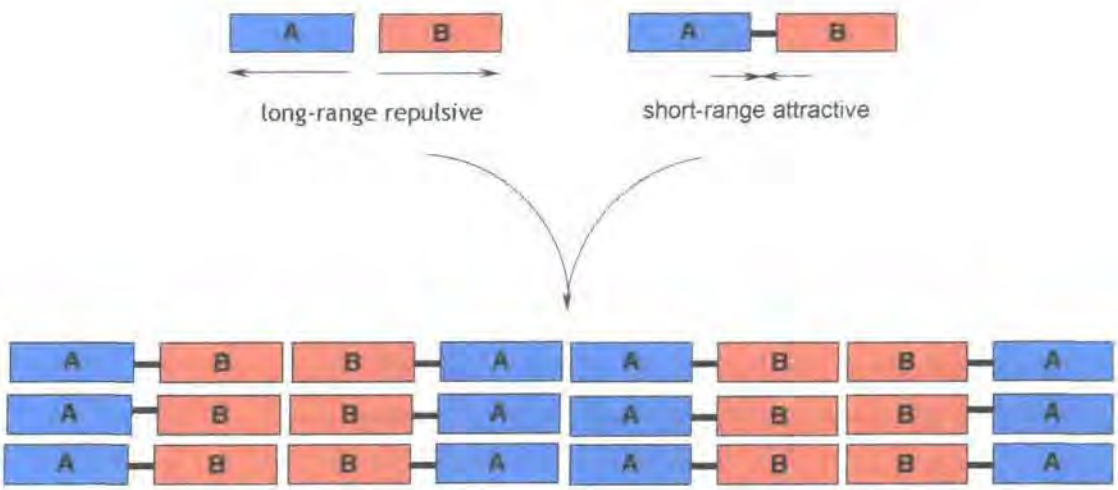

Figure 1.1 - *Schematic representation of self-assembly process showing the role of long range repulsive and short range attractive forces*

In the case of block copolymers in the bulk the long-range repulsive forces are due to incompatibility between the blocks, and the short-range attractive forces are the covalent bonds between the blocks. Similarly for micelle formation the long-range repulsive forces are hydrophobic/hydrophilic interactions, whilst the short-range attractive forces are the same as in the melt.[6]

The two forces compete with one another, long-range forces trying to force the blocks apart, and short-range forces trying to keep the blocks together. As the covalent bond between the blocks is a strongly attractive force, it wins the battle to a certain degree. The result is microphase separation into domains of each block, minimising the unfavourable interactions and maximising the favourable interactions, between the blocks and the solvent if there is one present.

1.1.1. Architecture

The architecture of block copolymers can be controlled by the synthetic procedure employed. For a copolymer containing two different blocks, A and B, it is possible to produce diblock, triblock, star block and graft copolymer architectures, which are shown schematically in figure 1.2.

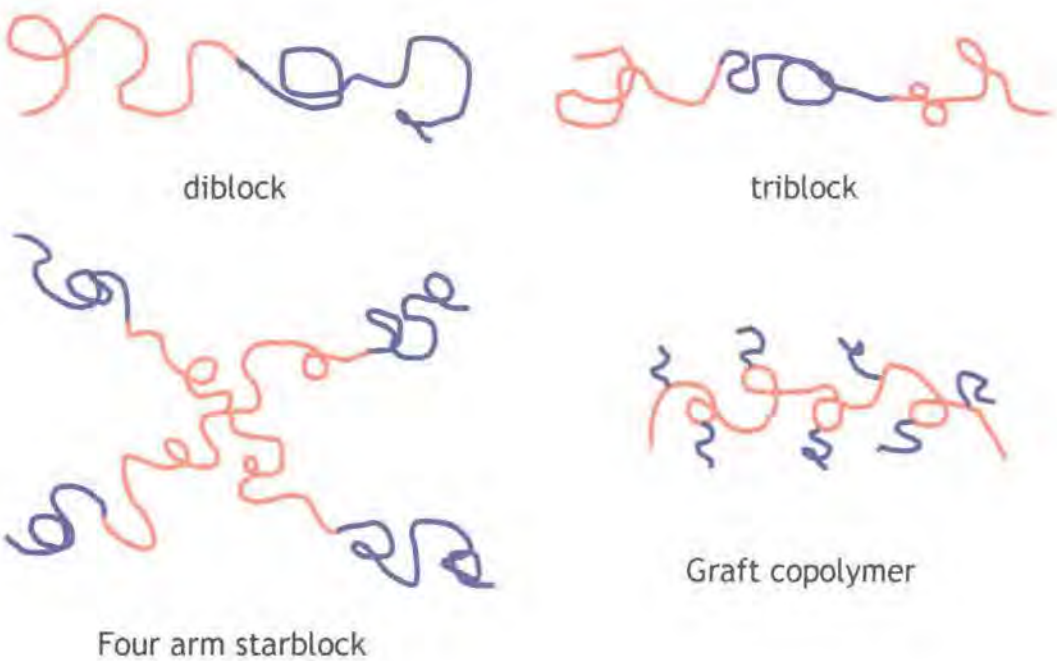

Figure 1.2 -*Schematic representation of common AB block copolymer architectures*

Other, more exotic architectures such as miktoarm or H-shaped polymers are possible by careful control over the synthetic conditions, and reagents.

1.1.2. Nomenclature

The concept of using different letters to distinguish blocks was introduced above. Throughout this work, A is the soluble block, whilst B is the insoluble block. In addition to this, it is possible to define a degree of polymerisation for each block, N_A, and N_B, and for the entire copolymer, N. The copolymer can be defined in terms of the weight fraction of one of the blocks, e.g. $w_A = {}^{N_A}/_{N}$. The volume fraction of copolymer in solution can be given the symbol, ϕ, and the concentration given the symbol c. By convention, the copolymers are named in the order poly(monomer B)-poly(monomer A), irrespective of the order in which they were synthesised. Deuteration of one of the blocks is denoted by *d*poly(monomer A). The micelle association number, which is the number of copolymer chains making up a micelle, is given the symbol, p.

1.1.3. Copolymer synthesis

The preparation of well-defined block copolymers is commonly accomplished using a living polymerisation technique involving sequential block growth. Living polymerisations are advantageous because they yield narrow molecular weight distributions with degrees of polymerisation controlled by the stoichiometry of the reaction. The first technique of this type to be demonstrated was the anionic polymerisation of styrene and isoprene by Szwarc and co-workers.[8] Since then other living polymerisation methods have become available, expanding the range of accessible monomers and copolymer architectures.

Table 1.1 lists the common living polymerisation techniques, and the monomers that they are used to polymerise.[6, 9]

Polymerisation technique	Active species	Monomers
Anionic polymerisation	anion	styrenes, vinylpyridines, methacrylates, acrylates, dienes, epoxides
Group transfer polymerisation (GTP)		methacryaltes, acrylates
Ring-opening metathesis polymerisation (ROMP)		Norbornenes
Cationic polymerisation	cation	vinyl ether, isobutylene, epoxides
Nitroxide mediated	radical	Styrenes
Atom transfer radical polymerisation (ATRP)		styrenes, methacrylates, acrylates, acrylonitriles
Reversible-Addition-Fragmentation chain transfer polymerisation (RAFT)		methacrylates, styrene, acrylates

Table 1.1 - *Overview of the common polymerisation techniques used to synthesise block copolymers, the active species associated with each and the monomers to which they are applied.*

Of the methods listed in table 1.1, anionic polymerisation is still the method of choice for many monomers, and was applied to the synthesis of the polymers used in this research. Chapter two provides a more detailed description of the first principles and experimental execution.

This chapter aims to provide an overview of the process of micellisation alongside a survey of experimental investigations. The possibilities of rendering micelles permanent structures by physical or chemical fixation will also be discussed. This will be succeeded by an outline of the aims and objectives of the research.

1.2. Micellisation

As mentioned in section 1.1 block copolymers self-assemble to form micelles when dispersed in a solvent selective towards one of the blocks. The self-assembly process is the result of competing interactions; long-range repulsive hydrophilic/hydrophobic interactions, and short-range attractive covalent bonding interactions. The micelles formed, (shown schematically in figure 1.3), consist of a lyophobic core of B blocks where the solvent is excluded, surrounded by a solvent swollen corona of A chains stretching away from the core-shell interface. The incompatibility between the two blocks is assumed sufficiently large that the core-shell interface is sharp.

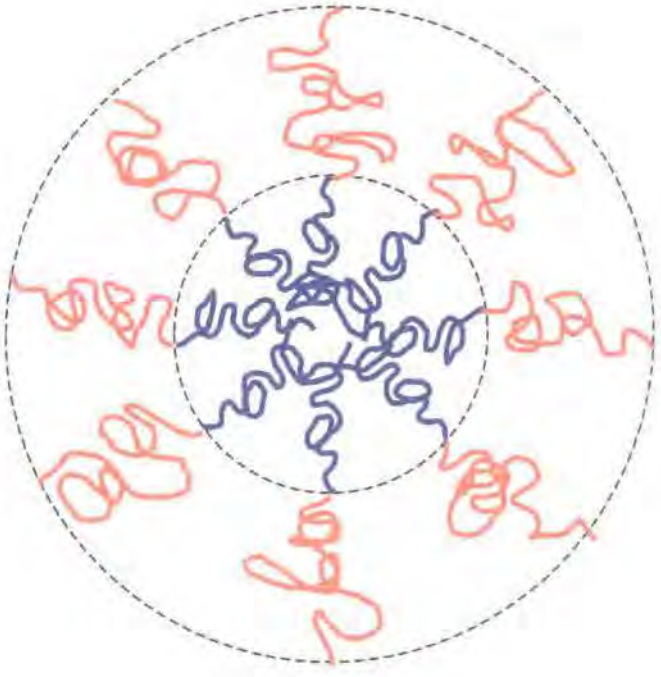

Figure 1.3 - *Schematic representation of a spherical micelle showing the core-shell structure.*

Depending upon the composition of the copolymer, figure 1.3 could be either a sphere, or a cylinder viewed "end-on". For the purposes of what follows, and indeed the experimental investigations carried out, the former is assumed, unless explicitly stated.

Micelle formation is generally observed above a critical micelle concentration (cmc), which can be defined as the concentration at which micelles become detectable by a given technique.[10] Below this concentration it is assumed that the copolymers are dispersed as unimers in solution.

As the concentration is increased above the cmc it is possible for the arrangement of the micelles to become more ordered, and at sufficiently high concentrations they can be ordered onto a lattice. The concentration at which this happens is the critical gel concentration (cgc). Figure 1.4 presents a schematic representation of the different concentration regimes of micellar dispersions.

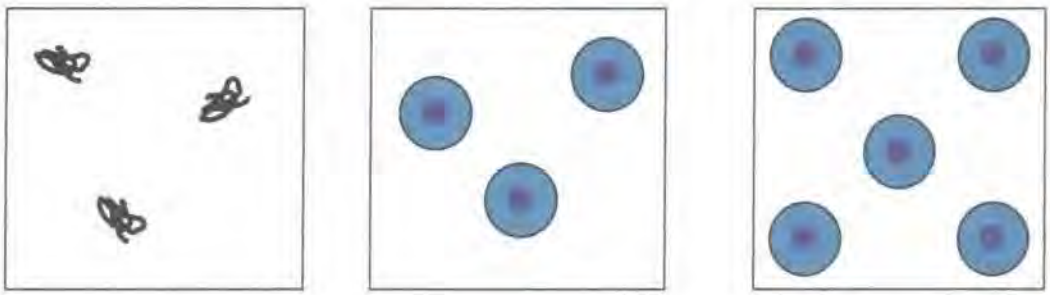

Figure 1.4 - *Schematic representation of the different micellar regimes observed when changing the concentration of the dispersion.*

There are two models, proposed by Elias[10], for the association of molecules into micelles, open and closed association. In the open association model, micelle formation can be represented by a series of stepwise equilibria, shown in figure 1.5, each having an associated equilibrium constant.

$$A_1 + A_1 \overset{k_2}{\rightleftharpoons} A_2$$

$$A_2 + A_1 \overset{k_3}{\rightleftharpoons} A_3$$

$$A_3 + A_1 \overset{k_4}{\rightleftharpoons} A_4$$

$$A_{N-1} + A_1 \overset{k_N}{\rightleftharpoons} A_N$$

Figure 1.5 - *Open association model of micelle formation.*

Should the association steps be equivalent, then the system can be defined by a single association constant, k_0:

$$k_0 = \frac{[A_N]}{[A_1][A_{N-1}]} \qquad \text{Equation 1.1}$$

The model does not lead to a cmc and predicts a broad distribution of micelle sizes.

In the closed association model, micelle formation is represented by an equilibrium between dispersed molecules and micelles having association number, p, as shown in figure 1.6.

$$pA_1 \rightleftharpoons A_p$$

Figure 1.6 - *Closed association model of micelle formation*

The association constant, k_c is given by equation 1.2.

$$k_c = \frac{[A_p]}{[A]^p} \qquad \textbf{Equation 1.2}$$

The model does lead to a cmc and predicts a narrow micelle size distribution. The closed association model is the most applicable to block copolymer systems, since a cmc is almost invariably observed and the micelles formed exhibit narrow size distributions.

The experimental determination of the cmc is discussed in section 3.2.1.1.

1.2.1. Theoretical description of micellisation

Many models have been postulated to describe the micelles formed by block copolymers in dilute dispersions. These can be divided into two classes:

i.) Scaling approaches, which provide simple relationships pertaining to how micelle dimensions such as the core radius or shell thickness depend on the number of segments of the different blocks.

ii.) Mean field models, where a block profile is usually assumed, and the association number, cmc, and phase diagram can be calculated from an expression for the free energy.

1.2.1.1. Scaling theories

de Gennes[11] made a major advance in this area in 1978, with the scaling relationship he proposed, essentially an extension of Alexander-de Gennes[12, 13] theory for polymer brushes. In his model of a micelle he assumed that the micelle consisted of p chains, which in the core were uniformly stretched, giving a core radius R_B. He also assumed uniform densities for the both the core and the corona. The model was reported for the limit of short A chains,

i.e. $N_B >> N_A$, resulting in a thin corona, with the core radius expected to scale as:

$$R_B \sim aN_B^{2/3}\left(\frac{\gamma a^2}{T}\right)^{1/3} \qquad \text{Equation 1.3}$$

where a is the segment length, N_B is the core chain degree of polymerisation, γ is the interfacial tension and T is temperature
and the association number as:

$$p \sim N_B \frac{\gamma a^2}{T} \qquad \text{Equation 1.4}$$

Daoud and Cotton[14] formulated a model to describe star-like polymers in a good solvent based on the principle of polymer "blobs" from Alexander-de Gennes theory, with the chain-ends confined to a spherical surface, as in figure 1.7.

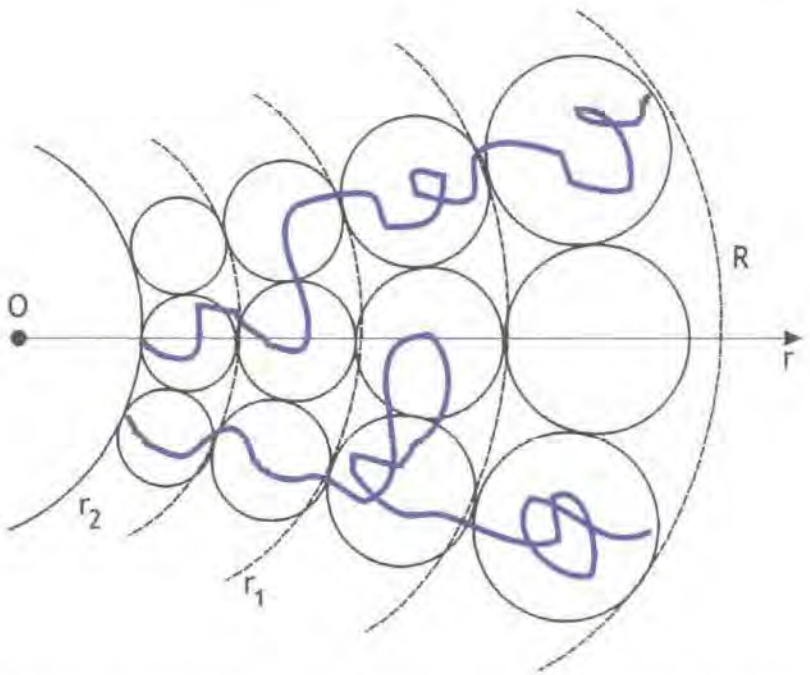

Figure 1.7 - *Representation of the blob analogy utilised by Daoud and Cotton*

Unlike the de Gennes model where the polymer concentration was assumed to be uniform across the corona, Daoud and Cotton postulated that it was dependent upon the distance, r, from the centre of the star. This was accomplished by increasing blob size with distance from the centre of the star, with the result being greater swelling on the outside of the molecule. The model can be applied to micelles by replacement of the number of arms, f, with the association number, p.

Three regions with distinct concentration profiles were identified:

i.) An inner melt-like core

ii.) An intermediate concentration region

iii.) A swollen outer region

The authors found that the radius of a star polymer in a good solvent in the long A chain limit, scaled as:

$$R \sim N_A^{3/5} f_A^{1/5} a \qquad \textbf{Equation 1.5}$$

Zhulina and Birshtein[15] applied scaling arguments to micelles, both spherical and cylindrical, formed by diblock copolymers in selective solvents. They identified four regimes, depending upon the composition of the copolymer, which are shown in figure 1.8.

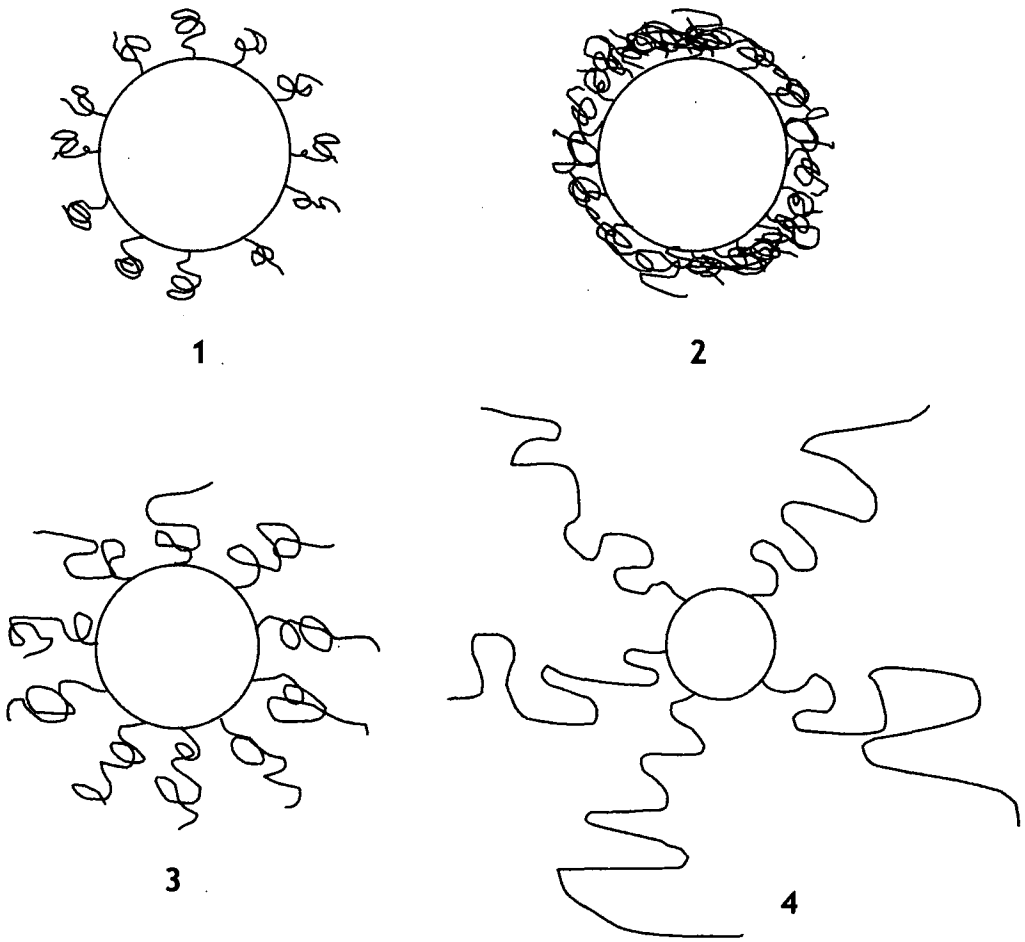

Figure 1.8 - *Micellar regimes identified by Zhulina and Birshtein*

Scaling relationships were proposed for the core radius, the shell thickness, the association number and the interfacial area per chain for each of the four regimes, and these are detailed in table 1.2.

Regime	Copolymer composition	R_B	R_A	p	σ
1	$N_A < N_B^{\nu/6}$	$N_B^{2/3}$	N_A^{ν}	N_B	$N_B^{1/3}$
2	$N_B^{\nu/6} < N_A < N_B^{(1+2\nu)/6\nu}$		$N_A N_B^{(\nu-1)/6\nu}$		
3	$N_B^{(1+2\nu)/6\nu} < N_A < N_B^{(1+2\nu)/5\nu}$	$N_B N_A^{-2\nu/(1+2\nu)}$	$N_A^{3\nu/(3\nu+1)}$	$N_B^2 N_A^{-6\nu/(1+2\nu)}$	$N_A^{2\nu/(1+2\nu)}$
4	$N_A < N_B^{(1+2\nu)/5\nu}$	$N_B^{3/5}$	$N_A^{\nu} N_B^{2(1-\nu)/5}$	$N_B^{4/5}$	$N_B^{2/5}$

Table 1.2 - *Scaling relationships associated with each of the regimes identified by Zhulina and Birshtein, along with the copolymer compositions giving rise to each.*

Using the Daoud and Cotton model as a starting point, Halperin[16] produced a scaling description of the micelles formed by AB diblock copolymers in a highly selective solvent. The constraints of the model were that the micelles had a small core and an extended corona (i.e. $N_A >> N_B$), and that the micelles were assumed to be spherical and monodisperse, each consisting of f monomers. The concentration of the corona was not assumed to be constant, as in the work be de Gennes, but was allowed to "fall off" as in star polymers. i.e.

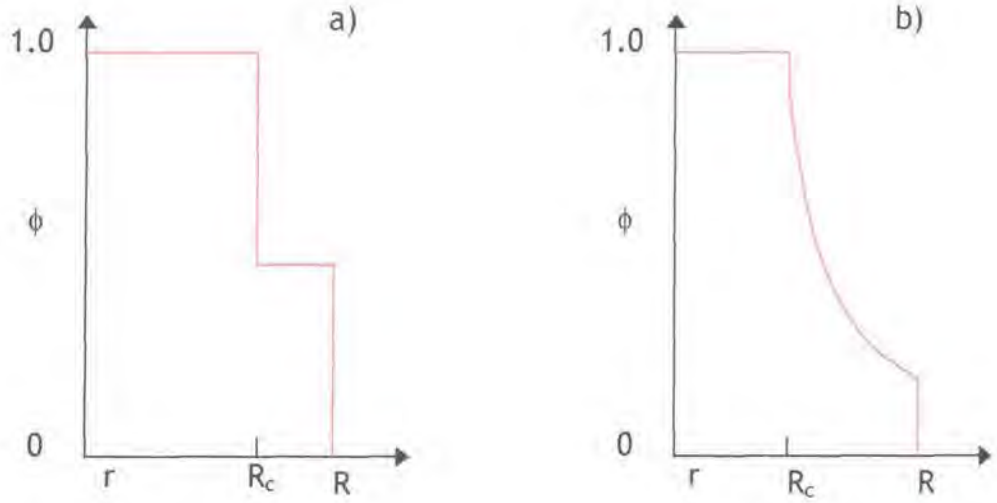

Figure 1.9 - *Plots of monomer volume fraction vs. distance from micelle centre (r). a) large core limit ($N_B >> N_A$), b) small core limit ($N_B << N_A$).*

Scaling relationships were produced for the radius of the core, and the overall micelle radius, and were:

$$R_c \approx N_B^{3/5} a$$ **Equation 1.6**

and

$$R \approx N_B^{4/25} N_A^{3/5} a$$ **Equation 1.7**

The scaling laws are only valid for high values of p, and therefore can only be used to describe micelle structure beyond the cmc, and not to determine the cmc itself.

All of the models discussed so far predict that the association number and core radius are independent of the length of the chains forming the corona. In contrast to this observation Zhang and co-workers[17] produced a scaling relationship for the core radius from the experimental data from poly(styrene)-poly(acrylic acid) micelles in water. They found that the core radii determined from transmission electron microscopy (TEM) scaled as:

$$R_B \sim N_B^{0.4} N_A^{-0.15}$$ **Equation 1.8**

The relationship was found not to be universal when applied to other experimental data. The authors concluded that the length of the soluble block influenced the core radius and proposed the more general relationship:

$$R_B \sim N_B^{\alpha} N_A^{-\gamma}$$ **Equation 1.9**

with α and γ being dependent upon the system in question. The observation that the length of the soluble block exerts influence on the core radius is one that was also made by Whitmore and Noolandi,[18] and indeed Zhang *et al.* use this as support for their observation.

1.2.1.2. Self-consistent field theories

Noolandi and Hong[19] proposed a model for AB diblock micelles based on a spherical shape, and the fact that the insoluble B block forms a uniform core and the A block forms a uniform corona. By applying a mean field theory, and using an approximation for the surface tension, along with known copolymer composition, molecular weight, and concentration in solution, the equilibrium size of micelles was obtained. The theory was compared to results obtained previously by Plestil and Baldrian[20] for PS-PB micelles in heptane, and was found to be in good agreement with the SAXS data. Agreement was also noted with the results of de Gennes, with respect to the scaling of micelle size, association number and radii with the degree of polymerisation.

Leibler *et al.*[21] proposed a mean field theory model for micelles formed by a diblock copolymer in a homopolymer solvent. Their model allowed the calculation of both the micelle size and the association number. The model assumed a symmetric copolymer, i.e. $N_A=N_B$, and that the homopolymer chains were much shorter than those of the copolymer. Spherical morphology was considered with a core consisting of only B blocks, and a corona containing a fraction, η, of A blocks and of homopolymer $(1-\eta)$. For the case of small incompatibility between the two blocks it was found that:

$$p \sim N^{0.6} \qquad \textbf{Equation 1.10}$$

and

$$R_B \sim N^{0.53} \qquad \textbf{Equation 1.11}$$

whilst for strong incompatibility

$$p \sim N \qquad \textbf{Equation 1.12}$$

and

$$R_B \sim N^{2/3} \qquad \textbf{Equation 1.13}$$

with the latter case showing good agreement with the relationships proposed by de Gennes.[11]

In an extension of the earlier work of Noolandi and Hong[19], Whitmore and Noolandi[18] proposed scaling relationships for diblock copolymer micelles dispersed in a homopolymer They found that the core radius exhibited a slight dependence upon the length of the soluble block, with it scaling as:

$$R_B \sim N_b^{\beta} N_A^{\mu} \quad 0.67 \leq \beta \leq 0.76,\ -0.1 \leq \mu \leq 0 \qquad \textbf{Equation 1.14}$$

The corona thickness was found to scale primarily with the length of the soluble A block, i.e.

$$R_A \sim N_a^{\omega} \quad 0.5 \leq \omega \leq 0.86 \qquad \textbf{Equation 1.15}$$

The model was compared to the SANS results of Selb *et al.*[22] They measured the core radius of poly(styrene)-poly(butadiene) copolymers in a poly(butadiene) homopolymer of different molecular weights. Good agreement between theory and experiment was observed, with the exponents of the core radius differing slightly.

Nagarajan and Ganesh[23] proposed a theory for the formation of block copolymer micelles in a selective solvent. The micelles were assumed to have a core consisting solely of the insoluble B blocks with the corona composed of A chains and solvent. In common with the work of Whitmore and Noolandi[18] the authors found that the solvent compatible block exerts an influence on the micelle properties, especially in a good solvent. Scaling relationships were obtained for block copolymers in a good solvent, poly(propylene oxide)-poly(ethylene oxide) in water, and in a near theta solvent, poly(butadiene)-poly(styrene) in *n*-heptane, and were respectively:

$R_B \sim N_A^{0.17} N_B^{0.73}$ **Equation 1.16** $p \sim N_A^{-0.9} N_B^{1.19}$ **Equation 1.17** $R_A \sim N_A^{0.74} N_B^{0.06}$ **Equation 1.18**

$R_B \sim N_A^{0.08} N_B^{0.70}$ **Equation 1.19** $p \sim N_A^{-0.24} N_B^{1.10}$ **Equation 1.20** $R_A \sim N_A^{0.68} N_B^{0.07}$ **Equation 1.21**

Combining these results, and those from two model systems, generic scaling relationships were proposed:

$$R_B = \frac{3N_B^2\left(\frac{\gamma_{BS}a^2}{k_BT}\right) + N_B^{3/2} + N_B N_A^{1/2}\left(\frac{R_B}{R_A}\right)^{1/3}}{\left[1 + N_B^{-1/3} + \left(\frac{N_B}{N_A}\right)\left(\frac{R_A}{R_B}\right)^2\right]^{1/3}} a \qquad \textbf{Equation 1.22}$$

$$p = \frac{4\pi N_B\left(\frac{\gamma_{BS}a^2}{k_BT}\right) + \left(\frac{4\pi}{3}\right)N_B^{1/2} + \left(\frac{4\pi}{3}\right)N_A^{1/2}\left(\frac{R_B}{R_A}\right)}{1 + N_B^{-1/3} + \left(\frac{N_B}{N_A}\right)\left(\frac{R_A}{R_B}\right)^2} \qquad \textbf{Equation 1.23}$$

$$\frac{R_A}{R_B} = 0.867\left[\frac{1}{2} + \frac{N_A N_B^2}{(N_A + N_B)^3} - \chi_{AS}\right]^{1/5} N_A^{6/7} N_B^{-8/11} \qquad \textbf{Equation 1.24}$$

Where γ_{BS} is the interfacial tension between the B block and the solvent, and χ_{AS} is the Flory-Huggins interaction parameter between the A block and the solvent.

There are many other theories relating to block copolymer micelles, and the interested reader is referred to Hamley,[4] or Linse[24] for further details.

1.3. Polymer Brushes

The size of an isolated polymer coil in solution is determined by the thermodynamic quality of the solvent. In a thermodynamically good solvent where the interactions between the chain segments and the solvent molecules

are attractive, the coil will expand to maximise favourable contacts with the solvent. In a thermodynamically poor solvent where the interactions between the components are repulsive the coil collapses in on itself to minimise unfavourable interactions with the solvent.

Polymer molecules attached or tethered to a surface or interface by one end exhibit different behaviour to free chains in solution. This is due to the grafting surface limiting the configurational space of the chain, and the anchoring changes the way in which neighbouring chains interact with one another. Block copolymer micelles can be considered as polymer brushes, with the corona chains grafted to the core surface.

Consider a polymer brush consisting of a set of polymer chains grafted to a solid/liquid interface. The chains are assumed to be monodisperse and to have a degree of polymerisation, N. The grafting density, σ, is assumed to be uniform and can be defined in a dimensionless way as the number of chains grafted in an area equal to the square of the segment size a^2, with the segment size being approximately equal to the cube root of the monomer volume. The polymer is assumed to be in a good solvent. For this scenario, two different regimes can be defined as shown in figure 1.10.

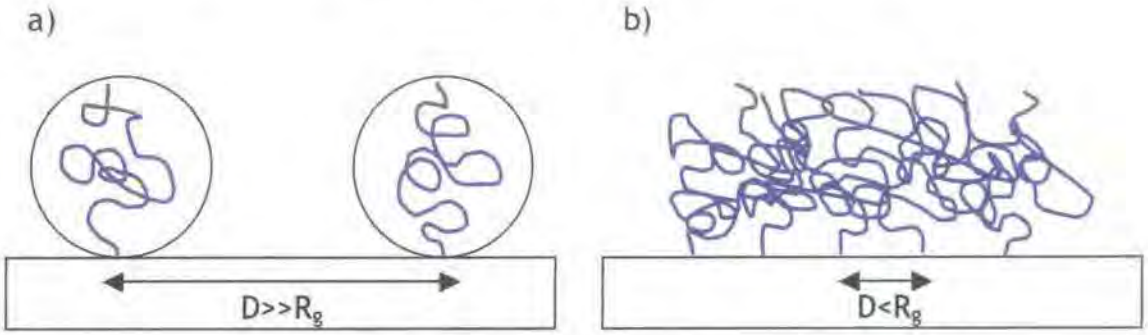

Figure 1.10 - *Schematic representation of the two regimes for polymers grafted to a surface. a) $D>>R_g$ "mushrooms", b) $D<R_g$ polymer brush*

If the distance, D, between the points of attachment is greater than the radius of gyration, R_g, then each chain is isolated from its neighbours and no interactions occur. This result in an array of little "mushrooms", the dimensions of which are comparable to the radius of gyration of the free chains.

If $D<R_g$ then the chains interact with one another. In this instance excluded volume interactions between neighbouring chains causes them to stretch normal to the grafting surface minimising unfavourable contact with one another and maximising favourable contact with the solvent molecules. The result is an array of interacting chains known as a brush.

The brush height, h, can be defined as the distance from the grafting surface at which the polymer volume fraction equals zero, i.e. just solvent. In a good solvent h is usually several times greater than the unperturbed radius of gyration of the polymer chains. As the quality of the solvent decreases the brush layer collapses as the polymer segments attempt to minimise unfavourable interactions with the solvent molecules.

The variation of the polymer volume fraction with distance from the grafting surface has been a subject of numerous theoretical models.[25]

Alexander[12] proposed scaling arguments relating the brush height to σ and N at low grafting densities, where conditions in the brush can be considered semi-dilute. The average distance between grafting sites can be expressed as:

$$D = a\sigma^{-1/2}$$ **Equation 1.25**

The brush can be divided into a series of "blobs" (figure 1.11), with the size of the blobs equal to D.

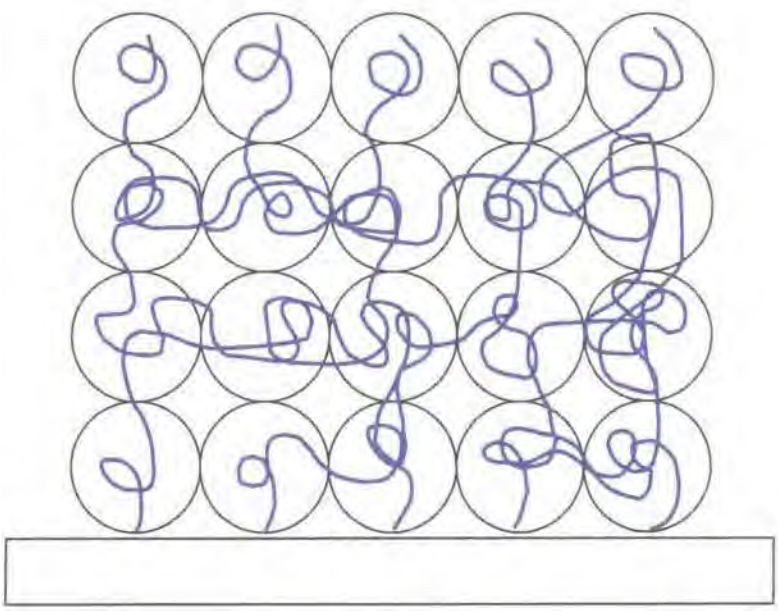

Figure 1.11 - *The blob picture of a polymer brush in the semi-dilute regime*

Each blob contains N_b subunits and D can be defined as:

$$D = aN_b^{3/5} \qquad \text{Equation 1.26}$$

As space is filled by the blobs the polymer volume fraction, ϕ_b, inside the brush has the form:

$$\phi_b \sim \frac{a^3 N_b}{D^3} \qquad \text{Equation 1.27}$$

The polymer volume fraction can be related to the grafting density by;

$$\phi_b \sim \sigma^{2/3} \qquad \text{Equation 1.28}$$

The volume of one chain containing N monomer units is hD^2, where h is the height of the grafted chain (or brush height). This gives an expression for the brush height:

$$h \sim Na\sigma^{1/3} \qquad \text{Equation 1.29}$$

At higher grafting densities, when conditions inside the brush are more concentrated the brush characteristics can be described by an energy balance argument proposed by de Gennes.[13] The free energy cost associated with stretching a chain from its Gaussian statistics to the brush height, h, is given by:

$$\frac{F_{stretch}}{k_B T} = \frac{h^2}{a^2 N} \qquad \text{Equation 1.30}$$

The excluded volume interaction free energy per unit volume can be expressed as:

$$\frac{F_{vol}}{k_B T} = \frac{1}{2}\frac{v\phi^2}{a^6} k_B T \qquad \text{Equation 1.31}$$

where the excluded volume parameter, v, is defined in terms of the segment size and the Flory-Huggins parameter as $v = a^3(1-2\chi)$. As the volume associated with a single chain is ha^2/σ the total free energy per chain can be expressed in terms of the height as:

$$\frac{F_{chain}}{k_B T} \sim \frac{h^2}{2a^2 N} + \frac{vN^2\sigma}{2ha^2} \qquad \text{Equation 1.32}$$

which minimising with respect to h gives:

$$h \sim N(v\sigma)^{1/3}$$ **Equation 1.33**

It is evident from equations 1.29 and 1.33 that both the Alexander and the de Gennes theories predict a linear relationship between brush height and degree of polymerisation, and a cube-root dependence on the grafting density. Only the latter incorporates the effect of solvent quality, with the brush height expected to increase with the quality of the solvent.

Both models proposed by Alexander and de Gennes assume that all chains within the brush behave the same with the free chain ends all located at the tip of the brush. The polymer volume fraction profile corresponding to both models is constant throughout the brush, falling abruptly to zero at the edge of the brush, i.e. a step-function.

Milner *et al.*[26] used a self-consistent field model to determine the concentration profile of polymer brushes. The solution of the SCF equations indicated a parabolic decay could be used to represent the polymer volume fraction within the brush, in contrast to the step function of Alexander-de Gennes theory[12, 13]. In their model, the brush height, h is given by:

$$h = \left(\frac{12}{\pi^2}\right)^{1/3} N(\sigma v)^{1/3}$$ **Equation 1.34**

Equation 1.34 shows that the brush height predicted by SCFT has the same cube root dependence on N and σ as the scaling relationships of Alexander[12] and de Gennes.[13] Unlike the scaling arguments that assume all the chains behave alike, with their free ends located at the tip of brush, the SCF calculations reveal that the free chain ends are distributed throughout the entire brush. These differences mean that scaling theory predicts a step function for the volume fraction profile whilst SCFT predicts a parabolic profile, as shown in figure 1.12.

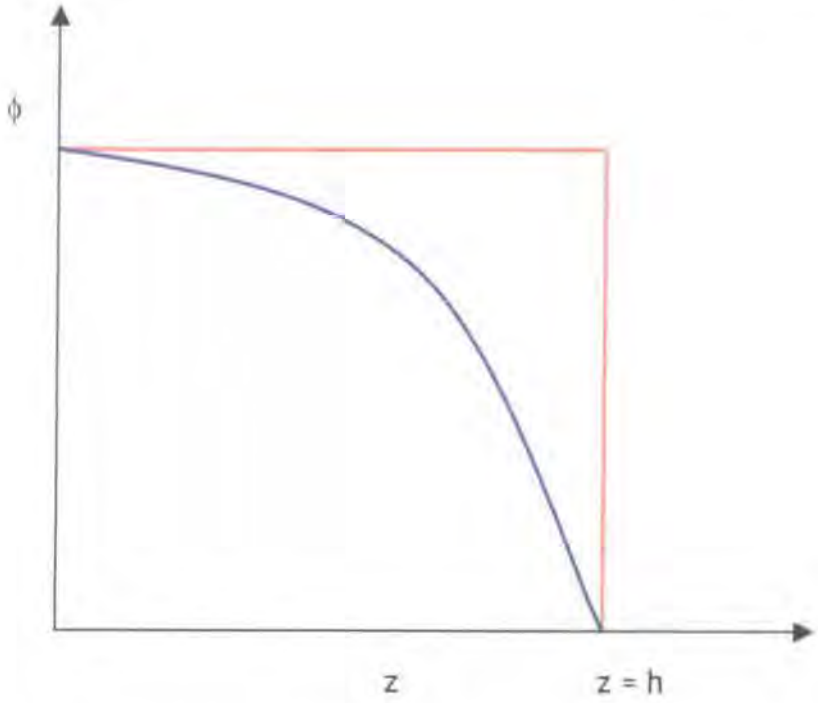

Figure 1.12 - *representation of step function — predicted by Alexander-de Gennes theory, and the parabolic volume fraction — due to the SCFT of Milner et al.*[26]

1.4. Micellar behaviour of poly(butadiene)-poly(ethylene oxide)

Investigations into the micellar behaviour of poly(butadiene)-poly(ethylene oxide) (PB-PEO) have only begun to appear in the literature within the last five or so years. Many of the investigations have been carried out in the group of Frank Bates, these are reviewed first, followed by investigations made by others.

1.4.1. Investigations of the Bates group

Won, Davis and Bates[27] investigated the solution behaviour of a PB-PEO diblock copolymer of molecular weight 4900g mol^{-1} containing 50wt% PEO in water at concentrations of up to 17%, and temperature between 298 and 348K. They observed that under all conditions cylindrical micelles consisting of a PB core surrounded by a PEO corona were formed. Small angle X-ray and neutron scattering (SAXS and SANS) were used to probe the ordering of the micelles over the concentration and temperature range stated, and a phase diagram was constructed (fig 1.13)

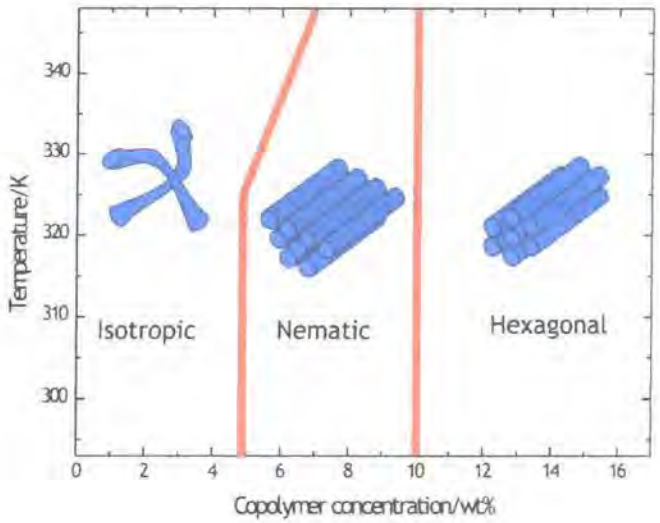

Figure 1.13 - *Phase diagram as a function of temperature and concentration for micelles of PB-PEO investigated by Won, Davis and Bates. Replicated from reference 27.*

The phase diagram shows that below 5% the micelles were present as an isotropic dispersion. As the concentration was increased, so did the order of the system and a one-dimensional ordered Nematic phase was observed between 5 and 10%. At concentrations greater than 10% the cylinders were ordered on a regular hexagonal lattice. Cryo-Transmission electron microscopy (cryo-TEM) yielded some interesting micrographs, with the long worm-like micelles clearly visible.

The authors cross-linked the PB core of the micelles using a redox combination of potassium persulphate, sodium metabisulphite, and iron(II) sulphate heptahydrate, which allowed coupling of the 1,2 double bonds of the PB backbone. SANS was used to investigate the differences between the micelles before and after cross-linking, with a reduction in the core radius of 13% observed. It was also noted that the cross-linking was confined to the core of the micelles by comparing solutions cross-linked at 5% then diluted ten-fold, to those cross-linked at 0.5%, with the scattering being indistinguishable between the two. This fact suggested that both solutions have the same inter and intra micellar structure.

Zheng *et al.*[28] used cryo-TEM to image vitrified films of PB-PEO dispersions. Several copolymers were used, having molecular weights in the range 4900-

13100g mol^{-1} and PEO contents between 51 and 70%. The authors noted that those copolymers with the lower PEO content formed cylindrical micelles, whilst those with the higher PEO content formed spheres when dispersed in water. The dimensions of the two morphologies were similar with the cylinders having a core radius of 160Å and total radius 490Å, whilst those of the spheres were 150Å and 480Å respectively. Comparisons of the ratio of R_{core}:R_{total} were made with the star model of Halperin[16] and the mean field model of Liebler *et al.*[21] with the former providing the better agreement.

Won *et al.*[29] used SANS to investigate the micelles formed from PB-PEO dispersed in water. The micelles formed were either spherical or cylindrical in nature depending upon the copolymer composition. Deuteration of the PB blocks was used to enhance the SANS contrast. Micellar dispersions of 1 and 3% were investigated both of which showed no evidence of a structure factor peak. The model used to fit the data assumed a uniform PB density in the core, with a sharp boundary between the core and corona.
Core radii were obtained by contrast matching the solvent to the corona and fitting the data to the appropriate form factor, whilst the corona thickness were determined under core contrast match conditions with the density profile approximated by a Fermi-Dirac distribution. The values determined are given in table 1.3.

M_n/g mol^{-1}	5380	8180
% PEO	49	66
Micelle morphology	Cylinder	Sphere
R_c/Å	74±1	112±1
R_s/Å	132±4	178±4
R_s:R_g	2.59	2.36

Table 1.3 - *Parameters for PB-PEO micelles obtained from fits to SANS data by Won et al*[29]*. R_c-core radius, R_s-shell thickness, R_g-unperturbed radius of gyration of PEO chains*

Both spheres and cylinders had concave concentration profiles in the corona. It was also suggested that despite favourable interactions with the solvent the

ethylene oxide segments were accumulated next to the core, possibly shielding it from unfavourable interactions with the solvent.

Won *et al.*[30] investigated the differences between core cross-linked and unreacted worm-like micelles in terms of their rheological properties and depletion effects upon the addition of PEO. The cross-linking was accomplished using the same redox combination detailed in their earlier paper, with a polymer of 4900g mol^{-1} and 50% PEO being used.
The authors observed that the cross-linked micelles had a storage modulus that was more than two orders of magnitude larger than their unreacted counterparts, which was attributed to an elastically interacting physical network of the cross-linked micelles. Also when subjected to shear the cross-linked micelles retained their orientation isotropy in contrast to the unreacted micelles, which aligned in the flow direction.

Using a series of PB-PEO block copolymers ranging in molecular weight from 3600 to 13100g mol^{-1} and PEO compositions from 28 to 66%, as well as some poly(ethyl ethylene)-poly(ethylene oxide) di and tri-block copolymers, Won *et al.*[31] utilised cryo-TEM to determine the boundaries for shape transitions between different morphologies. This led to the construction of a morphology diagram as function of PEO volume fraction in the polymer, and length of the hydrophobic block, as shown in figure 1.14. The vertical lines on the morphology diagram serve merely as an indication of the boundaries and are not absolute.

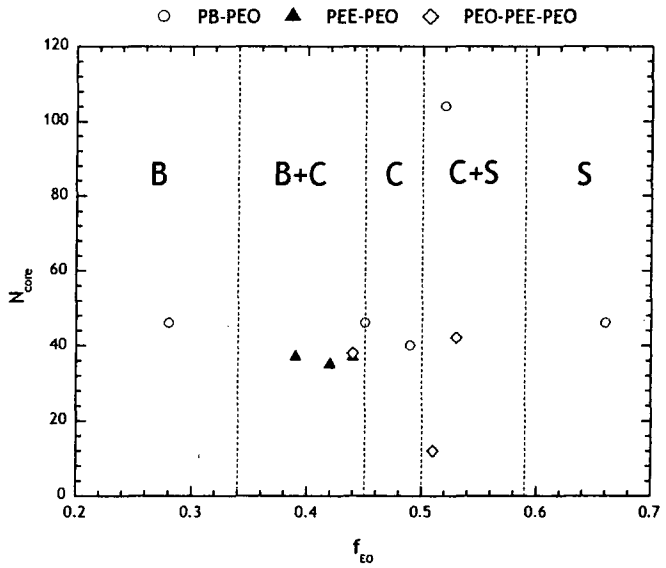

Figure 1.14 - *Morphology diagram as a function of PEO composition, f_{EO}, and PB degree of polymerisation, N_{core}, from Won et al.*[31] *B-Bilayered vesicles, C-cylinders, S-spheres*

In addition to the basic geometries of membrane-like bilayer, cylinder and sphere, more exotic compound structures were observed in the ranges near to the bilayer-cylinder and cylinder-sphere boundaries. These structures were observed in both freshly prepared and long-term stored solutions indicating their long lifetime. Their presence was attributed to the metastability of amphiphilic polymeric materials.

Packing properties such as the interfacial area per chain and degree of hydrophobic stretching were determined, and it was noted that for a given morphology the interfacial area per chain was inversely proportional to the hydrophobic stretching.

Jain and Bates[32] investigated the solution properties of two series of PB-PEO diblock copolymers, each having constant PB molecular weights, but varying PEO content. One of PB molecular weight 2500g mol^{-1} and $0.3 \leq w_{PEO} \leq 0.64$, and the other of 9200 g mol^{-1} and $0.24 \leq w_{PEO} \leq 0.62$. 1% dispersions were examined using cryo-TEM, and the authors were able to construct a morphology diagram (figure 1.15) relating the morphology observed to the degree of polymerisation of PB and the PEO content of the copolymer.

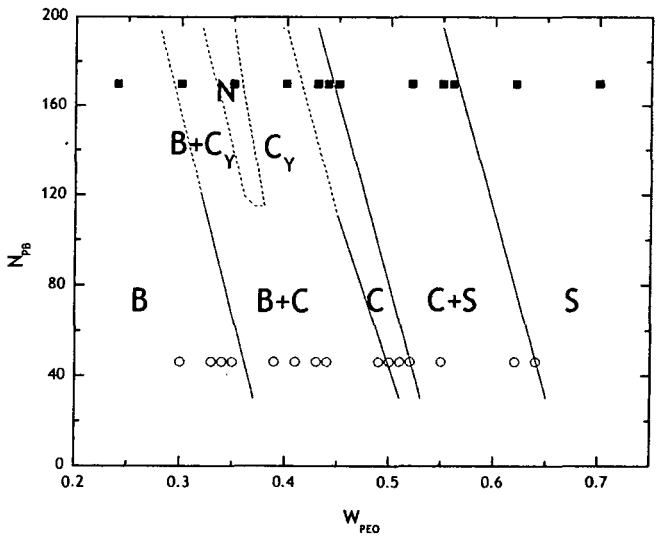

Figure 1.15 - *Morphology diagram as a function of PEO composition, w_{PEO}, and PB degree of polymerisation, N_{PB}, from Jain and Bates.*[32] *Abbreviations as in figure 1.14, and N-Network, C_Y-cylinder with Y-junctions*

In common with the work of Won *et al.*[31] they observed the "classical" sequence of dispersed structures, i.e. bilayered vesicles, cylinders and spheres with increasing PEO content. The large increase in copolymer molecular weight caused the core dimensions to increase three fold, and shift the morphology boundaries to lower PEO content, as shown in figure 1.15. They also observed the formation of Y-junctions in cylindrical micelles at compositions between the B and C regimes. Even at w_{PEO}=0.42 where cylinders would be expected occasional branches were observed. At w_{PEO}=0.39 an extended three-dimensional network morphology dominated by Y-junctions was formed; behaviour that was not observed in the lower molecular weight copolymers. Fragmentation of the network by stirring or sonication produced individual micelles of complex morphology, exhibiting a high degree of symmetry. The authors attributed this to the redistribution of diblock copolymer molecules within the particles after fragmentation in order to balance the internal energy.

Won, Davis and Bates[33] used a combination of fully hydrogenous and dPB-hPEO to investigate the molecular exchange in spherical and cylindrical micelles. They examined 1% dispersions that were prepared using two different methods:

i.) Pre-mixing, where both isotopic variants were dissolved in chloroform, dried, annealed, then dispersed in D_2O.

ii.) Post-mixing, where 1% dispersions of both isotopic variants were mixed directly.

SANS experiments on dispersions produced by the two methods revealed differences in the scattering curves. The eight-day-old post-mixed sample could be accurately reproduced by scattering from an unmixed sample (the mean of the scattering from the two isotopic variants), suggesting that no exchange had taken place. The authors concluded that intermicellar equilibration time may be of the order of years, and that the residence time of a copolymer molecule within a micelle may be immeasurably large.

1.4.2. Investigations by other researchers

Hentze *et al.*[34] investigated the lyotropic mesophases of PB-PEO co-polymers. Two different polymers were used, one having a molecular weight of 13900gmol^{-1}, and containing 55% PEO, and the other 28400gmol^{-1} and 64% PEO. The entire concentration range from 0-100%, with temperatures ranging from 293-373K were used. Phase diagrams were constructed for both polymers, (figure 1.16 a and b) following elucidation of the nature of phases formed by the polymers under various conditions using polarised light optical microscopy.

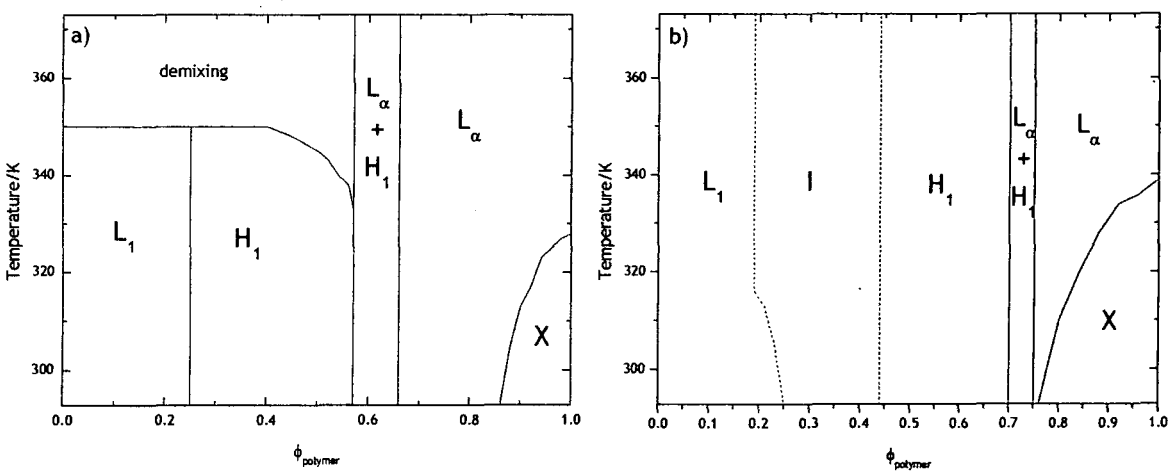

Figure 1.16 - *Phase diagrams from Henze et al[34]. for PB-PEO block copolymers as a function of copolymer concentration and temperature. a) M_n = 13900gmol^{-1}, w_{PEO} = 0.55 PEO, b) M_n = 28400gmol^{-1}, w_{PEO} = 0.64. L_1-isotropic micellar solution, H_1-hexagonal phase, L_α - lamellar phase, X-semi-crystalline phase, I-cubic phase*

Cross-linking of the ordered phases, using γ-rays, resulted in the formation of solid, mechanically stable, "elastic" hydrogels that swelled on the addition of water but did not dissolve. The morphology of the mesophases was retained upon cross-linking, and SAXS measurements revealed a decrease of 5-10% in the d-spacings.

Expanding their earlier study, Förster *et al.*[35] used SAXS, SANS, TEM and polarised light microscopy to investigate the mesophases formed by PB-PEO block copolymers with a range of molecular weights greater than in their earlier study. As in the earlier work they observed increasing order with concentration from micellar solutions through bcc lattice, and hexagonal arrays to lamellae. Their results are summarised in table 1.4.

Polymer 1, 26750gmol^{-1}, w_{PEO}=0.524	
$\phi_{polymer}$	Morphology
0.4	Bcc spheres
0.5	Cylinders
0.6	Cylinders
	Ribbons
	Vesicles
0.7	Cylinders
	Platelets
	Vesicles
0.8	Lamellae
1.0	Lamellae

Polymer 4, 13570gmol^{-1}, w_{PEO}=0.434	
$\phi_{polymer}$	Morphology
0.001	Cylinders
0.02	Cylinders
0.3	Hexagonal cylinders
0.5	Hexagonal cylinders
0.6	Hexagonal cylinders
	Lamellae
0.7	Lamellae
1.0	Lamellae

Polymer 2, 44625gmol^{-1}, w_{PEO}=0.409	
$\phi_{polymer}$	Morphology
0.3	Spheres
0.5	Hexagonal cylinders
0.7	Lamellae
1.0	Lamellae

Polymer 3, 82330gmol^{-1}, w_{PEO}=0.409	
$\phi_{polymer}$	Morphology
0.3	Spheres
	Cylinders
0.5	Sponge
0.7	Lamellae
1.0	Lamellae

Table 1.4 - *Summary of morphologies observed by Förster et al[35]. for PB-PEO block copolymers of varying molecular weights and compositions in aqueous solution*

They noted that increasing the molecular weight of the copolymer reduced the order in the system, especially in the bcc lattice and hexagonal regimes. In common with the work of the Bates group, the formation of loops and junctions from cylindrical morphology was observed.

Egger *et al.*[36] investigated a mixed system of PB-PEO and Dodecyltrimethylammoniumbromide, DTAB, using light scattering, SAXS and SANS. The polymer they used had a molecular weight of 4330gmol^{-1}, a PEO content of 54% and formed cylindrical micelles upon dispersion in water. Adding DTAB at concentrations greater than its cmc resulted in a transformation from cylindrical to spherical morphology being observed. The authors proposed that this was due to the formation of mixed micelles, the driving force for which was the dilution of charges by embedding the cationic surfactant head group in the matrix of neutral ethylene oxide segments.

Maskos and Harris[37] investigated the micellar structures of a PB-PEO diblock copolymer of molecular weight 3350gmol^{-1} containing 40% PEO. A dispersion of ca 0.1% was cross-linked using γ-rays, and the structures produced, the most common of which were bilayered vesicles, imaged using TEM. The authors noted that the vesicles were stable enough to be transferred to THF, a good solvent for both blocks, whilst retaining the same shape. Small numbers of other structures were observed such as cylinders, strings of vesicles and vesicle sheets. The authors suggested that the strings were formed by fusion of the outer layers of the vesicles.

1.5. Micellar behaviour of poly(butylene oxide)-poly(ethylene oxide)

Over the last decade or so, Booth and co-workers have investigated the micellisation of poly(butylene oxide)-poly(ethylene oxide) (PBO-PEO) in aqueous solution. For brevity a brief summary of the important conclusions is presented here, and the interested reader is referred to recent reviews summarising their efforts and the references contained therein for more detail.[38, 39]

Studies have been carried out on several architectures, diblock, PEO-PBO-PEO and PBO-PEO-PBO triblocks and cyclic copolymer; schematic representations of the micelles formed by each are shown in figure 1.17.

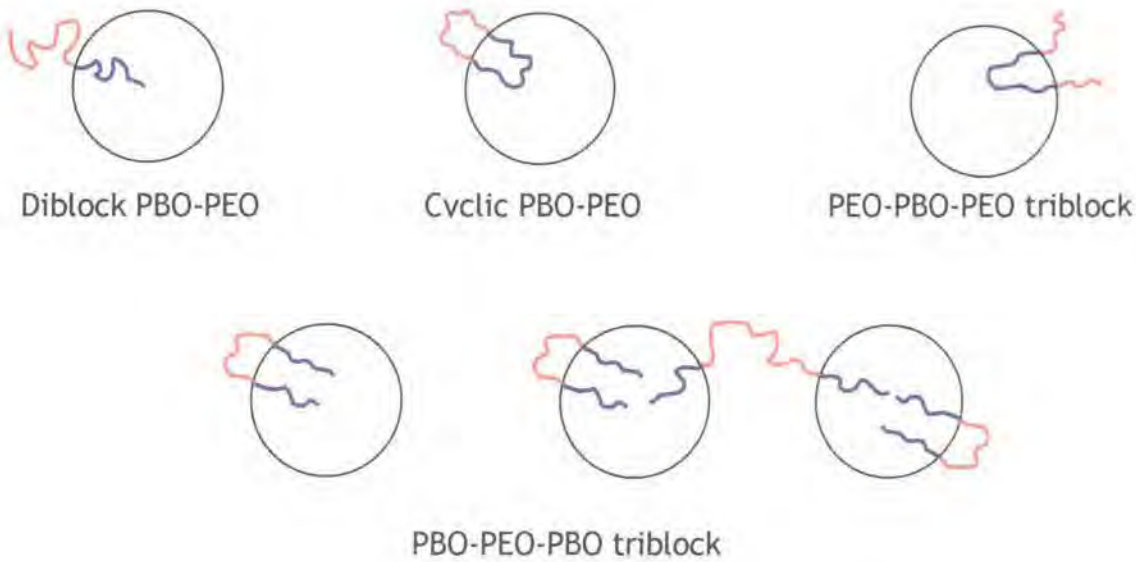

Figure 1.17- *Schematic representation of block copolymer architecture for PBO-PEO block copolymers studied by Booth and co-workers*

The majority of the copolymers investigated were synthesised "in-house" utilising sequential anionic polymerisation of the two monomers with a potassium salt as the initiator. Static and dynamic light scattering, nuclear magnetic resonance spectrometry, gel permeation chromatography, polarised optical microscopy, rheology, surface tension and differential scanning calorimetry have all been used to provide information of the micelles and the micellisation process.

In common with observation for other PEO containing copolymers, the length of the hydrophobic PBO block was found to be the primary determinant of the cmc and association number, with the former decreasing and the latter increasing with increasing hydrophobe length. The effect of the PEO block length was less clear, with the data suggesting a small increase in the cmc and decrease in the association number with an increase in PEO block length for a constant PBO block length; behaviour common with other PEO containing copolymers such as poly(propylene oxide)-poly(ethylene oxide) (PPO-PEO).

Increasing the temperature resulted in a decrease in the cmc, an observation that was common to all of the architectures studied, whilst the association number increased with a temperature as the quality of the solvent for PEO decreased. The hydrodynamic radii exhibited little temperature dependence, an effect observed for PPO-PEO block copolymers and that was attributed to a balance between an increase in association number, accompanied by a decrease in the swelling of the PEO block corona as the solvent quality decreases.

The enthalpy of micellisation was determined for a number of solutions by plotting log (c) *vs.* 1/cmt, yielding values in the range $24 \leq \Delta_{mic}H° \leq 125$ kJ mol^{-1}, smaller than those determined for PPO-PEO copolymers ($115 \leq \Delta_{mic}H° \leq 331$ kJ mol^{-1}). The standard Gibbs energies were comparable to those of PPO-PEO block copolymers, with values of $-10 \leq \Delta_{mic}G° \leq -30$ kJ mol^{-1}. The results indicated the entropy driven nature of the micellisation of PBO-PEO in aqueous solution, which is consistent with the hydrophobicity of the PBO block.

Comparisons were made between the different architectures at constant composition and chain length, and for a given hydrophobe length, the cmc's were found to be in the order PBO-PEO<cyclic PBO-PEO<PBO-PEO-PBO≤PEO-PBO-PEO. The association number was found to follow a similar trend, but with the two triblock architectures forming micelles having approximately equivalent association numbers.

1.6. Micellar behaviour of poly(propylene oxide)-poly(ethylene oxide)

Much research has been devoted to the study of the commercially available poly(propylene oxide)-poly(ethylene oxide) (PPO-PEO) block copolymers. There are in excess of 1000 papers relating to the micellisation properties of these copolymers. Chu and Zhou[40] recently collated and summarised some of the important results from different groups relating to the micellisation process and resulting micelle structures. The results are complicated by the high polydispersities of the commercially manufactured triblock copolymers as well as the large numbers of polymer available. In addition to these

complications, there are also some slight discrepancies between results obtained from different techniques or laboratories. Never the less, some useful comparisons can be made between the data and some interesting trends observed.

The properties of PPO-PEO copolymers in aqueous solution are strongly temperature dependent, with the hydrophobic nature of the PPO block increasing with temperature. Homo-PPO is water-soluble at temperatures below ca 283-288K, as a result PPO-PEO block copolymers exist in solution as dispersed unimers at lower temperatures.

From the data summarised by Chu and Zhou[40] it is possible to make some generalisations about the micellisation process and the resulting structures:

i.) For a given temperature, increasing the length of the PPO block results in an exponential decrease of the cmc.

ii.) The effect of the PEO block length is less pronounced than that of the PPO block, with only small increases in the cmc and cmt observed on increasing its length.

iii.) For a constant copolymer composition the cmc and cmt values decrease with increasing copolymer molecular weight.

iv.) The chain architecture has a profound effect on the micelle formation with PPO-PEO-PPO copolymers displaying reduced micellisation ability in comparison to a PEO-PPO-PEO copolymer of the same composition.

v.) The micellisation process is entropically driven, with a large positive enthalpy of micellisation commonly observed.

vi.) The association number increases with temperature, whilst the micelle radius remains relatively constant.

vii.) Increasing the length of the PPO block results in an increase in association number, this is also observed for decreasing length of PEO block.

1.7. Cross-linked micelles

As discussed in section 1.1 the self-assembly process leading to the formation of micelles is the result of non-covalent interactions; consequently the process is reversible, and the micelles are capable of reverting back to dispersed molecules should the conditions be suitable, e.g. dilution to c<cmc. As has been discussed in section 1.4 for PB-PEO block copolymers it is possible

to render the micelles permanent structures by chemically cross-linking the core either though redox chemistry or γ irradiation. There are however other examples reported in the literature of cross-linked micelles in both aqueous and hydrocarbon media. Depending upon the chemical functionality of the block copolymer forming the micelles it is possible to effect cross-linking in the core as already seen, or in the shell. This section aims to provide an overview of both types of cross-linking.

1.7.1. Core cross-linked micelles

One of the earliest reports of micelle cross-linking was that of Tuzar and co-workers.[41] They cross-linked the poly(butadiene) cores of poly(butadiene)-poly(styrene), (PB-PS), micelles in several mixed solvent systems selective for the PS using either UV radiation and a peroxide initiator or a high energy electron beam. They reported little in terms of the micelle properties either before or after cross-linking.

Wilson and Riess[42] also used UV radiation and a photo initiator, to cross-link micelles of the same chemical nature (i.e. PB-PS in solvents selective for PS)). Two different solvents were used, namely DMF and DMA, depending upon the solubility of the polymer. The cross-linking efficiencies were determined by precipitation into methanol, followed by THF addition to solubilise any non-stabilised material, and ranged from 23-86%. QELS was used to determine the hydrodynamic radii of the micelles both before and after the cross-linking reaction. In all cases a small decrease in R_h was observed upon cross-linking, which the authors attributed to reduced swelling of the core by the solvent.

Saito and Ishizu[43] cross linked the 2-vinyl pyridine core of poly(vinyl pyridine)-poly(styrene)-poly(vinyl pyridine) (PVP-PS-PVP) triblock copolymers in toluene/cyclohexane mixtures using 1,4 diiodobutane. TEM and QELS were used to study the micelles before and after cross-linking, with the latter revealing that the hydrodynamic radii of the micelles decreased upon cross-linking in toluene, but remained unchanged when the reaction was carried out in toluene/cyclohexane.

Iijima *et al.* [44] cross-linked the micelles of a poly(lactide)-poly(ethylene oxide), PLA-PEO, diblock copolymer in water by polymerising a methacryloyl end group "built in" to the PLA during synthesis, (fig 1.18).

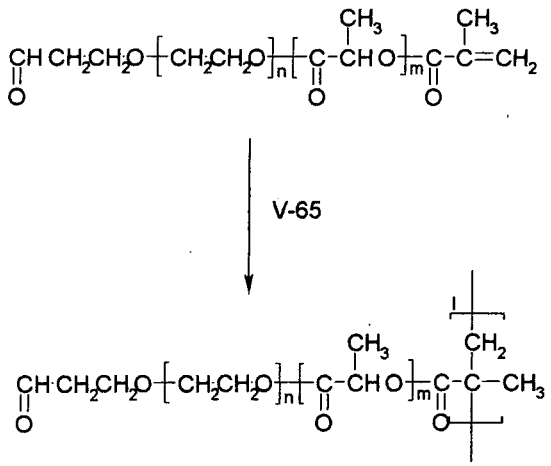

Figure 1.18 - *Cross-linking of PLA-PEO micelles in aqueous solution by polymerisation of terminal methacrolyl group due to Iijima et al.*

The success of the reaction was determined by the absence of vinyl protons in the NMR spectrum. QELS was used to characterise the micelles before and after cross-linking, with the micelle diameter remaining unchanged following the cross-linking reaction. The micelles were inherently stable, both in terms of temperature and long-term storage, and it was possible to recover them from aqueous solution and dissolve them in a good solvent for both blocks (DMF), without any disruption of the micelle structure.

Guo, Liu, and Tao[45] cross-linked the Poly(2-cinnamoylethyl methacrylate) (PCEMA) core of PCEMA-PS micelles, (fig 1.19), in THF/cyclohexane and chloroform/cyclohexane by irradiating the samples with UV radiation.

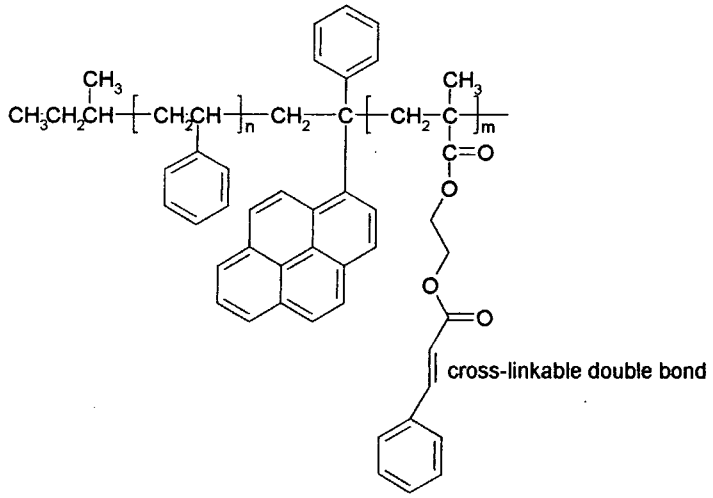

Figure 1.19 - *structure of PCEMA-PS block copolymer as prepared by Guo, Liu and Tao, with the site of cross-linking indicated.*

The resulting particles were characterised by QELS, GPC and TEM. The success of the reaction was demonstrated by the bimodal GPC trace, one peak corresponding to the copolymer, and the other, of a much greater intensity, to the cross-linked micelles; the former was attributed to unimers in equilibrium with the micelles prior to cross-linking. QELS experiments on the micelles before and after cross-linking revealed a slight decrease in the hydrodynamic radius but still with a monomodal size distribution. The decrease in size was attributed to a possible reduction in core volume upon polymerisation. TEM revealed the micelles to be spherical in nature.

Henselwood and Liu[46] cross-linked the PCEMA core of PCEMA-poly(acylic acid) (PAA) micelles in water/DMF (80:20) mixtures by irradiation with UV light. Characterisation of the cross-linked micelles with TEM confirmed their spherical nature. QELS experiments were only carried out after the cross-linking reaction and so it was not possible to determine whether the micelle size had changed.

Rheingans *et al.*[47] cross-linked the poly(dimethyl siloxane) core of PDMS-PEO micelles in water by photopolymerisation of methacrylic acid groups in the DMS core, (fig 1.20)

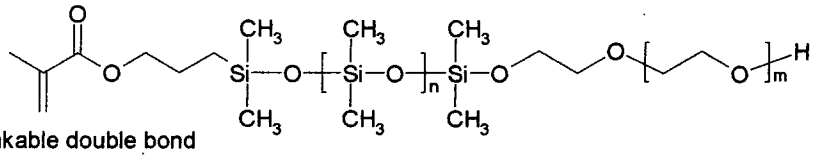

Figure 1.20 - *PDMS-PEO block copolymer with methacrylic acid end-group suitable for cross-linking the PDMS core of the micelle due to Rheingans et al.*

AFM characterisation before and after cross-linking revealed no change in the micelle dimensions.

There are other examples of core cross-linked micelles in the literature in addition to those presented here. The group of Reiko Saito[43, 48-53] have cross-linked several micellar systems with the emphasis on the synthetic procedure rather than the characterisation of the micelles. The interested reader is referred to the cited references for further details.

1.7.2. Shell cross-linked micelles

Much of the research in this area has been instigated by the group of Karen Wooley, indeed a review summarising their efforts was recently published.[54] The micelles are formed from amphiphilic block copolymers, usually in aqueous solution, with a hydrophobic core and a hydrophilic corona containing a suitable reactive group. Cross-linking is usually accomplished by chemical reaction of the functional group in the corona to give the cross-linked particles termed Knedels. A brief overview of some of the systems and key observations reported is presented here, with more detailed information available in reference 54.

Thurmond *et al.* [55] prepared shell cross-linked knedels (SCK) by cross-linking a partially quaternised PVP shell of PS-PVP in THF/water mixtures (fig 1.21) by irradiation in the presence of a photo-initiator.

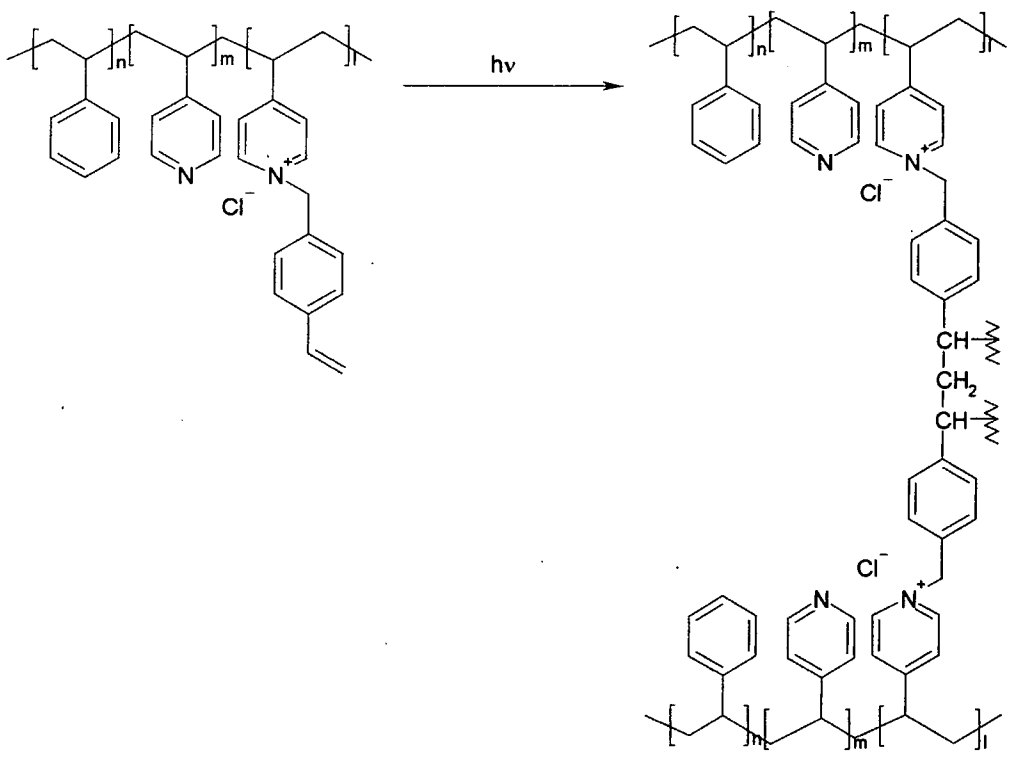

Figure 1.21 - *Cross-linking reaction of the part-quaternised PVP shell of PS-PVP copolymer micelles due to Thurmond et al.*

AFM was used to determine the size of the SCK's, with large variations in size observed depending upon the relative block lengths. Typical diameters were of the order of 10-300Å for copolymers of molecular of ca. 15000 $gmol^{-1}$.
PS-PAA micelles in THF/water mixtures were cross-linked by amidation of the acid group by Huang *et al* [56] (figure 1.22).

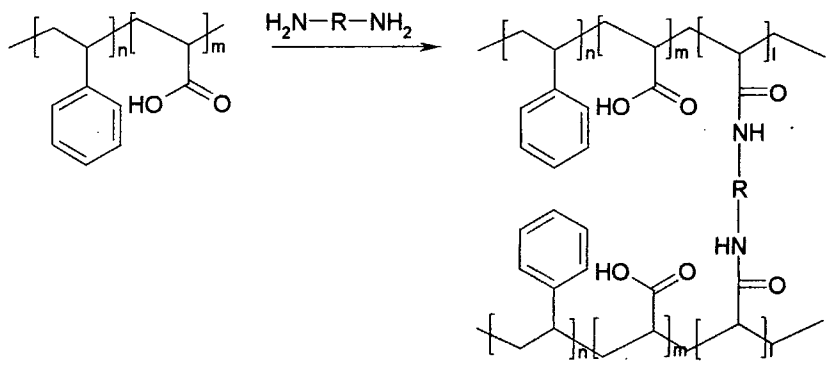

Figure 1.22 - *cross-linking reaction of PAA corona of PS-PAA micelles by amidation reaction due to Huang et al.*

The sizes and shapes of the SCK's were studied and compared to the micelles by AFM and TEM. It was observed that the micelle height when adsorbed onto

mica was less than that of the SCK's, which was attributed to spreading of the micelles whilst the SCK's remained spherical in shape due to their more rigid structure. This observation was supported by TEM, which showed the micelles to be ellipsoidal in shape whilst the SCK's remained spherical.

Other systems have been exploited including poly(ε-caprolactone-acrylic acid).[57] The poly(acrylic acid) shell was cross-linked by reaction with the amine groups of 2,2'(ethylendioxy)bis(ethylamine).

1.8. Aims and objectives

The aims and objectives of the research presented in this thesis can be summarised as follows.

- To synthesise two molecular weight series of poly(butadiene)-poly(ethylene oxide) diblock copolymers with fully hydrogenous and perdeuterated variants. Each copolymer should contain ca. 15wt% poly(butadiene) which should have a majority 1,2 microstructure.
- To elucidate the structure of the micelles formed by the copolymers upon dispersion in aqueous solution.
- To probe the organisation of the micelles at higher concentrations and to determine subsequent inter-micellar interactions.
- To develop a synthetic procedure to facilitate the cross-linking of poly(butadiene) core of the micelles without disrupting the local structure.
- To characterise the cross-linked micelles in terms of their structure and organisation, comparing them to the virgin micelles and rationalising any differences.

1.9. Glossary of symbols

The symbols used in the body of the text and the equations are defined here in the order in which they appear in the text.

1.9.1. Micellisation

p	micelle association number
R_B	core radius formed by insoluble B block
a	segment length
N_B	degree of polymerisation of insoluble block
γ	interfacial tension
T	temperature
r	distance from micelle/star centre
f	number of arms in a star
N_A	degree of polymerisation of soluble block
σ	distance between coronal chains on core surface
ν	exclude volume parameter
γ_{BS}	interfacial tension between insoluble B block and solvent
k_B	Bolztman constant

1.9.2. Polymer Brushes

D	separation distance between grafted chains
R_g	radius of gyration
a	segment length
σ	grafting density
N	degree of polymerisation of brush forming layer
N_b	number of segments in a blob
ϕ_b	polymer volume fraction inside a blob
h	brush height
$F_{stretch}$	stretching free energy
k_B	Boltzman constant
T	temperature
F_{vol}	excluded volume interaction free energy
ν	excluded volume parameter
χ	Flory-Huggins interaction parameter
z	distance from grafting surface

1.10. Bibliography

1 G. Riess, G. Hurtrez, and P. Badahur, in '*Enclycopedia of Polymer Science and Engineering*', ed. H. F. Mark and J. I. Kroschwitz, Wiley, New York, 1985.

2 A. M. Urbas, *et al.*, *Adv. Mater.*, 2002, **14**, 1850.

3 F. S. Bates and G. H. Fredrickson, *Annu. Rev. Phys. Chem.*, 1990, **41**, 525.

4 I. W. Hamley, 'The Physics of Block Copolymers', Oxford University Press, New York, 1998.

5 F. S. Bates and G. H. Fredrickson, *Phys. Today*, 1999, **52**, 32.

6 S. Forster and T. Plantenberg, *Agnew. Chem. Int. Ed.*, 2002, **41**, 688.

7 M. Muthukumar, C. K. Ober, and E. L. Thomas, *Science*, 1997, **277**, 1225.

8 M. Szwarc, *Nature*, 1956, **178**, 1168.

9 S. Forster and M. Antonietti, *Adv. Mater.*, 1998, **10**, 195.

10 H. G. Elias, in '*Light Scattering from Polymer Solutions*', ed. M. B. Huglin, Academic Press, London, 1972.

11 P. G. de Gennes, in '*Solid State Physics, Supplement*', ed. L. Liebert, Academic, New York, 1978.

12 S. Alexander, *J. Physique*, 1977, **38**, 983.

13 P. G. de Gennes, *J. Physique*, 1976, **37**, 1445.

14 M. Daoud and J. P. Cotton, *J. Physique*, 1982, **43**, 531.

15 E. B. Zhulina and T. M. Birshtein, *Polymer Science USSR*, 1986, **27**, 570.

16 A. Halperin, *Macromolecules*, 1987, **20**, 2943.

17 L. Zhang, R. J. Barlow, and A. Eisenberg, *Macromolecules*, 1995, **28**, 6055.

18 M. D. Whitmore and J. Noolandi, *Macromolecules*, 1985, **18**, 657.

19 J. Noolandi and K. M. Hong, *Macromolecules*, 1983, **16**, 1443.

20 J. Plestil and J. Baldrian, *Macromol. Chem.*, 1975, **176**, 1009.

21 L. Leibler, H. Orland, and J. C. Wheeler, *J. Chem. Phys.*, 1983, **79**, 3550.

22 J. Selb, *et al.*, *Polymer Bulletin*, 1983, **10**, 444.

23 R. Nagarajan and K. Ganesh, *J. Chem. Phys.*, 1989, **90**, 5843.

[24] P. Linse, in '*Amphiphilic block copolymers: Self assembly and applications*', ed. P. Alexandridis and B. Lindman, Elsevier, Amsterdam, 2000.

[25] R. A. L. Jones and R. W. Richards, 'Polymers at Surfaces and Interfaces', Cambridge University Press, Cambridge, 1999.

[26] S. T. Milner, T. A. Witten, and M. E. Cates, *Macromolecules*, 1988, **21**, 2610.

[27] Y. Y. Won, H. T. Davis, and F. S. Bates, *Science*, 1999, **283**, 960.

[28] Y. Zheng, *et al.*, *J. Phys. Chem. B*, 1999, **103**, 10331.

[29] Y. Y. Won, *et al.*, *J. Phys. Chem. B*, 2000, **104**, 7134.

[30] Y. Y. Won, *et al.*, *J. Phys. Chem. B*, 2001, **105**, 8302.

[31] Y.-Y. Won, *et al.*, *J. Phys. Chem. B*, 2002, **106**, 3354.

[32] S. Jain and F. S. Bates, *Science*, 2003, **300**, 460.

[33] Y. Y. Won, H. T. Davis, and F. S. Bates, *Macromolecules*, 2003, **36**, 953.

[34] H. P. Hentze, *et al.*, *Macromolecules*, 1999, **32**, 5803.

[35] S. Forster, *et al.*, *Macromolecules*, 2001, **34**, 4610.

[36] H. Egger, *et al.*, *Macromol. Symp.*, 2000, **162**, 291.

[37] M. Maskos and J. R. Harris, *Macromolecular Rapid Communications*, 2001, **22**, 271.

[38] C. Booth and D. Attwood, *Macromol. Rapid Commun.*, 2000, **21**, 501.

[39] C. Booth, G. E. Yu, and V. M. Nace, in '*Amphiphilic block copolymers: Self assembly and applications*', ed. P. Alexandridis and B. Lindman, Elsevier, Amsterdam, 2000.

[40] B. Chu and Z. Zhou, in '*Nonionic surfactants: Polyoxyalkylene block copolymers*', ed. V. M. Nace, Marcel Dekker, New York, 1996.

[41] Z. Tuzar, *et al.*, *Macromol. Chem. Phys.*, 1982, **183**, 399.

[42] D. J. Wilson and G. Reiss, *European Polymer Journal*, 1988, **24**, 617.

[43] R. Saito and K. Ishizu, *Polymer*, 1997, **38**, 225.

[44] M. Iijima, *et al.*, *Macromolecules*, 1999, **32**, 1140.

[45] A. Guo, G. Liu, and J. Tao, *Macromolecules*, 1996, **29**, 2487.

[46] F. Henselwood and G. Liu, *Macromolecules*, 1997, **30**, 488.

[47] O. Rheingans, *et al.*, *Macromolecules*, 2000, **33**, 4780.

[48] R. Saito, *et al.*, *Colloid. Surf. A: Physiochem. Eng. Aspects*, 1999, **153**, 305.

[49] R. Saito, K. Ishizu, and T. Fukutomi, *Polymer*, 1990, **31**, 679.

[50] R. Saito, K. Ishizu, and T. Fukutomi, *Polymer*, 1991, **32**, 2258.

[51] R. Saito, K. Ishizu, and T. Fukutomi, *Polymer*, 1991, **32**, 531.

[52] R. Saito, K. Ishizu, and T. Fukutomi, *Polymer*, 1992, **33**, 1712.

[53] R. Saito, S. Yoshida, and K. Ishizu, *J. Appl. Polym. Sci.*, 1997, **63**, 849.

[54] K. L. Wooley, *J. Poly. Sci. A: Polym. Chem.*, 2000, **38**, 1397.

[55] K. B. Thurmond II, T. Kowalewski, and K. L. Wooley, *J. Am. Chem. Soc.*, 1997, **119**, 6656.

[56] H. Huang, *et al.*, *J. Am. Chem. Soc.*, 1997, **119**, 11653.

[57] Q. Zhang, E. E. Remsen, and K. L. Wooley, *J. Am. Chem. Soc.*, 2000, **122**, 3642.

2. Synthesis and Experimental Methods

2.1. *Synthetic background*

2.1.1. Anionic Polymerisation

Anionic Polymerisation is one type of "living" polymerisation; that is:

"a chain polymerisation proceeding in the absence of the kinetic steps of termination or chain transfer"[1]

Generally:

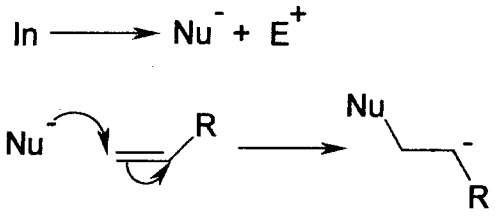

Figure 2.1 - *Initiation reaction in anionic polymerisation*

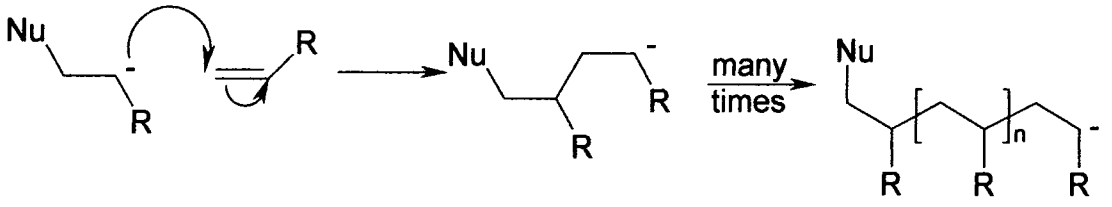

Figure 2.2 - *Propagation reaction in anionic polymerisation*

In order for a monomer to be susceptible to anionic polymerisation one of the substituents on the double bond needs to be capable of stabilising the negative charge present. Typically these would be electron-withdrawing groups such as other double bonds, aromatic rings, carbonyls etc. The electron-withdrawing groups themselves must be stable to, or capable of being protected from, the reactive chain ends. Types of monomer that can be polymerised anionically include styrenes, dienes and methacrylates. Typical initiators would be alkyl lithium compounds such as *sec*-butyl lithium or *n*-butyl lithium, alkali metals or radical anions such as potassium naphthalene. As the anionic chain end is associated with a counter ion e.g. Li^+, the solvent in which the reaction is carried out has a profound influence; solvents that promote dissociation (e.g. aromatic and polar solvents) lead to faster rates of reaction due to the increased nucleophilicity of the anion. Whilst chain propagation is dependent on the separation of the living chain end and the counter ion, the solvent influences the mode of entry of any

incoming monomer. Thus careful consideration should be given to solvent/initiator combination due to the dramatic effect that can be achieved with regards to the stereochemistry of the resulting polymer. Common solvents used for the polymerisation of styrenes and dienes include benzene, tetrahydrofuran (THF) and diethyl ether.

Anionic polymerisations are sensitive to trace quantities of impurities including water, oxygen and carbon dioxide. These impurities may participate in the polymerisation in a number of ways but the most influential process is the termination or "killing" of living chains leading to loss of control. Thus "clean" conditions are therefore necessary; one way of achieving such conditions is through the use of high vacuum techniques.

A distinct advantage of anionic polymerisations is the ability to replace hydrogen with deuterium without discernable affect on the polymerisability of a monomer, meaning that deuterated polymers can be prepared that can subsequently be utilised in neutron scattering experiments.

2.1.2. Why Use Anionic Polymerisation?

As previously mentioned, anionic polymerisation can be considered "living", affording control over the major variables affecting the polymer properties, namely molecular weight, molecular weight distribution, molecular architecture, stereochemistry and copolymer composition.

2.1.2.1. Molecular weight

This is probably the single most important variable affecting polymer properties. In anionic polymerisation, as with all living polymerisations, the molecular weight is controlled by the stoichiometry of the reaction and the degree of conversion. For a monofunctional initiator under ideal conditions one polymer chain is formed per initiating molecule. At complete conversion, the expected number average molecular weight can be calculated using equation 2.1[2]

$$\overline{M}_n = \frac{monomer\ mass}{initiator\ moles}$$ **Equation 2.1**

2.1.2.2. Molecular weight distribution

If the rate of initiation is much more rapid than that of propagation, polymers with a narrow molecular weight distribution can be obtained. Under these conditions all of the chains are initiated at the same time and the duration of chain propagation is identical. The rate of reaction is affected by several different factors including the nature of the initiator and the quality of the solvent, (with rates being enhanced in solvents such as aromatics and polar solvents which strongly solvate the cation of the initiating species enhancing its nucleophilicity).

The degree of polymerisation, X, and the polydispersity can be related by equation 2.2.[2]

$$\frac{X_w}{X_n} = 1 + \left[\frac{X_n}{(X_n + 1)^2}\right] \cong 1 + \frac{1}{X_n} \qquad \text{Equation 2.2}$$

This implies that the polydispersity decreases with increasing molecular weight.

2.1.2.3. Molecular Architecture

In a living polymerisation, once all of the monomer has been consumed the chain ends retain their active centres. This leads to the possibility of producing several different polymer architectures depending on the monomer added. Addition of a monomer different to that used initially results in the formation of a block copolymer. The addition of an electrophile gives an end-functionalised polymer.

$$P^- + E^+ \longrightarrow P{-}E$$

Figure 2.3 - *Electrophile addition to living anionic chain*

By controlling termination reactions with multifunctional linking agents star-branched polymers can be formed.

$$nP^- + L \longrightarrow \left[P\right]_n L$$

Figure 2.4 - *Addition of linking agent to living anionic chain*

2.1.2.4. Stereochemistry

Anionic polymerisation allows stereospecific polymers to be synthesised from monomers where there is more than one possible mode of addition by careful choice of the solvent/initiator combination. For example in the case of 1,3 butadiene three modes of addition are possible, 1,2 addition, *cis* 1,4 addition and *trans* 1,4 addition. The proportions in which they are obtained are influenced greatly by the solvent and counter ion.[3, 4] Different stereoisomers of the same polymer can have vastly different properties. For example in the case of poly(butadiene) the 1,2 stereoisomer has a glass transition temperature of 258K, whereas the two 1,4 isomers *cis* and *trans* have glass transition temperatures of 218 and 170K respectively.[5]

2.2. Synthetic strategy

Two different molecular weight series of poly(butadiene)-poly(ethylene oxide) block copolymers were synthesised, one of which was approximately 5000 $gmol^{-1}$, the other being approximately 10000 $gmol^{-1}$. Each series had the same molecular composition of approximately 15wt% poly(butadiene), and all H and D variants of the two blocks were to be synthesised, with the polybutadiene block having a mainly 1,2 microstructure to facilitate post-polymerisation cross-linking.

The synthesis of poly(ethylene oxide) block copolymers is complicated by the lack of reactivity of ethylene oxide in the presence of a lithium counter ion due to the formation of a strong ion pair between the active chain end and the Li^+ counter ion.[6, 7] As a result even in large excesses of ethylene oxide (EO) only one EO unit adds to the end of the active chain.

Bywater *et al.*[3] investigated the effect of solvent and counter ion on the microstructure of poly(butadiene). They found that a lithium counter ion in THF at temperatures less than 273K gave 1,2 content of the order of 90%. It was also interesting to note that the use of potassium in the same solvent at similar temperatures resulted in polymers having almost 70% 1,2 microstructure. These results are in contrast to those of Milner and Young[4] who showed that carrying out the same reaction in benzene at room

temperature with a lithium counter ion produced polymers with a majority of 1,4 microstructure.

2.2.1. Literature Procedures

Poly(butadiene)-poly(ethylene oxide) (PB-PEO) block copolymer syntheses have been reported in the literature, the earliest of which was by Hillymer and Bates in 1996.[8] Although they did not directly synthesise poly(butadiene)-*block*-poly(ethylene oxide) (the poly(butadiene) was hydrogenated in the presence of a Palladium catalyst) the method was subsequently used to produce poly(butadiene)-poly(ethylene oxide) block copolymers.[9]

The polymerisation of 1,3 butadiene in THF at 223 to 213K using *t-butyl* lithium or *sec*-butyl lithium initiator, resulted in a polymer that was end-capped by the addition of excess ethylene oxide, with the polymeric alcohol isolated upon addition of methanolic HCl. The alcoholic polymer was titrated with potassium naphthalenide, resulting in the potassium salt of the polymer, which initiated the co-polymerisation of ethylene oxide. Under these reaction conditions, formation of the 1,2 isomer of PB predominates, with polymers containing on average 90% 1,2 units (scheme 2.1).

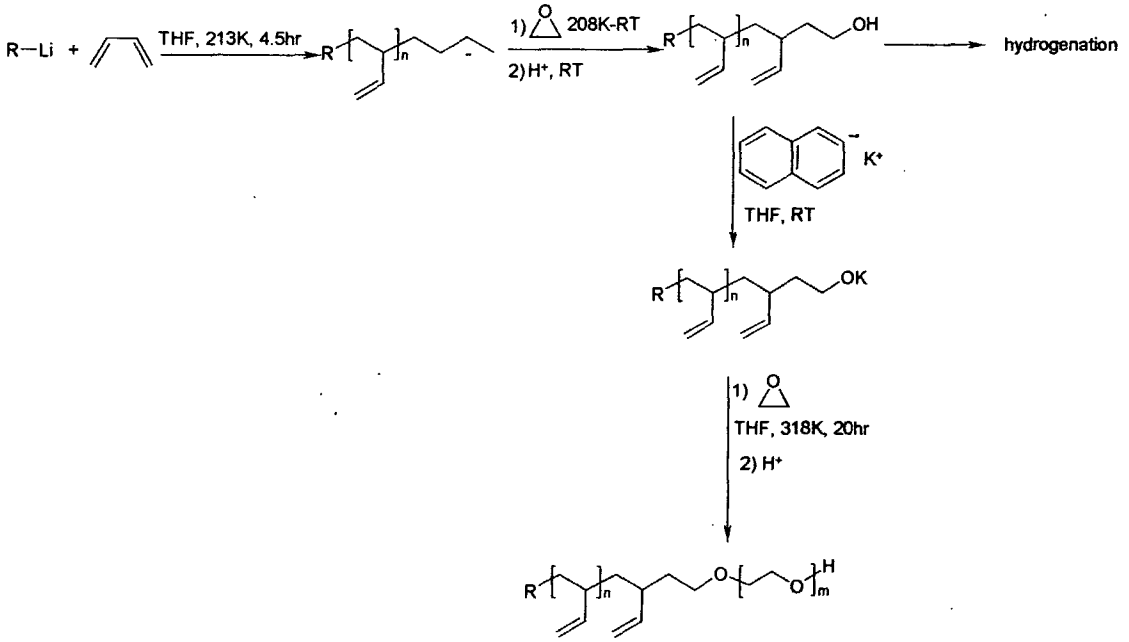

Scheme 2.1- *Reaction scheme of Hillmyer and Bates*[8]

Hoerner *et al.*[10] (scheme 2.2) used cumyl potassium to initiate the polymerisation of butadiene in THF at 213K, followed by the addition of

ethylene oxide monomer to produce poly(butadiene)-poly(ethylene oxide) block copolymers having 67% 1,2 microstructure.

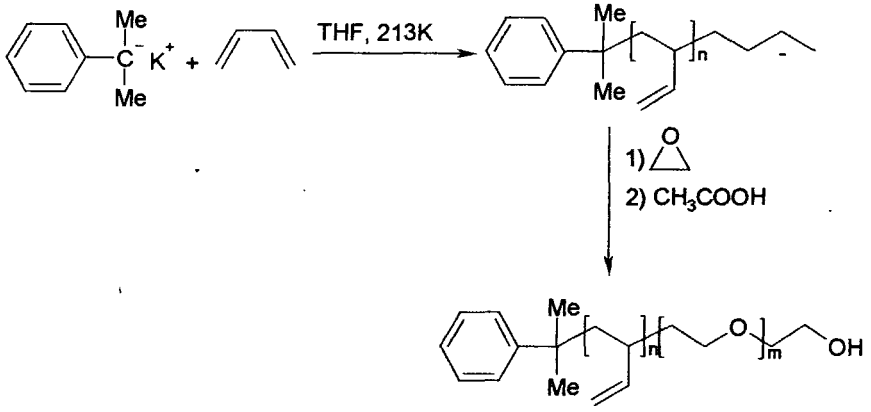

Scheme 2.2- *Reaction scheme of Hoerner et al.*[10]

Förster and Krämer[7] (scheme 2.3) used a one-step procedure with the polymerisation of butadiene being carried out using *sec*-butyl lithium in THF in the presence of phosphazene base that complexed lithium ions, thereby suppressing the ion pair association. This permitted the direct polymerisation of ethylene oxide onto the end of the poly(butadiene) chains without the need for a metallation step. The presence of base had minimal effect on the stereochemistry of the reaction, with 89% of the poly(butadiene) being in the form of 1,2 units which was the same as that observed in the analogous reaction without the base present.

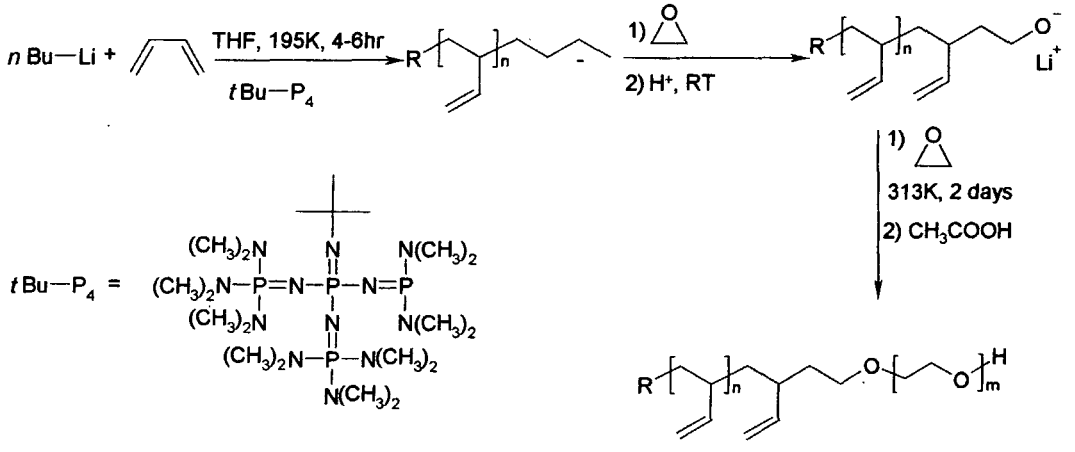

Scheme 2.3- *Reaction scheme of Förster and Krämer*[11] *showing the structure of phosphazene base*

The three procedures outlined above give poly(butadiene)-poly(ethylene oxide) block copolymers with the butadiene being predominantly in its 1,2 form. However, which was preferable?

The method of Hoerner *et al.*[10] was considered to be most desirable, with the inherent advantage of it being a one-pot procedure. A variation on this method was to be pursued in the first instance using diphenymethyl potassium as the initiator in place of cumyl potassium, scheme 2.4.

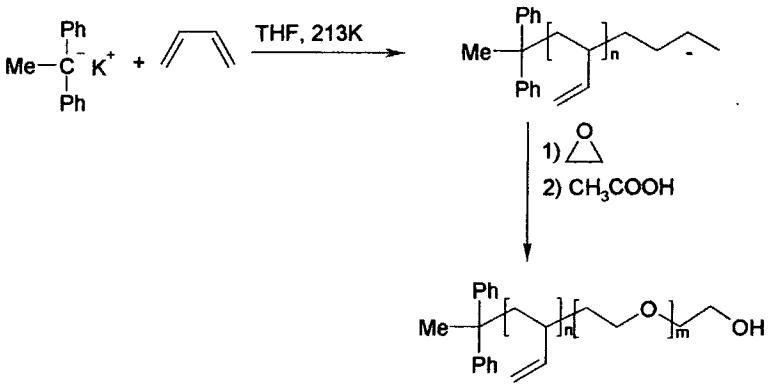

Scheme 2.4- *Proposed one pot reaction scheme*

The method of Hillmyer and Bates[8] had been successfully used by Bowers *et al.*[12] and an adaptation of this route was to be employed if scheme 2.4 was unsuccessful. The adaptation was to use a potassium mirror to metallate the ethylene oxide end-capped poly(butadiene) rather than titrate with potassium napthalenide, in a procedure analogous to that employed by Jialanella *et al*[13]. for poly(styrene)-poly(ethylene oxide). The route can be seen in scheme 2.5.

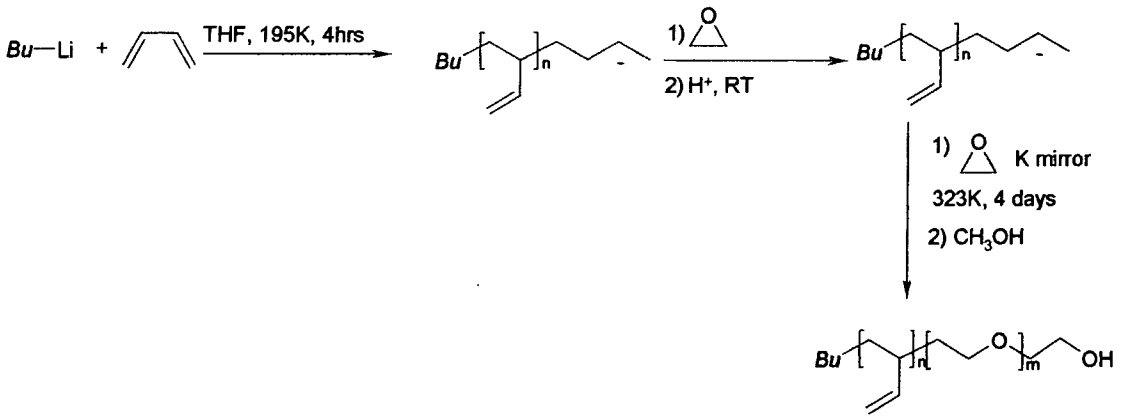

Scheme 2.5- *Proposed two-step reaction scheme*

2.2.2. Cross-linking reactions

Block copolymer micelles dispersed in selective solvents are not permanent structures[14] and the unsaturation of the poly(butadiene) in the copolymers synthesised as part of this research was to be exploited to cross-link the cores rendering the micelles permanent structures. This is shown schematically in figure 2.5.

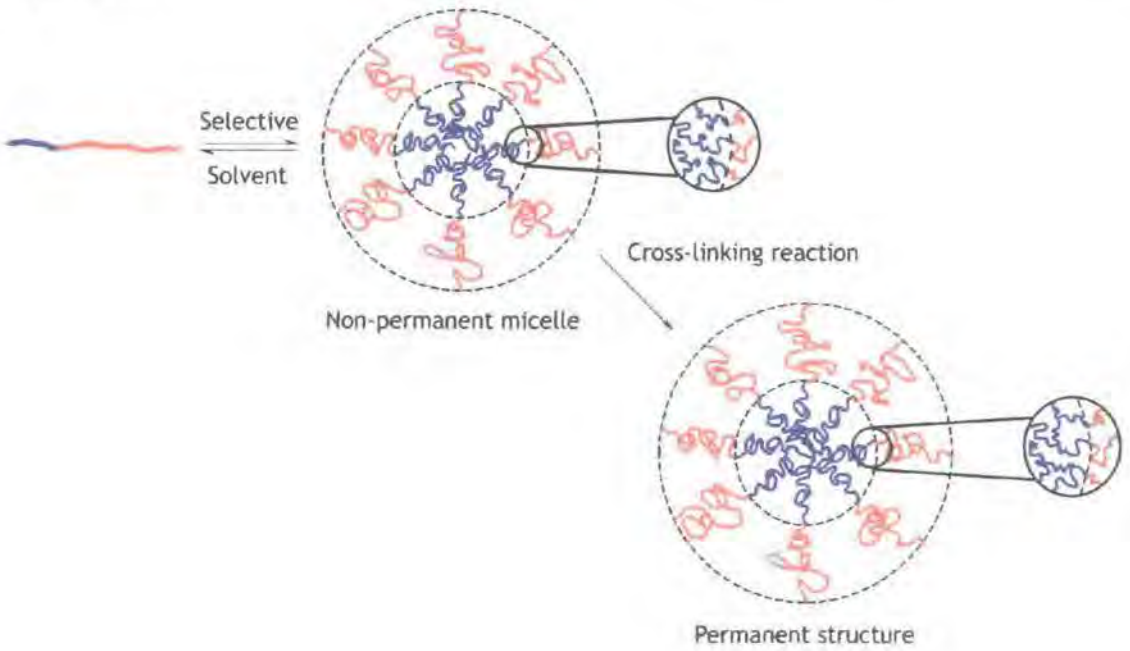

Figure 2.5 - *Schematic representation of cross-linked micelles*

Because aqueous dispersions of micelles were desired, common free-radical initiators were unsuitable because of their insolubility in water. Additionally to preserve the structure of the micelle the use of initiators that required elevated temperature was also prohibited.

Several groups have used photo initiators in conjunction with UV light to generate free-radicals and cross-link micelles having a poly(butadiene) core. Tuzar *et al.*[15] utilised dibenzoyl peroxide as a photo initiator to cross-link poly(butadiene)-poly(styrene) micelles in THF/ethanol dispersions. Wilson and Riess[16] used benzoin ethyl ether to cross-link the micelles of the same polymer but this time in DMF. Both of the methods are relatively straight forward, but require the use of quartz vessels to transmit the UV light.

A redox initiator system often used for free-radical polymerisation was thought to be the most appropriate. Redox initiators can be used in aqueous conditions at room temperature using combinations of inorganic salts to

generate free radicals at an acceptable rate.[17] Bates and co-workers have used this method to cross-link poly(butadiene)-poly(ethylene oxide) micelles in aqueous solution.[9, 18]

2.3. Synthetic procedures

2.3.1. Block Copolymer synthesis

All of the reactions were carried out under high vacuum conditions using "Christmas tree" type reaction vessels, which can be seen in figure 2.6.

Figure 2.6 - *Single reaction bulb "Christmas-tree"*

2.3.1.1. Materials

All materials were supplied by Aldrich Chemicals unless stated otherwise.

Tetrahydrofuran (THF) (250mL) was purified *via.* degassing over sodium wire and benzophenone. Ethylene oxide was vacuum distilled onto potassium hydroxide contained in a 50mL reaction flask that was partially immersed in iced water, and the EO/KOH mixture stirred for 15hrs. The monomer was then vacuum distilled into a flask containing calcium hydride and degassed several times by free-evacuate-thaw cycles. The flask was again immersed in iced water and stirred for ca. 15hrs. After vacuum transfer to a new flask, dibutyl magnesium (1ml) was injected for final purification. The deuterated ethylene oxide (Fluka) was treated in the same manner as the hydrogenous version, with the omission of the potassium hydroxide step.

Butadiene was purified by passing through a series of columns filled with different grades of molecular sieves to remove any moisture.

Deuterated butadiene was supplied by Dr. Zaijun Lu and was passed through only one drying column prior to use.

2.3.1.2. Polymerisation

The initial attempt to prepare block copolymers with sufficient control utilised diphenyl methyl potassium to initiate the polymerisation of butadiene in THF solution. On completion of the butadiene polymerisation, ethylene oxide was distilled into the flask and the reaction mixture stirred at 323K for four days. The reaction was then terminated by addition of methanol and the copolymer recovered. Analysis of the copolymer, especially the determination of molecular weight showed a large variation in values that should in principle have been equal. Evidently, there was insufficient control and thus this method was abandoned. Good control of molecular weight and block copolymer composition was essential in view of the ranges of isotopic variants that need to be synthesised.

For the second polymerisation method a slightly different reactor was used, with a separate large reaction vessel, as shown in figure 2.7.

Figure 2.7 - *Twin reaction bulb "Christmas tree"*

Ethylene oxide, THF and butadiene were purified as described previously. The reactor was evacuated for ca. 15hrs, before being cleaned by rinsing with "living" polystyryl lithium solution, and evacuated for a further 15hrs. THF (150-200mL) was distilled into one of the flasks of the reaction vessel over liquid nitrogen, and allowed to warm to room temperature before being

stirred. Butadiene (2.99g) was distilled into the reaction vessel immersed in a solid CO_2/acetone bath, followed by injection of *sec*-butyl lithium (0.00199mol, 1.4mL) initiator solution, which caused the solution to turn yellow in colour. The reaction was stirred at 195K for 4hrs, before adding ethylene oxide (1g) to end-cap the living poly(butadiene) chains, and stirred for a further 2hrs (when a sample of the reaction mixture (10-15mL) was decanted into a side arm flask and terminated with degassed methanol (0.5mL)) The main mass of the reaction mixture was also terminated by injecting degassed methanol (1ml). The solvent was distilled out of the flask to leave a slightly opaque white oil. Fresh THF (150mL) was distilled onto the copolymer cooled by immersing the flask in a CO_2/acetone bath. The polymer solution was left stirring for 2hrs before the solvent was distilled out again leaving behind the oily polymer, which was pumped on at high vacuum for 2 days. More THF (150-200mL) was distilled onto the cooled polymer (195K) in order to redissolve it prior to the metallation. Potassium (0.00995mol, 0.4g) was cleaned in hexane and added to the unused flask of the vessel whilst a flow of dry nitrogen through the flask was maintained. The flask was re-evacuated, and the potassium vaporised by gentle warming, with it condensing on the cooler parts of the flask generating a mirror *in situ*. The polymer solution from the first reaction vessel was decanted onto the mirror, agitated periodically over two hours to ensure efficient metallation by the potassium mirror, after which time the solution was decanted back to the first flask. Ethylene oxide (16.29g) was distilled on to the cooled (195K) solution which was stirred at room temperature for ca 15hrs, and then stirred at 323K for three days, during which time a yellow colour developed. After cooling to room temperature, degassed methanol (1mL) was injected to terminate the reaction, followed by stirring for ½hr. The polymer was recovered by precipitation into stirred hexane (800mL), yielding a white solid, which was dried at room temperature *in vacuo*. for 24hrs.

The identical synthesis procedure was applied to all the isotopic variants for each molecular weight copolymer, these isotopic variants being hPB-hPEO, dPB-hPEO and hPB-dPEO. (section 2.6 pg 70)

2.3.1.3. Polymer and copolymer characterisation

The poly(butadiene) block was characterised using size exclusion chromatography (SEC or GPC) and ^{1}H NMR; and the copolymer analysed by SEC in THF, ^{1}H NMR or ^{13}C NMR depending on isotopic labelling, and differential scanning calorimetery (DSC)

NMR spectra were recorded using a Varian Mercury spectrometer operating at 399.97 MHz for ^{1}H and 100.57 MHz for ^{13}C. SEC data were obtained using Viscotek 200 chromatograph equipped with refractive index, viscosity and light scattering detectors using THF as the eluent. Poly(butadiene) blocks were analysed using poly(butadiene) calibrants. For the copolymers poly(styrene) standards were used as calibrants.

DSC data were obtained using a Perkin Elmer Pyris 1 DSC and a heating rate of 10 K min^{-1}.

2.3.2. Micelle core cross-linking

Attempts to cross-link the micelle cores using the redox couple of sodium meta bisulphite, Iron(II) sulphate heptahydrate and *tert*-butylhydroperoxide reported by M^{c}Carthy *et al.*[19] proved unsuccessful. The combination of initiators proved not to be robust, with the reaction difficult to reproduce upon scaling up.

Initial attempts at using the method reported by Won, Davis and Bates were also unsuccessful in that although the micelles were cross-linked, upon their recovery from the reaction mixture by freeze-drying, they were no longer dispersible in water.

The method eventually settled upon was a slight variation of that used by Won *et. al.*[9, 18] in that higher concentration dispersions were used, with samples prepared by dilution directly from the reaction mixture.

An aqueous copolymer dispersion in D_2O (10mL, 10%) was added to a 100mL round-bottomed flask, having a septum, side arm connector, and Young's tap, which was stirred gently and sparged with nitrogen for 2hrs. Potassium persulphate (10wt%, 1g) was added to the polymer dispersion prior to stirring. Initiator solutions were prepared in the same solvent as the polymer solution, as detailed in table 2.1

Initiator	Amount/g	Volume H_2O/mL	Conc/wt%	Amount injected/mL	Ratio to polymer mass
Sodium metabisulphite	2.00602	5	40	1.25	0.5
Iron (II) sulphate heptahydrate	1.58944	5	30	0.09	0.02

Table 2.1 - *Quantities of initiators used*

The initiator solutions were injected through the septum turning the solution yellow in colour. After initial stirring the reaction was left quiescent for 15hrs, after which it was colourless. The solutions were diluted directly for use in small-angle neutron scattering experiments using the appropriate solvent. The product was characterised by ^1H NMR in D_2O.

2.4. Experimental methods

2.4.1. Small-Angle Scattering Techniques

Small-angle X-ray and neutron scattering (SAXS and SANS respectively) are simple diffraction techniques that exploit the wave-particle duality of the respective radiation to provide information about the size and shape of molecules and their interactions with each other.[20, 21] Even though X-rays and neutrons interact with different parts of the atom, electrons and nuclei respectively, and are sensitive to inhomogeneities in different properties, namely electron density and neutron scattering length density, the underlying principles for both techniques are identical. The two techniques along with static light scattering are complementary to each other yielding information on different length scales. Table 2.2 provides an overview of the techniques, and outlines the information obtainable from each.[20, 22]

Parameter	Radiation			
	Light		X-rays	Neutrons
Radiation scattered by	Electrons		Electrons	Nuclei
Typical wavelengths (nm)	400-700		0.15	0.01-3
Typical length scales probed (nm)	25-25000		0.1-2500	0.5-1000
Typical sample volumes (cm^3)	0.05-5		0.0001-0.5	0.05-3.5
Information yielded	*Static* M_w, A_2. R_g, p, cmt, cmc	*Dynamic* D_t, D_r, R_h, size distribution	R_g & internal structure, unimer/micelle size and shape, detection of structural parameters and ordered mesophases (at high conc)	Similar to SAXS but *via*, H-D substitution.

Table 2.2 - *Comparison of radiation scattering techniques. M_w is weight average molecular weight, A_2 is the second virial coefficient, R_g is the radius of gyration, p is the micelle association number, cmc and cmt are the critical micelle concentration and temperature respectively, D_t and D_r are the translational and rotational diffusion coefficients respectively, and R_h is the hydrodynamic radius.*

2.4.1.1. General Principles

The scattering geometry of a typical small-angle scattering experiment is shown in figure 2.8

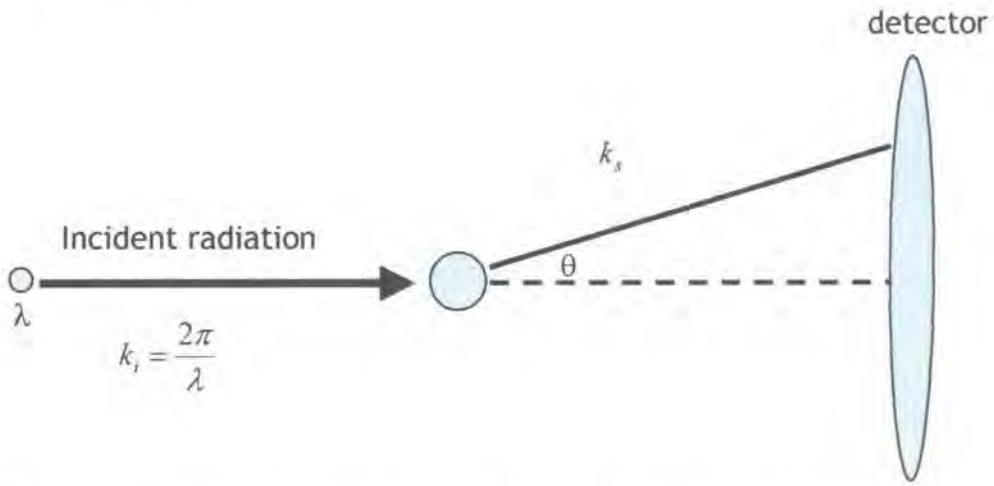

Figure 2.8 - *Representative geometry of a small-angle scattering experiment*

The incident $\mathbf{k_i}$, and scattered, $\mathbf{k_s}$ wave vectors can be related to the scattering vector **Q** whose magnitude is given by equation 2.3

$$Q = |\mathbf{Q}| = |\mathbf{k}_s - \mathbf{k}_s| = \frac{4\pi n}{\lambda}\sin(\theta/2) \qquad \textbf{Equation 2.3}$$

The modulus of the scattering vector, **Q**, is the independent variable in any small-angle scattering experiment and has the units of length^{-1}. Substituting equation 2.3 into Braggs law of diffraction ($\lambda = 2d\sin(\theta/2)$) gives

$$d = 2\pi/Q \qquad \textbf{Equation 2.4}$$

which can be used for either sizing the scattering centre in a sample from a scattering intensity peak in Q-space or for configuring an instrument to ensure its Q-range is appropriate.

In a small-angle scattering experiment the number of "events" received by a detector element or pixel is measured.[23] This can be expressed as

$$I(Q) = I_0(\lambda)\Delta\Omega\eta(\lambda)T(\lambda)V_s\frac{\partial\Sigma}{\partial\Omega}(Q) \qquad \textbf{Equation 2.5}$$

where I(Q) is the scattering intensity, I_0 is the incident flux, $\Delta\Omega$ is the solid angle element defined by the size of a detector pixel, η is the detector efficiency, T is the neutron transmission of the sample, V_s is the volume of the sample illuminated by the neutron beam, and $\partial\Sigma/\partial\Omega$ is the differential scattering cross-section

The differential cross-section is the independent variable in small-angle scattering experiments and contains all of the information on the size, shape and interactions between the scattering centres in the sample.

Generally

$$\frac{d\Sigma}{d\Omega}(Q) = NV_p^2(\Delta\rho)^2P(Q)S(Q) + B \qquad \textbf{Equation 2.6}$$

where N is the number concentration of scattering centres, V_p is the volume of one scattering centre, $(\Delta\rho)^2$ is the contrast, P(Q) is the particle form factor, S(Q) is the particle structure factor, and B is the background.

2.4.1.2. Contrast

In order to be able to obtain scattering from a system there must be a degree of contrast present; that is the property governing the interaction with the incident radiation must be different in the scattering body to that of its surroundings. If this is not the case then the system is said to be at contrast match and no scattering is observed. In SAXS the contrast arises from the electron density difference and in SANS from the neutron scattering length density difference. Table 2.3 shows the atomic scattering lengths and neutron scattering lengths for some common atoms and their isotopes for both X-rays and neutrons.[24]

Element	X-ray scattering length/10^{-12}cm	Neutron coherent scattering lengths/10^{-12}cm
H	0.282	-0.374
D	0.282	0.667
B	1.41	0.54
^{12}C	1.69	0.665
^{14}N	1.97	0.94
O	2.26	0.580

Table 2.3 - *Comparison of x-ray and neutron scattering lengths for common atomic species*

As can be seen from table 2.3 the variation of the atomic scattering lengths for neutrons varies somewhat irregularly with atomic number. This is not the case for X-rays, where the X-ray scattering length scales with increasing number of electrons, thus increasing linearly with atomic number. Of particular significance is the difference in both sign and magnitude for hydrogen and deuterium scattering lengths. This allows manipulation of the scattering length by replacing hydrogen with deuterium in a molecule and is thus highly relevant for small angle neutron scattering.

The scattering length density of a molecule is obtained using equation 2.7.[20, 25]

$$\rho = \frac{\delta N_A}{M} \sum_i b_i \qquad \textbf{Equation 2.7}$$

For polymers it is only necessary to calculate the scattering length or electron density for one repeat unit, since these are the scattering centres.

Table 2.4 shows the scattering length and electron densities for the solvent and polymers investigated here.

Compound	Electron density/10^{10}cm^{-2}	Neutron scattering length density/10^{10}cm^{-2}	
		h-form	d-form
Water	9.3	-0.56	6.38
PEO	10.29	0.64	6.46
PB	9.00	0.47	6.82

Table 2.4 - *Comparison of x-ray and neutron scattering lengths for the scattering centres investigated*

As mentioned earlier, the contrast $(\Delta\rho)^2$ is the square of the difference between the scattering length/electron density of the solute and the solvent and if this is zero, then no scattering is observed. Due to the differences in hydrogen and deuterium scattering length densities noted earlier, molecules or parts of molecules can be differentially labelled to contrast match a scattering centre with its surroundings and thus simplify the scattering pattern. For example, in micellar systems where the core and the corona of the micelle are made from different materials, deuterating one part of the molecule e.g. the hydrophilic part, and matching the scattering length density of the solvent to the hydrogenous part by mixing light and heavy solvents in appropriate amounts, the hydrogenous part becomes "invisible" to the neutrons and the scattering observed is due to the deuterium labelled portion of the molecules. [26] This can be visualised as in figure 2.9

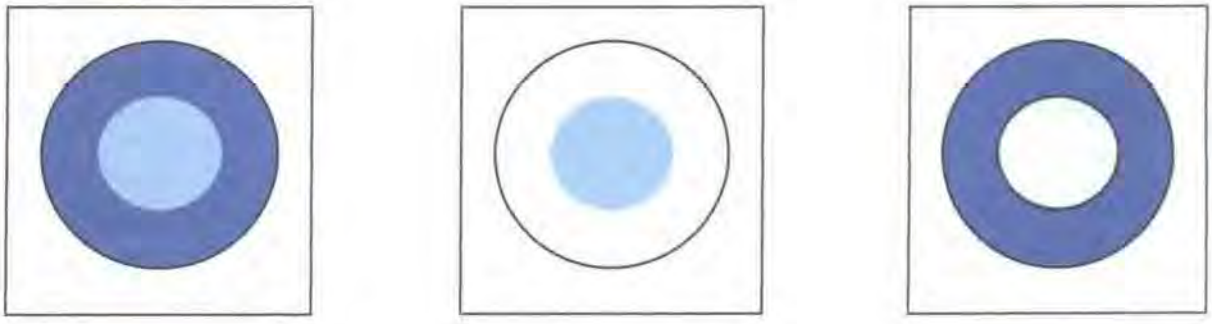

Figure 2.9 - *Schematic representation of contrast matching in spherical micelles*

As was noted in section 2.3.1.2 per-deuterated analogues of the block copolymers were synthesised by using anionic polymerisation.

2.4.1.3. Form Factor

The form factor (P(Q) in equation 2.6) describes how $d\Sigma/d\Omega(Q)$ is modulated by interference effects between radiation scattered from different parts of the same scattering particle. Consequently it is sensitive to the size and shape of the scattering particles. Analytical expressions for P(Q) exist for many particle morphologies, a large number of which have been set out by Pedersen.[27] Perhaps the most common is that of a uniform sphere, equation 2.8, derived by Lord Rayleigh in 1911.[28]

$$P(Q) = \left[\frac{3(\sin(QR) - QR\cos(QR))}{QR^3}\right]^2 \qquad \textbf{Equation 2.8}$$

For solutions of spherical micelles the form factor of a sphere is not appropriate because the micelle consists of two concentric spheres, that of the poorly solvated component surrounded by a second of the well solvated component, shown schematically in figure 2.10. In this case a core-shell model for P(Q) would be used.[20, 29]

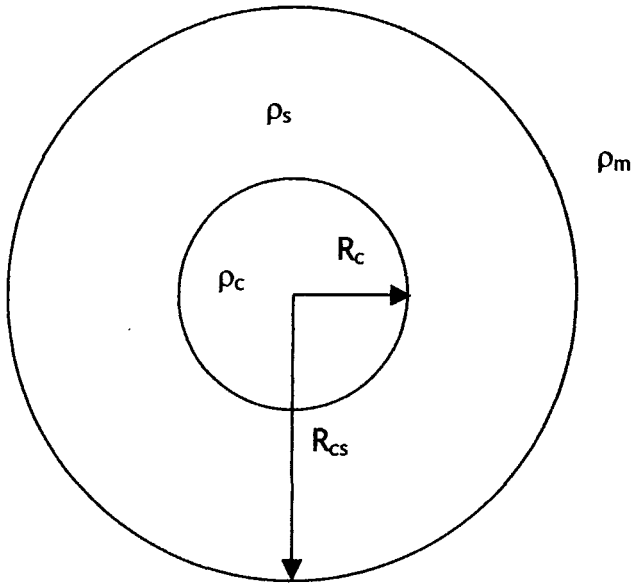

Figure 2.10 - *Schematic representation of a core-shell particle. R_c is the core radius, R_{cs} is the micelle radius, ρ is the scattering length density, where subscript c implies the core, s implies the shell and m the solvent.*

The scattering is now that from a sphere of radius R_{cs} and scattering length density ρ_s, minus the scattering from a sphere of radius R_c and scattering length density ρ_s, plus the scattering from a sphere of radius R_c and scattering length density ρ_c. Equation 2.6 can be rewritten as:[20, 29]

$$\frac{d\Sigma}{d\Omega}(Q) = \frac{16\pi^2}{9} N_p P(Q) S(Q) + B \qquad \textbf{Equation 2.9}$$

and P(Q) is given by

$$\left[\begin{array}{l} (\rho_s - \rho_m)\left[3R_{cs}^3 \left(\frac{\sin QR_{cs} - QR_{cs}\cos QR_{cs}}{Q^3 R_{cs}^3} \right) - \left(\frac{\sin QR_c - QR_c \cos QR_c}{Q^3 R_c^3} \right) \right] \\ + (\rho_c - \rho_m) 3R_c^3 \left(\frac{\sin QR_c - QR_c \cos QR_c}{Q^3 R_c^3} \right) \end{array} \right]^2 \qquad \textbf{Equation 2.10}$$

2.4.1.4. Structure Factor

The structure factor (S(Q)) describes quantitatively how $d\Sigma/d\Omega(Q)$ is modified by interference effects between radiation scattered by different scattering particles in the sample. It is dependant on the degree and extent of order between the scattering particles in the sample and thus is determined by the interaction potential between the scattering particles.

The simplest form of interaction between particles is *via* a hard-sphere potential.[30, 31] In this situation at a particular distance of separation the energy between the particles rises steeply to infinity as shown by figure 2.11.[32]

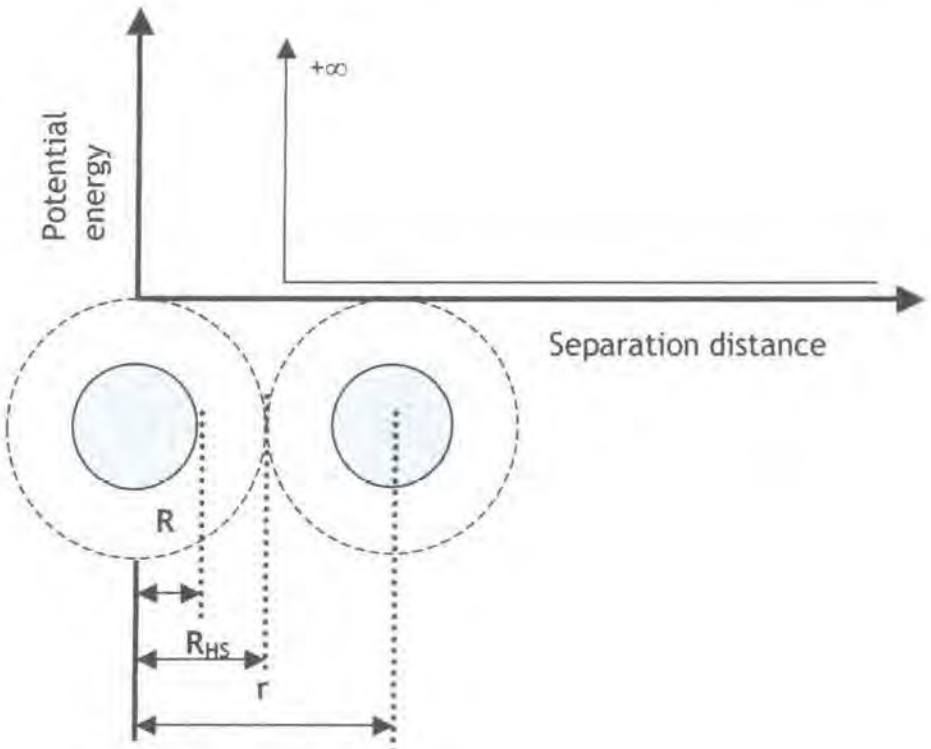

Figure 2.11 - *Schematic representation of hard sphere interactions*

The structure factor arising from this potential is given by equation 2.11

$$S(Q) = \frac{1}{1 + 24\eta\left(\frac{G(2QR)}{2QR}\right)}$$ **Equation 2.11**

where η is the hard sphere volume fraction and $G(2QR)$ is given by equation 2.12.

$$G(2QR) = \frac{\alpha}{(2QR)^2}(\sin 2QR - 2QR\cos 2QR) + \frac{\beta}{(2QR)^3}(2\cdot 2QR\sin 2QR + (2-(2QR)^2)\cos 2QR - 2)$$
$$+ \frac{\gamma}{(2QR)^5}(-(2QR)^4\cos 2QR + 4[(3\cdot(2QR)^2 - 6)\cos 2QR + ((2QR)^3 - 6\cdot 2QR)\sin 2QR + 6])$$

Equation 2.12

α, β, and γ are functions of the hard sphere volume fraction given by:

$$\alpha = \frac{(1+2\eta)^2}{(1-\eta)^4}$$ **Equation 2.13**

$$\beta = -\frac{6\eta\left(1+\frac{\eta}{2}\right)^2}{(1-\eta)^4}$$ **Equation 2.14**

$$\gamma = \frac{\frac{\eta}{2}(1+2\eta)^2}{(1-\eta)^4}$$ **Equation 2.15**

2.4.2. Light scattering

Light scattering is a non-invasive, non-destructive technique that can be utilised for the characterisation of complex fluids such as polymer solutions.[33] Light incident on a solution of molecules gives rise to scattering by virtue of the interaction of its electric field with the electrons of the molecules in solution.[34] These molecules are in constant random motion, Brownian motion, and so on a microscopic scale cause density fluctuations in the solution. These density fluctuations cause a small shift in the frequency of the scattered light relative to that of the incident frequency[35] and the process is said to be quasi-elastic, hence the name quasi-elastic light scattering (QELS) given to this form of study. As the movements of the molecules are very fast it is possible to collect scattered light in time periods sufficiently longer than those associated with the movements of the molecules, giving an average over the number of particles in the scattering volume. In this instance the frequency shift is not observed and the process is said to be elastic. This technique is known as static or classical light scattering (SLS).

The two scattering processes yield complementary information for the scattering molecules; static light scattering provides information on the molecular weight, radius of gyration and thermodynamics of interaction with the solvent, whilst quasi-elastic light scattering yields diffusion coefficients from which size parameters can be obtained. Each of the two techniques will be discussed in turn.

2.4.2.1. Static Light scattering[33, 34, 36, 37]

The size of a molecule has a profound effect on its scattering properties and the key parameter is the molecular size relative to the wavelength of the incident light. If the molecular dimensions are less than $\lambda/20$ the molecule can be considered as a point scatterer; i.e. a Rayleigh scatterer. Those particles with dimensions comparable to the incident wavelength are large; i.e. Debye scatterers.

When $d<\lambda/20$ the intensity of light scattered from a dilute solution of polymer molecules consists of two contributions:

i.) Intensity due to density fluctuations of the solvent

ii.) Intensity due to the scattering from concentration fluctuations of the polymer molecules

The presence of small amounts of polymer molecules has little effect on the density fluctuations, and so two scattering intensities have to be measured, that of the pure solvent and of the polymer solution. The difference in the two intensities is the contribution from the dissolved polymer molecules to the overall intensity, which is referred to as the excess scattering.

If the polymer molecules can be considered to be independent of one another, i.e. in dilute solution, then the scattering intensity from that solution at an angle θ to the incident beam is given by equation 2.16

$$I_\theta = I_0 \frac{4\pi^2 n_0^2}{r^2 \lambda_0^4 N_A}\left(\frac{dn}{dc}\right)^2 Mc \qquad \textbf{Equation 2.16}$$

where I_θ is the intensity of polarised light scattered from a dilute polymer solution at angle θ, I_0 is the incident light intensity, n_0 is the solvent refractive index, r is the distance between the scattering molecule and the detector, λ_0 is the incident wavelength radiation, N_A is Avogadro's number, dn/dc is the specific refractive index increment, M is the molecular weight of the polymer and c is its concentration.

The specific refractive index increment, dn/dc, is the change in refractive index of a dilute polymer solution for a unit increase in the concentration of the polymer, the units are customarily ml g^{-1}.

The increase in scattered intensity from a solution in relation to the pure solvent is due to fluctuations in the solute concentration within small volume elements, the dimensions of which are such that they can be considered point scatterers in relation to the incident wavelength; they must also be large enough to hold many solvent and a few solute molecules. As a result of the number of solute molecules within a volume element changing concentration fluctuations occur. Allowing for these concentration fluctuations the scattered intensity is now given by:

$$I_\theta = I_0 \frac{4\pi^2 n^2}{r^2 \lambda_0^4 N_A}\left(\frac{dn}{dc}\right)^2 c \frac{1}{M^{-1} + 2A_2 c + 3A_2 c^2 + \ldots} \qquad \textbf{Equation 2.17}$$

Often measurements are performed in solutions sufficiently dilute that the third and higher virial coefficients are negligible and can be discarded.

Equation 2.17 can be re-written as:

$$R_\theta = \frac{I_\theta r^2}{I_0} = \frac{Kc}{M^{-1} + 2A_2 c}$$ **Equation 2.18**

where $K = \frac{4\pi^2 n_0^2}{r^2 \lambda_0^4 N_A}\left(\frac{dn}{dc}\right)^2$ **Equation 2.19**

R_θ is the Rayleigh ratio, which is a measure of reduced intensity of scattered light at any angle to the incident beam, and is independent of the instrument. It eliminates intensity changes due to the angular dependence of scattering intensity upon the degree of polarisation of the incident beam and on the parameters of the apparatus.

If the dimensions of the solute are greater than $\lambda/20$, then light scattered from different parts of the molecule is coherent and capable of interference, with the beams reaching the detector with different phases potentially resulting in an intensity which is reduced in comparison to the sum of the intensities of the constituent beams. As the light is scattered from different parts of the same molecule, the effect is one of intramolecular interference. As a result of this interference, the intensity of scattered light depends upon the angle of observation. This angular dependence can be described by the particle scattering factor $P(\theta)$, which can be defined as the Rayleigh ratios at the angle of observation θ, and at zero angle, i.e. $P(\theta) = R_\theta / R_0$. $P(\theta)$ is analogous to $P(Q)$ in small angle scattering, and is characteristic of molecular shape.

From this definition, $P(0)=1$ for particles of any size and shape. For small particles $P(\theta)=1$ at any angle as the Rayleigh ratio is independent of the angle of observation under this condition.

The basic equation given earlier for light scattering from dilute polymer solutions with small dimensions compared to the incident wavelength is only valid for large polymers when θ equals zero, as there is no reduction in the scattered intensity due to intramolecular interference. Thus

$$\frac{Kc}{R_0} = \frac{1}{M} + 2A_2c \qquad \text{Equation 2.20}$$

but $R_0 = {R_\theta}/{P(\theta)}$, so substituting this into equation 2.20 gives

$$\frac{Kc}{R_\theta} = \frac{1}{MP(\theta)} + 2A_2c \qquad \text{Equation 2.21}$$

which is the classical form of equation for static light scattering from polymer molecules presented by Zimm.

P(θ) can be related to the radius of gyration by equation 2.22

$$\frac{1}{P(\theta)} = 1 - \frac{16\pi^2}{3\lambda^2}\langle R_g^2\rangle \sin^2\left({\theta}/{2}\right) \qquad \text{Equation 2.22}$$

substituting equation 2.22 into 2.21 gives

$$\frac{Kc}{R_\theta} = \left|_{\substack{c\to 0\\ \theta\to 0}}\right. \frac{1}{M}\left[1 + \frac{16\pi^2}{3\lambda^2}\langle R_g^2\rangle \sin^2(\theta/2)\right] + 2A_2c \qquad \text{Equation 2.23}$$

Equation 2.23 can be used to determine the molecular weight, radius of gyration and second virial coefficient from a plot of Kc/R_θ *vs.* $\sin^2(\theta/2)+kc$ where k is a plotting constant via a double extrapolation procedure (see section 3.4).

2.4.2.2. Quasi-elastic Light Scattering[33, 35, 38]

The Brownian motion of polymer molecules in solution gives rise to density fluctuations on a microscopic scale that appear and disappear at a rate determined by the speed of the molecules' Brownian motions.

Quasi-elastic light scattering allows measurement of the density fluctuations as a function of time to yield information about the diffusion coefficients from which molecular size can be obtained. This is achieved *via.* the intensity autocorrelation function, $g(t)$, equation 2.24

$$g(t) = \int_0^\infty I(t).I(t+\tau)dt \qquad \text{Equation 2.24}$$

where $I(t)$ is the intensity of scattered light at time t, and $I(t+\tau)$ is the intensity of scattered light at time $t+\tau$.

For a system of hard, spherical, non-interacting particles in a fluid the correlation function, $g(\tau)$, is given by

$$g(\tau) = \exp(-\Gamma t) \qquad \textbf{Equation 2.25}$$

The relaxation rate, Γ, is related to the scattering vector, Q, and the diffusion coefficient, D, by:

$$\Gamma = -Q^2 D \qquad \textbf{Equation 2.26}$$

$$Q = \frac{4\pi n}{\lambda}\sin(\theta/2) \qquad \textbf{Equation 2.27}$$

The relaxation rate can be obtained by fitting the experimental correlation data to one of several models and since Q is known, the diffusion coefficient can be calculated. The diffusion coefficient can be used to determine the hydrodynamic radius, R_h, using the Stokes-Einstein equation

$$D = \frac{k_B T}{6\pi\eta R_h} \qquad \textbf{Equation 2.28}$$

where k_B is Boltzmann's constant, T is the temperature and η is the solvent viscosity.

Often, for a monodisperse or highly dilute sample, a simple exponential fit is sufficient to extract the relaxation rate from the correlation function. Sometimes however, polydisperse or more concentrated samples are examined and the correlation function can no longer be expressed by equation 2.25. The autocorrelation now has the form of a distribution of exponentials expressed as a Laplace integral:

$$g(\tau) = \int_0^\infty G(\Gamma) e^{-\Gamma\tau} d\Gamma \qquad \textbf{Equation 2.29}$$

There are several methods of analysing correlation functions of polydisperse or non-dilute systems with two of the most common being the cumulants[39] and CONTIN[40] methods.

In the cumulants[39] method a Taylor series expansion of the logarithm of equation 2.29 is used to average over all of the light scattering particles, i.e.

$$\ln g(\tau) = -K_1\tau + \frac{K_2\tau^2}{2} + \ldots \qquad \textbf{Equation 2.30}$$

where K_1 and K_2 are the first and second cumulants respectively.

The cumulants of the expansion give the average diffusion coefficient and the normalised distribution width for the first and second cumulants respectively. Higher cumulants are not usually justifiable due to the quality of the data.
In the CONTIN[40] method, $g(\tau)$ is represented by a series of discrete steps, each of width $\Delta\Gamma$. In this instance $g(\tau)$ is given by equation 2.31.

$$g(\tau) = \sum_{i=1}^{J} G(\Gamma_i) \int_{\Gamma_i - \Delta\Gamma/2}^{\Gamma_i + \Delta\Gamma/2} e^{-\Gamma/\Delta\tau} d\Gamma \qquad \text{Equation 2.31}$$

The step width and number of steps are varied until a best fit is obtained.

2.5. Experimental procedures

2.5.1. Specimen preparation

2.5.1.1. Dispersion Preparation

All glassware was cleaned using permanganic acid prior to use to remove any impurities adhering to the glass surface. Potassium Permanganate (ca. 100mg) was dissolved in concentrated sulphuric acid (200mL) producing a pale green viscous liquid. The acid was poured into any glassware to be cleaned and left overnight, after which it was rinsed with ultra high quality water, followed by ethanol and then dried *in vacuo* at room temperature.
Aqueous dispersions were prepared by mixing a known weight of the copolymer with an appropriate volume of UHQ water, and/or heavy water (Aldrich, 99.9% inclusion), and leaving in the dark for several days to equilibrate.

2.5.2. Light Scattering measurements

Light scattering measurements were performed at the universities of Durham and Sheffield on apparatus equipped with either a Laser Quantum Torus 532 (Durham) or a Uniphase microgreen (Sheffield) frequency doubled Nd-YAG laser with an incident wavelength of 532nm. These were both used in conjunction with a Brookhaven BI200SM goniometer coupled to either an avalanche photo diode (Durham) or a photo multiplier tube (Sheffield), with the outputs measured by a Brookhaven BI9000AT digital autocorrelator.

All of the dispersions were filtered several times through a cellulose ester filter (Millipore), having a pore size of 0.22μm, in order to remove dust particles.

Quasi-elastic light scattering measurements were carried out at an angle of 90° to the incident beam and results presented are the averages of several repeated runs.

Static light scattering measurements were performed over the angular range $30 \leq \theta \leq 150°$.

The specific refractive index increment of the copolymer dispersions was determined using a Brice-Phoenix differential refractometer. The difference in refractive index between a copolymer dispersion and the pure solvent was determined for a series of solutions ranging in concentration from 0.5 to 2% at four wavelengths between 436 and 633nm. A plot of refractive index change *vs.* concentration for each wavelength gave the dn/dc value for the respective wavelength, with these being plotted against $1/\text{wavelength}^2$ to give the wavelength dependence of dn/dc. The procedure was repeated for solutions of the polymer in chloroform, which is a good solvent for both blocks of the copolymer.

2.5.3. Small-Angle X-ray Scattering

SAXS data were obtained using a Kratky compact camera equipped with a Braun 50M position sensitive wire detector with 1024 position sensitive channels. The X-ray generator was operated at 25mA and 25kV using CuKα radiation. All of the measurements were performed *in vacuo*. Liquid samples were housed in a quartz capillary tube.

Data were the result of repeated runs averaged and corrected for both sample transmission and background scattering. Use was made of the ITR[41] software to desmear the raw data to correct for the influence of a finite slit width.

2.5.4. Small-Angle Neutron Scattering

SANS experiments were carried out on the LOQ diffractometer at the UK pulsed neutron source, ISIS, located at the Rutherford Appleton Laboratory, Didcot, Oxfordshire.[42] The dispersions were transferred to rectangular quartz cells having a 1mm path length that were maintained at 298K during the data collection. Data collected was corrected for transmission and the background scattering was subtracted before being converted to absolute scattering cross-sections by comparison to the scattering of a well-defined blend of hydrogenous and deuterated polystyrene.

SANS data for concentrations in the range 0.2 to 10% (w/v) were collected for all contrasts. The dispersions remained liquid-like in their properties across the entire concentration range. Higher concentrations of up to 50% w/v were investigated for the fully hydrogenous copolymer dispersed in heavy water systems. For concentrations greater than 30% w/v solid gels formed for the higher molecular weight copolymer, for the lower molecular weight a concentration of greater than 40% was needed to form a gel.

Gel samples were housed in an instrument resident sample rack consisting of two circular quartz windows with a Teflon spacer ring between them, which were secured in an aluminium disc by brass screws. The aluminium disc was supported in a thermo stated sample rack, shown in figure 2.12.[43]

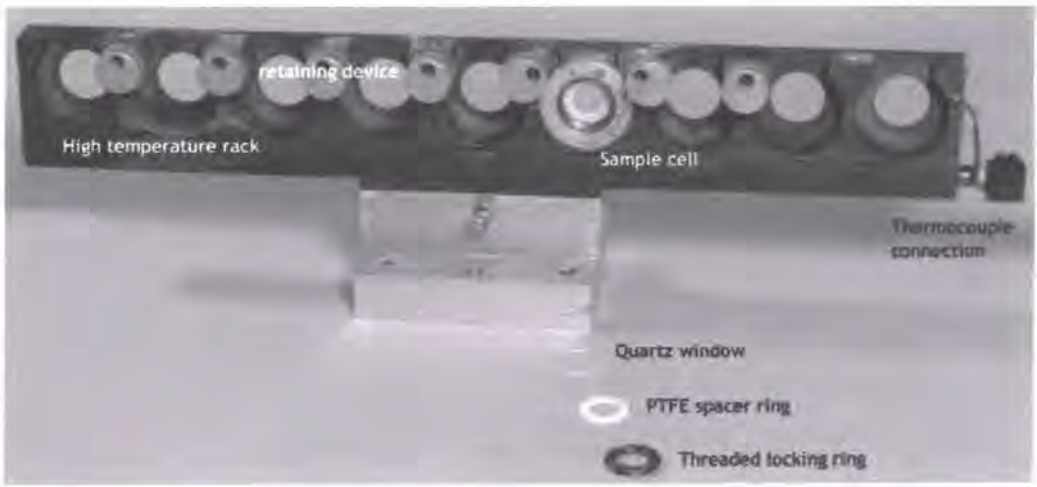

Figure 2.12 - *Sample rack utilised for gel samples*

2.6. *Results and discussion*

2.6.1. Copolymer synthesis

The method detailed in section 2.3.1.2 was employed to synthesise the copolymers investigated during this research and afforded control over the molecular weight and polydispersity. Table 2.5 gives the characterisation data of all the copolymers

Isotopic variation	PB block			Copolymer		
	Mwt/g mol^{-1}	PDI	1,2 content /%	Mass % PEO	Mwt/g mol^{-1}	PDI
10k hPB-hPEO	1470	1.06	91	83	8754	1.11
10k hPB-dPEO	1200	1.08	89	77	5247	1.30
10k dPB-hPEO	1110	1.25	90	87	8538	1.25
5k hPB-hPEO	780	1.08	86	81	4180	1.14
5k dPB-hPEO	770	1.09	85	85	4974	1.11
5k hPB-dPEO	540	1.19	79	90	5449	1.25

Table 2.5 - *Copolymer characterisation results*

Some sample results from the characterisation of the copolymers are presented here in order to demonstrate the characteristics outlined in table 2.5.

In contrast to the first method employed, the synthesis of the polybutadiene block using a lithium counter ion provided greater control over the molecular weight and its distribution, yielding polymers with a relatively narrow polydispersity, and molecular weights of the magnitude expected. The GPC trace of one of the poly(butadiene) blocks isolated during the synthetic procedure is shown in figure 2.13. This shows that the poly(butadiene) block is close to the target molecular weight of 1500 g mol^{-1} and has a narrow molecular weight distribution.

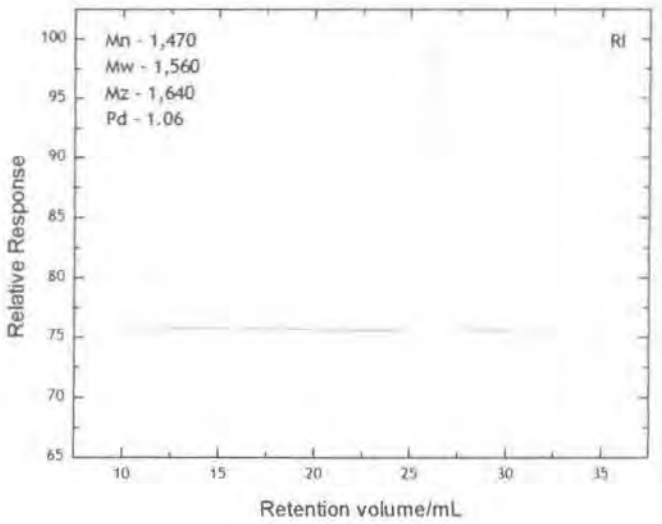

Figure 2.13 - *GPC trace of lithium initiated butadiene polymerisation*

Figure 2.14 shows the ^{1}H NMR spectrum of the polybutadiene block from the 10k hPB-hPEO copolymer after end-capping with EO.

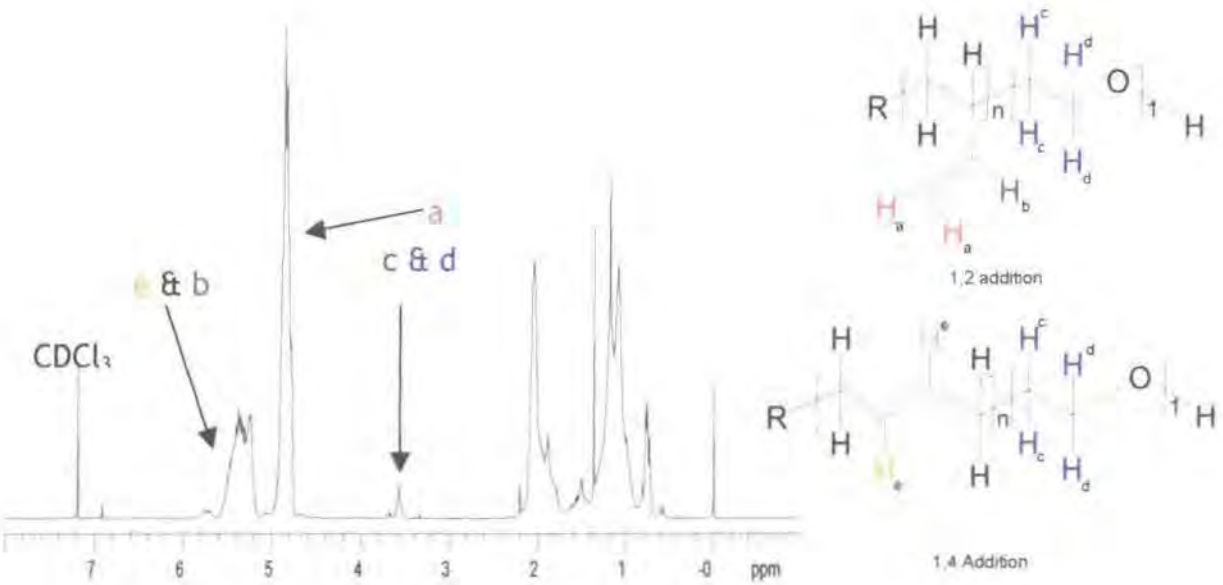

Figure 2.14 - *^{1}H NMR spectrum of ethylene oxide end-capped polybutadiene, with important peaks labelled*

Calculation of the amount of ethylene oxide incorporated into the polymer at this stage reveals that it is of the order of 2% by mass, which based on the

molecular weight of the polymer being 1470 g mol^{-1}, gives a value of 30 g mol^{-1} for the molar mass of the ethylene oxide unit. Because the poly(butadiene) is the dominant component, there are large errors in estimating the mass of ethylene oxide incorporated, but this result does agree with the more rigorous investigation of Quirk and Ma.[6]

Figure 2.15 shows a GPC trace from the 5k hPB-hPEO copolymer, a single peak only is observed.

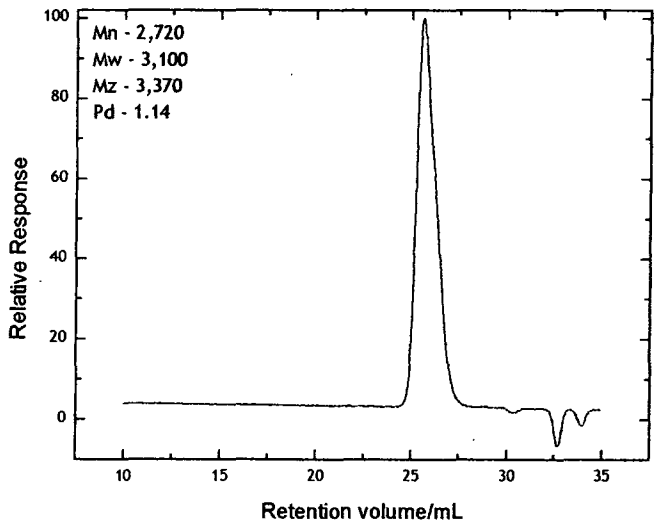

Figure 2.15 - *GPC trace of 5k hPB-hPEO copolymer*

Hence there was no excess potassium in solution. Had there been it would have been highly likely that some homo poly(ethylene oxide) would also have been formed which would have manifested itself on the GPC trace as either a second peak, or a small shoulder on the main peak.

The ^{1}H NMR spectra of the copolymers shows that the polymerisation of ethylene oxide from the site of metallation on the end-capped chain has been successful. ^{1}H NMR spectroscopy was used to calculate the compositions of the fully hydrogenous copolymers whilst ^{13}C was used for the per-deuterated variants. The compositions calculated from these are of the order expected from the stoichiometry of the reaction, and is in contrast to that shown in figure 2.14 for the end-capped poly(butadiene) chain. Figure 2.16 shows a typical ^{1}H NMR spectrum of the 10k hPB-hPEO copolymer.

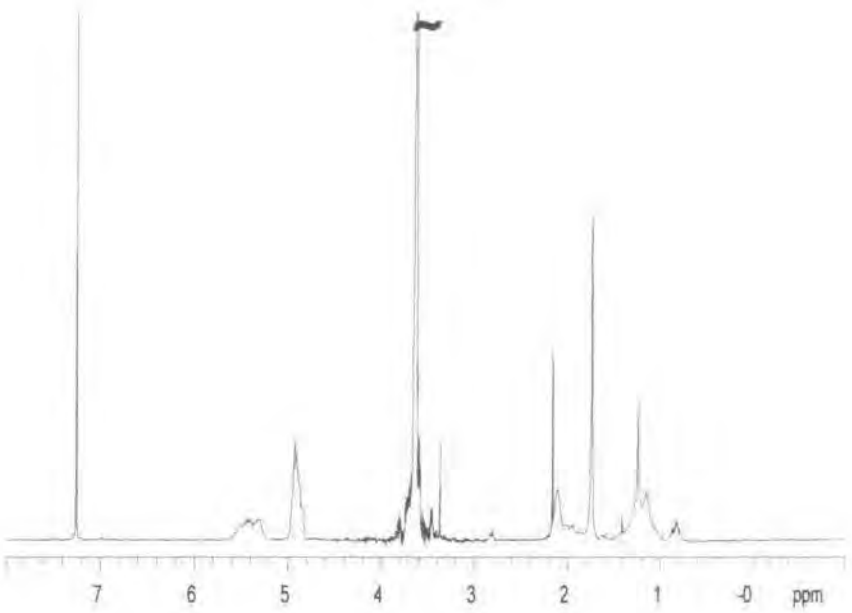

Figure 2.16 - *^{1}H NMR of 10k hPB-hPEO. Peak assignments are the same as those in figure 2.14.*

Thermal analysis of the two fully hydrogenous polymers shows sharp endotherms (figure 2.17) for the PEO block with melting points of 319K and 331K for the 5k and the 10k hPB-hPEO copolymers respectively.

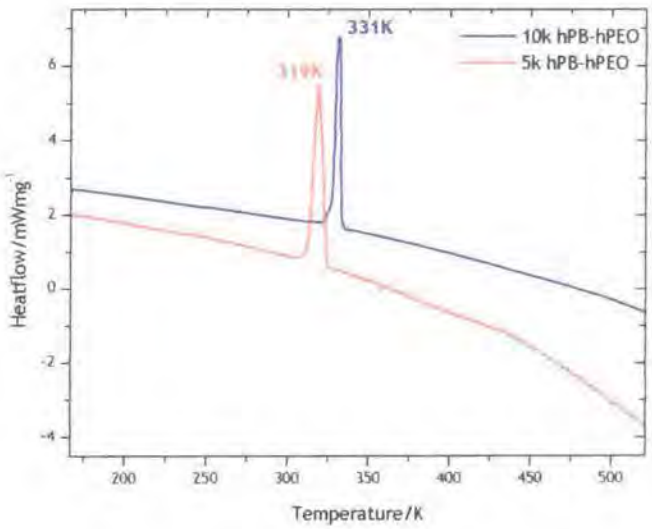

Figure 2.17 - *DSC traces from 5k and 10k hPB-hPEO copolymers showing melting points of 319K and 331K respectively. The heatflow has been normalised to the mass of sample used.*

2.6.2. Cross-linking reactions

Initial attempts to cross-link a micellar dispersion using this method of M^{c}Carthy and co-workers[19] proved successful. The reaction was attempted on a relatively small scale, (ca. 0.2g polymer), and analysis of the end product by ^{1}H NMR spectroscopy revealed there to be no olefinic protons present, indicating a successful reaction. Interestingly, the polymer proved soluble in water but not organic solvents making GPC analysis impossible. Attempts to repeat the reaction on a larger scale were unsuccessful with copolymer being recovered. Quite why this is the case remains unclear, although it is possible that the procedure may not have been robust enough to be successfully scaled up. Perhaps larger amounts of the initiators should have been used.

As with the previous method initial attempts to produce cross-linked micelles using the method of Won, Davis and Bates[9, 18] were successful, with the product proving soluble in water, but not organic media. However, when the reaction was scaled up to produce sufficient material for subsequent investigations, the product recovered was cross-linked, but was only very slightly soluble in water, and not at a level suitable for further studies. Again the reason for this is unknown, but may become apparent with further investigations.

Following the limited success of the previous method it was decided to perform the reaction using the same basic procedure, but to use the solvent which would be used in the SANS experiments to form the dispersion. This way the reaction mixture could be diluted and used directly for the experiments. As the SANS experiments required concentrations of up to 10% it was decided to carry out the reaction at this concentration.

The reaction proved successful as demonstrated by the absence of olefinic protons in the ^{1}H NMR spectra, an example of which is shown in figure 2.18 along with that of the copolymer.

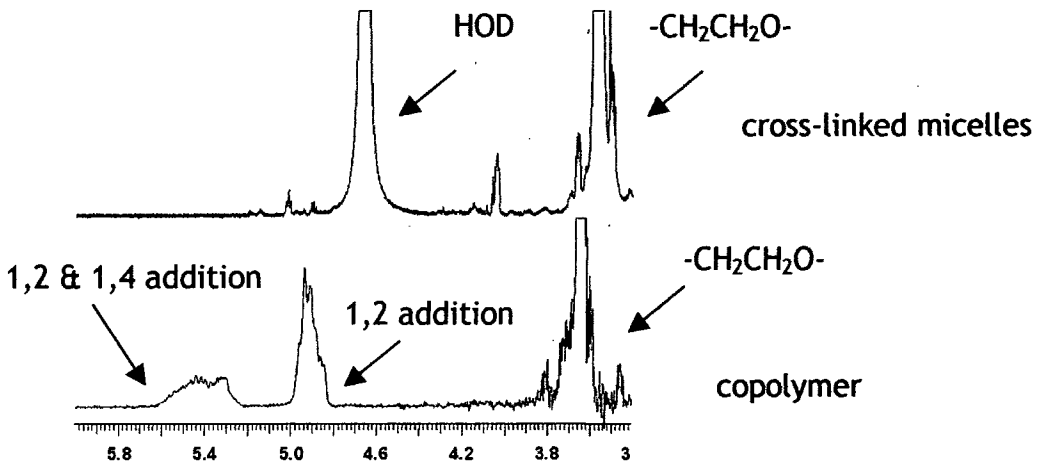

Figure 2.18 - *Olefinic region of 1H NMR spectra of copolymer and cross-linked micelles showing the absence of the vinyl protons in the cross-linked species*

The procedure was used to produce cross-linked micellar dispersions for all of the contrast conditions utilised for the micellar dispersions, with the products being used for subsequent SANS, SAXS, and light scattering experiments.

2.6.3. Light Scattering

2.6.3.1. Aqueous dispersions

Quasi-elastic light scattering was used to determine the critical micelle concentrations of the two fully hydrogenous copolymers in aqueous solution. Figure 2.19 shows the graph obtained when plotting the average count rate *vs.* log (conc) for 10k hPB-hPEO.

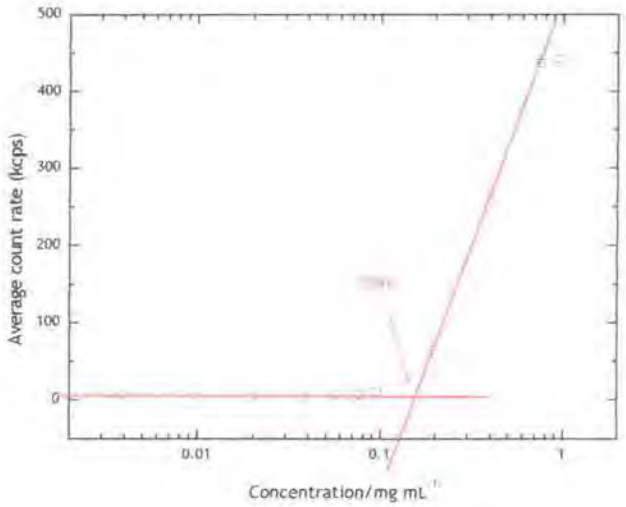

Figure 2.19 - *Intensity vs. log (conc) for 10k hPB-hPEO. Break point indicated represents the cmc, a value of 0.148 mg mL^{-1}. Lines are guides for the eye.*

The two cmc's were determined as 0.148 mg mL^{-1} for 10k hPB-hPEO and 0.268 mg mL^{-1} for 5k hPB-hPEO.

QELS measurements suggest average diffusion coefficients of 1.46×10^{-7} cm^2 s^{-1} and 1.82×10^{-7} cm^2 s^{-1}, giving hydrodynamic radii via equation 2.28 of 170Å and 140Å for the 10k and the 5k hPB-hPEO polymers respectively. CONTIN[40] analysis of the autocorrelation functions suggests monomodal populations in dilute solutions as shown in figure 2.20 for the 5k hPB-hPEO copolymer.

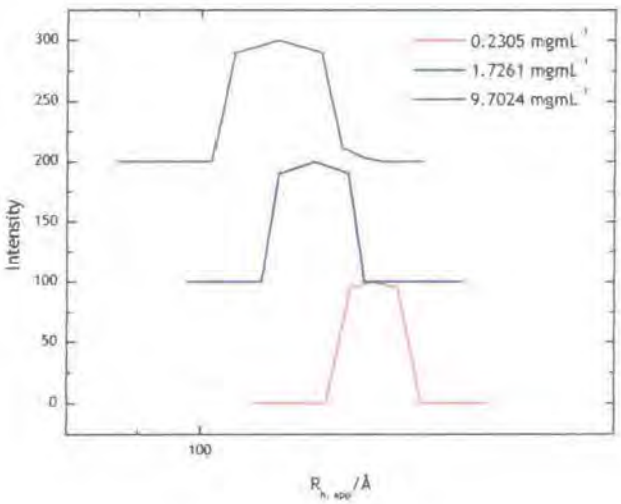

Figure 2.20 - *Size distribution for 5k hPB-hPEO in dilute solutions at c>cmc.* The distributions are shifted successively by 100 for clarity

SLS data proved inconclusive, with the molecular weights, and radii of gyration determined not matching what could be reasonably expected. Both Zimm and Debye methods[34] were applied to the hPB-hPEO copolymers for both molecular weights, with figure 2.21 showing a Zimm plot for the 10k hPB-hPEO copolymer.

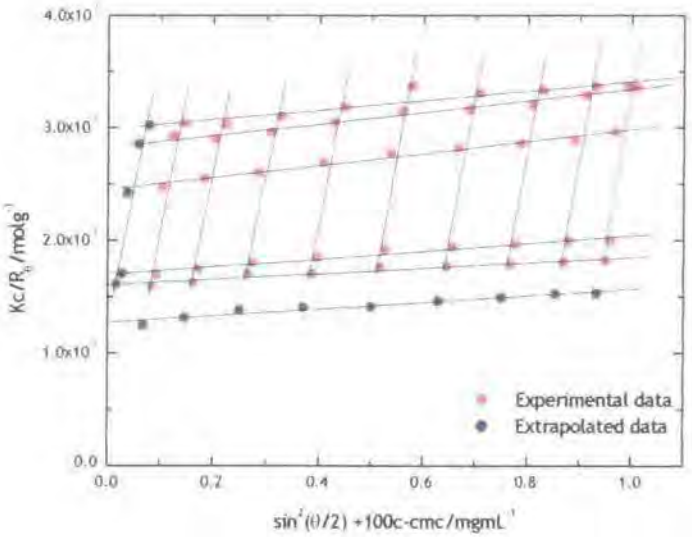

Figure 2.21 - *Zimm plot for 10k hPB-hPEO in water generated using equation 2.23. Vertical lines are fits through concentration series at a given angle and the horizontal lines are fits through angular series at a given concentration.*

The cmc determination and QELS data are dealt with in sections 3.2 and 3.3, and the SLS in section 3.4.

2.6.3.2. Cross-linked micelles

QELS and SLS experiments were performed on the cross-linked micelles and comparisons made between them and the "virgin" micelles.

QELS experiments revealed that the micelle dimensions were smaller following cross-linking with the 10k micelles having a hydrodynamic radius of 156Å and the 5k 94Å. The size distributions were still monomodal in dilute solution, although they had increased in width (figure 2.22).

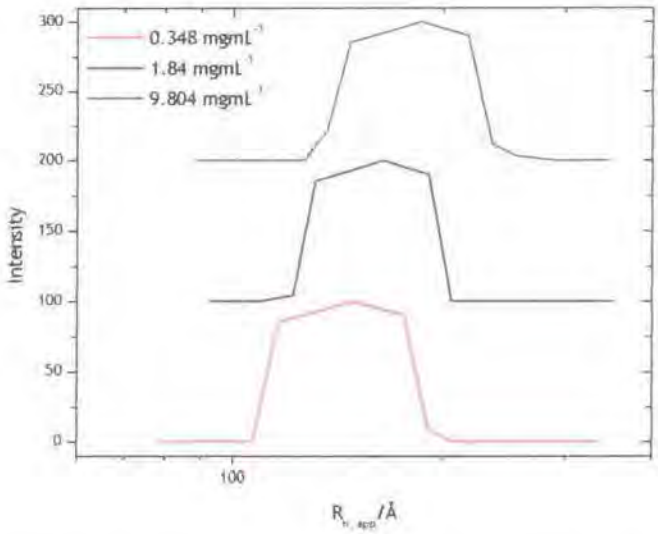

Figure 2.22 - *Size distribution for 10k hPB-hPEO in dilute solutions. The distributions are shifted successively by 100 for clarity.*

SLS data proved as troublesome as for the virgin micelles, with the data not being reliable.

The QELS studies of cross-linked micelles are discussed in section 4.3, with the SLS studies in section 4.4.

2.6.4. Small-angle X-ray scattering

2.6.4.1. Aqueous dispersions

Typical examples of the data collected are presented in figures 2.23 and 2.24 for the 5k and 10k hPB-hPEO respectively, but discussion and treatment of these and other data are left until later chapters.

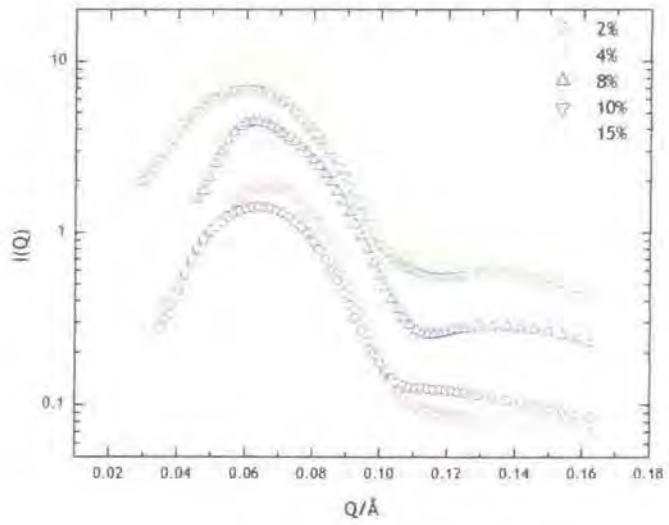

Figure 2.23 - *SAXS data from 5k hPB-hPEO in the concentration range 2-15%.*

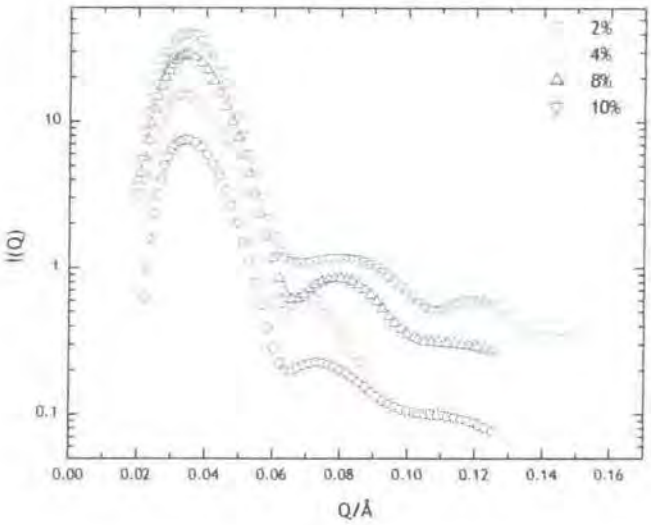

Figure 2.24 - *SAXS data from 10k hPB-hPEO in the concentration range 2-10%.*

Both molecular weights showed a structure factor peak at low Q due to intermolecular interactions. Attempts were made to fit the data but proved troublesome due to the lack of SAXS contrast. Consequently it was not possible to obtain realistic estimates of the micelle dimensions or their interactions with one another. Section 3.4 deals with the treatment of the SAXS data.

2.6.4.2. Cross-linked micelles

SAXS experiments of the cross-linked micelles were carried out in the same manner as for the virgin micelles. The results were complicated by the presence of residual inorganic salts from the cross-linking reaction, which enhanced the SAXS contrast, but reduced the quality of the solvent. Consequently it was just as hard to obtain realistic parameters from the data as for the virgin micelles. Figure 2.25 shows a comparison between SAXS data from the micelles before and after cross-linking.

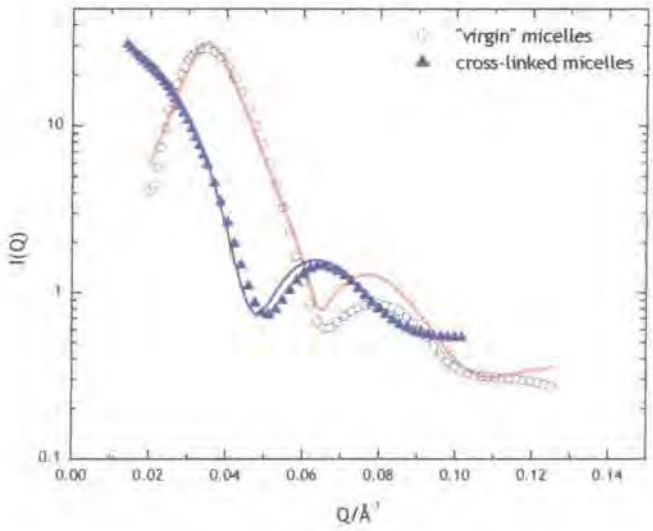

Figure 2.25 - *SAXS data from 10k 8% hPB-hPEO before and after cross-linking. Lines are fits to the data.*

Figure 2.25 clearly shows the reduction in the interactions between the micelles, manifesting itself in the less pronounced structure factor peak. Section 4.5 deals with the treatment of the SAXS data from the cross-linked micelles.

2.6.5. Small-Angle Neutron scattering

2.6.5.1. Aqueous dispersions

Data providing an overview of that collected is presented here. As with the data from the previous sections it will be discussed in more detail later.

Figures 2.26 and 2.27 show the scattering from 1% and 10% dispersions of all three contrasts for the 10k and 5k series respectively.

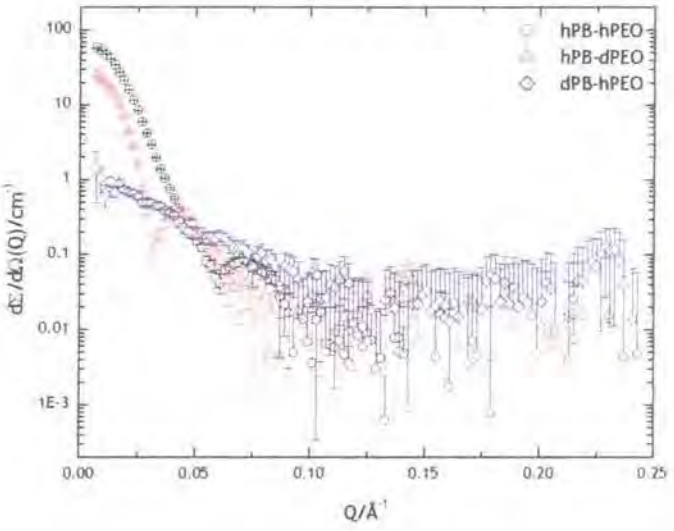

Figure 2.26 - *SANS data from 1% dispersions of 10k series*

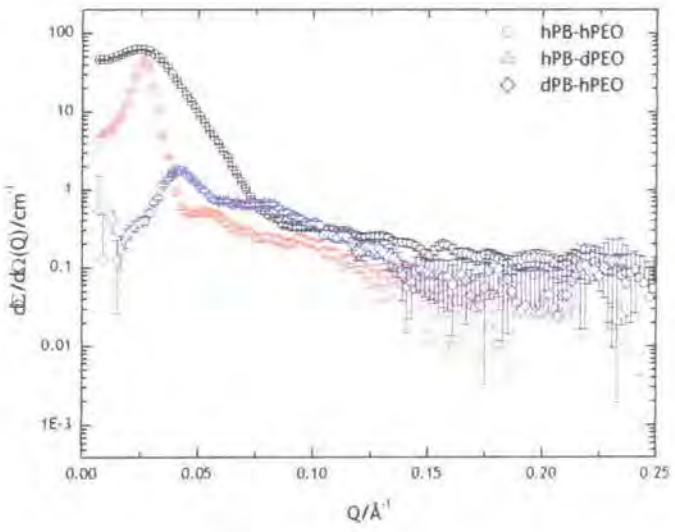

Figure 2.27 - *SANS data from 10% dispersions of 5k series*

Figures 2.26 and 2.27 clearly show the differences in the scattering due to the effects of both concentration and contrast. The 10% dispersions show a pronounced structure factor peak at low Q due to intermicellar interactions, whilst this is distinctly absent in the 1% dispersions suggesting the concentration is sufficiently dilute that the micelles do not exhibit a high degree of long-range order. The scattering from the dispersions where the corona is contrast matched (i.e. scattering from the core only) is considerably weaker than for the other two contrasts as one would expect given that the core-forming block is the minority component of the copolymers.

From fits to the data it was possible to determine the micelle dimensions and association numbers, with the 5k micelles having core radii of ca 20Å and a shell thickness of between 60 and 100Å, whilst the 10k micelles had core radii of 40Å and a corona thickness of ca 115Å. The two molecular weights exhibited contrasting association behaviour with the 5k micelles having only moderate association numbers of 30-40 whilst the 10k micelles had high association numbers of 100-200. The treatment of the dilute micellar dispersion is dealt with in section 3.5.2, whilst the more concentrated dispersions with greater organisation are tackled in section 3.5.3

2.6.5.2. Cross-linked micelles

The cross-linked micelles were investigated by SANS over the same concentration range as for the virgin micelles. Figure 2.28 demonstrates the differences in the data between the micelles before and after cross-linking, with scattering from a 1% dispersion of the 5k hPB-hPEO micelles shown.

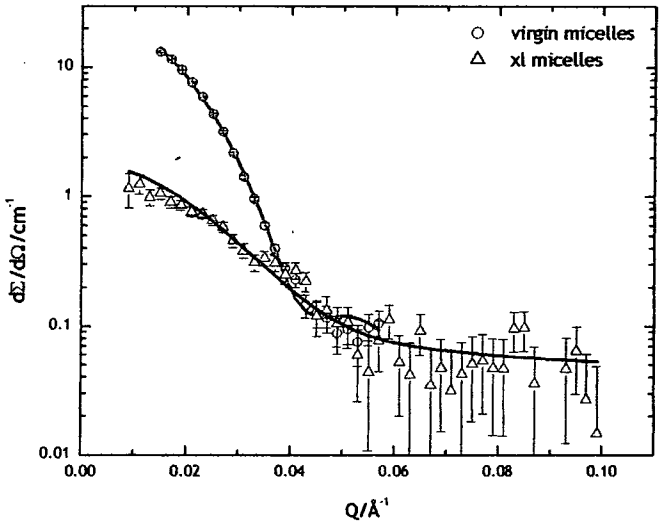

Figure 2.28 - *Differences in the scattering from cross-linked and virgin micelles of a 1% dispersion of 5k hPB-hPEO. Lines are fits to the data.*

Fits to the data revealed that the core radius had decreased by 16-30% depending on the molecular weight and contrast conditions, whilst the corona thickness was between 15-50% smaller. The former can be attributed to a reduction in the core volume associated with the polymerisation reaction, whilst the latter was due to a reduction in the quality of the solvent caused by the presence of residual inorganic salts from the cross-linking reaction resulting in the coronal chains being less stretched. Section 4.6 deals with the SANS data from the cross-linked micelles.

2.7. *Glossary of symbols*

The symbols used in the body of the text and the equations are defined here in the order in which they appear in the text.

2.7.1. Small-angle scattering

M_w - weight average molecular weight

A_2 - second virial coefficient

R_g - radius of gyration

p - micelle association number

cmc - critical micelle concentration

cmt - critical micelle temperature

D_t - translational diffusion coefficient

D_r - rotational diffusion coefficient

R_h - hydrodynamic radius

λ - radiation wavelength

k_i - incident wave vector

k_s - scattered wave vector

θ - scattering angle

Q - scattering vector

d - domain size

I(Q) - scattering intensity

I_0 - Incident flux

$\Delta\Omega$ - solid angle element defined by the size of a detector pixel

η - detector efficiency

T - neutron transmission of sample

V_s - volume of sample illuminated by neutron beam

$\partial\Sigma/\partial\Omega$ - differential scattering cross-section

N - number concentration of scattering centres

V_p - volume of one scattering centre

$(\Delta\rho)^2$ - contrast factor

P(Q) - particle form factor

S(Q) - particle structure factor

B - background

ρ - X-ray/neutron scattering length density

δ - bulk density

N_A - Avogadro's number

M - molar mass

b_i - X-ray/neutron scattering length

R - sphere radius

ρ_c - core scattering length density

ρ_s - shell scattering length density

ρ_m - solvent scattering length density

R_c - core radius

R_{cs} - micelle radius

r - separation distance

R_{HS} - hard sphere radius

h - hard sphere volume faction

2.7.2. Static light scattering

I_θ - intensity of scattered light at angle θ

I_0 - incident intensity

n_0 - solvent refractive index

r - distance between scattering molecule and detector

λ_0 - incident wavelength radiation

N_A - Avogadro's number

dn/dc - specific refractive index increment

M - molar mass

c- concentration

A_2 - second virial coefficient

R_θ - Rayleigh ratio at angle θ

K - optical constant

R_g - radius of gyration

k - plotting constant

2.7.3. Quasi-elastic light scattering

g(t) - intensity autocorrelation function

I(t) - intensity at time t

$I(t+\tau)$ - intensity at time $t+\tau$

τ - delay time

Γ - relaxation rate

Q - scattering vector

D - diffusion coefficient

k_B - Boltzmann's constant

T - temperature

η - solvent viscosity

R_h - hydrodynamic radius

K - cumulant coefficient

2.8. Bibliography

1 M. Szwarc, *Nature*, 1956, **178**, 1168.

2 H. L. Hsieh and R. P. Quirk, 'Anionic Polymerisation: Principles and Practical Applications', Marcel Dekker, New York, 1996.

3 S. Bywater, Y. Firat, and P. E. Black, *J Polym Sci, A, Polym Chem.*, 1984, **22**, 669.

4 R. Milner and R. N. Young, *Polymer*, 1982, **23**, 1636.

5 J. Brandup and E. H. Immergut, 'Polymer Handbook', 3rd, ed., John Wiley and Sons, Toronto, 1989.

6 R. P. Quirk and J. J. Ma, *J. Polym. Sci. A, Polym. Chem.*, 1988, **26**, 2031.

7 S. Forster and E. Kramer, *Macromolecules*, 1999, **32**, 2783.

8 M. A. Hillmyer and F. S. Bates, *Macromolecules*, 1996, **29**, 6994.

9 Y. Y. Won, H. T. Davis, and F. S. Bates, *Science*, 1999, **283**, 960.

10 P. Hoerner, *et al.*, *Macromol. Chem. Phys.*, 1998, **199**, 343.

11 S. Forster and M. Antonietti, *Adv. Mater.*, 1998, **10**, 195.

12 J. Bowers, *et al.*, *Langmuir*, 2001, **17**, 131.

13 G. L. Jialanella, E. M. Firer, and I. Piirma, *J Polym Sci, A, Polym Chem.*, 1992, **30**, 1925.

14 M. Muthukumar, C. K. Ober, and E. L. Thomas, *Science*, 1997, **277**, 1225.

15 Z. Tuzar, *et al.*, *Macromol. Chem. Phys.*, 1982, **183**, 399.

16 D. J. Wilson and G. Reiss, *Eur. Polym. J.*, 1988, **24**, 617.

17 G. Odian, 'Principles of Polymerisation', 3rd, ed., John Wiley & Sons Inc., New York, 1991.

18 Y. Y. Won, *et al.*, *J. Phys. Chem. B*, 2001, **105**, 8302.

19 T. F. McCarthy, *et al.*, *J. App. Polym. Sci.*, 1998, **70**, 2211.

20 S. M. King, in '*Modern Techniques of Polymer Characterisation*', ed. R. A. Pethrick and J. V. Dawkins, John Wiley & Sons, London, 1999.

21 C. E. Williams, R. P. May, and A. Guinier, in '*X-ray Characterisation of Materials*', ed. E. Lifshin, Wiley-VCH, Weinheim, 1999.

22 B. Chu and Z. Zhou, in '*Nonionic surfactants: Polyoxyalkylene block copolymers*', ed. V. M. Nace, Marcel Dekker, New York, 1996.

23 R. W. Richards, in '*Comprehensive Polymer Science*', ed. C. Booth and C. Price, Pergamon, Oxford, 1989.

24 L. A. Feigin and D. I. Svergum, 'Structure Analysis by Small-angle X-ray and Neutron Scattering', Plenum Press, New York, 1987.

25 '*Small Angle X-ray Scattering*', ed. O. Glatter and O. Kratky, Academic Press, 1982.

26 R. H. Ottewill, in '*Colloidal Dispersions*', ed. J. W. Goodwin, Royal Society of Chemistry, London, 1982.

27 J. S. Pedersen, *Adv. Colloid Interface Sci.*, 1997, **70**, 171.

28 L. Rayleigh, *Proc. Roy. Soc. London, Ser. A.*, 1911, **84**, 25.

29 G. J. Bown, R. W. Richards, and R. K. Heenan, *Polymer*, 2001, **42**, 7663.

30 J. K. Perkus and G. J. Yevick, *Phys. Rev*, 1958, **110**, 1.

31 N. W. Ashcroft and J. Lekner, *Phys. Rev*, 1966, **145**, 83.

32 R. H. Ottewill, in '*Colloidal Dispersions*', ed. J. W. Goodwin, Royal Society of Chemistry, London, 1982.

33 P. N. Pusey, in '*Colloidal Dispersions*', ed. J. W. Goodwin, Royal Society of Chemistry, London, 1982.

34 P. Kratochvil, 'Classical Light Scattering From Polymer Solutions', A. D. Jenkins, Elsevier, New York, 1987.

35 R. B. Filippen, in '*Modern Methods of Polymer Characterisation*', ed. H. G. Barth and J. W. Mays, Wiley and Sons, New York, 1991.

36 I. A. Katime and J. R. Quintana, in '*Comprehensive Polymer Science*', ed. C. Booth and C. Price, Pergamon, Oxford, 1989.

37 W. Burchard, in '*Applied Fibre Science*', ed. F. Happey, Academic Press, 1978.

38 G. D. Phillies, *J. Appl. Polym. Sci: Appl. Polym. Symp.*, 1989, **43**, 275.

39 D. E. Koppel, *J. Chem. Phys.*, 1972, **57**, 4814.

40 S. W. Provencher, *Makromol. Chem.*, 1979, **180**, 201.

41 O. Glatter and K. Gruber, *J. Appl. Cryst.*, 1993, **26**, 512.

42 http://www.isis.rl.ac.uk/largescale/loq

43 R. K. Heenan and S. M. King, 'The LoQ Handbook', RAL-TR-96-036, Rutherford Appleton Laboratory, Didcot, 1996.

3. Block Copolymer Micelles

3.1. Introduction

Poly(butadiene)-Poly(ethylene oxide) (PB-PEO) block copolymers synthesised by the route described in chapter two are amphiphilic, and as a consequence form micelles when dispersed in water, which is a selective solvent for the poly(ethylene oxide) block. Micelle formation is generally only observed above the critical micelle concentration (cmc), which can be defined as the concentration at which micelle formation becomes sufficiently appreciable to be detected by a given experimental technique.[1]

A considerable amount of research has been invested in the study of the structure, organisation and properties of amphiphilic block copolymers in aqueous solutions over the past decade.[2-7] The key results of this work were presented in chapter one, with particular emphasis on the work of Bates and co-workers into the study of PB-PEO in aqueous solution. A comparison of this work with new results presented herein will now be discussed; a perspective of these new results compared to those for different amphiphilic block copolymers will also be presented.

3.2.1. How do we study block copolymer micelles?

Chapter two discussed the basic theory underpinning radiation scattering techniques that have formed the backbone of this research. The information obtainable from each technique was also presented, but will be briefly reviewed here for clarity.

The structural detail that can be resolved from a particular technique is inversely proportional to the magnitude of the scattering vector, which is given by equation 3.1

$$|\mathbf{Q}| = Q = \frac{4\pi n}{\lambda}\sin(\theta/2) \qquad \textbf{Equation 3.1}$$

Thus static light scattering, whose Q values range from ca. 5×10^{-3} to 5×10^{-2} nm^{-1} yields information on the radius of gyration but not the internal structure. Conversely, SAXS and SANS with Q values of 3×10^{-3} to 5 nm^{-1} allows

intramicellar structure to be elucidated. Table 3.1 details the information that each of the techniques can yield.

	SLS	QELS	SAXS	SANS
Q values/nm^{-1}	~5×10^{-3}-5×10^{-2}	~5×10^{-3}-5×10^{-2}	5×10^{-3}-5	
Information obtainable	R_g, M_w, A_2, p	D, R_h, size distribution	R_g, internal structure, micelle shape, structure and ordering	

Table 3.1 - *Q values and information yielded from scattering techniques. R_g is the radius of gyration, M_w is the weight average molecular weight, A_2 is the second virial coefficient, D is the diffusion coefficient, R_h is the hydrodynamic radius.*

The techniques are complementary to one another, and in order to obtain the maximum amount of information for the micelles a combination of the four should be employed, as used here. The results obtained from each of the techniques will be presented and discussed individually, with the final part of this chapter drawing all of the results together.

3.2. Quasi-Elastic Light Scattering

QELS is a powerful, widely used tool for the study of block copolymer micelles.[8-11] As discussed earlier in section 2.4.2.2, QELS yields an intensity autocorrelation function, which when suitably analysed provides invaluable information about the hydrodynamic behaviour of micelles. As the intensity is sensitive to low mass concentrations of micelles it provides a convenient method for demonstrating their presence in aqueous solution.[3, 12]

Using the method of CONTIN[13] analysis discussed in section 2.4.2.2 the intensity distribution of the apparent translational diffusion coefficient can be obtained, and by applying the Stokes-Einstein equation (equation 2.28), *viz* $D_{app} = \frac{k_B T}{6\pi\eta R_{h,app}}$ the apparent diffusion coefficient can be converted to the corresponding distribution of apparent hydrodynamic radii, $R_{h,\,app}$.

Examples of such distributions are shown in figure 3.1 for both the 10k and the 5k hPB-hPEO copolymers after micellisation.

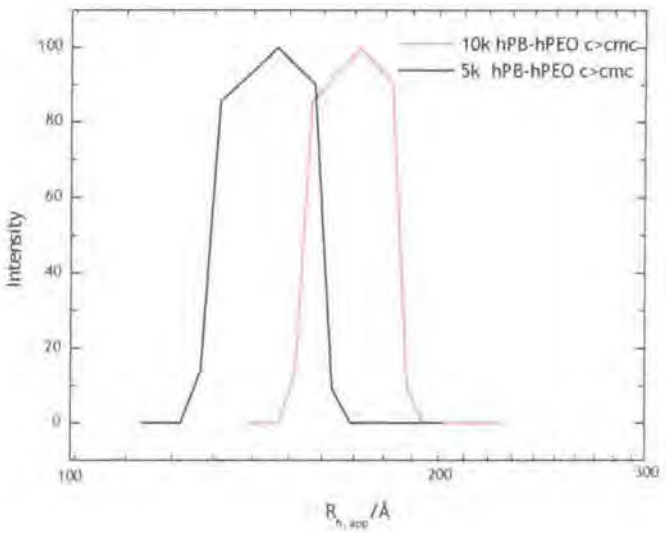

Figure 3.1 - *Typical size distributions for the 10k and 5k hPB-hPEO polymers above the cmc from CONTIN analysis of QELS data. The distributions are actually rounded in nature, similar to a Gaussian distribution, but the CONTIN routine (cf pg 67) evaluates the data as discrete steps leading to the distributions observed.*

The size distributions shown in figure 3.1 suggest that micelles formed by 10k hPB-hPEO and 5k hPB-hPEO have radii of the order of 174 and 140Å respectively. It was not possible to obtain size distributions for either of the two polymers below the cmc due to the weak nature of the scattering.
Scattered light intensity increase dramatically for very low concentrations of micelles, and thus QELS was chosen to determine the cmc's of the two copolymers.

3.2.1. Critical Micelle concentration

As touched upon in section 3.1, the cmc is the concentration at which micelles are detectable by a given experimental technique. Micelle formation results from the association of molecules in a selective solvent above this concentration. Elias[14] proposed two models for the association of molecules into micelles. In the first, termed open association, micelle formation can be represented as a series of successive equilibrium steps, (as shown in figure 3.2), each having an associated equilibrium constant.

$$A_1 + A_1 \overset{k_2}{\rightleftharpoons} A_2$$

$$A_2 + A_1 \overset{k_3}{\rightleftharpoons} A_3$$

$$A_3 + A_1 \overset{k_4}{\rightleftharpoons} A_4$$

$$A_{N-1} + A_1 \overset{k_N}{\rightleftharpoons} A_N$$

Figure 3.2 - *Open association*

If the different association steps are equivalent, then one association constant, k_0 that is given by equation 3.2, can define the system.

$$k_0 = \frac{[A_N]}{[A_1][A_{N-1}]} \qquad \textbf{Equation 3.2}$$

This model leads to a broad continuous distribution of micelle sizes, and is similar to the equilibrium in condensation polymerisation in terms of the size distribution. However it does not lead to a definable cmc.

The second model, termed closed association, can be represented by an equilibrium between micelles of association number p, and unimers, as shown in figure 3.3.

$$pA_1 \rightleftharpoons A_p$$

Figure 3.3- *Closed association*

The association constant, k_c is given by equation 3.3.

$$k_c = \frac{[A_p]}{[A]^p} \qquad \textbf{Equation 3.3}$$

This model gives rise to a narrow distribution of micelle sizes and can be compared to the monomer/polymer equilibrium in addition polymerisation. It also allows for the concept of a cmc.

Block copolymers undergoing micellisation exhibit a cmc, and show a narrow distribution of particle sizes, suggesting the closed association model is the most appropriate.[15]

3.2.1.1. Experimental determination

Light scattering is a convenient way of demonstrating the presence of micelles, as the intensity of scattered light is sensitive to low mass concentrations of micelles. It was for this reason that it was chosen to determine the cmc's of the two fully hydrogenous polymers.

The procedure for the QELS experiments was outlined in section 2.5.2, but briefly, the intensity autocorrelation functions of aqueous copolymer dispersions in the concentration range 1×10^{-5} to 2×10^{-3} gml^{-1} were recorded. Plots of the scattered intensity *vs.* log concentration were constructed, with the cmc defined as the point at which the scattering increased from the value established for dispersed molecules.

Figures 3.4 and 3.5 show plots of scattering intensity *vs.* concentration for the two copolymers, with the break-point marked on each.

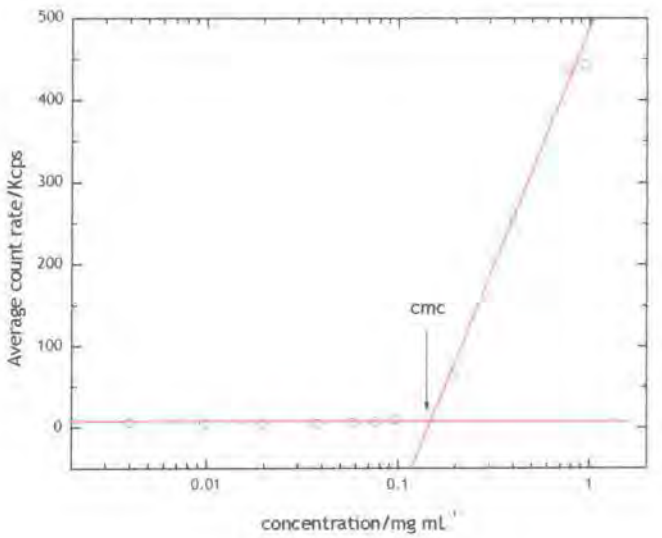

Figure 3.4 - *Intensity vs. concentration for 10k hPB-hPEO. Break point indicated represents the cmc, a value of 0.148 mg mL^{-1}. Lines are guides for the eye.*

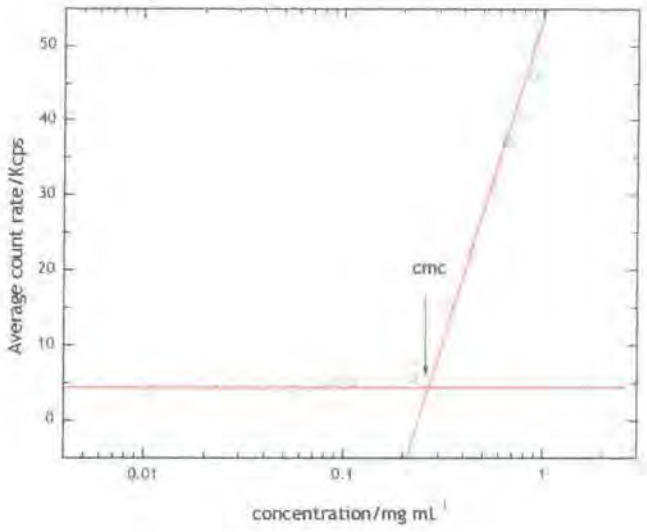

Figure 3.5 - *Intensity vs. concentration for 5k hPB-hPEO. Break point indicated represents the cmc, a value of 0.268 mg mL^{-1}. Lines are guides for the eye.*

The two cmc's were determined as 0.148 mg mL^{-1} for 10k hPB-hPEO and 0.268 mg mL^{-1} for 5k hPB-hPEO. The magnitude of these values in relation to one another is as expected, with the higher molecular weight copolymer having a cmc that is approximately half that of its lower molecular weight counterpart.

It is well documented that in poly(ethylene oxide) containing diblock copolymers, the principle determinants of the cmc are the nature and length of the hydrophobic block; the length of the ethylene oxide block exerting only a small influence.[2-4]

For the model of closed association, introduced earlier, if the association number, p, is large, typically greater than 50, the association constant given by equation 3.3 can be related to the Gibbs energy of association given by equation 3.4.[14]

$$\Delta_{mic}G^{\circ} = -RT\ln K \approx RT\ln[A] \qquad \text{Equation 3.4}$$

For molecules and micelles in equilibrium just above the cmc:

$$\Delta_{mic}G^{\circ} = -RT\ln(cmc) \qquad \text{Equation 3.5}$$

Plotting log(cmc) *vs.* hydrophobe length allows comparison of the micellisation process in block copolymers containing different hydrophobic

groups.[16, 17] Such a comparison is useful as it enables determination of the relative hydrophobicities of the poorly solvated blocks. Booth and co-workers have employed such a comparison for the block copolymers they have studied,[2, 16, 17] and it is extended here to encompass the results from the present work in addition to selected results from the literature.

Table 3.2 outlines the cmc's determined for six different species of diblock copolymer, each forming spherical micelles in aqueous solution.

Copolymer	Hydrophobe length	cmc/mg mL^{-1}	Log(cmc/mol dm^{-3})	Reference
PB-PEO	14	0.148	-4.193	Present work
	27	0.268	-4.772	Present work
	45	0.500	-4.210	18
PPO-PEO	34	52	-2.097	2
	37	6.6	-3.004	
	52	1.5	-3.699	
	55	1.3	-3.745	
	60	0.64	-4.102	
	73	0.13	-4.824	
PBO-PEO	5	5.7	-2.444	2
	8	0.3	-3.959	
	10	0.034	-4.721	
	13	0.016	-5.301	
	16	0.0045	-6.114	
	16	0.0038	-6.432	
PSO-PEO	3.5	0.29	-3.959	17
	5.1	0.058	-4.678	
	6.5	0.042	-4.854	
PS-PEO	10	0.01270	-5.498	5
	14	0.03200	-5.424	12
	17	0.00290	-6.467	6
	17	0.00100	-7.149	
C_nE_m	6		-1.040	16
	8		-2.280	
	10		-2.870	
	12		-3.810	
	12		-4.000	
	12		-3.300	
	14		-4.900	
	14		-4.200	
	16		-5.300	
	16		-4.900	

Table 3.2 - *cmc values for PEO based block copolymers having different hydrophobes taken from both the present research and the literature. PB=poly(butadiene), PPO=poly(propylene oxide), PBO=poly(butylene oxide), PSO=poly(styrene oxide), PS=poly(styrene)*

Figure 3.6 shows a plot of log(cmc) *vs.* hydrophobe length, n, constructed using the data from table 3.2.

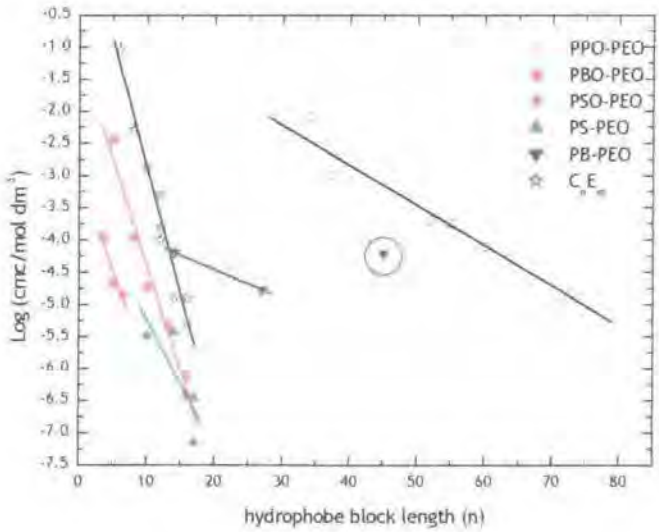

Figure 3.6 - *Plot of log(cmc) vs hydrophobe length for PEO based block copolymers with different hydrophobes, abbreviations are as in table 3.2. The circled point is that due to Zheng and Davis.*

One of the most striking features of figure 3.6 is the difference in the slope for the PB-PEO copolymers when compared to the other species, with it being significantly shallower. The line through the PB-PEO points was calculated using only the results from the present research, as there was some question mark over the validity of the result produced by Zheng and Davis[18] (that circled in figure 3.6). The result used originates from graphical interpretation of their data rather than the result quoted in the text of the paper, with the two values being vastly different, the latter quoted as 1.1×10^{-4}g L^{-1}.

Using the chain length required to attain a given cmc value as an indicator, the relative hydophobicities can be calculated from the linear relationships determined in figure 3.6. Such a comparison yields relative hydrophobicities in the ration of 1:3:5:6:11:13 for PPO:PB:C_n:PBO:PS:PSO respectively.

Davies and Rideal proposed a system to calculate a hydrophile-lipophile balance (HLB) based upon the functional groups present in the molecule.[19, 20] This can be used as an indication of the hydrophobic nature of a molecule by the score given from equation 3.6

$$HLB = \sum(hydrophilic\ group\ numbers) - \sum(hydrophobic\ group\ numbers) + 7$$

Equation 3.6

The lower the total score, the more hydrophobic a molecule is. Lipophilic groups such as CH_2 units are given a group number of 0.475, whilst PEO has a group number of 0.33. Charged species have higher group numbers still. Calculation of HLB numbers for PPO-PEO, PBO-PEO and PB-PEO give values of 5.905, 5.43 and 5.43 respectively, indicating that PB and PBO have similar hydrophobic character, and are more hydrophobic that PPO. This can only be taken as an indicative value and not an absolute one.

For some polymer blocks in the list given the data set available is very small, therefore the ratio of hydophobicities given should be taken as indicative rather than quantitative.

3.2.2. Average Hydrodynamic radii

The concentration dependence of the apparent average diffusion coefficient (D_{app}) determined from analysis of the intensity autocorrelation function can be related to the translational diffusion coefficient of the micelles at zero concentration by equation 3.7[8, 21-23]

$$D_{app} = D_0(1 + k_d(c - cmc))$$ **Equation 3.7**

k_d is the diffusion second virial coefficient, which can be related to the thermodynamic second virial coefficient by equation 3.8[8, 23]

$$k_d = 2A_2M_w - k_f - 2v$$ **Equation 3.8**

k_f is the frictional coefficient and v is the partial specific volume of micelles in solution.

Figure 3.7 shows plots of D_{app} *vs.* (c-cmc) for polymers 10k hPB-hPEO and 5k hPB-hPEO in aqueous solution.

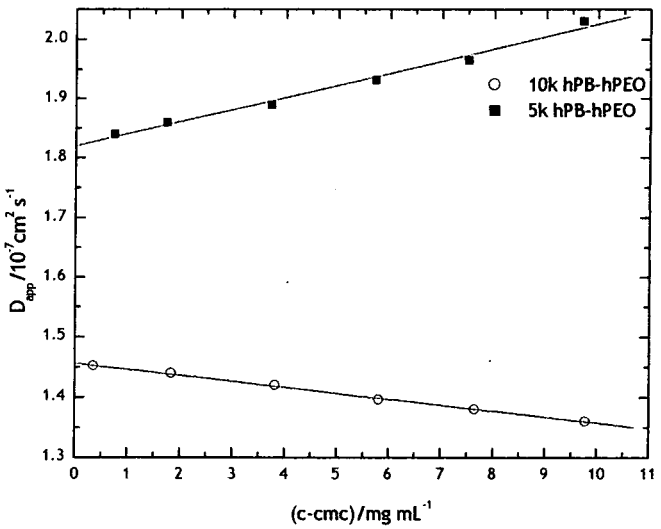

Figure 3.7 - *Apparent diffusion coefficient vs. concentration for 10k hPB-hPEO and 5k hPB-hPEO in dilute solutions. Lines are linear fits to the data.*

Extrapolating to zero micelle concentration gives the diffusion coefficient of the micelle at infinite dilution, and hence the hydrodynamic radius.

Table 3.3 lists the parameters obtained from figure 3.7 for the two copolymers.

Copolymer	$D_0/10^{-7}cm^2s^{-1}$	R_h/Å	k_d/mL mg^{-1}
10k hPB-hPEO	1.456±0.012	168±0.8	-0.00682±0.0001
5k hPB-hPEO	1.820±0.008	136±0.3	0.011±0.001

Table 3.3 - *Diffusion coefficient, Hydrodynamic radii, and second virial diffusion coefficient calculated from extrapolation to infinite dilute for 10k hPB-hPEO and 5k hPB-hPEO.*

One particularly striking feature of figure 3.7 is the difference in slope, and thus the value of k_d for the two copolymers. Quite why this is so remains unclear. A positive value of k_d is the normal occurrence for diblock copolymer micelles,[24-26] implying a repulsion between them. This is usually associated with the micelles acting as hard spheres.[24] A negative k_d value is more commonly associated with triblock copolymers in a solvent selective for the

middle block.[21, 27, 28] Under these conditions flower-like micelles are formed with some of the end blocks dangling in solution leading to attractive interactions. The synthetic procedure employed precludes the formation of such copolymers and so the negative value must be due to some other factor.

Table 3.4 details hydrodynamic radii of poly(ethylene oxide) based diblock copolymers of comparable molecular characteristics to those studied here.
Chapter one introduced the scaling approaches applied to micelles by Halperin[29] and others. These are discussed in more detail in section 3.5.2.3, but briefly, the values of the micelle radius, R, can be estimated from the degree of polymerisation of both blocks and the segment length using equation 3.9

$$R \approx N_B^{4/25} N_A^{3/5} a \qquad \textbf{Equation 3.9}$$

where N_B is the degree of polymerisation of the core block, N_A is the degree of polymerisation of the shell block, and a is the segment length.
The model assumes the segment length to be equal for both blocks, which although not strictly correct, the errors associated with such an assumption are sufficiently small as to allow it to be used. The segment length can be determined by the cube root of the volume of one repeat unit, which Nagarajan and Ganesh[30] reported as 64.6Å for ethylene oxide, giving a segment length of 4.01Å. The values expected from this relationship are also given in table 3.4 for the copolymers listed, using the segment length of ethylene oxide in all of the calculations.
Strictly speaking, the degree of polymerisation of the two blocks in the copolymers should be normalised with respect to the melt densities of each block, using equation 3.10.

$$r_v = N_A + N_B\left(\frac{M_B}{\rho_B} + \frac{M_A}{\rho_A}\right) \qquad \textbf{Equation 3.10}$$

where r_v is the normalised degree of polymerisation, N_A and N_B are the respective degrees of polymerisation of each block, M_A and M_B are the molecular weights of each block, and ρ_A and ρ_B are the melt densities of each block. This correction was not applied here, but in any future efforts to fit

similar data should be applied. This changes the molecular volumes by ca 15%.

Copolymer	Wt % EO	M_w copolymer	R_h/Å	R/Å	R_h:R	Reference
$B_{14}E_{89}$	81	4100	135	92.4	1.46	Present work
$B_{27}E_{164}$	83	8800	168	146.6	1.15	Present work
$E_{43}BO_9$	74	2620	69	54.5	1.27	31
$E_{40}BO_{10}$	71	2580	73	53.0	1.38	
$E_{90}BO_{10}$	85	4820	95	86.3	1.10	
$E_{96}BO_{18}$	77	5690	155	98.5	1.57	
$E_{184}BO_{18}$	86	9670	195	145.6	1.34	
$E_{106}BO_{16}$	80	5990	73	102.6	0.71	24
$E_{216}BO_{16}$	89	10700	200	157.3	1.27	
$E_{50}SO_{3.5}$	84	2670	66	51.3	1.29	17
$E_{50}SO_{5.1}$	78	2920	69	54.4	1.27	
$E_{51}SO_{6.5}$	74	3110	72	57.3	1.26	
$S_{16}E_{155}$	80	8500	100	128.9	0.78	32
$S_{36}E_{237}$	74	14100	150	189.3	0.79	
$S_{9.6}E_{68.2}$	75	4000	140	72.6	1.93	5

Table 3.4 - *Hydrodynamic radii, and theoretically predicted radii, R, for poly(ethylene oxide) based diblock copolymers R_h:R is the ration of experimental radii to theoretical radii. Hydrophobe abbreviations are as in table 3.2.*

There is a reasonable correlation between the radii determined by QELS and those estimated using Halperin's model, with the latter generally being smaller than the experimental values. The dimensions of the micelles investigated here are slightly larger than those predicted by Halperin's model, but comparable to those reported in the literature for poly(butylene oxide) containing copolymers having similar molecular characteristics. Unfortunately, there appear to be few k_d values reported for diblock copolymer micelles, with many authors preferring to use the analogous method of plotting $1/R_{h,\,app}$ *vs.* concentration in order to determine the true R_h value.

3.2.3. Concentration effects

The effect of concentration upon the size distribution of the micelles was investigated at concentrations as high as 100 mg mL^{-1} for both copolymers. Figures 3.8 and 3.9 show the $R_{h,\ app}$ distributions for 10k hPB-hPEO and 5k hPB-hPEO with varying concentration.

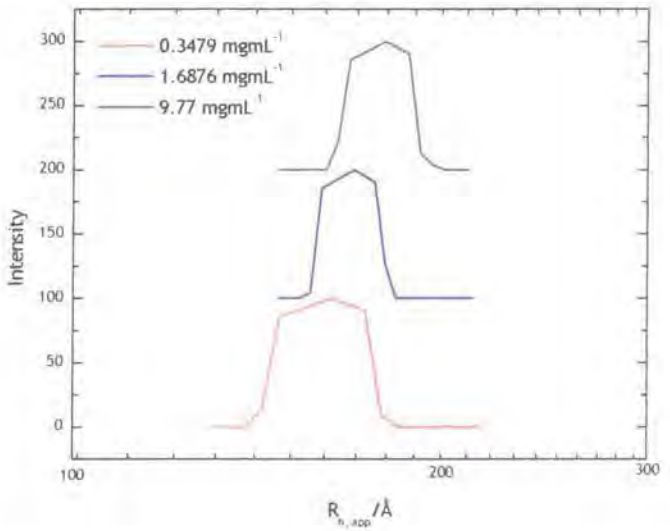

Figure 3.8 -Size distribution for 10k hPB-hPEO in dilute solutions at c>cmc. The distributions are shifted successively by 100 for clarity.

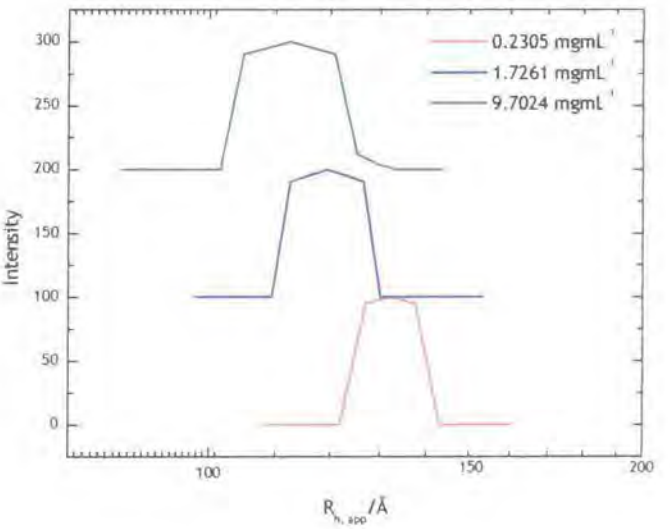

Figure 3.9 - Size distribution for 5k hPB-hPEO *in dilute solutions at c>cmc.* The distributions are shifted successively by 100 for clarity.

It is apparent from figures 3.8 and 3.9 that the observations made in the previous section are supported by the data presented therein; namely that the size of the micelles decreases with increasing concentration for 5k hPB-hPEO and vice versa for 10k hPB-hPEO. The distributions observed in the dilute regime, where c≤10 mg mL^{-1} are narrow, indicative of a closed association process. The observation of a shift in $R_{h,\,app}$, to lower values with increasing concentration has been commonly observed in the literature for other poly(ethylene oxide) based block copolymer micelles.[11]

Distributions of the two copolymers at higher concentrations are shown in figures 3.10 and 3.11.

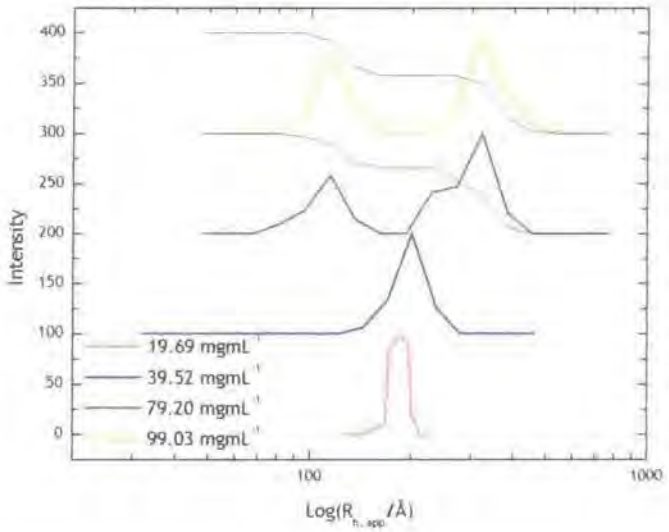

Figure 3.10 - *Size distribution for 10k hPB-hPEO at higher concentrations showing the development of dual populations at c>40 mg mL^{-1}. The black lines on the cumulative distributions represent the relative amounts of each present. The distributions are shifted successively by 100 for clarity.*

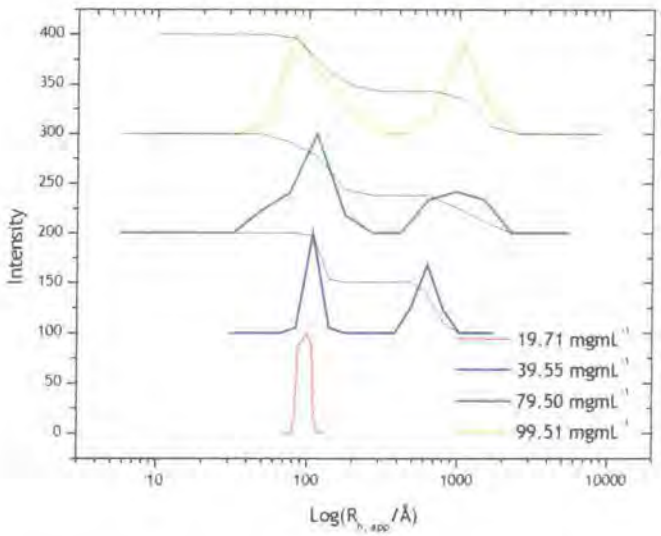

Figure 3.11 - *Log normal size distribution for 10k hPB-hPEO at higher concentrations showing the development of dual populations at c>20 mg mL^{-1}. The black lines on the cumulative distributions represent the relative amounts of each present. The distributions are shifted successively by 100 for clarity*

From figures 3.10 and 3.11 it can be seen that micelles of both copolymers exist in bimodal distributions at higher concentrations. For 10k hPB-hPEO this occurs when c>4 mg mL^{-1} with the smaller size population having a radius of ca 110Å and the larger populations 330Å. The relative occurrence of the two populations is ca. 1:3 in favour of the larger population. It is worthwhile pointing out that this dual population is not always observed at these concentrations, although it is more prevalent than the monomodal case. For 5k hPB-hPEO, the situation is a little different. Bimodal populations are observed at c>2mg mL^{-1} with the smaller species having a radius of ca 110Å and the larger species between 600 and 1000Å depending upon the concentration. The dimensions of the larger population are more akin to those of micellar clusters observed by Xu *et al.*[7] for poly(styrene)-poly(ethylene oxide). The relative occurrence for these populations is ca 3:2 in favour of the smaller populations.

One possible reason for the difference in size of the micellar clusters could be that those formed by 10k hPB-hPEO may be more tightly packed due to the attractive nature of the micelles suggested by the diffusion second virial coefficient, whereas those formed by 5k hPB-hPEO may be more loosely

packed as the same parameter for this copolymer suggests micellar interactions of a repulsive nature.

The observation of micellar clusters at higher concentrations is not entirely unexpected since the degree of ordering in the system is expected to increase with concentration, and with it the level of micellar interactions. These dominate the properties of the dispersion at higher concentrations, and are readily observable in the small-angle scattering data that will be introduced in subsequent sections.

3.2.4. Effect of temperature

The effect of temperature upon the properties of the micelles in aqueous solutions for both copolymers was investigated. Temperatures in the range 283-353K in 5k increments were explored. The experiments were carried out much in the same manner as for those detailed earlier, with the exception that for a given experiment the concentration was fixed whilst the temperature was varied. The concentration dependence of D_{app} at each temperature was used to ascertain the micelle radius and the second virial diffusion coefficient.

Table 3.5 details the parameters determined from the concentration dependence of D_{app} at different temperatures for polymers 10k hPB-hPEO and 5k hPB-hPEO, typical examples of which are shown in figures 3.12 and 3.13.

	10k hPB-hPEO			5k hPB-hPEO		
T/K	$D_0/10^{-7}$ cm^{2}s^{-1}	R_h/Å	k_d/mL mg^{-1}	$D_0/10^{-7}$ cm^{2}s^{-1}	R_h/Å	k_d/mL mg^{-1}
283	0.866	182.9	0.041	1.190	133.1	3.43
288	0.923	200.5	0.145	1.239	149.3	3.14
293	1.139	187.8	0.096	1.419	150.8	3.15
298	1.407	174.0	-0.098	1.553	157.7	5.01
303	1.634	170.1	-0.086	1.880	147.9	2.90
308	1.925	162.7	-0.130	2.200	142.4	5.35
313	2.175	161.2	-0.115	2.890	121.4	1.56
318	2.489	156.8	-0.277	3.030	128.8	1.71
323	2.735	158.0	-0.185	3.600	120.1	0.92
328	2.910	163.6	-0.105	3.780	126.0	1.88
333	2.922	178.8	-0.198	4.115	126.9	1.17
338	3.764	151.5	-0.175	4.250	134.2	2.52
343	4.007	155.0	-0.210			
348	4.889	137.7	-0.266			
353	5.326	140.3	-0.257			

Table 3.5 - *Diffusion coefficients, hydrodynamic radii, and second virial diffusion coefficients for 10k hPB-hPEO and 5k hPB-hPEO at different temperatures determined by extrapolation to infinite dilution*

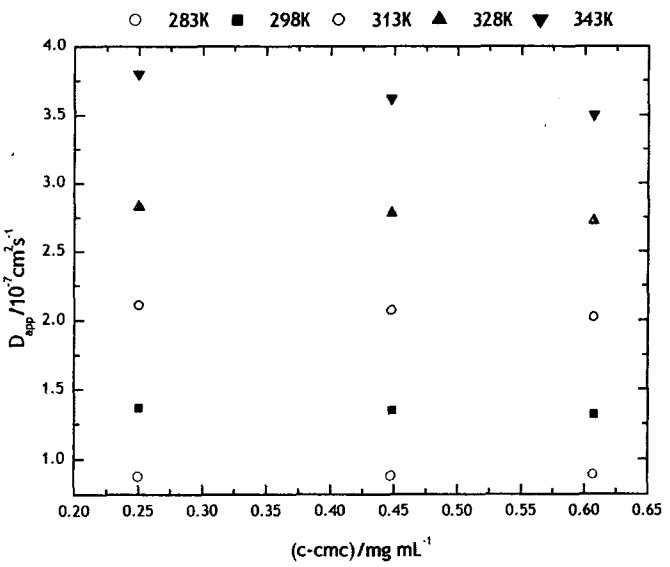

Figure 3.12 - *Variation of apparent diffusion coefficient with concentration at different temperatures for 10k hPB-hPEO*

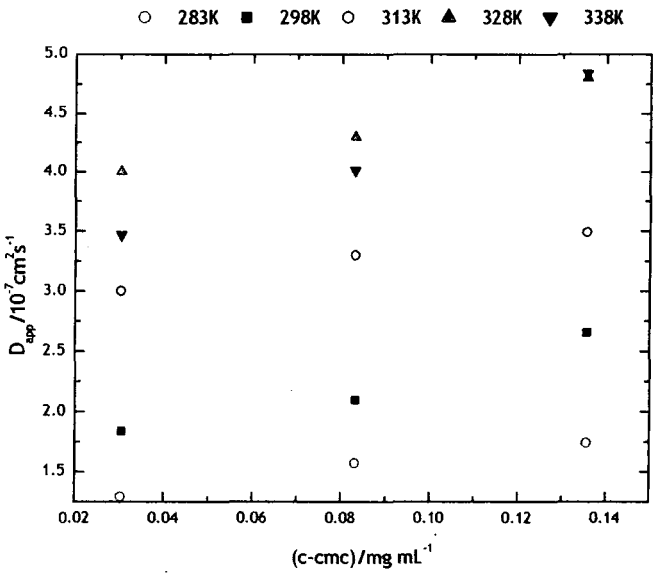

Figure 3.13 - *Variation of apparent diffusion coefficient with concentration at different temperatures for 5k hPB-hPEO*

Figures 3.12 and 3.13 reveal some interesting behaviour about the micelles. Below ambient temperature the behaviour of the micelles of 10k hPB-hPEO conforms to that considered normal for diblock copolymers, i.e. the second diffusion virial coefficient is positive, suggesting repulsive interactions. At ambient temperature and above, the slope of the concentration dependence of D_{app} is reversed and the nature of the interactions becomes attractive. With small exceptions, there appears to be a trend of an increase in the magnitude of k_d suggesting stronger interactions of micelles at elevated temperatures. This is accompanied by an apparent decrease in R_h. The latter observation is one that is subject to conflicting data in the literature. It was initially accepted that R_h was approximately constant with an increase in temperature, with this constancy attributed to a decrease in the swelling of the ethylene oxide fringe of the micelle as the solvent becomes poorer, accompanied by an increase in association number.[2, 4] Recently, however, Mingvanish *et al.*[25] observed a decrease in R_h with an increase in temperature. No explanation was offered for this, although the results presented here appear to support the authors' observations.

In contrast to 10k hPB-hPEO, 5k hPB-hPEO displays the same behaviour in terms of the micellar interactions regardless of the temperature, with k_d always taking a positive value. The R_h values were, in the main, relatively

constant with temperature with slight variations observed, which may be purely due to statistical errors. This observation supports those of several authors e.g Zhou *et al.*[21]

3.2.5. Conclusions

For clarity, the important facts that have been concluded from the QELS data are presented here.

- Both of the block copolymers investigated form micelles at low concentrations, and appear to do so *via* a closed association process.
- The cmc's were determined as 0.148 mg mL^{-1} for 10k hPB-hPEO and 0.268 mg mL^{-1} for 5k hPB-hPEO.
- Poly(butadiene) has a relative hydrophobicity that lies between that of poly(propylene oxide) and poly(butylene oxide), an observation that is approximately supported by an HLB calculation.
- The micelles formed have an average hydrodynamic radius of 168Å for 10k hPB-hPEO and 136Å for 5k hPB-hPEO.
- The micelles of 5k hPB-hPEO show repulsive tendencies towards each other at all temperatures, whilst the data suggests those of 10k hPB-hPEO are attracted to one another when the temperature is at or greater than ambient temperature.
- The micelles of 10k hPB-hPEO decrease in size with an increase in temperature, whilst those of 5k hPB-hPEO show little change in size with temperature.

3.3. Static Light Scattering

3.3.1. Introduction

As discussed in section 2.4.2.1, SLS can be used to determine size parameters of molecules. For homopolymers the treatment is relatively uncomplicated as each molecule can be assumed to have the same refractive index; this is not true for block copolymers. It is rarely possible to synthesise block copolymers of uniform composition. As a result, the refractive index is dependent upon the composition. The two blocks also occupy different positions with respect to the molecules' centre of gravity, and thus the angular distribution of

scattered light is different from that of a homopolymer. These two factors have to be considered when treating light scattering data from block copolymers.

Homopolymers can be described in terms of their molecular weight and polydispersity index, but for block copolymers knowledge of the total molecular weight as well as that of the individual blocks is required. If the block copolymer is polydisperse, then account must be taken of two-fold polydispersity, namely mass and structure. Consequently, characterisation is somewhat complicated.

In what follows,[33] M is the molecular weight of a molecule; M^A and M^B are the molecular weights of the polymers of monomers A and B respectively. For a monodisperse system, the composition by weight, w, of the sample is defined by:

$$w = \frac{M^A}{M^A + M^B} \qquad \text{Equation 3.11}$$

Similarly, for a polydisperse system, the number-average (M_n, M_n^A, M_n^B) and weight-average (M_W, M_W^A, M_W^B) molecular weights can be defined, with an average composition w_n given by:

$$w = \frac{M_n^A}{M_n^A + M_n^B} \qquad \text{Equation 3.12}$$

3.3.1.1. Molecular weight

For a monodisperse homopolymer of concentration c, the excess Rayleigh ratio, $R-R_0$, for an ideal solution (i.e. $A_2=0$), is given by

$$R - R_0 = KM\left(\frac{dn}{dc}\right)^2 P(\theta)c \qquad \text{Equation 3.13}$$

$P(\theta)$ is the particle scattering factor, M is molecular weight, $\left(\frac{dn}{dc}\right)$ is the specific refractive index increment, c is concentration

where $K = \frac{4\pi^2 n_o^2}{N_A \lambda_0^4}$ Equation 3.14

n_0 is solvent refractive index, N_A is Avogadro's number and λ_0 is the incident wavelength.

As P(θ) nears 1 when θ approaches 0, for extrapolation of scattering intensity to zero angle:

$$R - R_0 = KcM\left(\frac{dn}{dc}\right)^2 \qquad \textbf{Equation 3.15}$$

For a polydisperse homopolymer, having a uniform specific refractive index increment, the molecular weight can be replaced by an average value, $\overline{M}$:

$$R - R_0 = Kc\overline{M}\left(\frac{dn}{dc}\right)^2 \qquad \textbf{Equation 3.16}$$

Similarly for a copolymer, an apparent average molecular weight, M_{app} can be introduced

$$R - R_0 = KcM_{app}\left(\frac{dn}{dc}\right)^2 \qquad \textbf{Equation 3.17}$$

where $\left(\frac{dn}{dc}\right)$ is the specific refractive index increment of the copolymer solution. It can either be measured experimentally, or calculated using equation 3.18.

$$\frac{dn}{dc} = w_A\left(\frac{dn}{dc}\right)_A + w_B\left(\frac{dn}{dc}\right)_B \qquad \textbf{Equation 3.18}$$

where $\left(\frac{dn}{dc}\right)_i$ is the specific refractive index increment of species i.

This will be revisited in a later section.

In the case of a micellar solution, the value of c is replaced by (c-cmc) as assuming the model of closed association, the solution at the cmc can be considered as the solvent for the micelles.

The apparent molecular weight can be related to the true value by equation 3.19:

$$M_{w,app}\left(\frac{dn}{dc}\right)^2 = M_w\left(\frac{dn}{dc}\right)_A\left(\frac{dn}{dc}\right)_B + \left(\left(\frac{dn}{dc}\right)_A^2 - \left(\frac{dn}{dc}\right)_A\left(\frac{dn}{dc}\right)_B\right)w_A M_w^A + \left(\left(\frac{dn}{dc}\right)_B^2 - \left(\frac{dn}{dc}\right)_A\left(\frac{dn}{dc}\right)_B\right)w_B M_W^B$$

Equation 3.19

In the case of micelles having a narrow distribution of association numbers, p, dividing by this value gives the corresponding number-average dependence shown in equation 3.20:

$$\frac{M_{w,app}\left(\frac{dn}{dc}\right)^2}{p} = M_n\left(\frac{dn}{dc}\right)_A\left(\frac{dn}{dc}\right)_B + \left(\left(\frac{dn}{dc}\right)_A^2 - \left(\frac{dn}{dc}\right)_A\left(\frac{dn}{dc}\right)_B\right)w_A M_n^A + \left(\left(\frac{dn}{dc}\right)_B^2 - \left(\frac{dn}{dc}\right)_A\left(\frac{dn}{dc}\right)_B\right)w_B M_n^B$$

Equation 3.20

3.3.2. Specific refractive index increment determination

As discussed earlier the specific refractive index increment of a block copolymer can be related to its composition and component blocks by:[34]

$$\frac{dn}{dc} = w_A\left(\frac{dn}{dc}\right)_A + w_B\left(\frac{dn}{dc}\right)_B \qquad \textbf{Equation 3.21}$$

It is possible to measure the value of $\left(\frac{dn}{dc}\right)$ directly using a differential refractometer, or it can be calculated. Both of these approaches will be discussed here, with the latter tackled first.

3.3.2.1. Calculation of dn/dc

The dn/dc of a given polymer is dependent upon several factors, solvent being one of the most important, but also wavelength and temperature. As all of the SLS measurements were carried out at 298K the effect of temperature was not considered.

PEO is soluble in water, and thus the wavelength dependence of its dn/dc can be readily determined from published data by a plot of dn/dc *vs.* $1/\lambda_0^2$, i.e. a Cauchy dispersion.[34] Such a plot is shown in figure 3.14 using data from reference. [35]

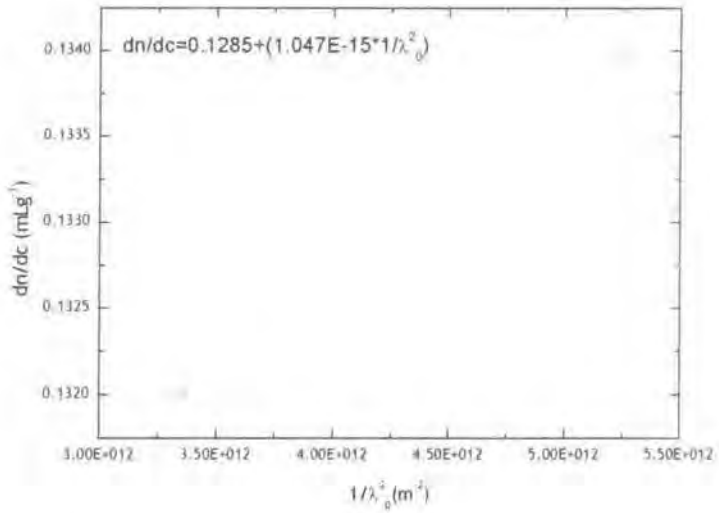

Figure 3.14 - *Cauchy dispersion of dn/dc PEO in water.*

From figure 3.14 the dn/dc of PEO in water at 532nm can be determined as 0.132 mL g^{-1}.

As poly(butadiene) is insoluble in water, the case is a little more complicated. The dn/dc can be determined at 532nm in different solvents, using a Cauchy dispersion as for PEO in water, as shown in figure 3.15 for chloroform, heptane and cyclohexane.[34]

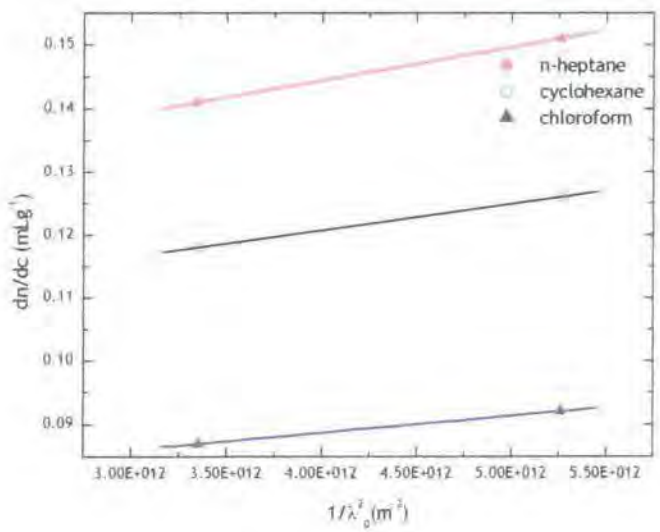

Figure 3.15 - *Cauchy dispersion for poly(butadiene) in n-heptane, cyclohexane and chloroform.*

Interpolation of the data gives the dn/dc values at 532nm for each of the three solvents. These are given in table 3.6 along with the refractive indices of the respective solvents.[36]

Solvent	Refractive index	dn/dc at 532nm/mL g^{-1}
Cyclohexane	1.426	0.1188
Chloroform	1.446	0.0875
n-heptane	1.387	0.1420

Table 3.6 - *Specific refractive index increment values for poly(butadiene) at 532nm in cyclohexane, chloroform and n-heptane determined from figure 3.15*

Using equation 3.22, the dn/dc can be related to the refractive index of the solvent:[34]

$$\frac{dn}{dc} = \left(\frac{dn}{dc}\right)_2 (n_2 - n_0) \qquad \textbf{Equation 3.22}$$

Thus a plot of dn/dc *vs.* solvent refractive index, n_0, gives a slope equal to $-\left(\frac{dn}{dc}\right)_2$, which allows determination of the dn/dc in any solvent whose refractive index is known, in this case water. Such a plot is shown in figure 3.16.

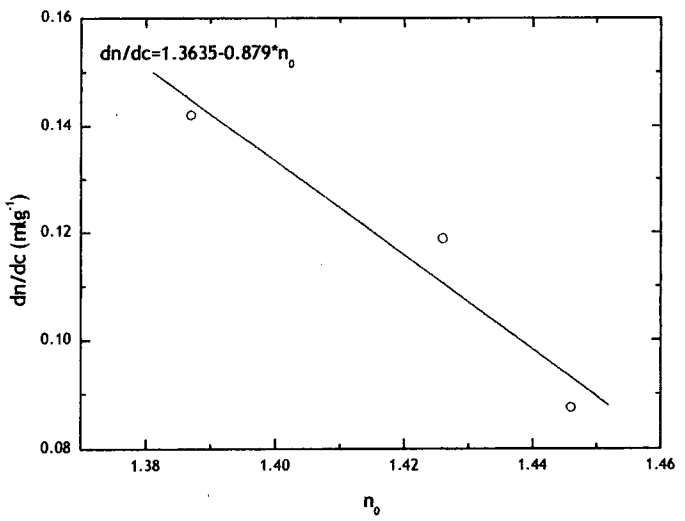

Figure 3.16 - *Plot of dn/dc vs solvent refractive index for poly(butadiene) at 532nm. The red line is a linear fit to the data. Extrapolation to the refractive index of water (1.3329) gives a dn/dc value of 0.192 mL g^{-1}.*

From figure 3.16 the dn/dc of poly(butadiene) in water at 532 nm can be determined as 0.192 mL g^{-1}.

Using equation 3.19, this value can be considered alongside that of PEO, and their relative contributions to the overall molecular weight of the polymer to give its average dn/dc value. This can be calculated as 0.144 mL g^{-1}.

The dn/dc value of the two fully hydrogenous polymers can be considered equal, since it depends only on the composition of a molecule and is independent of its molecular weight.

3.3.2.2. Experimental determination of dn/dc

The procedure used was outlined in section 2.5.2, producing a plot of change in refractive index, Δn, *vs.* concentration, (figure 3.17), the slope of which was the dn/dc at each different wavelength.

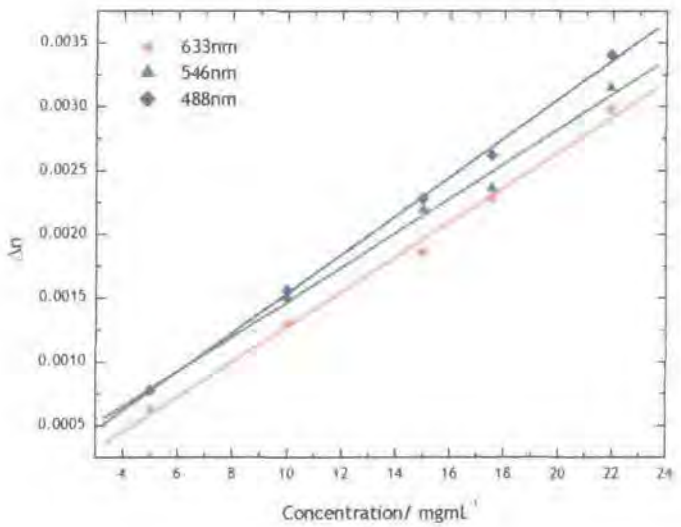

Figure 3.17 - *Plot of change in refractive index (Δn) vs concentration for 5k hPB-hPEO in water at wavelengths of 633, 546 and 488nm, the slope of which yields the dn/dc value at the respective wavelength. The lines are fits to the data.*

Using the dn/dc values calculated from figure 3.17 for the different wavelengths a plot of dn/dc *vs.* $1/\lambda_0^2$ can be constructed (figure 3.18) as before to allow determination of the wavelength dependence, and thus calculation of the dn/dc at the desired wavelength.

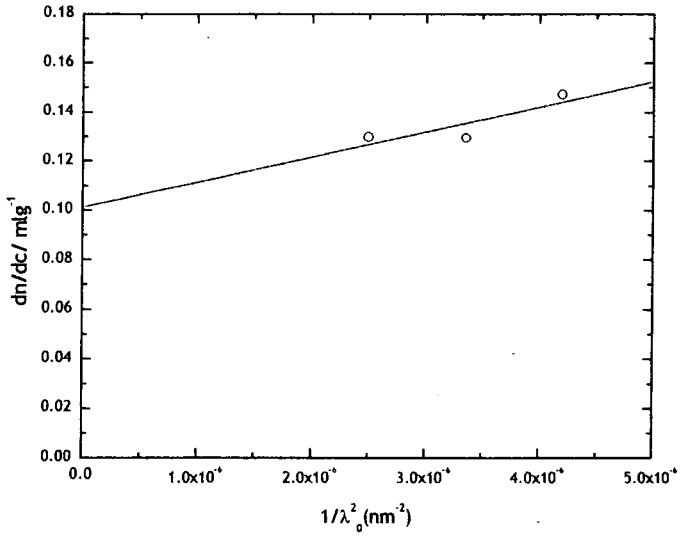

Figure 3.18 - *Cauchy dispersion for 5k hPB-hPEO in water*

From the relationship observed in figure 3.18, the dn/dc for the fully hydrogenous copolymers at 532nm was dtermined as 0.137 mL g^{-1}. This is in reasonable agreement with the value calculated in section 3.3.2.1.

3.3.3. Molecular weight and size determination

3.3.3.1. Zimm plot method

Using the procedure described in section 2.4.2.1 SLS measurements were carried out on polymers 10k hPB-hPEO and 5k hPB-hPEO. The dn/dc value used was that measured experimentally in the previous section.

The Zimm plots constructed use equation 2.23 as their theoretical basis, *viz.*

$$\frac{Kc}{R_\theta} = \lim_{\substack{c\to 0 \\ \theta\to 0}} \frac{1}{M}\left[1+\frac{16\pi^2}{3\lambda^2}\left\langle R_g^2\right\rangle \sin^2(\theta/2)\right] + 2A_2c \qquad \textbf{Equation 3.23}$$

Figures 3.19 and 3.20 show Zimm plots for 10k hPB-hPEO and 5k hPB-hPEO respectively.

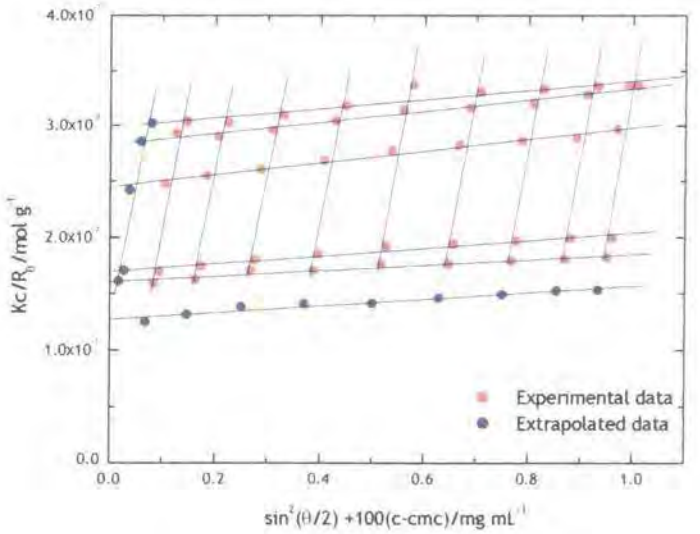

Figure 3.19- *Zimm plot for 10k hPB-hPEO in water generated using equation 3.22. Vertical lines are fits through concentration series at a given angle and the horizontal lines are fits through angular series at a given concentration.*

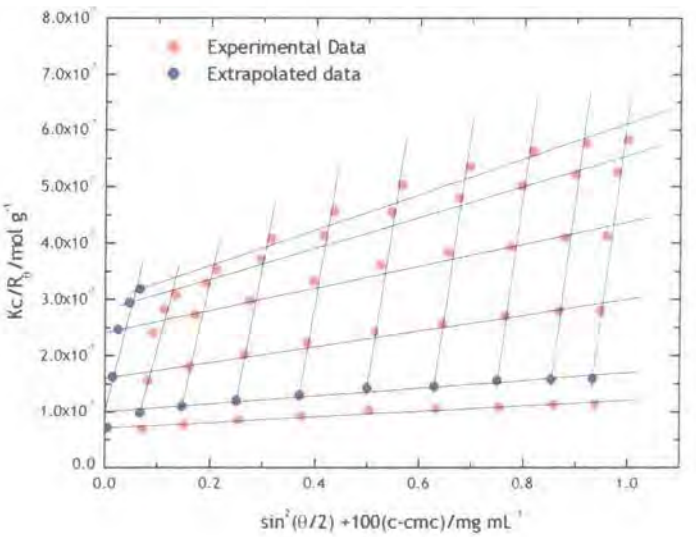

Figure 3.20 - *Zimm plot for polymer 5k hPB-hPEO in water generated using equation 3.22. Vertical lines are fits through concentration series at a given angle and the horizontal lines are fits through angular series at a given concentration.*

The parameters determined from the extrapolations to zero angle and zero concentration are listed in table 3.7.

Polymer	M_{app}/g mol^{-1}	A_2/cm^{3}mol g^{-1}	$R_{g,\ app}$/Å
10k hPB-hPEO	$7.9\times10^6\pm4\times10^4$	1.216×10^{-4}	350
5k hPB-hPEO	$9.9\times10^6\pm2\times10^4$	1.872×10^{-4}	600

Table 3.7 - *Molecular weights, second virial diffusion coefficients (A_2) and radii of gyration calculated from extrapolated data in figures 3.19 and 3.20.*

The striking feature of the data in table 3.7 is the two $R_{g,\ app}$ values. Their magnitudes are somewhat different to those observed in the QELS experiments. If the micelles were acting as hard spheres then R_g:R_h~0.77[37]; for the two polymers here this value is far in excess of that. A larger value of this ratio, is usually associated with a cylindrical morphology, but small-angle scattering data shown in later sections supports the notion that micelles are spherical.

The 10k hPB-hPEO should have the larger radii of the two due to its greater molecular weight. The likely explanation for this is the "shape" of the scattering data. The radius of gyration is calculated from the limiting slope of the extrapolation to zero concentration, which should be the lowest horizontal line in the Zimm plot. In figure 3.20 this is clearly not the case, and most probably leads to the erroneous value given in table 3.7. This observation could be due to a phenomenon in the system, several examples exist of Zimm plots exhibiting upward curvature at low angles caused by ordering of the system.[38] The solutions used here were kept in the dilute range to minimise such effects, and so the likely explanation is experimental error.

In addition to the reversal in the trend of the micelle size, the apparent molecular weights of the micelles are also the inverse of what would be expected. Theory predicts that the association number (calculated later) increases with the length of the hydrophobic block.[29, 39] This would mean that the molecular weight of a micelle composed of 10k hPB-hPEO would have a higher association number, and thus molecular weight than one composed of 5k hPB-hPEO, which is clearly not the case here.

Treatment of the radius of gyration to yield the true value is more involved than for the molecular weight,[33] and given the quality of the data it was decided not to pursue this any further.

Using equation 3.18, and the dn/dc values calculated for the individual blocks, and their respective molecular weights calculated from the Zimm plots the true value of the micelle molecular weight can be calculated. These values are listed in table 3.8.

Polymer	M_{app}/gmol^{-1}	M_w/gmol^{-1}
10k hPB-hPEO	$7.9\times10^6\pm4\times10^4$	5.88×10^6
5k hPB-hPEO	$9.9\times10^6\pm2\times10^4$	7.34×10^6

Table 3.8 - *True molecular weights of 10k and 5k hPB-hPEO calculated using equation 3.18.*

From the molecular weights determined the average association number of the micelles can be calculated by dividing the micelle molecular weight by that of the copolymer. The values determined are given in table 3.9.

Polymer	M_w/gmol^{-1}	p
10k hPB-hPEO	5.88×10^6	640
5k hPB-hPEO	7.34×10^6	1657

Table 3.9 - *Association numbers, p, for 10k and 5k hPB-hPEO calculated from the molecular weights of the micelles.*

As discussed earlier the association number is expected to increase with the length of the block forming the core of the micelle. The values determined here are considerably higher than those obtained for poly(ethylene oxide) copolymers of comparable molecular weight and composition, with values of up to ca 400 being common.

In addition to the radii of gyration calculated from the data it is also possible to estimate the micelle radius from the second virial coefficient using equation 3.22, which has been applied by Mortensen and co-workers.[5]

$$R_{A_2} = \left[\frac{3M_w^2 A_2}{16\pi N_A}\right]^{1/3} \qquad \textbf{Equation 3.24}$$

These values are shown in table 3.10.

Polymer	M_w/gmol^{-1}	A_2/cm^{3}molg^{-1}	R_{A_2} /Å
10k hPB-hPEO	5.82×10^6	1.216×10^{-4}	740
5k hPB-hPEO	7.37×10^6	1.872×10^{-4}	1000

Table 3.10 - *Estimates of micelle radius for 10k and 5k hPB-hPEO from the second virial coefficient, using equation 3.23.*

As with the previous treatments of the Zimm plot data the validity of the results in table 3.10 is open to question.

3.3.3.2. Debye treatment of SLS data

Several groups including those of Booth[16, 24, 28] and Chu[8, 9, 21] have employed the Debye equation when treating light scattering data, which at 90° takes the form

$$\frac{K(c-cmc)}{R_{90}} = \frac{1}{M_{app}} + 2A_2(c-cmc) \qquad \textbf{Equation 3.25}$$

Thus a plot of $K(c\text{-}cmc)/R_{90}$ *vs.* (c-cmc) has an intercept of $1/M_{app}$, and a gradient of $2A_2$. The apparent molecular weight can be related to the true molecular weight in the same manner as for the Zimm type data treatment. Debye plots at 90° for polymers 10k and 5k hPB-hPEO are shown in figures 3.21 and 3.22 respectively.

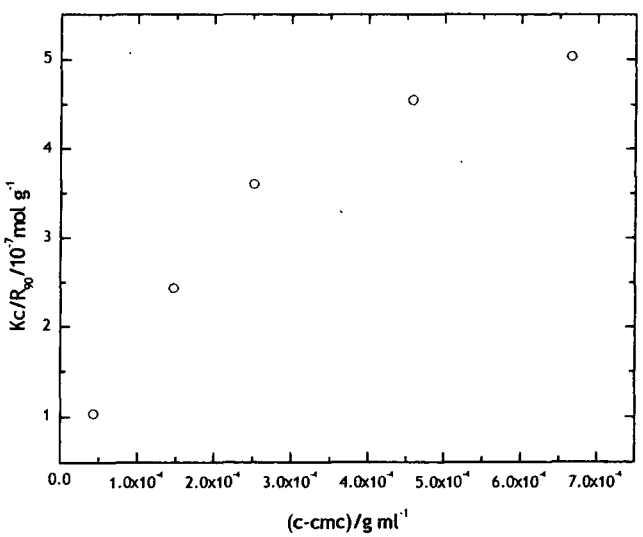

Figure 3.21 - *Debye plot for 10k hPB-hPEO using equation 3.24*

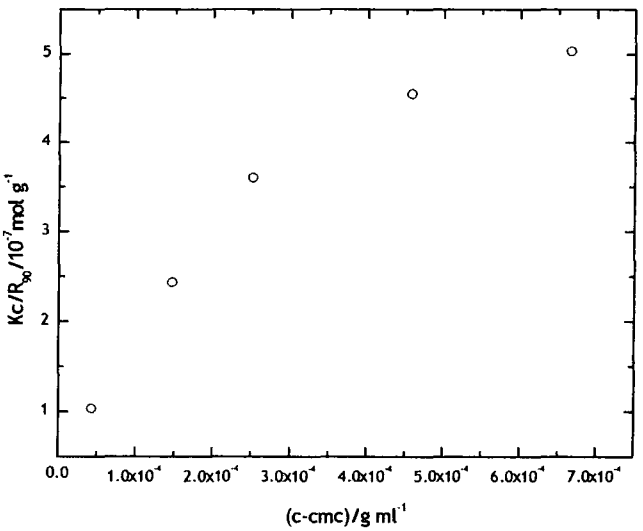

Figure 3.22 - *Debye plot for 5k hPB-hPEO using equation 3.24.*

In the concentration range explored curvature is evident. The curvature observed is different to that seen by the Booth group[16, 17] who used the Carnahan-Starling[40] approximation to fit their light scattering data. By doubling the concentration range, linear Debye plots could be obtained, figures 3.23 and 3.24. Table 3.11 sets out the values obtained from linear fits to the data.

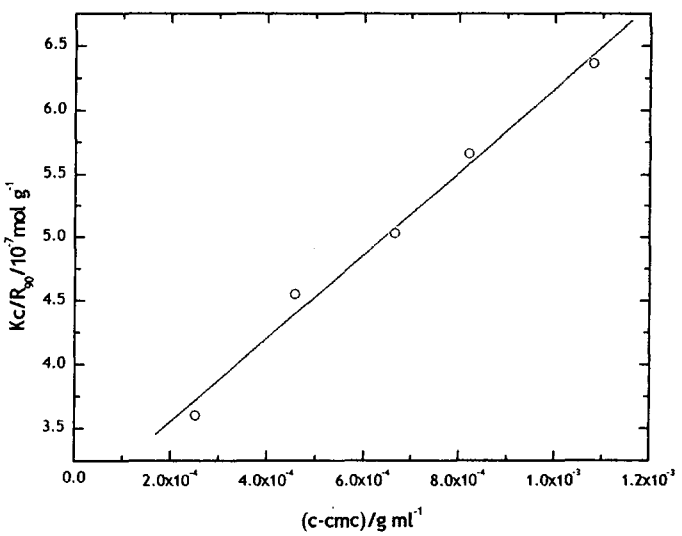

Figure 3.23 - *Debye plot for 10k hPB-hPEO over a modified concentration range. The line is a linear fit to the data.*

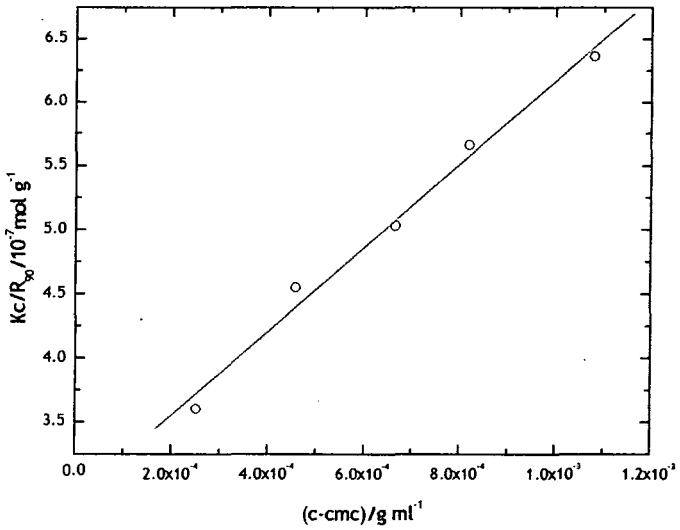

Figure 3.24 - *Debye plot for 5k hPB-hPEO over a modified concentration range. The line is a linear fit to the data*

Polymer	M_{app}/g mol^{-1}	M_w/g mol^{-1}	A_2/cm^{3}mol g^{-1}
10k hPB-hPEO	4.29×10^6	3.18×10^6	6.23×10^{-5}
5k hPB-hPEO	3.45×10^6	2.63×10^6	1.64×10^{-5}

Table 3.11- *Data obtained from linear fits to figures 3.23 and 3.24 constructed using the Debye equation, along with the true molecular weight.*

The values of the molecular weights obtained from the Debye analysis of the data are more in line with those expected, namely the higher molecular weight polymer forms micelles of a higher molecular weight.

As with the Zimm plot methods it is possible to calculate the association number, and to estimate the micellar radii using the second virial coefficient. The values obtained are given in table 3.12

Polymer	M_w/g mol^{-1}	p	A_2/cm^{3}mol g^{-1}	R_{A_2} /Å
10k hPB-hPEO	3.18×10^6	346	6.23×10^{-5}	397
5k hPB-hPEO	2.63×10^6	594	1.64×10^{-5}	224

Table 3.12 - *Association numbers, p, and estimates of the micelle radius from figures 3.23 and 3.24.*

As with the previous Zimm treatment of the data, the association numbers do not follow the pattern expected, with the lower molecular weight copolymer having a higher association number than its higher molecular weight counterpart. The estimate of the micelle radius follows the pattern expected but the values are still higher than those obtained from the QELS experiments.

3.3.4. Conclusions

Interpretation of the data obtained during the SLS experiments is open to question. Estimates of the sizes of the micelles are larger than those from the QELS experiments and theoretical predictions. The association numbers are not as expected, with the lower molecular weight polymer showing a higher association number than its higher molecular weight counterpart.

3.4. Small-angle X-ray Scattering

3.4.1. Introduction

As discussed in section 2.4.1 small-angle X-ray scattering, (SAXS), provides a powerful tool for probing the structure and interactions of block copolymer micelles in solution. Unlike light scattering studies that can be performed on relatively dilute solutions, SAXS experiments usually need higher concentration solutions due to the lower flux of the technique. This fact allows the micellar interactions to be probed, but also introduces complications, as structure factors (which provide information about micellar interactions) are described by somewhat complicated expressions. Therefore, in order to extract the maximum amount of useful information from the data,

modelling techniques must be used. There are a variety of models that can be employed, many of which have been reviewed by Pedersen and Svaneborg,[41] and Castelletto and Hamley.[42]

In this instance, it is the core-shell model described by Ottewill[43] and introduced in chapter two that forms the basis of the analysis of the form factor. For the structure factor, two possible models will be considered; that of a hard sphere based on Perkus-Yevick[44-46] theory, and the mean spherical approximation due to Hayter and Penfold.[47]

3.4.2. Dilute dispersions

It was not possible to observe sufficient scattering at c<1% and so the only data in dilute solution is that at 1%. The scattering observed for both copolymers at this concentration was quite weak, leading to a degree of uncertainty in the values obtained.

3.4.2.1. Preliminary analysis

Following correction of the scattering data for solvent and instrument effects, plots of log(I(Q)) *vs.* log(Q) for the dilute solutions were constructed in order to determine whether any cylindrical micelles were present. These are shown in figure 3.25 for 1% dispersions of both 5k and 10k hPB-hPEO.

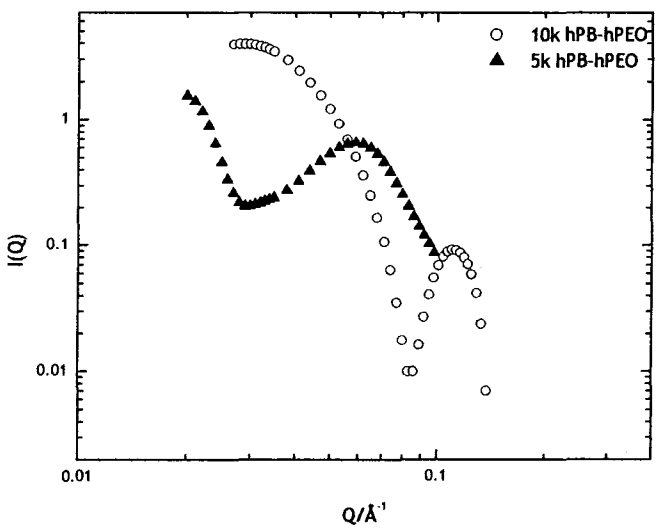

Figure 3.25 - *Log-Log plot for 5k and 10k hPB-hPEO after correcting for solvent and instrument effects*

Neither of the two scattering curves shows Q^{-1} exponents at low Q indicative of cylindrical micelles.[48, 49]

Using a Guinier approximation:[50]

$$I(Q) \approx NV^2(\Delta\rho)^2 \exp\left(-\frac{(QR)^2}{5}\right) \approx NV^2(\Delta\rho)^2 \exp\left(-\frac{(QR_g)^2}{3}\right) \qquad \textbf{Equation 3.26}$$

both the radius of gyration and the radius of a sphere can be determined from the scattering data. A plot of $\ln(I(Q))$ vs. Q^2 gives a gradient of $-R^2/5$ or $-R_g^2/3$. Figure 3.26 shows a Guinier approximation for 5k and 10k hPB-hPEO.

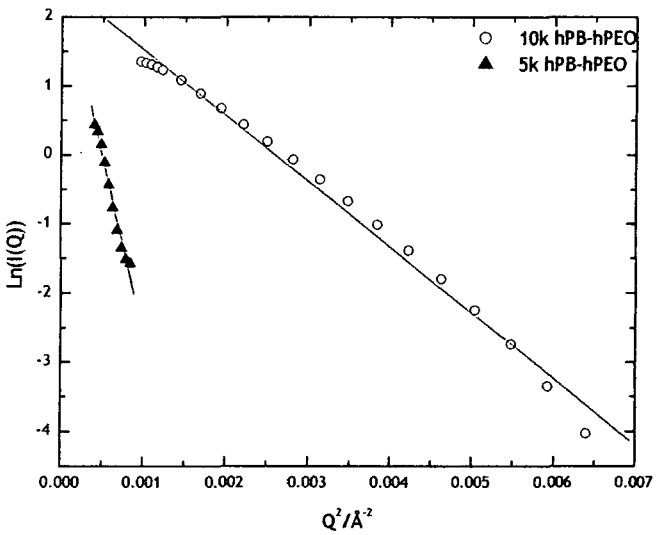

Figure 3.26 - *Guinier approximations for 5k and 10k hPB-hPEO constructed using equation 3.25. Sphere radii determined from linear fits are 70 and 160 Å respectively*

The radii determined from the linear fits to the data are 70Å and 160Å for 10k hPB-hPEO and 5k hPB-hPEO respectively. These values are somewhat different to those obtained from dynamic light scattering, with the former being smaller and the latter being larger. As stated earlier, any values obtained from these concentrations should be treated with caution due to the weak nature of the scattering.

3.4.2.2. Fitting to a core-shell model

The core-shell model was introduced in chapter two, and is shown schematically in figure 3.27

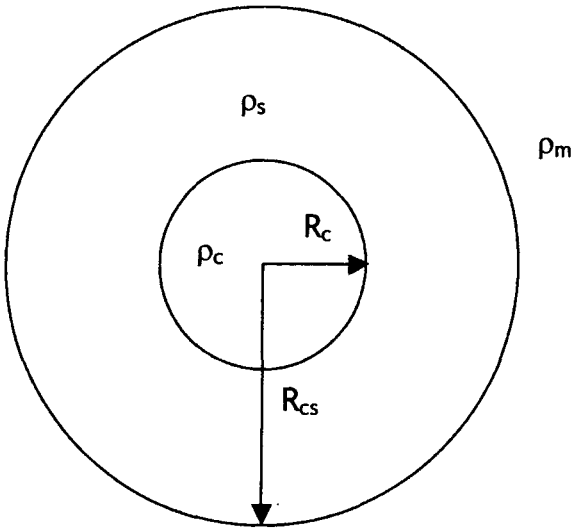

Figure 3.27 - *Schematic representation of a core-shell particle. R_c is the core radius, R_{cs} is the micelle radius, ρ is the electron density, where subscript c implies the core, s implies the shell and m the solvent.*

If it is assumed that the core consists solely of PB, and the shell is dry, then:

$\rho_c = 8.991\times10^{10}cm^{-2}$

$\rho_s = 10.291\times10^{10}cm^{-2}$

$\rho_m = 9.333\times10^{10}cm^{-2}$

If however the shell contains a percentage of water, as is suggested by the SANS data (see later section), then the value of ρ_s consists of weighted contributions from the two components namely PEO and H_2O. For this concentration the average amount of water across the entire shell, from SANS experiments, is 84%; this gives $\rho_s = 9.484\times10^{10}cm^{-2}$.

In the case of a core-shell particle, the scattering can be represented by:[49]

$$I(Q) = \frac{16\pi^2}{9} N_p P(Q) S(Q) + B \qquad \textbf{Equation 3.27}$$

where P(Q) is given by

$$\left[(\rho_s - \rho_m)\left[3R_{cs}^3 \left(\frac{\sin QR_{cs} - QR_{cs}\cos QR_{cs}}{Q^3 R_{cs}^3} \right) - \left(\frac{\sin QR_c - QR_c \cos QR_c}{Q^3 R_c^3} \right) \right] + (\rho_c - \rho_m) 3R_c^3 \left(\frac{\sin QR_c - QR_c \cos QR_c}{Q^3 R_c^3} \right) \right]^2 \qquad \textbf{Equation 3.28}$$

Dr Richard Heenan's FISH2 analysis software[51] was used to fit the experimental data. The core-shell model used consists of nine parameters that are detailed in table 3.13

Parameter	Definition
ρ_c-ρ_s	Electron density difference between core and shell
R_c	Core radius
ρ_s-ρ_m	Electron density difference between shell and solvent
R_{cs}	Total micelle radius
R_s	Shell thickness
Scale	Scaling parameters based upon volume fraction
$\overline{R}$	Average core radius (see below)
$\sigma/\overline{R}$	Standard deviation of Schultz distribution (see below)
Background	Flat background added to data

Table 3.13 - *Parameters used in the core-shell model utilised by the FISH2 software.*

The parameters $\overline{R}$ and $\sigma/\overline{R}$ relate to a Schultz distribution used to allow for micelle polydispersity. The Schultz distribution due to Kotlarchyk and Chen[52] can be represented by:

$$f_s(R) = \left(\frac{Z+1}{\overline{R}}\right)^{Z+1} R^Z \exp\left[-\left(\frac{Z+1}{\overline{R}}\right)R\right] \Big/ \Gamma(Z+1) \qquad \textbf{Equation 3.29}$$

Z is a width parameter computed by the software.

The standard deviation, σ, of the distribution is given by:

$$\sigma = \frac{\overline{R}}{(Z+1)^{1/2}} \qquad \textbf{Equation 3.30}$$

During the fitting all of the parameters listed in table 3.13 were varied, with the exception of the two electron density differences, as allowing these to vary produced unrealistic values for them in the final fitted parameters.

Figure 3.28 shows the fits obtained for 5k and 10k hPB-hPEO using the dry value of the shell electron density, both in linear, and semi-logarithmic form, with the parameters obtained given in table 3.14.

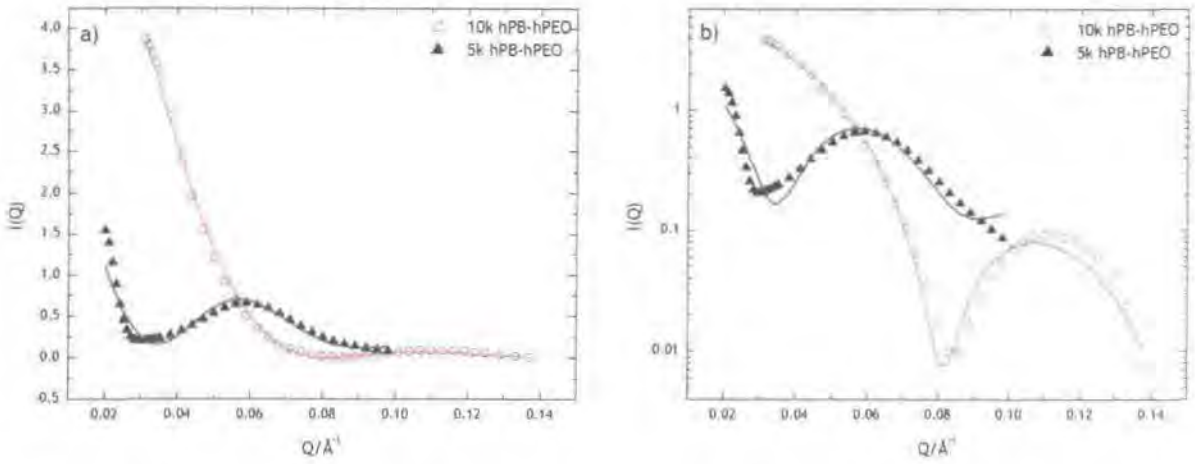

Figure 3.28 - *Fits obtained to 1% dispersion data for 5k and 10k hPB-hPEO using the FISH2 software program. a) shows a linear intensity scale, and b) shows a logarithmic intensity scale. Lines are fits to the data*

Parameter	10k hPB-hPEO	5k hPB-hPEO
R_c/Å	13.5	59.6
R_{cs}/Å	53.5	72.1
R_s/Å	40	12.4
σ/R	0.121	0.131

Table 3.14 - *Parameters obtained from fits to 5k and 10k hPB-hPEO, shown in figure 3.28, using the core-shell model*

The micelle radii obtained from these fits are somewhat smaller than those from the light scattering studies, although the shell thickness for 5k hPB-hPEO is somewhat questionable in relation to the value of the core given the composition of the copolymer. As mentioned earlier the shell is likely to be wet, containing a percentage of water. Attempts were made to fit the data with varying the volume fraction of water, ϕ_w, in the shell. This was achieved by altering the electron density differences detailed in table 3.13.

Table 3.15 gives the parameters obtained for different water contents in the shell, along with the respective electron density differences.

Copolymer	ϕ_w	ρ_c-ρ_s	ρ_s-ρ_m	R_c/Å	R_{cs}/Å	R_s/Å	σ/R
10k hPB-hPEO	0.5	-0.821	0.479	8.69	53.95	45.26	0.262
5k hPB-hPEO				54.52	76.05	21.48	0.141
10k hPB-hPEO	0.6	-0.7252	0.3832	9.30	53.92	44.61	0.256
5k hPB-hPEO				52.43	77.31	24.88	0.144
10k hPB-hPEO	0.7	-0.6294	0.291	36.42	115.56	79.14	0.572
5k hPB-hPEO				49.68	78.81	29.13	0.149
10k hPB-hPEO	0.8	-0.5336	0.1916	37.63	116.12	78.48	0.575
5k hPB-hPEO				44.84	81.10	36.26	0.158
10k hPB-hPEO	0.84	-0.493	0.151	33.84	113.59	79.74	0.607
5k hPB-hPEO				42.11	82.40	40.29	0.162

Table 3.15 - *Parameters obtained from fits to 5k and 10k hPB-hPEO using the core-shell model, by varying the volume fraction of water, ϕ_w in the shell.*

Figure 3.29 shows the fits generated in semi-logarithmic form.

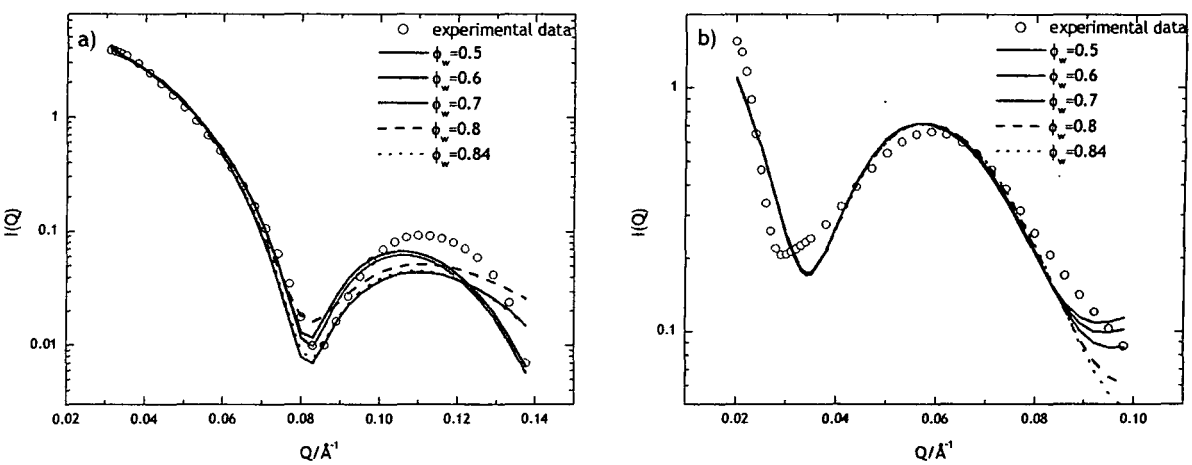

Figure 3.29 - *Fits to 10k hPB-hPEO a) and 5k hPB-hPEO b) generated using the core shell model with varying volume fractions of water, ϕ_w, in the shell. Lines are fits to the data.*

As is quite evident from table 3.15 and figure 3.29 the fits are not of a particularly good quality, with the values obtained varying considerably depending upon the ϕ_w value used.

The electron densities of the three components in this system are quite similar, and therefore the contrast is small. It may not be possible to distinguish between the core and the shell of the micelle because of this, especially if the shell contains quite a large volume fraction of water, as this reduces the contrast further.

For this reason it was decided to fit the data to a uniform sphere model.

3.4.2.3. Fitting to a uniform sphere model

The sphere model used was similar to the core-shell model in that it used a Schultz distribution to account for polydispersity in micelle size, only this time it was for the entire micelle, as opposed to the core. The parameters remain much the same except the contrast factor forms part of the scaling parameter, and the core radius is no longer present.

Figure 3.30 shows the fit generated using this model for the 10k 1% dispersion, again in linear and semi-logarithmic form.

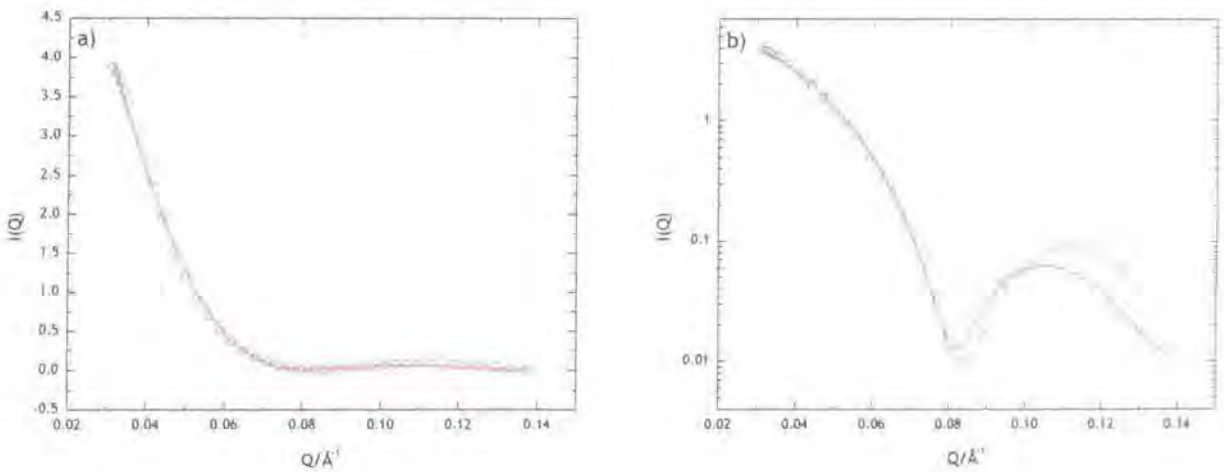

Figure 3.30 - *10k hPB-hPEO fitted to a simple sphere model. a) Shows a linear intensity scale, whilst b) shows a logarithmic intensity scale*

The fit shown in figure 3.30 suggests a micellar radius of 55Å. This is somewhat smaller than the values suggested by light scattering. It is evident from figure 3.30 that the uniform sphere model does not fit the data adequately enough, and so its use was not pursued further.

Because of the lack of SAXS contrast and weak scattering intensity, the 1% dispersions of the two copolymers reveal little in terms of the micelle dimensions. Fits to the data suggest they are spherical core-shell particles that are approximately 150-200Å in diameter.

3.4.3. Higher Concentration dispersions

When a scattering system is sufficiently dilute, or there is no long-range ordering between the particles, then $S(Q)=1$, and the features of the scattering are determined by P(Q). As the concentration increases, so does the number of scattering particles and usually the degree of order in the system. Under these conditions $S(Q)\neq 1$, and the scattering pattern becomes more complex.

Two methods of modelling S(Q) were explored here, the first of which, based on a hard-sphere potential,[44-46] was introduced in chapter two. The second uses the mean spherical approximation of Hayter and Penfold.[47]

3.4.3.1. Hard-sphere potential[44-46]

A hard-sphere potential is the simplest form of interaction between particles. At a certain distance of separation, the energy of interaction rises steeply to infinity, as shown in figure 3.31.

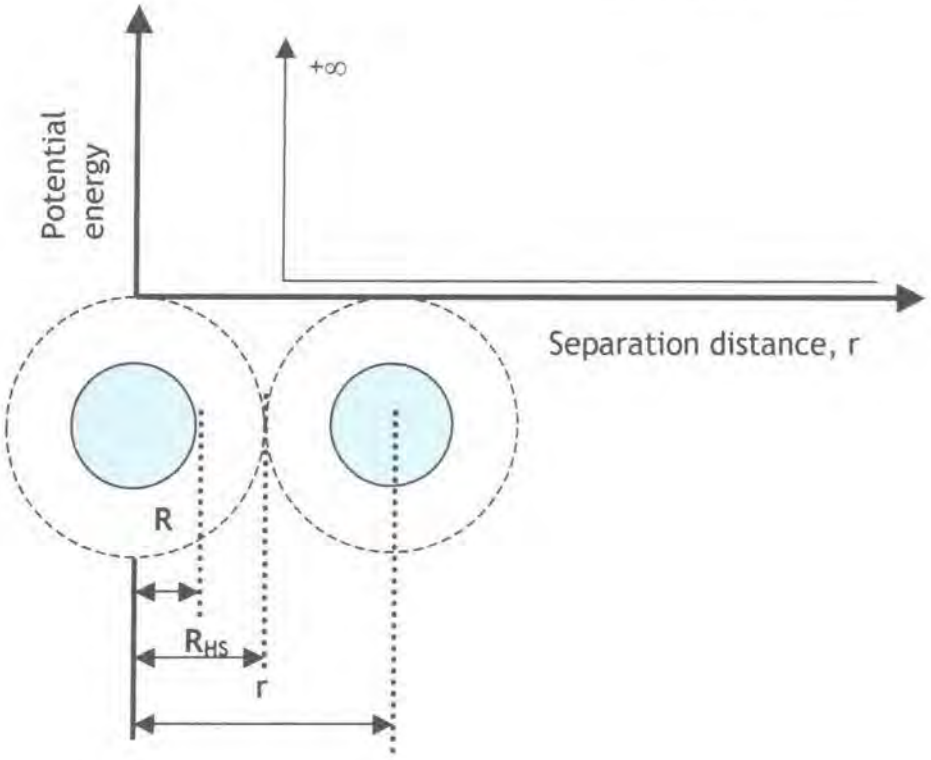

Figure 3.31 - *schematic representation of a hard-sphere interaction potential between two spheres. R is sphere radius, R_{HS} is the hard sphere radius.*

This distance, r, can be defined as $2R_{hs}$, where R_{hs} is the effective hard sphere radius. Generally $R_{hs}>R$.

The hard sphere volume fraction, η, is:

$$\eta = \frac{\frac{4}{3}\pi R_{hs}^3 N_p}{V} \qquad \textbf{Equation 3.31}$$

where V is the total volume of the system and N_p is the number of particles in the system.

The structure factor is then given by equation 3.30

$$S(Q) = \frac{1}{1 + 24\eta\left(G(2QR)/2QR\right)} \qquad \textbf{Equation 3.32}$$

where

$$G(2QR)=\frac{\alpha}{(2QR)^2}(\sin 2QR-2QR\cos 2QR)+\frac{\beta}{(2QR)^3}(2\cdot 2QR\sin 2QR+(2-(2QR)^2)\cos 2QR-2$$

$$+\frac{\gamma}{(2QR)^5}(-(2QR)^4\cos 2QR+4[(3\cdot(2QR)^2-6)\cos 2QR+((2QR)^3-6\cdot 2QR)\sin 2QR+6])$$

Equation 3.33

α, β, and γ are functions of the hard sphere volume fraction given by:

$$\alpha=\frac{(1+2\eta)^2}{(1-\eta)^4}$$ **Equation 3.34**

$$\beta=-\frac{6\eta\left(1+\eta_2\right)^2}{(1-\eta)^4}$$ **Equation 3.35**

$$\gamma=\frac{\eta_2(1+2\eta)^2}{(1-\eta)^4}$$ **Equation 3.36**

Figure 3.32 shows a typical fit generated using a core-shell model for the particle form factor, with a hard-sphere potential effective between micelles. It is evident from the figure that the hard-sphere potential does not describe adequately the structure observed in the data. For this reason it was decided not to pursue the use of the hard sphere model any further, either for the SAXS or the SANS data, and concentrate instead on the mean spherical approximation.

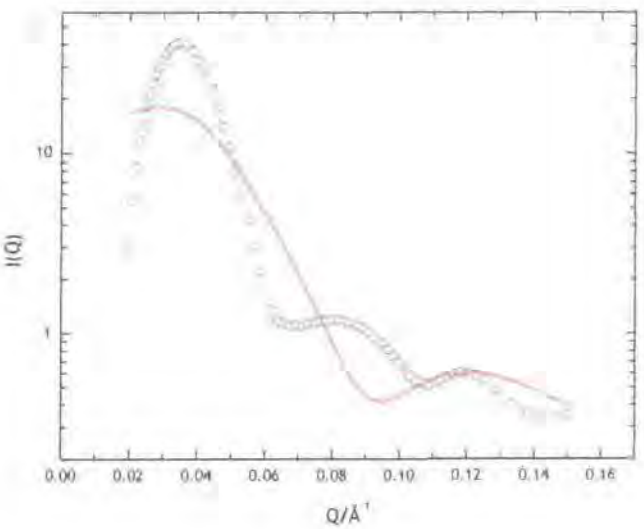

Figure 3.32 - *Fit to a 10% dispersion of 10k hPB-hPEO using a hard-sphere potential to describe the structure factor*

3.4.3.2. Mean Spherical Approximation[47]

The mean spherical approximation was developed for charged particles in solution but has been successfully applied to non-ionic species.[53, 54]

The repulsive potential between two identical spherical macroions of diameter, σ, is given by:

$$U(r) = \frac{\pi\varepsilon_0\varepsilon\sigma^2\psi_0^2 \exp[-\kappa(r-\sigma)]}{r} \quad \text{Equation 3.37}$$

where ε_0 is the permitivity of free space, ε is the solvent relative permitivity, ψ_0 is the surface potential, κ is the Debye-Hückel inverse screening length and r is the macroion centre-to-centre distance.

The surface potential, ψ_0, can be related to the electronic charge, z_m, of the macroion by:

$$\psi_0 = \frac{z_m}{\pi\varepsilon_0\varepsilon\sigma(2+\kappa\sigma)} \quad \text{Equation 3.38}$$

Defining $x = r/\sigma$, $k = \kappa\sigma$, and $K = Q\sigma$ equation 3.37 can be expressed in dimensionless units as:

$$\beta U(x) = \frac{\gamma \exp(-kx)}{x} \qquad x > 1 \quad \text{Equation 3.39}$$

where $\beta = 1/k_B T$, and $\gamma \exp(-k) = \beta\pi\varepsilon_0\varepsilon\sigma\psi_0^2$ Equation 3.40

is the contact potential for a macroion pair in units of $k_B T$.

The particle volume fraction, η, is given by:

$$\eta = \frac{\pi n\sigma^3}{6} \quad \text{Equation 3.41}$$

The structure factor can then be expressed in closed analytic form as:

$$S(Q\sigma) = \frac{1}{1-24\eta a(2Q\sigma)} \quad \text{Equation 3.42}$$

where a(2Qσ) is a complex trigonometrical expansion, given in Appendix A.

Attempts were made to fit the data using the mean spherical approximation, and typical fits can be seen in figures 3.33 to 3.36, with the associated parameters given in tables 3.16 and 3.17.

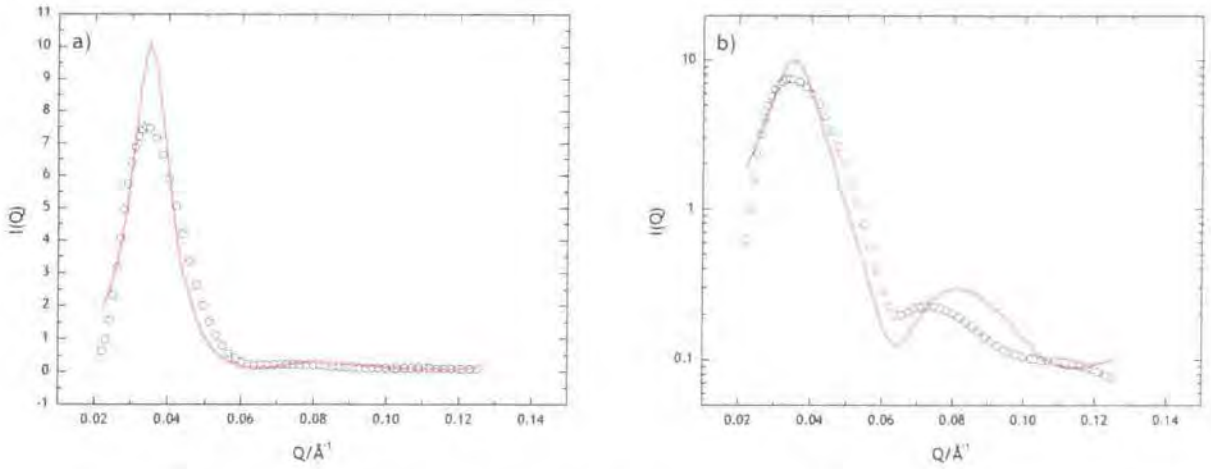

Figure 3.33 - *SAXS from a 2% dispersion of 10k hPB-hPEO. a) shows a linear cross-section and b) a logarithmic scale. Red lines are fits to the data.*

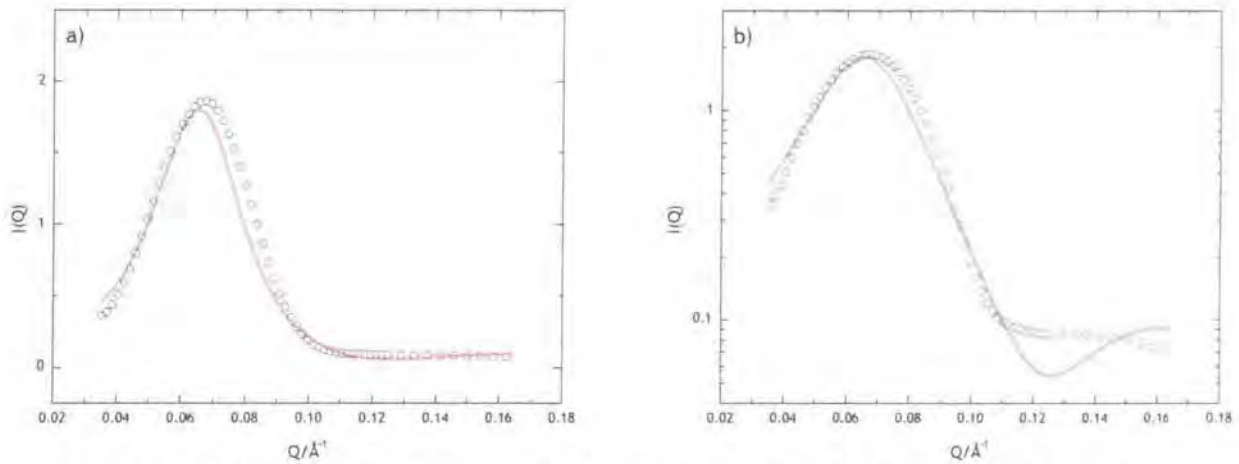

Figure 3.34 - *SAXS from a 4% dispersion of 5k hPB-hPEO. a) Shows a linear cross-section and b) a logarithmic scale. Red lines are fits to the data*

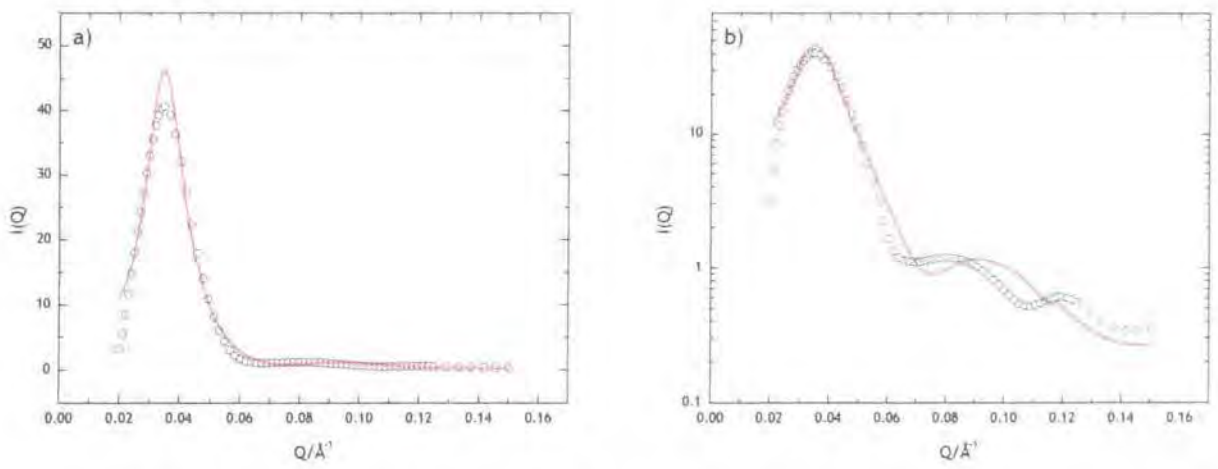

Figure 3.35 - *SAXS from a 10% dispersion of 10k hPB-hPEO. a) shows a linear cross-section and b) a logarithmic scale. Red lines are fits to the data*

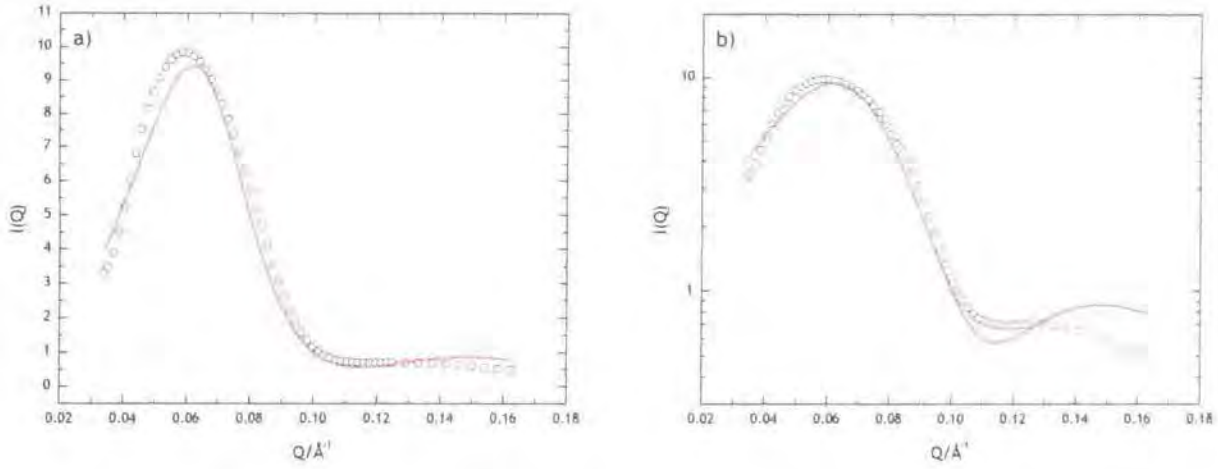

Figure 3.36 - *SAXS from a 15% dispersion of 5k hPB-hPEO. a) shows a linear cross-section and b) a logarithmic scale. Red lines are fits to the data*

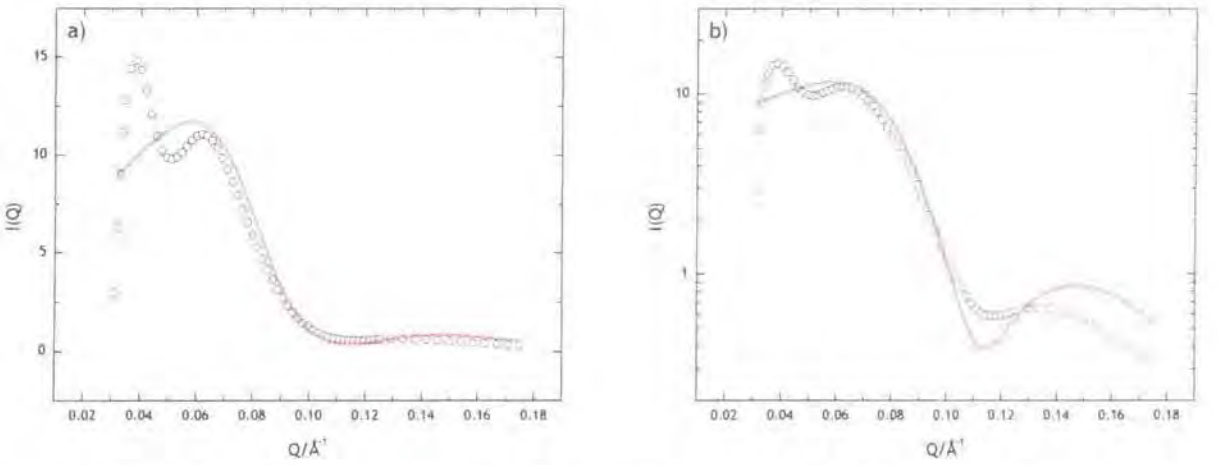

Figure 3.37 - *SAXS from a 20% dispersion of 5k hPB-hPEO. a) shows a linear cross-section and b) a logarithmic scale. Red lines are fits to the data*

Parameter	10%	8%	4%	2%
R_c/Å	15	16	13	11
R_s/Å	43	43	48	59
σ/R	0.397	0.246	0.250	0.350
H-P S(Q) R/Å	53.83	49.94	39.29	31.16
Charge	20.82	20.85	22.35	25.54
κ/Å^{-1}	2.159×10^{-3}	3.025×10^{-3}	6.365×10^{-3}	2.998×10^{-3}
γ	29.123	31.742	47.915	75.382
$\gamma\exp(-k)$	23.083	23.465	29.057	62.539

Table 3.16 - *Parameters from fits to dispersions of 10k hPB-hPEO using a core-shell model with the mean spherical approximation to model the structure factor*

Parameter	20%	15%	10%	8%	4%	2%
R_c/Å	5	6	6	6	6	6
R_s/Å	34	33	32	30	30	25
σ/R	0.126	0.219	0.225	0.224	0.25	0.25
H-P S(Q) R/Å	31.58	30.50	27.77	25.54	20.88	17.81
Charge	7.80	10.00	11.44	12.41	15.60	15.60
κ/Å^{-1}	4.000×10^{-2}	7.505×10^{-3}	3.615×10^{-3}	1.000×10^{-3}	1.907×10^{-2}	1.907×10^{-2}
γ	16.803	12.256	16.992	21.551	47.218	53.638
$\gamma\exp(-k)$	1.343	7.754	13.901	20.477	21.294	27.194

Table 3.17 - *Parameters from fits to dispersions of 5k hPB-hPEO using a core-shell model with the mean spherical approximation to model the structure factor*

The fits shown in figures 3.33 to 3.37 are a considerable improvement over those generated using the hard-sphere potential to model the structure factor, but still do not capture all the features seen in the data. As observed

with the 1% dispersions, the micellar dimensions are somewhat smaller than those observed by light scattering, likely due to the lack of SAXS contrast. Consequently, information extracted from the fits should be treated with caution, and perhaps assessed as qualitative rather than quantitative.

Particularly noteworthy is the shape of the scattering for the 20% dispersion of 5k hPB-hPEO. The structure factor peak appears to have two separate contributions, possibly due to a higher degree of ordering than the liquid-like structure observed at the lower concentrations.

3.4.4. Conclusions

The lack of SAXS contrast between the different components of the scattering system hampered attempts to extract quantitative information about the size and interactions between micelles both in dilute and more concentrated dispersions where the interactions are more prevalent. The scattering in the dilute regime was weak and the lowest concentration accessible was ca 1%. Consequently, fitting the data to suitable models proved troublesome.

For clarity, the main conclusions that can be inferred from the data are presented here.

- Micelle dimensions obtained from fits to a core-shell model at low concentration for 10k hPB-hPEO suggest a core radius of ca 14Å surrounded by a shell with a thickness of ca 40Å. This suggests a micelle radius of 54Å, which is smaller than that observed by QELS and that predicted by theory.
- The quality of the dilute dispersion data for 5k hPB-hPEO was poor due to the weak scattering, and so it was not possible to fit the data adequately to any model.
- A hard-sphere potential proved inadequate to model the structure factor for the more concentrated dispersions.
- The mean spherical approximation was used to model the structure factor for the concentrated dispersions with many but not all of the features in the data being captured.
- Higher concentration dispersions suggest a core radius of 13Å and a shell thickness of ca 50Å for 10k hPB-hPEO, whilst the data for 5k hPB-hPEO suggests a core radius of 6Å and a shell thickness of ca 30Å.

- For a 20% dispersion of 5k hPB-hPEO there appear to be two contributions towards the structure factor peak, which is possibly due to a change in the type of ordering in the system.
- Micelle interactions could not be determined quantitatively due to the uncertainty in the fits to the data.

3.5. Small-Angle Neutron Scattering

3.5.1. Introduction

In common with SAXS, SANS provides a powerful tool for probing micellar structure and determining intermicellar interactions at higher concentrations. Unlike SAXS however the information is gleaned *via* isotopic variation, namely exchanging deuterium for hydrogen as discussed in chapter two. The contrast in a typical SANS experiment, even one in which the scattering is due to the entire molecule far exceeds that accessible in SAXS enabling more detailed information with respect to micellar structure to be obtained. The information is yielded much in the same manner as for SAXS data, by fitting to a suitable model.

3.5.2. Dilute dispersions

3.5.2.1. Preliminary treatment

In common with the SAXS data, Log-Log plots of the dilute solutions showed no Q^{-1} dependencies associated with cylindrical micelles.[48] Typical plots for 1% dispersions of both molecular weights, for all three contrasts are shown in figure 3.38.

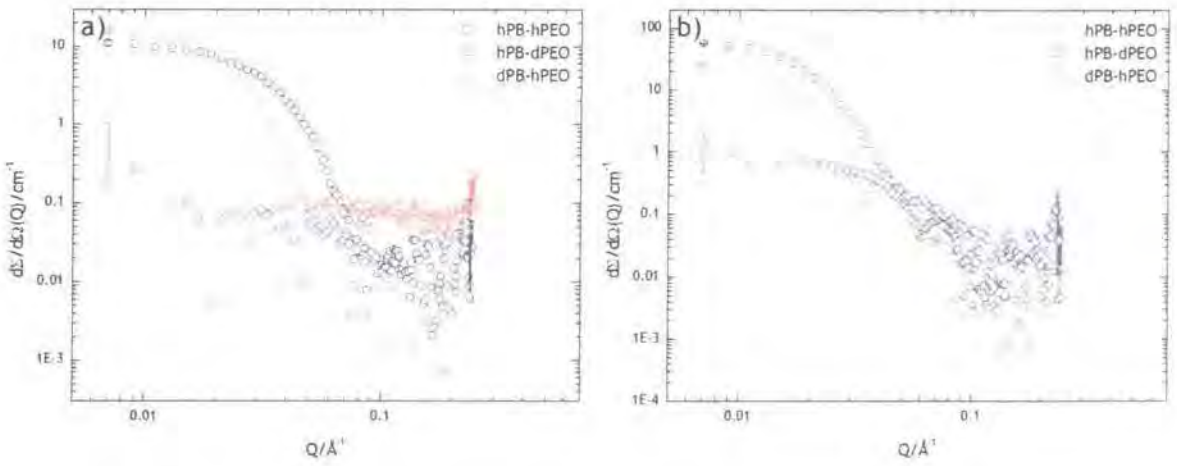

Figure 3.38 - *double logarithmic plots for a) 5k and b) 10k dispersions. Examples of error bars indicating their magnitude at the extremes of the data are shown for clarity.*

The Guinier approximation was applied to the dilute solution data.[50] Typical plots are shown in figure 3.39 again for both copolymers and all three contrasts, with the respective results obtained detailed in table 3.18.

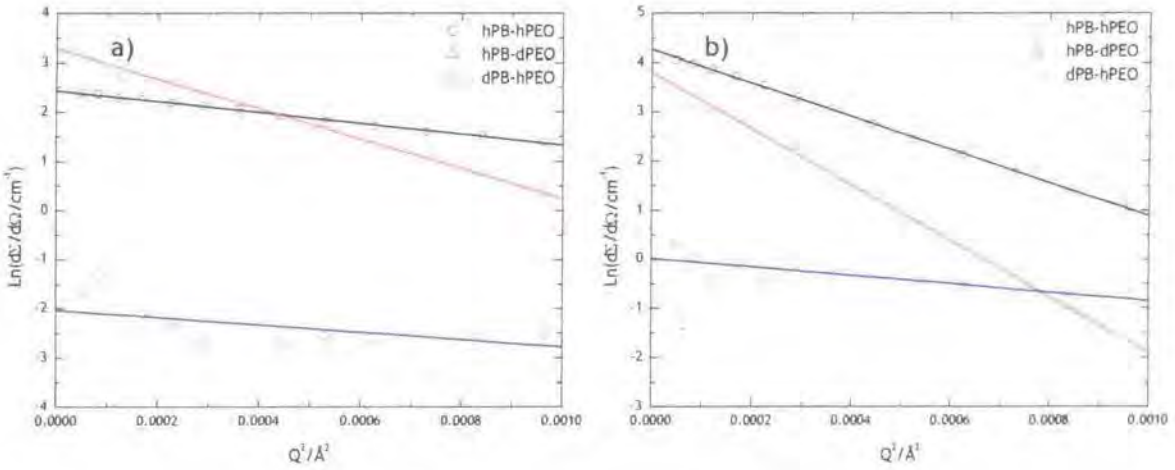

Figure 3.39 - *Guinier plots for 1% dispersions of a) 5k and b) 10k generated using equation 3.24. Lines are linear fits to the data*

Conc/%	Sphere Radius/Å					
	hPB-hPEO		hPB-dPEO		dPB-hPEO	
	5k	10k	5k	10k	5k	10k
0.2	76	132	126	161	n/a	56
0.4	74	131	125	173	n/a	65
0.6	77	130	120	168	48	60
1	74	130	123	169	61	66

Table 3.18 - *radii determined from slopes of the linear fits to Guinier plots of the type shown in figure 3.41 for 5k and 10k dispersions at c≤1%. The part of micelle scattering neutrons is highlighted in bold.*

It can be seen from table 3.18, that there are differences between the micelle radii determined for the fully hydrogenous polymer and those for the deuterated shell polymer for both molecular weights. These are likely due to the difference in the molecular weights of the copolymers and to the different weightings given by the contrasts factors to the individual from factors in equation 3.27.

3.5.2.2. Fitting to a core-shell model

The greater degree of contrast available in SANS enabled the use of slightly more sophisticated models to fit the data. For the SAXS data the polymer volume fraction in the shell was assumed to be uniform across its entire width. Polymer brush theory discussed in chapter one suggests this is not the case,[55] with a decrease in volume fraction with increasing distance from the core-shell interface being predicted. This was taken into account in the models utilised.

The core was assumed to consist exclusively of PB, and to be of uniform density. The volume fraction of PEO in the corona was modelled by a series of six linear steps approximating to a parabolic profile. As a result, the corona was essentially split into six sub-shells, each having a local concentration profile of PEO. Figure 3.40 shows the variation of the neutron scattering length density with distance from the micelle core for each of the contrasts used.

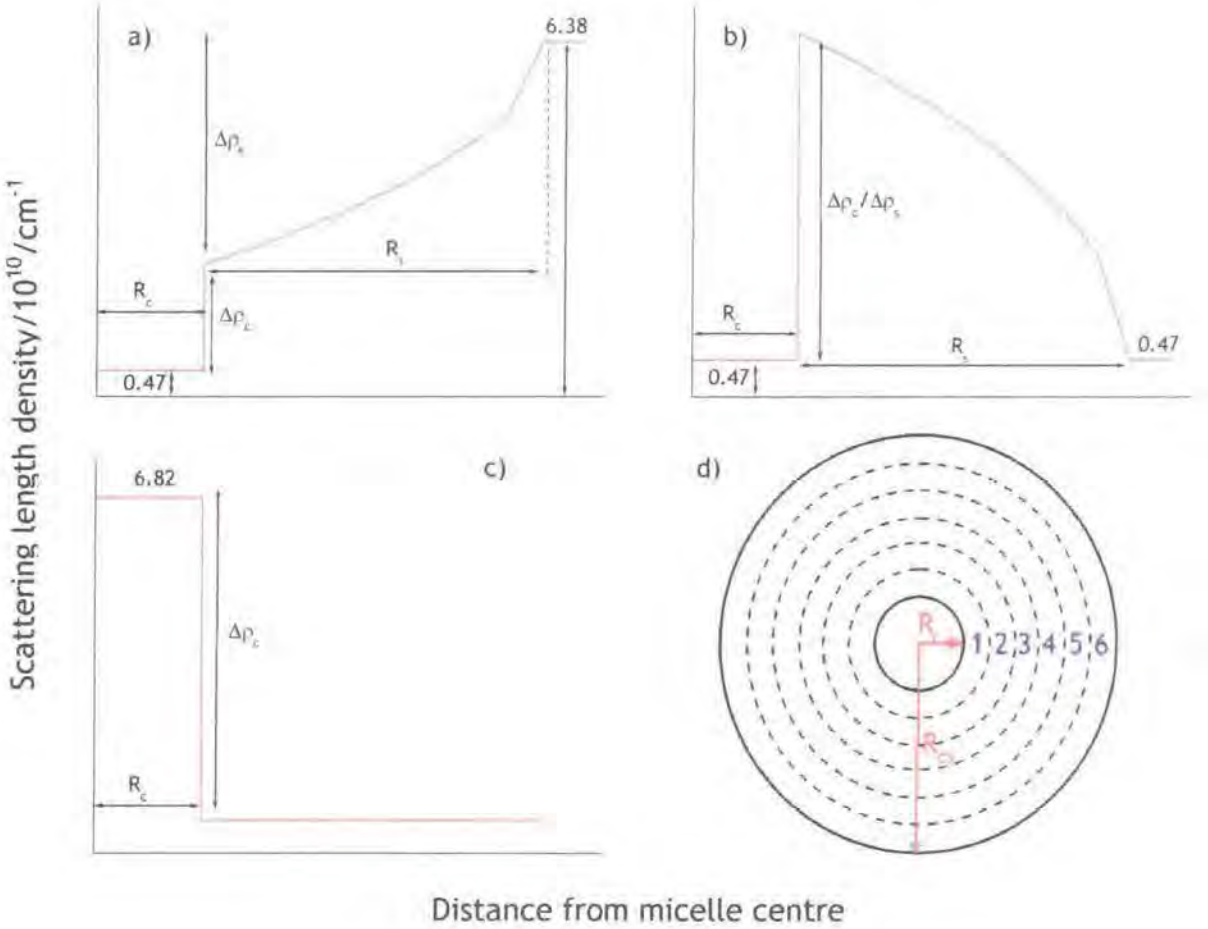

Figure 3.40 - *Schematic representations of the scattering length density distributions used in the core model to fit dilute dispersions. a) hPB-hPEO in D_2O, b) hPB-dPEO in hPB contrast match H_2O, c) dPB-hPEO in hPEO contrast match H_2O, d) representation of the core shell model.*

With the exception of the varying scattering length density, the model was much the same as that used to fit the SAXS data. A Schultz distribution[52] was incorporated into the core radius to account for any micelle polydispersity and the adjustable parameters were much the same as those detailed in table 3.13. However, the scattering length density differences at the core-corona interface $\Delta\rho_c$, and that across the shell $\Delta\rho_s$, were not allowed to vary whilst fitting the data. They were fixed at values corresponding to a given water volume fraction, ϕ_w in the innermost sub-shell of the corona (number 1 in figure 3.40 d)). The reason being that allowing these parameters to vary during fitting returned unrealistic values for them. Different values of ϕ_w

were explored for all of the data fitted and the optimum values chosen based upon the quality of the fits.

Figures 3.41 to 3.43 show representative fits for the different contrasts and concentrations explored for the two molecular weights, with the parameters from all of the fits for the dilute dispersions given in tables 3.19 and 3.20.

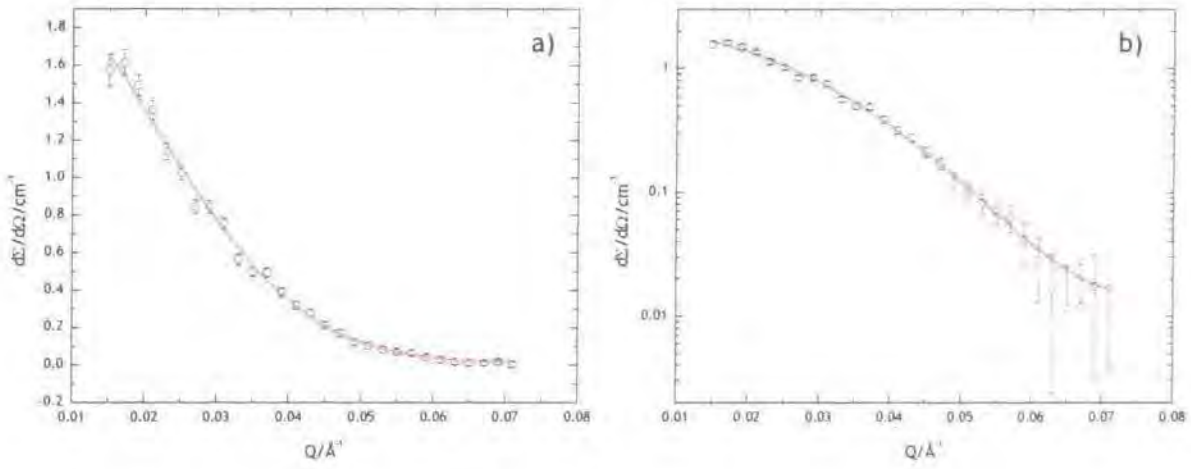

Figure 3.41 - *0.2% dispersion of 5k hPB-hPEO in D_2O. a) linear scale, b) semi-logarithmic. Red lines are fits to the data.*

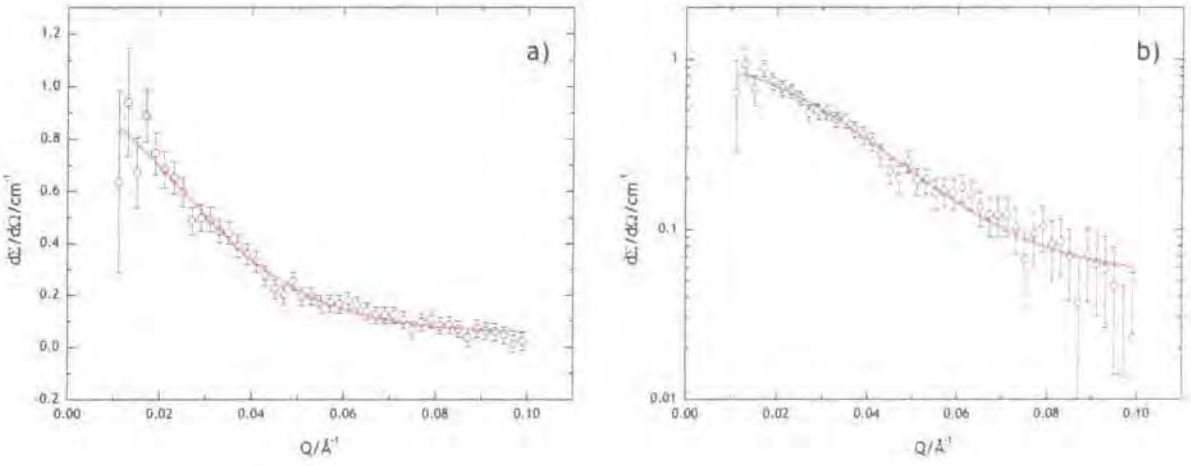

Figure 3.42 - *1% dispersion of 10k dPB-hPEO in hPEO contrast match H_2O. a) linear scale, b) semi-logarithmic. Red lines are fits to the data.*

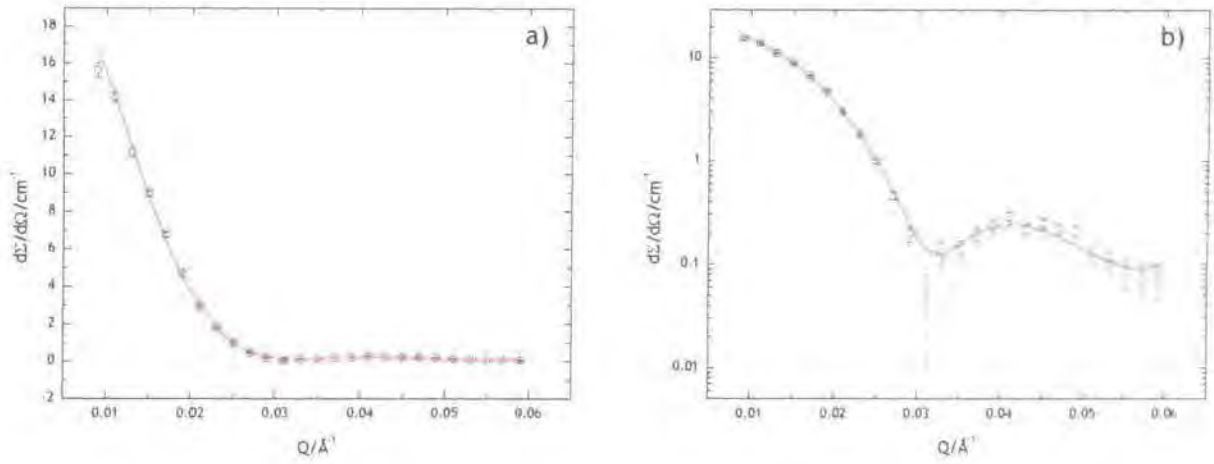

Figure 3.43 - *0.6% dispersion of 10k hPB-dPEO in hPB contrast match H_2O. a) linear scale, b) semi-logarithmic Red lines are fits to the data.*

Copolymer	Conc/%	R_cÅ	R_sÅ	$\Delta\rho_c/10^{10}cm^{-2}$	$\Delta\rho_s/10^{10}cm^{-2}$	σ/R	ϕ_w
hPB-hPEO	0.2	21	67	-5.049	-0.861	0.225	0.85
	0.4	19	62	-4.877	-1.033	0.463	0.82
	0.6	19	59	-4.762	-1.148	0.502	0.8
	1.0	20	58	-4.590	-1.320	0.468	0.77
hPB-dPEO	0.2	24	97	-0.898	0.898	0.371	0.85
	0.4	24	96	-1.078	1.078	0.456	0.82
	0.6	25	93	-1.198	1.198	0.465	0.80
	1.0	25	91	-1.198	1.198	0.455	0.80
dPB-hPEO	0.2						
	0.4			Scattering too weak to fit			
	0.6						
	1.0	27	-	6.180	0	0.009	-

Table 3.19 - *Parameters obtained from 5k dispersions fitted to the core model shown in figure 3.40, using FISH 2with the parameters as detailed therein.*

Copolymer	Conc/%	R_cÅ	R_sÅ	$\Delta\rho_c/10^{10}cm^{-2}$	$\Delta\rho_s/10^{10}cm^{-2}$	σ/R	ϕ_w
hPB-hPEO	0.2	35	115	-5.049	-0.861	0.1	0.85
	0.4	40	108	-4.877	-1.033	0.35	0.82
	0.6	39	112	-4.475	-1.435	0.35	0.80
	1.0	38	113	-4.647	-1.263	0.36	0.78
hPB-dPEO	0.2	40	118	-0.899	0.899	0.15	0.85
	0.4	44	110	-1.078	1.078	0.15	0.82
	0.6	42	113	-1.198	1.198	0.17	0.80
	1.0	45	107	-1.318	1.318	0.2	0.78
dPB-hPEO	0.2	46	-	6.18	-	0.2	-
	0.4	46	-	6.18	-	0.2	-
	0.6	47	-	6.18	-	0.2	-
	1.0	45	-	6.18	-	0.2	-

Table 3.20 - *Parameters obtained from 10k dispersions fitted to the core model shown in figure 3.40, using FISH 2with the parameters as detailed therein.*

From tables 3.19 and 3.20 it is evident that the total micelle radius for the 5k series is of the between 80 and 120Å, with the core radius being circa 25Å. The former is slightly smaller than the value of 136Å determined by QELS measurements in section 3.2.2, but is in reasonable agreement. The 10k series shows a micelle radius of 150Å, again slightly smaller than the value of 168Å from QELS measurements but still with reasonable agreement, whilst a core radius of circa 40Å is observed.

The goodness of the fits obtained using FISH was assessed using intensity calculations. The volume fractions of PB and PEO from any given fit can be calculated and compared to the values expected from the original composition and concentration. The closeness of these values provides an indication as to the goodness of fit. Table 3.21 details the results of such calculations for the fits on the dilute solutions.

Polymer	Conc/%	ϕPB^a	ϕPB^b	ϕPEO^a	ϕPEO^b
5k hPB-hPEO	0.2	0.00041	0.00040	0.00189	0.00146
	0.4	0.00072	0.00080	0.00290	0.00292
	0.6	0.00088	0.00120	0.00346	0.00438
	1	0.00160	0.00199	0.00693	0.00729
5k hPB-dPEO	0.2	0.00026	0.00031	0.00179	0.00153
	0.4	0.00045	0.00063	0.00293	0.00305
	0.6	0.00112	0.00094	0.00424	0.00458
	1	0.00156	0.00157	0.00958	0.00763
5k dPB-hPEO	1	0.00104	0.00115	-	-
10k hPB-hPEO	0.2	0.00051	0.00036	0.00295	0.00149
	0.4	0.00099	0.00071	0.00341	0.00299
	0.6	0.00129	0.00107	0.00561	0.00448
	1	0.00185	0.00178	0.00868	0.00747
10k hPB-dPEO	0.2	0.00040	0.00048	0.00178	0.00139
	0.4	0.00085	0.00097	0.00323	0.00278
	0.6	0.00137	0.00145	0.00814	0.00834
	1	0.00243	0.00242	0.00572	0.00695
10k dPB-hPEO	0.2	0.00026	0.00027	-	-
	0.4	0.00053	0.00055	-	-
	0.6	0.00079	0.00082	-	-
	1	0.00135	0.00137	-	-

Table 3.21 - *Comparison of calculated [a] and experimental [b] volume fractions from dilute dispersions of the two molecular weight series*

It is evident from the values in table 3.21 that the observed and calculated volume fractions are in good agreement suggesting that the fits are acceptable in terms of the parameters they give.

The unperturbed radius of gyration, R_g, of a PEO chain in water at 298K can be calculated using equation 3.42.[56]

$$R_g = \left(4.08 \times 10^{-18} M_w^{1.1}\right)^{1/2}$$ **Equation 3.43**

Table 3.22 details the values calculated for the copolymers used here.

Isotopic variation	M_w PEO/gmol^{-1}	R_g PEO/Å
5k hPB-hPEO	3590	23
5k hPB-dPEO	4295	26
5k dPB-hPEO	5790	30
5k hPB-hPEO	7610	36
5k hPB-dPEO	4340	26
5k dPB-hPEO	9230	40

Table 3.22 - *Unperturbed radii of gyration of PEO blocks in copolymers calculated using equation 3.42*

The number of copolymer chains in a micelle, the association number, p, can be calculated using equation 3.43,[4] assuming that the core consists solely of PB.

$$p = \frac{4/3 \pi R_c^3}{V_{PB}}$$ **Equation 3.44**

where V_{PB} is the volume of the poly(butadiene) block given by:[4]

$$V_{PB} = \frac{m_{PB}}{N_A \rho_{PB}}$$ **Equation 3.45**

m_{PB} is the molecular weight of the polybutadiene block, ρ_{PB} is the density of poly(butadiene),[35] 0.964 gcm^{-3} and N_A is Avogadro's number.

The distance between PEO chains on the core surface, D_{PEO}, can be calculated using equation 3.45:[54]

$$D_{PEO} = \left(\frac{4\pi R_c^2}{p}\right)^{\frac{1}{2}}$$ **Equation 3.46**

Tables 3.23 and 3.24 give the values of the association number, the separation distance of the PEO chains on the core surface, and the ratio of the shell thickness to the unperturbed radius of gyration, R_s:R_g, for both copolymer series.

Copolymer	Conc/%	p	D_{PEO}/Å	R_s:R_g
hPB-hPEO	0.2	27	14.39	2.88
	0.4	20	15.13	2.66
	0.6	20	15.13	2.53
	1.0	23	14.75	2.49
hPB-dPEO	0.2	40	13.44	3.75
	0.4	40	13.44	3.71
	0.6	45	13.17	3.60
	1.0	45	13.17	3.52
dPB-hPEO	1.0	74	-	-

Table 3.23 - *Values of association number, p, distance between PEO chains on the core surface D_{PEO}, and the ratio of the shell thickness to the unperturbed radius of gyration R_s:R_g for dilute dispersions of the 5k series.*

Copolymer	Conc/%	p	D_{PEO}/Å	R_s:R_g
hPB-hPEO	0.2	71	14.73	3.17
	0.4	106	13.78	2.98
	0.6	98	13.96	3.09
	1.0	91	14.14	3.12
hPB-dPEO	0.2	130	12.45	4.48
	0.4	173	11.87	4.18
	0.6	150	12.15	4.29
	1.0	185	11.74	4.06
dPB-hPEO	0.2	213	-	-
	0.4	213	-	-
	0.6	227	-	-
	1.0	200	-	-

Table 3.24 - *Values of association number, p, distance between PEO chains on the core surface D_{PEO}, and the ratio of the shell thickness to the unperturbed radius of gyration R_s:R_g for dilute dispersions of the 10k series.*

The micelles of the two molecular weight series show quite contrasting association behaviour. The lower molecular weight series form micelles of modest association number ($p \geq 50$ is considered large), whereas the higher molecular weight series micelles have a relatively high association numbers. The relationship between the two molecular weight series is not unexpected, since the association number is predicted to scale with the length of the insoluble block,[29, 39] but is in contrast to the relationship observed from the SLS measurements.

The ratios of the shell thickness to the unperturbed radius of gyration for both copolymers suggest that the chains in the shell are highly stretched. Those for the case where the core is contrast matched are more highly stretched than the fully hydrogenous copolymers.

The distance between the poly(ethylene oxide) chains on the surface of the core is less than the radius of gyration of chains in all instances. This lends credence to the use of a model approximating to a polymer brush.

Using the values for the molecular volumes of water and ethylene oxide given by Nagarajan and Ganesh[30] it is possible to calculate the number of water molecules associated with one ethylene oxide segment in each of the sub-shells of the corona for the different volume fractions of water associated with the change in concentration. Figure 3.44 shows a plot of the number of water molecules per ethylene oxide segment as a function of increasing distance across the shell, with 0 being the core-shell interface and 1 being the edge of the micelle.

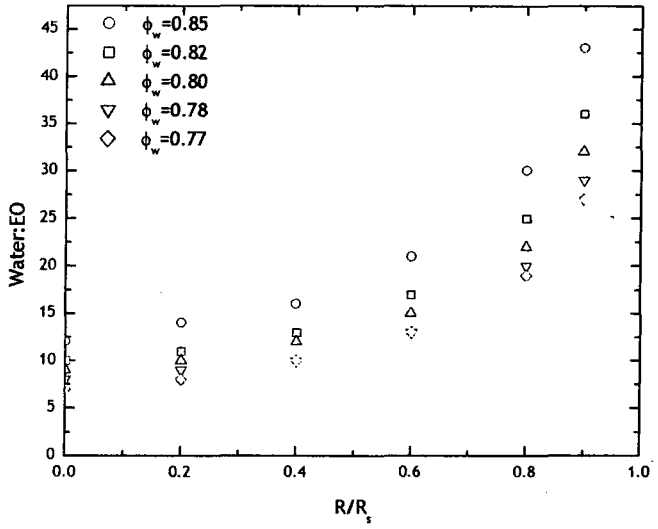

Figure 3.44 - *Plot of number of water molecules per ethylene oxide segment (Water:EO) vs. distance from core shell-boundary (R/R_s) for dilute dispersions with varying water volume fractions.*

Figure 3.44 shows that for all of the dilute dispersions the ethylene oxide segments next to the core-shell interface have a greater number of water molecules associated with them than would be found in the local hydration states, where between two and four bound water molecules are associated with each segment.[57]

3.5.2.3. Comparison with theory

Scaling and self-consistent field theories applicable to block copolymer micelles were introduced in chapter one. Perhaps the most useful of those discussed are the theories of Daoud and Cotton[58] and Halperin,[29] whose origins lie in the description of star polymers, and that of Zhulina and Birshtein.[39] The theories were discussed in detail in that chapter, and so will not be analysed here. Instead the relevant scaling laws from each and their applicability to the current results will be discussed. In the description that follows A is the soluble block having N_A repeat units each of length a, forming a shell of thickness R_s, B is the insoluble block having N_B repeat units each of length a, forming a core of radius R_c, with the total micelle radius being R_{mic},

p is the association number, σ is the interfacial area per chain, given by $\sigma = \frac{4\pi R_c^2}{p}$.

Table 3.25 details the scaling laws due to each of the theories in terms of the parameters detailed above.

Model	R_c	R_s	R_{cs}	p	σ
Daoud and Cotton	-	-	$N_A^{3/5} p^{1/5} v^{1/5} a$	-	-
Zhulina and Birshtein	$N_B^{3/5}$	$N_A^{v} N_B^{2(1-v)/5}$	-	$N_B^{4/5}$	$N_B^{2/5}$
Halperin	$N_B^{3/5} a$	-	$N_B^{4/25} N_A^{3/5} a$	$N_B^{4/5}$	-

Table 3.25 - *Scaling relationships for micellar parameters due to Daoud and Cotton, Zhulina and Birshtein and Halperin. R_c is core radius, R_s is shell thickness, R_{cs} is micelle radius, p is association number, σ is interfacial are per chain, v - excluded volume parameter, 0.588 for a good solvent, ½ for a θ solvent*

Using the scaling relationships in table 3.25 values for the parameters given by the scaling laws were calculated for each of the six block copolymers used.

Parameter	Model	5k series			10k series		
		hPB-hPEO	hPB-dPEO	dPB-hPEO	hPB-hPEO	hPB-dPEO	dPB-hPEO
N_A		89	106	140	164	90	163
N_B		16	16	12	29	24	26
R_c	Z-B	5.28	5.19	4.42	7.54	6.73	7.01
	Halperin	24.02	23.61	20.11	34.32	30.64	31.92
R_s	Z-B	22.11	24.45	27.51	34.94	23.77	34.07
R_{cs}	D-C	98.95	125.64	165.64	189.88	147.87	223.69
	Halperin	92.41	102.38	115.76	146.66	99.15	143.07
P	Z-B	9.19	8.98	7.25	14.79	12.71	13.42
	Halperin	9.19	8.98	7.25	14.79	12.71	13.42
σ	Z-B	3.03	3.00	2.69	3.85	3.57	3.66

Table 3.26 - *Micelle parameters calculated using the scaling relationships in table 3.25.*

Of the scaling relations utilised to calculate the above values, only those of Halperin[29] offer any definite magnitude in terms of size. Those of Daoud and Cotton[58] rely on the association number of the micelle being incorporated into the relationship, which essentially renders it dependent upon the experimental data, making a meaningful comparison difficult. The relationships of Zhulina and Birshtein[39] are the same as those of Halperin[29] with the former not incorporating the segment length into their equations. None of the relationships makes any allowances for the concentration of the solution, only specifying that it should be sufficiently high that micelles are present, but sufficiently dilute such that micellar interactions are not present. For this reason, the values obtained from fits to the data were averaged when there was more than one concentration. Comparison of the experimental results with those calculated from the scaling relationships of Zhulina and Birshtein[39] and those of Halperin[29] are given in table 3.27. Xu *et. al.*[32] used the ratio of experiment:model as a means of testing the applicability of the model to the experimental data. They took the constancy of the ratio as proof of the models' validity, and this approach is applied here.

Parameter	Model	5k series			10k series		
		hPB-hPEO	hPB-dPEO	dPB-hPEO	hPB-hPEO	hPB-dPEO	dPB-hPEO
N_A		89	106	140	164	90	163
N_B		16	16	12	29	24	26
R_cÅ	*Experiment*	*19.75*	*24.50*	*27.00*	*38.00*	*42.75*	*46.00*
	Halperin	24.02	23.61	20.11	34.32	30.64	31.92
	E:Hal	0.82	1.04	1.34	1.11	1.40	1.44
R_sÅ	*Experiment*	*61.50*	*94.25*	-	*112.00*	*112.00*	-
	Halperin	68.38	78.77	-	112.33	68.51	-
	E:Hal	0.90	1.20	-	1.00	1.63	-
R_{cs}Å	*Experiment*	*81.25*	*118.75*	-	*150.00*	*154.75*	-
	Halperin	92.41	102.38	115.76	146.66	99.15	143.07
	E:Hal	0.88	1.16	-	1.02	1.56	-
p	*Experiment*	*22.50*	*42.50*	*74.00*	*91.50*	*159.50*	*213.25*
	Halperin	9.19	8.98	7.25	14.79	12.71	13.42
	E:Hal	2.45	4.73	10.20	6.19	12.55	15.89
σ/Å	*Experiment*	*217.85*	*177.48*	*123.80*	*198.32*	*143.99*	*124.69*
	Z-B	3.03	3.00	2.69	3.85	3.57	3.66
	E:Z-B	71.86	59.23	45.97	51.57	40.39	34.03

Table 3.27 - *Comparison between experimentally determined and model calculated parameters.*

The agreement between theory and experiment in this case is somewhat mixed. The ratio between experimentally determined data and that expected from the scaling relationships varies between different parameters and copolymers. It appears however that the ratio for the micelle dimensions is relatively constant for a given polymer, e.g. for 5k hPB-hPEO the core has a ratio of 0.82, the shell 0.9, and the overall radius 0.88.

Neither the experimentally determined association numbers nor the interfacial area per chain match particularly well with those predicted from theory, with the ratio varying considerably between the polymers.

Theories relating to polymer brush-like layers were discussed in chapter one. It was noted that block copolymer micelles could be considered as polymer brushes with the core forming the tethering surface, and the corona chains forming the brush like layer. The relationships proposed by Alexander,[59] de Gennes[60] and Milner *et al.*[55] and Dan and Tirrell[61] are given in equations 3.46 to 3.49, and table 3.28 details the brush heights predicted from them for the polymers used here, along with the experimentally determined brush heights, (corona thickness).

$$h \sim Na\sigma^{1/3}$$ **Equation 3.47[59]**

$$h \sim N(v\sigma)^{1/3}$$ **Equation 3.48[60]**

$$h = \left(\frac{12}{\pi^2}\right)^{1/3} N(\sigma v)^{1/3}$$ **Equation 3.49[55]**

$$h \sim aN^{3/(3+d)}\sigma^{1/(3+d)}(R/a)^{d/(3+d)}$$ **Equation 3.50[61]**

where h is the brush height, σ is the grafting density $\sigma = a^2/D^2$, d is related to the dimensionality of curvature in the geometry under consideration and is equal to 2 for spheres, R is the radius of curvature of the tethering interface, in this case the core radius.

Parameter	Model	5k series		10k series	
		hPB-hPEO	hPB-dPEO	hPB-hPEO	hPB-dPEO
N_A		89	106	164	90
D/Å		14.85	13.30	14.15	12.05
σ		0.073	0.091	0.080	0.111
Experiment/Å		61.50	94.25	112.00	112.00
h/Å	Alexander	149.25	192.05	284.03	173.15
	E:Alex	0.412	0.491	0.394	0.647
h/Å	de Gennes	31.16	40.10	59.30	36.15
	E:dG	1.973	2.350	1.889	3.098
H/Å	Milner	33.26	42.80	63.29	38.59
	E:Milner	1.849	2.202	1.770	2.903
H/Å	D & T	66.43	84.05	126.86	99.05
	E:D & T	0.926	1.12	0.883	1.131

Table 3.28 - *Comparison between experimental and predicted brush heights, h, using the scaling relationships of Alexander, de Gennes and Milner et al. D is the distance between PEO chains on the core surface calculated in tables 3.23 and 3.24, σ is the grafting density,* $\sigma = a^2/D^2$ *where a is the segment size.*

For any given model, the ratios between experimentally determined corona thickness and theoretically predicted brush height vary considerably between the different polymers.

The model of Dan and Tirrell[61] provides the best agreement of all those applied. This is hardly surprising since it is the only one postulated for a curved interface as opposed to a planar interface, and thus the only taking account of the degree of curvature into consideration when calculating the brush height.

3.5.3. Higher concentration dispersions

As shown in chapter two, a structure factor peak was present at low Q when c≥2% for all of the dispersions analysed. Under such conditions it is no longer possible to fit the data assuming S(Q)=1 and an expression has to be introduced to account for this fact. Section 3.4.3 introduced two such

expressions, the hard-sphere potential[44,45] and the mean spherical approximation.[47] In common with the SAXS data, the mean spherical approximation[47] was used to fit the SANS data from the dispersions at 2, 4, 8, and 10% for all three contrasts and the two different molecular weights. The two fully hydrogenous copolymers were explored at concentrations as high as 50%. The results obtained and their significance is presented here.

3.5.3.1. Results and discussion

Figures 3.45 to 3.51 show typical examples of fits to the data for both molecular weights and all three contrasts, with the results obtained from the fits given in tables 3.29 to 3.36.

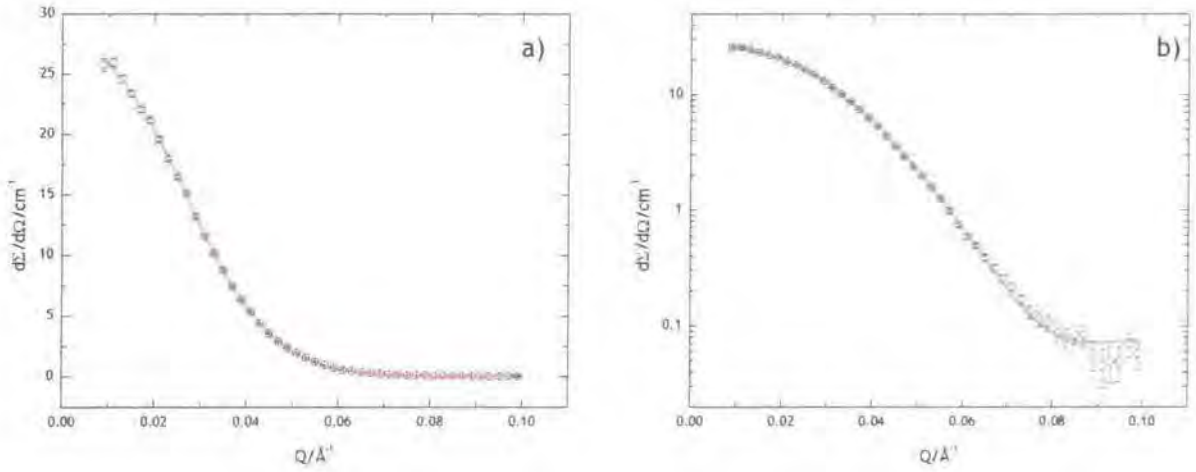

Figure 3.45 - *2% dispersion of 5k hPB-hPEO in D_2O. a) linear b)semi-logarithmic. Red lines are fits to the data.*

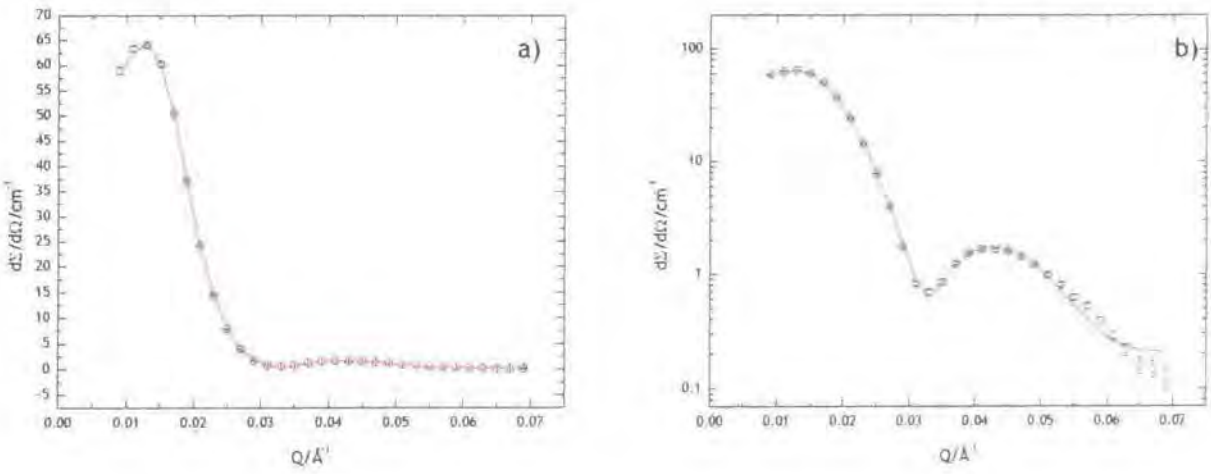

Figure 3.46 - *4% dispersion of 10k hPB-dPEO in hPB contrast match H_2O. a) linear b)semi-logarithmic. Red lines are fits to the data.*

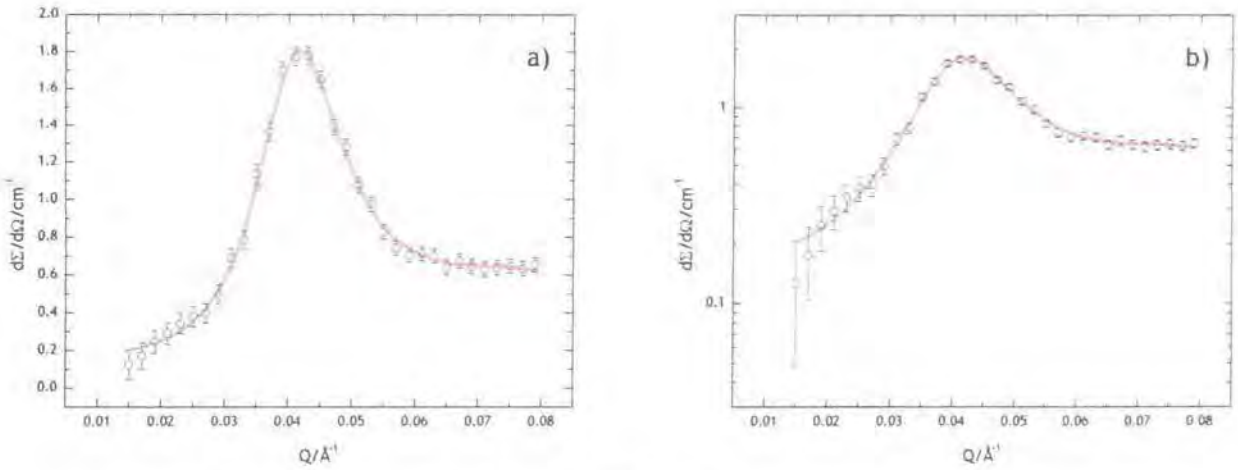

Figure 3.47 - *10% dispersion of 5k dPB-hPEO in hPEO contrast match H_2O. a) linear b)semi-logarithmic. Red lines are fits to the data.*

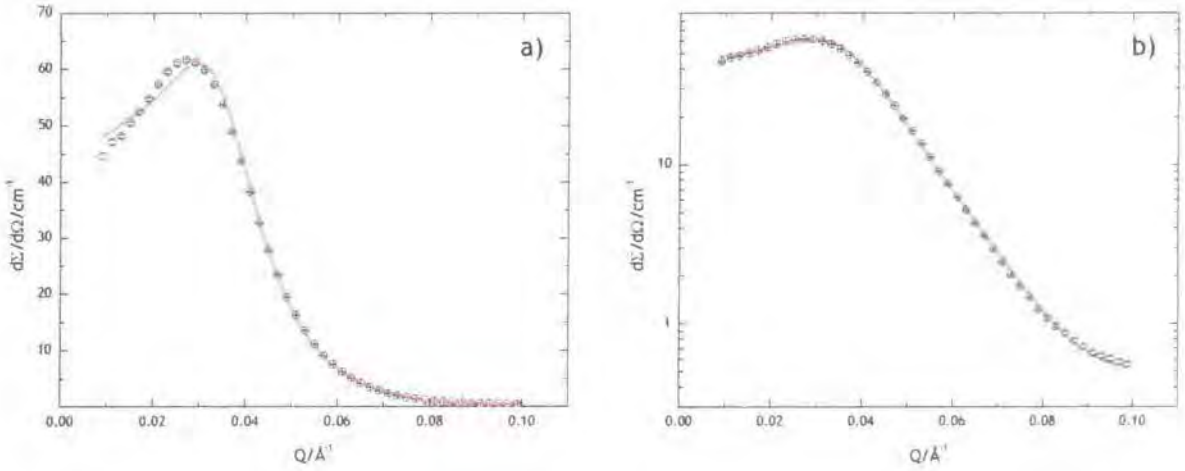

Figure 3.48 - *20% dispersion of 5k hPB-hPEO in D_2O. a) linear b)semi-logarithmic. Red lines are fits to the data.*

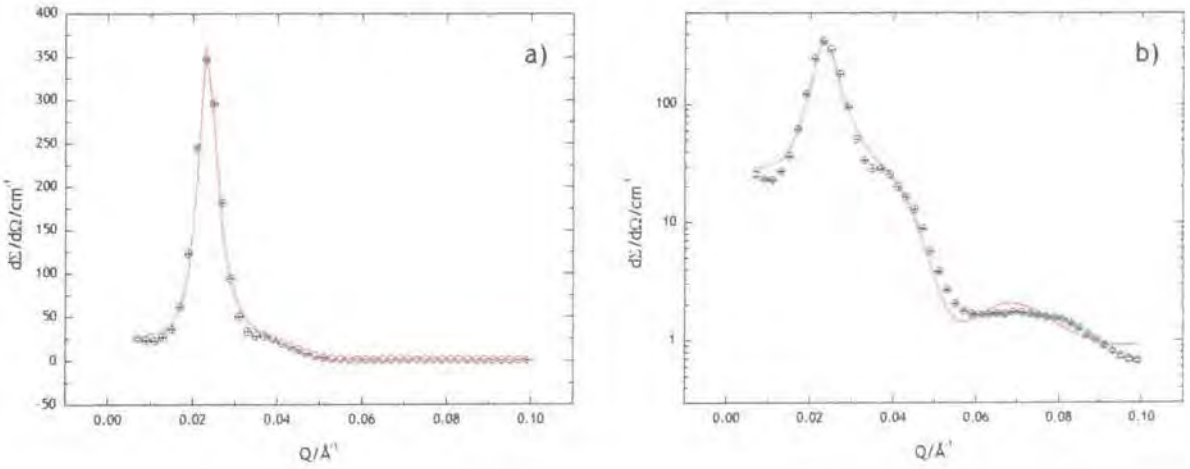

Figure 3.49 - *30% dispersion of 10k hPB-hPEO in D_2O. a) linear b)semi-logarithmic. Red lines are fits to the data.*

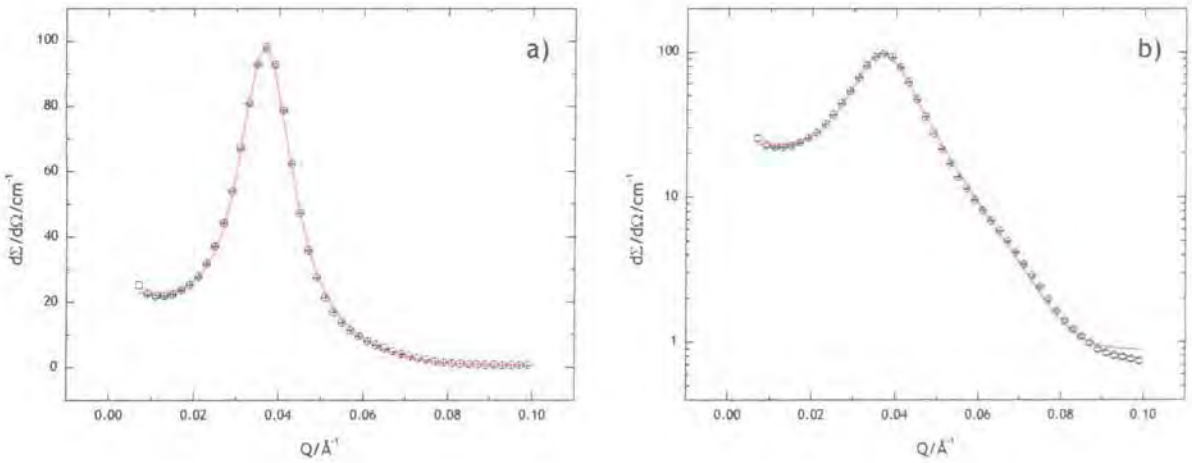

Figure 3.50 - *40% dispersion of 5k hPB-hPEO in D_2O. a) linear b)semi-logarithmic. Red lines are fits to the data.*

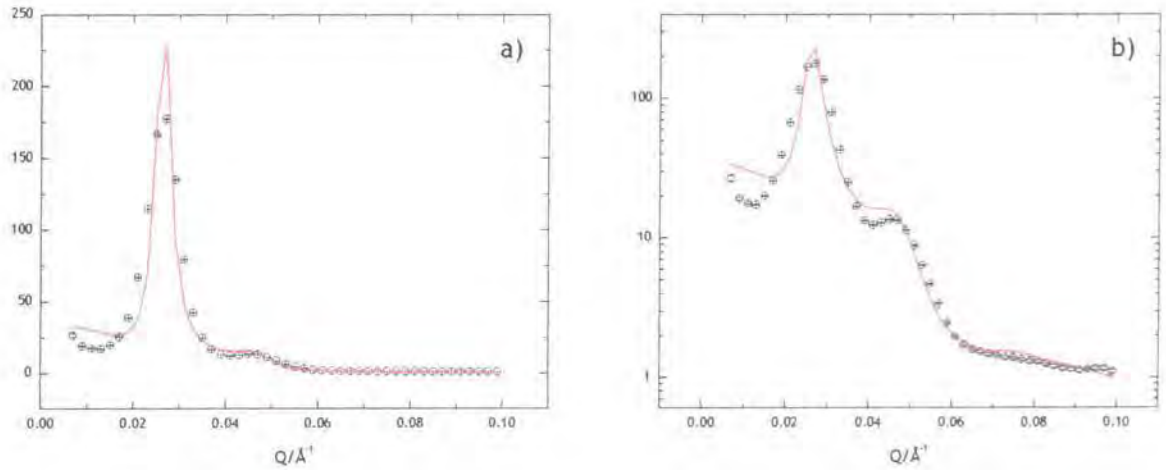

Figure 3.51 - *50% dispersion of 10k hPB-hPEO in D_2O. a) linear b)semi-logarithmic. Red lines are fits to the data.*

Parameter	10%	8%	4%	2%
R_c/Å	19	19	20	21
R_s/Å	48	48	48	50
σ/R	0.537	0.548	0.570	0.524
ϕ_w	0.50	0.55	0.60	0.65
p	27	23	23	20
D_{PEO}/Å	14.39	14.75	14.75	15.13
R_s:R_g	2.06	2.06	2.06	2.15
H-P S(Q) R/Å	66.85	63.92	55.08	60.85
Charge	12.84	12.18	9.90	14.48
κ/Å^{-1}	3.732×10^{-3}	6.526×10^{-3}	1.129×10^{-2}	2.752×10^{-2}
γ	9.293	9.504	8.367	48.987
$\gamma\exp(-k)$	5.642	4.130	2.407	1.721

Table 3.29 - *Parameters from fits to 5k hPB-hPEO in D_2O 2%≤c≤10%*

As for the dilute dispersions, the distinct steps in ϕ_w result from the model applied rather than being a real phenomenon of the system, with different values of this being investigated at each concentration until one providing a suitable fit was found.

Parameter	50%	40%	30%	20%
R_c/Å	19	17	24	24
R_s/Å	32	46	36	37
σ/R	0.351	0.377	0.292	0.393
ϕ_w	0	0	0	0
p	20	14	40	40
D_{PEO}/Å	15.13	16.00	13.46	13.46
R_s:R_g	1.37	1.97	1.55	1.59
H-P S(Q) R/Å	81.09	85.72	77.76	76.81
Charge	40.77	11	8.69	7.87
κ/Å^{-1}	5.792×10^{-2}	5.386×10^{-4}	7.21×10^{-4}	9.117×10^{-4}
γ	27061.997	5.054	3.485	2.891
$\gamma\exp(-k)$	2.256	4.573	3.116	2.513

Table 3.30 - *Parameters from fits to 5k hPB-hPEO in D_2O 20%≤c≤50%*

A point to note about the water volume fraction in table 3.30. Using values greater than zero resulted in fits of quite poor quality, in terms of both the parameters and the match to the data. So although the value of 0 is an unrealistic one, it is the only way a meaningful fit could be generated using the model applied to the other systems. It clearly demonstrates the limitations of the model with respect to higher concentration dispersions.

Parameter	10%	8%	4%	2%
R_c/Å	19	18	20	21
R_s/Å	97	100	99	97
σ/R	0.324	0.473	0.586	0.547
ϕ_w	0.60	0.65	0.70	0.75
p	20	17	23	27
D_{PEO}/Å	15.11	15.52	14.72	14.37
R_s:R_g	3.75	3.87	3.83	3.75
H-P S(Q) R/Å	70.11	72.58	68.95	68.14
Charge	32.43	29.25	21.83	17.30
κ/Å^{-1}	4.325×10^{-3}	8.65×10^{-3}	1.119×10^{-2}	1.177×10^{-2}
γ	57.851	55.752	36.810	24.032
$\gamma\exp(-k)$	31.545	15.884	7.867	4.833

Table 3.31 - *Parameters from fits to 5k hPB-dPEO in hPB contrast match H_2O 2%≤c≤10%*

Parameter	10%	8%	4%	2%
R_c/Å	25	24	25	23
σ/R	0.081	0.145	0.1726	0.160
p	59	52	59	46
H-P S(Q) R/Å	50.14	50.90	52.62	56.28
Charge	126.06	50.10	35.94	17.14
κ/Å^{-1}	6.848×10^{-2}	4.035×10^{-2}	3.594×10^{-2}	3.594×10^{-2}
γ	57910.105	1172.807	467.607	68.531
$\gamma\exp(-k)$	60.300	19.954	10.404	2.734

Table 3.32 - *Parameters from fits to 5k dPB-hPEO in hPEO contrast match H_2O 2%≤c≤10%*

Parameter	10%	8%	4%	2%
R_c/Å	40	39	39	39
R_s/Å	67	68	71	76
σ/R	0.489	0.540	0.495	0.505
ϕ_w	0.5	0.55	0.60	0.65
p	106	98	98	98
D_{PEO}/Å	13.78	13.96	13.96	13.96
R_s:R_g	1.85	1.88	1.96	2.10
H-P S(Q) R/Å	110.59	106.20	94.34	82.95
Charge	27.35	25.81	22.56	19.04
κ/Å^{-1}	2.267×10^{-3}	3.316×10^{-3}	6.413×10^{-3}	1.153×10^{-2}
γ	25.505	24.772	25.080	27.616
$\gamma\exp(-k)$	15.449	12.248	7.480	4.078

Table 3.33 - *Parameters from fits to 10k hPB-hPEO in D_2O 2%≤c≤10%*

Parameter	50%	40%	30%	20%
R_c/Å	58	63	41	40
R_s/Å	13	14	54	51
σ/R	0.177	0.138	0.10	0.255
ϕ_w	0	0	0	0
p	323	414	114	106
D_{PEO}/Å	11.44	10.98	13.61	13.78
R_s:R_g	0.36	0.39	1.49	1.41
H-P S(Q) R/Å	131.72	128.10	124.55	121.62
Charge	40.77	43.41	120.08	16.85
κ/Å^{-1}	2.000×10^{-2}	2.000×10^{-2}	4.439×10^{-2}	1.503×10^{-3}
γ	662.463	695.843	614728.672	8.528
$\gamma\exp(-k)$	3.411	4.142	9.702	5.905

Table 3.34 - *Parameters from fits to 10k hPB-hPEO in D_2O 20%≤c≤50%*

Parameter	10%	8%	4%	2%
R_c/Å	46	47	50	50
R_s/Å	101	100	97	99
σ/R	0.183	0.178	0.164	0.150
ϕ_w	0.50	0.55	0.60	0.65
p	197	210	253	253
D_{PEO}/Å	11.61	11.49	11.14	11.14
R_s:R_g	3.84	3.80	3.68	3.76
H-P S(Q) R/Å	94.46	95.88	102.32	100.39
Charge	30.85	33.01	34.26	31.16
κ/Å^{-1}	7.720×10^{-3}	1.176×10^{-2}	2.444×10^{-2}	3.43×10^{-2}
γ	51.726	55.752	495.985	1836.679
$\gamma\exp(-k)$	12.029	15.8834	3.345	1.677

Table 3.35 - *Parameters from fits to 10k hPB-dPEO in hPB contrast match H_2O 2%≤c≤10%*

Parameter	10%	8%	4%	2%
R_c/Å	40	40	40	42
σ/R	0.169	0.181	0.200	0.145
p	140	140	140	162
H-P S(Q) R/Å	83.83	92.11	91.58	98.78
Charge	19.50	17.67	13.42	12.71
κ/Å^{-1}	3.684×10^{-3}	4.586×10^{-3}	1.195×10^{-2}	3.215×10^{-2}
γ	17.534	13.920	467.607	68.531
$\gamma\exp(-k)$	9.456	5.980	10.404	2.734

Table 3.36 - *Parameters from fits to 10k dPB-hPEO in hPEO contrast match H_2O 2%≤c≤10%*

Figures 3.52 and 3.53 plot the variation of core radius and corona thickness respectively as a function of concentration for the contrasts explored.

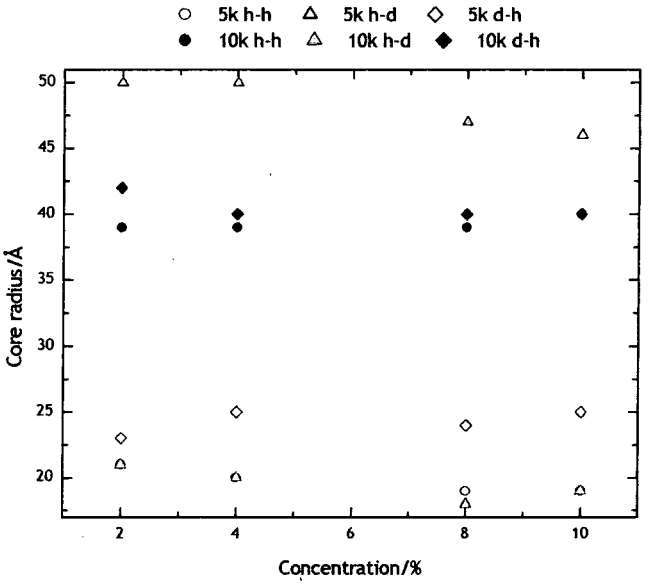

Figure 3.52 - *Variation of micelle core radius with concentration for the different molecular weights and contrasts investigated.*

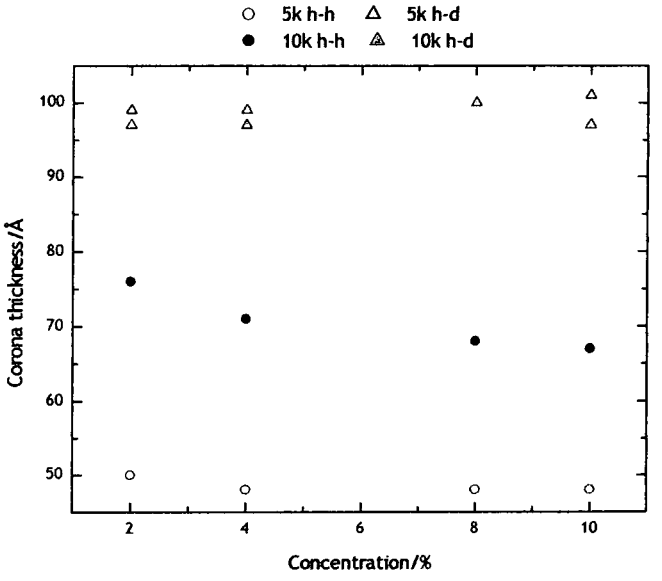

Figure 3.53 - *Variation of micelle corona thickness with concentration for the different molecular weights and contrasts investigated.*

From tables 3.29-3.36 and figure 3.52-3.53 the following trends are observed in the micelle dimensions for the different molecular weights and contrasts.

i.) The 5k hPB-hPEO copolymer shows a decrease in core radius and shell thickness with increasing concentration.

ii.) The 10k hPB-hPEO copolymer shows an increase in core radius and a decrease in shell thickness with increasing concentration.

iii.) The two hPB-dPEO copolymers show a decrease in core radius, whilst the shell thickness remains relatively constant.

iv.) The core radius remains relatively constant for the two dPB-hPEO copolymers as the concentration is increased.

With the exception of the fully hydrogenous copolymers when $c \geq 20\%$, the changes in the micelle dimensions are all relatively small, and so it is possible they may be due to the errors associated with the fitting process rather than a phenomenon of the system.

At the elevated concentrations however, the shape of the scattering changes, with the structure factor peak moving to higher Q and becoming more dominant, and it is possible that the ordering in the system that gives rise to the structure factor is no longer liquid-like and consequently the mean spherical approximation may no longer be a suitable model.

Interpretation of the parameters from the mean spherical approximation is somewhat difficult. It was developed to describe macroion solutions, but in the block copolymer micelle systems studied here there is no charge, and the interactions between the micelles are of a steric rather than an electrostatic nature. There are however two patterns that can be seen in the parameters giving rise to S(Q):

i.) κ decreases with increasing concentration

ii.) $\gamma\exp(-k)$ increases with increasing concentration.

$\gamma\exp(-k)$ is the contact potential between a macroion pair, and the fact that it increases with concentration suggests that the interaction between micelles also increases with concentration. In the case of the fully hydrogenous polymers it is also larger for a given concentration for the higher molecular weight variant.

Using equation 3.38 it is possible to calculate the dimensionless interaction potential as a function of the micelle centre-centre-distance. Such plots are shown in figures 3.54 and 3.55 for 10k hPB-hPEO and 5k hPB-hPEO respectively, for concentrations between 2 and 10%.

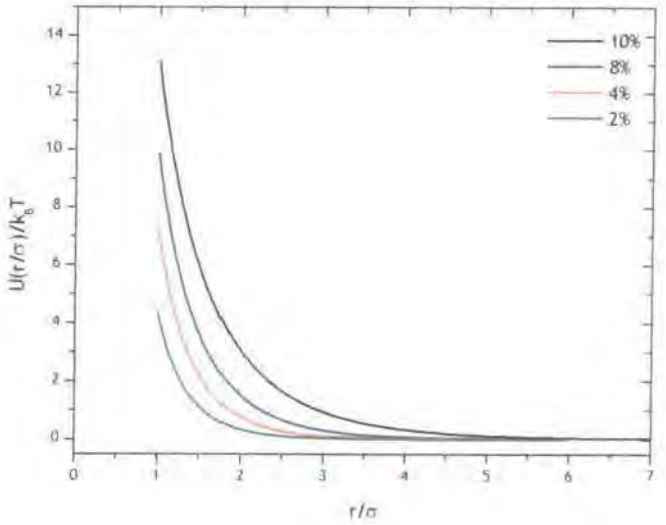

Figure 3.54 - *Dimensionless interaction potentials for 10k hPB-hPEO in D_2O at 2%≤c≤10% calculated using equation 3.38*

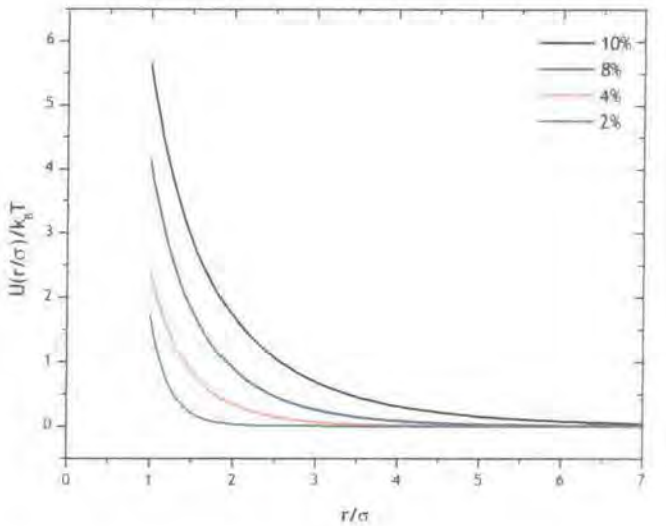

Figure 3.55 - *Dimensionless interaction potentials for 5k hPB-hPEO in D_2O at 2%≤c≤10% calculated using equation 3.38*

Both figures show that as the concentration increases so does the distance at which repulsion between the micelles is observed. The potentials are hard-sphere like at low separations showing a relatively steep rise, but with a softer tail at longer separations, which would be expected from the form of the potential used. They are similar in form to those of M^{c}Connell *et al.*[62] for poly(styrene)-poly(isoprene) block copolymers.

Figure 3.56 and 3.57 show the dimensionless interaction potentials for the two hPB-hPEO polymers at concentrations between 20 and 50%.

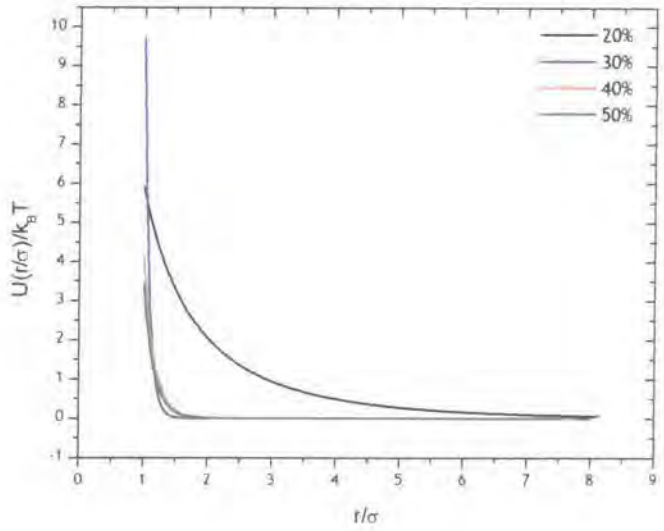

Figure 3.56 - *Dimensionless interaction potentials for 10k hPB-hPEO in D_2O at 20%≤c≤50% calculated using equation 3.38*

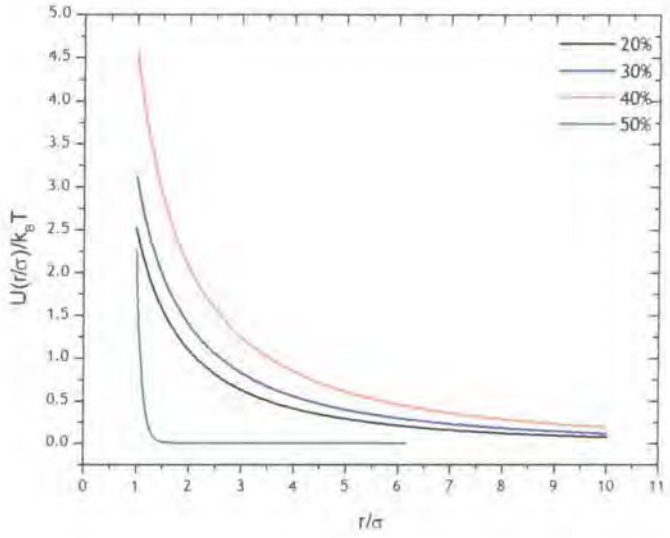

Figure 3.57 - *Dimensionless interaction potentials for 5k hPB-hPEO in D_2O at 20%≤c≤50% calculated using equation 3.38*

Figure 3.56 suggests that at concentrations greater than 20% the micelles behave as hard spheres. Figure 3.57 shows that at concentrations between 20 and 40% inclusive the micelles still interact with one another at distances up

to ten times their diameter; whilst above this they behave as hard spheres. The validity of these observations is open to question since the mean spherical approximation does not reproduce entirely all of the features of the data at these elevated concentrations. Indeed at the higher end of these values the dispersions no longer flow and are solid intractable gels, where different physical principles govern the micellar interactions compared to more dilute liquid-like dispersions.

In an approach applied by Bown *et al.*[54] it is possible to calculate reduced force-distance profiles for the fully hydrogenous polymers from the interaction potentials using the relationships of Patel *et al.*[63] (equations 3.50-3.52).

$$f = \frac{force}{\left(\sigma^{(2\nu+1)/2\nu} a^{1/\nu} N\right)}$$ **Equation 3.51**

where f is reduced force, σ is the grafting density, a is the segment length, ν is the excluded volume parameter, N is the degree of polymerisation of the corona forming block.

$$\delta = \frac{r}{\left(2\sigma^{(1-\nu)/2\nu} a^{1/\nu} N\right)}$$ **Equation 3.52**

where δ is the reduced distance.

$$F(r/D) = \pi R_c U(r/D)$$ **Equation 3.53**

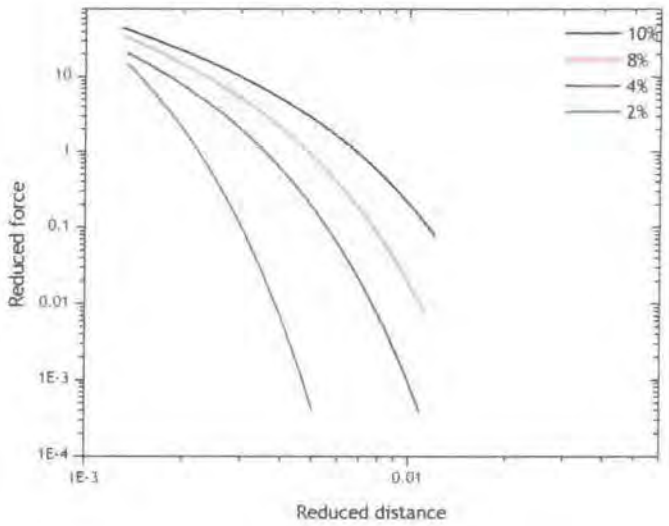

Figure 3.58 - *Reduced force as a function of reduced separation of micelle cores for 5k hPB-hPEO*

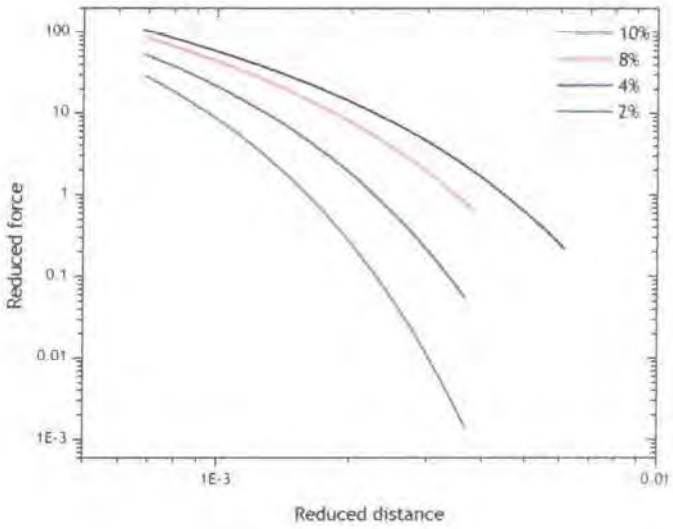

Figure 3.59 - *Reduced force as a function of reduced separation of micelle cores for 10k hPB-hPEO*

The potentials in figures 3.58 and 3.59 are comparable to those obtained by Bown *et al.*[54] and Patel *et al.*[63] with the former attributing the shape as being due to the corona behaving as a brush-like layer.

3.5.3. Conclusions

As with the previous sections, the main conclusions that can be inferred from the data are summarised here for clarity.

- The block copolymers investigated form micelles when dispersed in water that are spherical in nature.
- The average dimensions of the micelles have been determined by fitting the data to a spherical core-shell model with a parabolic volume fraction profile in the shell.
- The lower molecular weight micelles have core radii of ca 22Å and a shell thickness of ca 80Å.
- The higher molecular weight micelles have core radii of ca 40Å and a shell thickness of ca 110Å.
- The PEO chains composing the corona are highly stretched compared to the unperturbed radius of gyration, and the separation distance between them is less than the radius of gyration allowing them to be considered as a polymer brush.
- Reasonable agreement with predicted brush heights and experimentally determined corona thicknesses was observed, with the relationship of Dan and Tirrell[61] providing the best agreement.
- Micelles formed by the two molecular weight series have quite different association behaviour, with the lower molecular weight micelles having modest association numbers whereas the higher molecular weight micelles have high association numbers.
- Reasonable agreement was found between the experimental data and the scaling relations of Halperin's star model.[29]
- A structure factor due to intermicellar interactions is evident as the concentration is increased, and this has been successfully modelled using the mean spherical approximation.
- As the concentration is increased still further, the shape of the scattering changes suggesting that the type of ordering is changing from liquid-like to solid-like.

3.6. Final discussion

The poly(butadiene)-poly(ethylene oxide) block copolymers investigated here formed spherical micelles in aqueous solution with low cmc's that were seen to be inversely related to the molecular weight of the copolymer. Comparison of these cmc's with those of other PEO containing diblock copolymers reported in the literature suggests that the hydrophobic character of PB lies somewhere between that of poly(butylene oxide) and poly(propylene oxide) with the later being the least hydrophobic. Calculation of hydrophile-lipophile balance for the three respective hydrophobes suggests the PB and PBO have approximately equivalent hydrophobic character, whilst PPO is the most hydrophilic of the three. Deng *et al.*[64] suggested that PB was more hydrophobic than PBO, although offered no evidence to support this claim. Elucidation of the hydrophobic character of PB in PB-PEO block copolymers is complicated by the small data set existing for such species, and so the conclusions drawn here can only serve as indicative observations rather than quantitative answers.

In common with reports for other block copolymers, PB-PEO appears to undergo micellisation by the closed association process, forming micelles having narrow size distributions as determined by CONTIN analysis of QELS data. The concentration dependence of the apparent diffusion coefficient allowed the elucidation of the micelle hydrodynamic radii, with values of 168Å and 136Å determined for the 10k and the 5k micelles respectively. The two molecular weights exhibited different concentration dependencies of the for the diffusion coefficient, with the lower molecular weight variant displaying the usual positive dependence due to repulsive interactions between micelles expected for diblock copolymers. The higher molecular weight micelles showed a negative dependence more commonly associated with triblock copolymers due to attractive interactions between micelles. The reason for the latter observation remains unclear since the synthetic procedure precludes the formation of triblock copolymers and SEC analysis of the block copolymer showed a monomodal distribution suggesting that no homo PEO was formed during the polymerisation reaction. One can only speculate as to the reasons for this unusual observation, with perhaps the

presence of some impurity not detected by SEC or NMR, or indeed from the water used to prepare the samples has caused this tendency.

Comparison of the hydrodynamic radii determined from QELS experiments on other PEO containing block copolymers (table 3.4) reveal that for those copolymers having similar compositions and molecular weights to the two studied here, reasonable agreement between the radii is observed. This result is not unexpected since the copolymers considered formed spherical micelles due to PEO being the major constituent. Under such circumstances, the corona would be expected to be the largest part of the micelle since the PEO chains are in a good solvent, and as the nature of the corona forming chains is the same in all of the species reasonable agreement could be expected.

The determination of the micelle radii from the fitting of SANS data due to dilute dispersions concurred fairly well with the hydrodynamic radii from the QELS experiments, with the latter values being slightly larger. The model used to fit the SANS data also allowed determination of the core radius of the micelles, with a value of 19-25Å observed for the 5k series and 35-45Å for the 10k series. Interestingly these values are considerably smaller than those determined by Bates and co-workers using cryo-TEM[65] and SANS[66] for PB-PEO block copolymers having comparable molecular weights and compositions to those investigated here. Cryo-TEM experiments suggested a core radius of 150Å and a shell thickness of 330Å for an 8k copolymer containing 70% PEO,[65] whilst fits to SANS data suggested a core radius of 112Å and a shell thickness of 178Å for a similar copolymer.[66] The fact that the core radii are larger than determined here could be attributed to the larger PB block, but as the PEO block length of the two copolymers studied by Bates and co-workers are shorter than those examined here, one would expect the corona thickness to be less than that determined here. The increased dimensions from the TEM experiments may result from the vitrification procedure used to prepare the films of the micelles for examination. The micelles could potentially "spread out" on the grid used, a phenomenon observed by Wooley and co-workers,[67] resulting in increased dimensions. The differences from the SANS experiments are likely to result from the different models used to fit the data. Won *et*

al.[66] used a Fermi-Dirac function to model the density profile of the corona as opposed to the parabolic function employed here.

Determination of micelle dimensions from SLS proved troublesome due to the poor quality of the data, with Zimm plot analysis suggesting the 5k micelles had a larger radius of gyration than their 10k counterparts; an observation that is clearly erroneous. The shape of the Zimm plot for the 5k micelles showed the extrapolated data "hooking back up" from the lowest concentration. This may be due to experimental error in the preparation of one or more of the dispersions, although there is some evidence of similar phenomena in the literature.[38] The intensity of the laser utilised could also be a problem, with the power output measured as 53 mW, resulting in quite a weak scattering intensity

Modelling of SAXS data to give micelle dimensions was hampered by the weak scattering intensity and the lack of SAXS contrast between the three scattering components in the system. It was not possible to measure scattering at concentrations below 1%, and even at this concentration, the scattering from the dispersions was weak in intensity. The results obtained from fitting 5k hPB-hPEO were particularly unrealistic, with the model suggesting a core radius of 60Å and a shell thickness of 12Å, clearly out of proportion with the copolymer composition. Fits to the 10k data were a little more successful, revealing a core radius of ca 14Å and a shell thickness of 40Å, both smaller than the values obtained by SANS. With hindsight, it would have been better to perform the SAXS experiments using a synchotron source, which would have provided a far greater incident flux, and removed the need for desmearing, which can add complications to the data.

The association number of the micelles, p, could be calculated from the core radii determined from fits to the SANS data based upon the molecular weight and density of PB block forming the core. The two molecular weight series exhibited contrasting association behaviours, with the 5k series showing moderate association numbers of 20-45 and the 10k series exhibiting high association numbers of 70-230. Won *et al.*[66] used a similar method for their spherical PB-PEO micelles discussed above and determined an association

number of 1350, which is considerably larger than the values obtained here, and of other PEO based block copolymers reported in the literature. They attributed the large association number compared to PPO-PEO copolymers to the strongly hydrophobic nature of the PB core reducing the number particles in the system in order to minimise the unfavourable contact with water. Several authors including Mortensen *et al.*[5] and Bown *et al.*[54] have employed the same method for determining association numbers and obtained conflicting results, with the former reporting p=470 for a 4k PS-PEO block copolymer and the latter reporting ca 135 for an 8k PS-PEO. These two values are considerably smaller than that determined by Won *et al*[66]. and on polymers that are more hydrophobic than PB-PEO, so their result and explanation for it appear questionable.

Booth and co-workers have reported association numbers for PBO-PEO block copolymers determined by SLS,[2, 3] suggesting a similar pattern to that observed here; namely low to moderate values for lower molecular weight species increasing to higher values with molecular weight. They noted that the length of the hydrophobic block was the primary determinant of the association number, with the two being proportionally related. The length of the hydrophilic block was seen to exert less influence with a small increase in its length resulting in a small decrease of the association number. Given the limited data set available for PB-PEO block copolymers (these results and those of Won *et al.*[66]) one could speculate that the association numbers observed support the observations of Booth and co-workers previously stated.

Attempts to determine the association numbers from SLS data proved fruitless due to the poor quality of the data.

From the association number, the separation distance between PEO chains on the surface of the micelle core could be calculated. These distances were compared to the unperturbed radii of gyration of the corona-forming PEO chain in water calculated using the relationship of Kawaguchi *et al.*[56] In all instances the separation distance was less than the radius of gyration. Comparison of the corona thickness to the same radius of gyration revealed that the chains forming the corona were highly stretched, (2.5-4.5×), relative to the unperturbed state. These two observations supported the notion of

considering the coronal layer as a polymer brush, which was applied during the fitting procedure in terms of the polymer volume fraction profile.
Comparison of the experimentally determined brush heights to the theoretical models of Alexender,[59] de Gennes,[60] Milner *et al*[55]. and Dan and Tirrell[61] revealed that the latter of these provided the closest agreement. This was not surprising since the others were postulated for planar surfaces whilst the Dan and Tirrell[61] model was formulated for curved interfaces.

As the concentration was increased above 1% the size distributions observed by QELS were seen to change markedly; first a broadening effect, then a bimodal population was observed. The two molecular weights again showed contrasting behaviour, with the 10k polymer exhibiting bimodal populations at c≥8%, with the smaller particles having a radius of 110Å and the larger ones ca 3 times that. The 5k micelles on the other hand showed bimodal populations at c≥4%, with the smaller particles having radii of 110Å and the larger ones 6-10 times that. The larger particles in both instances are likely micelle clusters similar to those reported by Xu *et al*[7]. for PS-PEO in water. They observed that the dimensions of these micellar aggregates were of the order of 10 times greater than the micelles. In future in may be beneficial to be able to fit the SANS data to a model accounting for the dual populations observed from the QELS experiments. This is currently not possible using the model and the software applied here.
The 10k copolymer behaviour is a little unusual since the dimensions of the larger particles are not as large as those of the 5k micelles or similar examples reported in the literature.[7] This may result from the clusters being more tightly bound due to the attractive nature of the interactions between the micelles suggested by the concentration dependence of the diffusion coefficient. As the clusters were not always observed it is possible they are non-equilibrium structures or due to impurities in the dispersion causing temporary micelle bridging, which would explain the negative concentration dependence of the diffusion coefficient.

The SAXS intensity from dispersion where c≥2% was much greater than those from the 1% dispersions for both molecular weights. At these higher concentrations a structure factor peak due to intermicellar interactions was

clearly evident and so account had to be taken of this when fitting the data. Initial attempts at using a hard-sphere potential were unsuccessful, with it not adequately describing the structure observed in even the most dilute of these dispersions.

The use of the mean spherical approximation resulted in fits that reproduced most of the features of the data, although it did not quite capture all of them. As for the dilute dispersions the lack of contrast made it difficult to obtain accurate micelle dimensions, with the 10k micelles giving a core radius of 13Å and a shell thickness of 50Å, whilst the 5k micelles gave a core radius of 6Å and a shell thickness of 30Å. All of these values are smaller than those determined by fits to the SANS data where the degree of contrast is greatly enhanced. The intermicellar interactions could not be determined quantitatively since the fits did not accurately reproduce the data.

There are few reports of SAXS investigations on micellar dispersions in the literature, with most investigations focusing on higher concentration mesophases or solid samples.[24, 64, 68] Presumably, this is due to the lack of contrast experienced here.

Fits to the SANS data for higher concentration dispersions proved far more successful than those from the SAXS data, with the mean spherical approximation accurately reproducing the features observed in the scattering data for samples where the dispersion was still liquid-like rather than a gel. Consequently, it was possible to obtain a more complete picture of the intermicellar interactions.

As discussed in section 3.5.3.1 there were small changes in the micelle dimensions for those dispersions at $c \leq 10\%$. Whether these changes in dimensions were a result of the errors associated with the fitting process or a genuine phenomenon of the system remains unclear.

The degree of stretching, determined by $R_s:R_g$, was seen to decrease with increasing concentration, presumably due to the micelles coming closer together and causing the coronal chains to contract slightly.

At the lowest concentration the interaction between the micelles is close to that of a hard-sphere potential, with a steep rise in the potential energy at short separation distances, and a relatively short tail. As the concentration

increases, the rises in the potential energy at low separation become less dramatic and the tail longer and softer, with interactions between micelles evident at greater degrees of separation. Other researchers have reported similar potentials including M^{c}Connell *et al*[62]. whose potentials were calculated from self-consistent field theory.

Interpretation of the potentials at higher concentrations is complicated by the model not fully reproducing the features of the data. However, it appears that when the dispersions are still liquids the same pattern discussed above is observed, namely an increasingly softer tail and interactions at longer distances are observed. When the dispersions form gels the potential reverts to that approaching a hard sphere, with steep rises in the potential at low separations and little interaction at longer distances.

3.7. Glossary of symbols

The symbols used in the body of the text and the equations are defined here in the order in which they appear in the text.

3.7.1. Introduction

Q	scattering vector
n	refractive index
λ	wavelength
θ	scattering angle
R_g	radius of gyration
M_w	weight average molecular weight
A_2	second virial coefficient
p	association number
D	diffusion coefficient
R_h	hydrodynamic radius

3.7.2. Quasi-Elastic Light Scattering

D_{app}	apparent diffusion coefficient
k_B	Boltmann constant
T	temperature

η	solvent viscosity
$R_{h,\,app}$	apparent hydrodynamic radius
$\Delta_{mic}G°$	Gibbs energy of association
R	Universal gas constant
K	micelle association constant
cmc	critical micelle concentration
D_0	diffusion coefficient at infinite dilute
k_d	diffusion second virial coefficient
c	concentration
k_f	frictional coefficient
ν	partial specific volume of micelles in solution
R	micelle radius
N_B	degree of polymerisation of core forming B block
N_A	degree of polymerisation of corona forming A block
a	segment length

3.7.3. Static Light Scattering

w	weight fraction of component in copolymer
M^A	molecular weight of A block
M^B	molecular weight of B block
M_n^A	number average molecular weight of A block
M_n^B	number average molecular weight of B block
M_n	number average molecular weight of copolymer
M_w^A	weight average molecular weight of A block
M_w^B	weight average molecular weight of B block
M_w	weight average molecular weight of copolymer
$R-R_0$	excess Rayleigh ratio
K	optical constant
M	molecular weight
dn/dc	specific refractive index increment
$P(\theta)$	particle scattering factor
n_0	solvent refractive index
N_A	Avogadro's number

λ_0	incident wavelength
$\overline{M}$	average molecular weight
M_{app}	apparent molecular weight
w_A	weight fraction of A in copolymer
w_B	weight fraction of B in copolymer
$\left(dn/dc\right)_A$	specific refractive index increment of A block
$\left(dn/dc\right)_B$	specific refractive index increment of B block
$M_{w,app}$	weight average apparent molecular weight
p	micelle association number
n_2	polymer refractive index
Δn	change in refractive index
R_θ	Rayleigh ratio at angle θ
A_2	second virial coefficient
R_g	radius of gyration
R_{A_2}	thermodynamic radius
R_{90}	Rayleigh ratio at 90°

3.7.4. Small-angle X-ray scattering

I(Q)	scattering intensity
N	number of scattering particles
V	particle volume
Q	scattering vector
R	radius of a sphere
$(\Delta\rho)^2$	contrast (electron density difference)
R_g	radius of gyration
ρ_c	electron density of micelle core
ρ_s	electron density of micelle corona
ρ_m	electron density of solvent
$\overline{R}$	average core radius
σ	standard deviation of Schultz distribution
Z	width parameter of Schultz distribution
$\Gamma(Z+1)$	gamma function

r	separation distance
R_{HS}	hard sphere radius
η	hard sphere volume fraction
V	total volume of system
$U(r)$	repulsion potential between spherical macroions
σ	macroion diameter
ε_0	permitivity of free space
ε	solvent relative permitivity
ψ_0	surface potential
κ	Debye-Huckel inverse screening length
z_m	electronic charge
n	number of particles

3.7.5. Small-angle neutron scattering

Q	scattering vector
$(d\Sigma/d\Omega)(Q)$	differential scattering cross-section
$\Delta\rho_c$	scattering length density difference between core and inner most sub-shell of corona
$\Delta\rho_c$	scattering length density difference between innermost shell of corona and solvent
ϕ_w	volume fraction of water in inner most sub-shell of corona
σ/R	width of Schultz distribution
ϕ_{PB}	volume fraction of poly(butadiene)
ϕ_{PEO}	volume fraction of poly(ethylene oxide)
R_g	radius of gyration
M_w	weight average molecular weight
p	micelle association number
V_{PB}	volume of poly(butadiene) block
m_{PB}	molecular weight of poly(butadiene) block
N_A	Avogadro's number
ρ_{PB}	density of poly(butadiene) block
N_A	degree of polymerisation of corona forming A block
N_B	degree of polymerisation of corona forming B block

ν	excluded volume parameter
σ	interfacial area per chain
h	brush height
N	degree of polymerisation of brush forming polymer
σ	grafting density
R	radius of curvature (core radius)
κ	Debye-Huckel inverse screening length
$U(r/\sigma)$	dimensionless interaction potential
r/σ	dimensionless separation
f	reduced force
σ	reduced distance
D (same as σ for S(Q))	macroion diameter

3.8. Bibliography

1 D. J. Shaw, 'Introduction to Colloid and Surface Chemistry', 4th, ed., Butterworth-Heinemann, Oxford, 1998.

2 C. Booth and D. Attwood, *Macromol. Rapid Commun.*, 2000, **21**, 501.

3 C. Booth, G. E. Yu, and V. M. Nace, in 'Amphiphilic block copolymers: Self assembly and applications', ed. P. Alexandridis and B. Lindman, Elsevier, Amsterdam, 2000.

4 B. Chu and Z. Zhou, in 'Nonionic surfactants: Polyoxyalkylene block copolymers', ed. V. M. Nace, Marcel Dekker New York, 1996.

5 K. Mortensen, *et al.*, *Langmuir*, 1997, **13**, 3635.

6 M. Willhelm, *et al.*, *Macromolecules*, 1991, **24**, 1033.

7 R. L. Xu, *et al.*, *Macromolecules*, 1991, **24**, 87.

8 Z. Zhou, B. Chu, and V. M. Nace, *Langmuir*, 1996, **12**, 5016.

9 T. Liu, *et al.*, *J. Phys. Chem. B*, 1997, **101**, 8808.

10 L. Derici, *et al.*, *Phys. Chem. Chem. Phys.*, 1999, **1**, 2773.

11 W. Mingvanish, C. Chaibundit, and C. Booth, *Phys. Chem. Chem. Phys.*, 2002, **4**, 778.

12 P. F. Dewhurst, *et al.*, *Macromolecules*, 1998, **31**, 7851.

13 S. W. Provencher, *Makromol. Chem.*, 1979, **180**, 201.

14 H. G. Elias, in 'Light Scattering from Polymer Solutions', ed. M. B. Huglin, Academic Press, London, 1972.

15 I. W. Hamley, 'The Physics of Block Copolymers', Oxford University Press, New York, 1998.

16 Y.-W. Yang, *et al.*, *Langmuir*, 1995, **11**, 4703.

17 S. M. Mai, *et al.*, *Langmuir*, 2000, **16**, 1681.

18 Y. Zheng and H. T. Davis, *Langmuir*, 2000, **16**, 6453.

19 J. T. Davies and E. K. Rideal, 'Interfacial Phenomena', 2nd, ed., Academic Press, New York, 1963.

20 R. J. Hunter, 'Foundations of Colloid Science Vol 2', Oxford University Press, New York, 1989.

21 Z. K. Zhou, *et al.*, *Macromolecules*, 1996, **29**, 8357.

22 C. Konak, *et al.*, *Progr. Colloid Polym. Sci.*, 1985, **71**, 15.

23 J. Selser, in 'Dynamic Light Scattering - The method and some applications', ed. W. Brown, Clarendon Press, Oxford, 1993.

24 A. Kelarakis, *et al.*, *J. Chem. Soc., Faraday Trans.*, 1998, **94**, 3639.

25 W. Mingvanish, *et al.*, *J. Phys. Chem. B*, 1999, **103**, 11269.

26 A. Kelarakis, *et al.*, *J. Phys. Chem. B*, 2001, **105**, 7384.

27 Y.-W. Yang, *et al.*, *Macromolecules*, 1996, **29**, 670.

28 S.-M. Mai, *et al.*, *J. Chem. Soc., Faraday Trans.*, 1998, **94**, 567.

29 A. Halperin, *Macromolecules*, 1987, **20**, 2943.

30 R. Nagarajan and K. Ganesh, *J. Chem. Phys.*, 1989, **90**, 5843.

31 A. Kelarakis, *et al.*, *Phys. Chem. Chem. Phys.*, 2001, **3**, 4037.

32 R. L. Xu, *et al.*, *Macromolecules*, 1992, **25**, 644.

33 H. Benoit and D. Froelich, in 'Light Scattering from Polymer Solutions', ed. M. B. Huglin, Academic Press, London, 1972.

34 M. B. Huglin, in 'Light Scattering from Polymer Solutions', ed. M. B. Huglin, Academic Press, London, 1972.

35 J. Brandup and E. H. Immergut, 'Polymer Handbook', 3rd, ed., John Wiley and Sons, Toronto, 1989.

36 B. L. Johnson and J. Smith, in 'Light Scattering from Polymer Solutions', ed. M. B. Huglin, Academic Press, London, 1972.

37 W. Burchard, M. Schmidt, and W. H. Stockmayer, *Macromolecules*, 1980, **13**, 580.

38 W. Burchard, in 'Applied Fibre Science', ed. F. Happey, Academic Press, 1978.

39 E. B. Zhulina and T. M. Birshtein, *Polymer Science USSR*, 1986, **27**, 570.

[40] N. F. Carnahan and K. E. Starling, *J. Chem. Phys.*, 1969, **51**, 635.

[41] J. S. Pedersen and C. Svaneborg, *Curr. Opinion Coll. Interface Sci.*, 2002, **7**, 158.

[42] V. Castelletto and I. W. Hamley, *Curr. Opinion Coll. Interface Sci.*, 2002, **7**, 167.

[43] R. H. Ottewill, Ch7 in 'Colloidal Dispersions', ed. J. W. Goodwin, Royal Society of Chemistry, London, 1982.

[44] N. W. Ashcroft and J. Lekner, *Phys. Rev*, 1966, **145**, 83.

[45] J. K. Perkus and G. J. Yevick, *Phys. Rev*, 1958, **110**, 1.

[46] R. H. Ottewill, Ch 9 in 'Coloidal Dispersions', ed. J. W. Goodwin, Royal Society of Chemistry, London, 1982.

[47] J. B. Hayter and J. Penfold, *Molec. Phys.*, 1981, **42**, 109.

[48] I. W. Hamley, *et al.*, *Langmuir*, 2001, **17**, 6386.

[49] S. M. King, in 'Modern Techniques of Polymer Characterisation', ed. R. A. Pethrick and J. V. Dawkins, John Wiley & Sons, London, 1999.

[50] 'Small Angle X-ray Scattering', ed. O. Glatter and O. Kratky, Academic Press, 1982.

[51] R. K. Heenan, 'The "Fish" Reference Manual', RAL-TR-89-129, Rutherford Appleton Laboratory, Didcot, 2000.

[52] M. Kotlarchyk and S.-H. Chen, *J. Chem. Phys.*, 1983, **79**, 2461.

[53] J. S. Higgins, *et al.*, *Polymer*, 1988, **29**, 1968.

[54] G. J. Bown, R. W. Richards, and R. K. Heenan, *Polymer*, 2001, **42**, 7663.

[55] S. T. Milner, T. A. Witten, and M. E. Cates, *Macromolecules*, 1988, **21**, 2610.

[56] S. Kawaguchi, *et al.*, *Polymer*, 1997, **38**, 2885.

[57] K. Taskai, *J. Am. Chem. Soc.*, 1996, **118**, 8459.

[58] M. Daoud and J. P. Cotton, *J. Physique*, 1982, **43**, 531.

[59] S. Alexander, *J. Physique*, 1977, **38**, 983.

[60] P. G. de Gennes, *J. Physique*, 1976, **37**, 1445.

[61] N. Dan and M. Tirrell, *Macromolecules*, 1992, **25**, 2890.

[62] G. A. McConnell, *et al.*, *Faraday Discuss.*, 1994, **98**, 121.

[63] S. Patel, M. Tirrell, and G. Hadziioannou, *Colloids Surf.*, 1988, **31**, 157.

[64] Y. Deng, *et al.*, *Polymer*, 2002, **43**, 7155.

[65] Y. Zheng, *et al.*, *J. Phys. Chem. B*, 1999, **103**, 10331.

[66] Y. Y. Won, *et al.*, *J. Phys. Chem. B*, 2000, **104**, 7134.

[67] H. Huang, *et al.*, *J. Am. Chem. Soc.*, 1997, **119**, 11653.

[68] I. W. Hamley, *et al.*, *Langmuir*, 2002, **18**, 1051.

4. Cross-linked micelles

4.1. Introduction

Micelles formed from the self-assembly of block copolymers in selective solvents are non-permanent structures held together by molecular interactions such as hydrophobic-hydrophilic effects, hydrogen bonding or van der Waals forces.[1] These interactions are relatively weak, and impart a reversible nature to the self-assembly process. The physical properties of the self-assembled structures can be changed by subsequent post self-assembly manipulation. One such change is to chemically fix or cross-link part of the micelle having a suitable functional group. This area has received a growing amount of attention in recent years.[2-17] Chapter one surveyed the major advances in the field of cross-linked micelles, both of the core and shell-cross-linked variants. The various different methodologies and outcomes were reviewed and discussed.

This chapter focuses on the core cross-linked micelles produced, and their properties as determined by the scattering techniques utilised in chapter three for the study of virgin copolymer micelles. These properties will be compared to those of the micelles and differences rationalised.

4.2. Cross-linked micelle production

As demonstrated in chapter three, poly(butadiene)-poly(ethylene oxide) block copolymers readily form micelles when dispersed in water at low concentrations. The presence of double bonds in the core, should prove suitable functional groups to cross-link the micelles.

Chapter two provided the synthetic details relating to the cross-linking procedure and subsequent physical characterisation of the cross-linked micelles, and the reader is referred to sections 2.3.2 and 2.6.2 for further details.

The procedures outlined in chapters two and three for the collection and subsequent treatment of data were as employed for the micelles and so are not presented in detail here.

4.3. Quasi-elastic light scattering

In contrast to the studies of the block copolymer micelles, it was unnecessary to determine the cmc since at any concentration micelles were always present since they were now permanent structures. The concentration of the solutions was adjusted for the presence of dispersed unimers that may not have reacted during the cross-linking reaction, by subtracting the respective cmc from the dispersion concentration.

4.3.1. Average Hydrodynamic Radius

As seen in chapter three, the concentration dependence of the apparent average diffusion coefficient (D_{app}) determined from analysis of the intensity autocorrelation function can be related to the translational diffusion coefficient of the micelles at zero concentration by equation 4.1[18-21]

$$D_{app} = D_0(1 + k_d(c - cmc)) \qquad \textbf{Equation 4.1}$$

Thus a plot D_{app} *vs.* (c-cmc) yields D_0 as its intercept, and k_d from the gradient. Figure 4.1 shows such a plot for the two hydrogenous copolymers after cross-linking, with the values determined given in table 4.1.

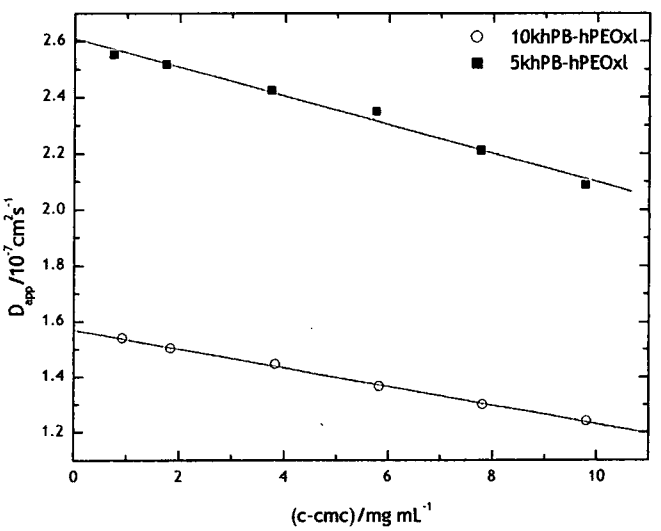

Figure 4.1 - *Apparent diffusion coefficient vs. concentration for hydrogenous polymers in dilute solutions. Lines are linear fits to the data.*

Copolymer	$D_0/10^{-7}cm^2s^{-1}$	R_h/Å	k_d/mL mg^{-1}
10k hPB-hPEOxl	1.567±0.006	156.1±0.5	-0.0216±0.002
5k hPB-hPEOxl	2.610±0.018	93.8±0.6	-0.0195±0.003

Table 4.1 - *Diffusion coefficient, Hydrodynamic radii, and second virial diffusion coefficient calculated from extrapolation to infinite dilute for hydrogenous polymers.*

The radii determined for the cross-linked micelles are smaller than those determined prior to core cross-linking (*viz.* 168.2 and 135.8Å for the 10k and 5k respectively). This result is not unexpected, since the core has essentially undergone a polymerisation reaction, and with this one would normally associate a decrease in volume. Other reports also note a decrease in radii on cross-linking. In common with the reports of Won and co-workers,[3] the reduction in the core volume exceeds that associated with the densification of rubber. From crude estimates based on the van der Waals radii and the length of carbon-carbon bonds the decrease in core radii upon polymerisation would be anticipated to be of the order of 7%, a value in the region of that observed.

One striking feature of the data is the reversal in sign of the diffusion second virial coefficient for the 5k micelles, from positive to negative, such now that both molecular weights exhibit values of the same sign. This may be due to the presence of residual inorganic salts from the cross-linking reaction, whose concentrations are close to that of the copolymer in the dispersion, giving rise to bridging effects in the corona of the micelles, and thus making them attractive rather than repulsive to one another.

The scaling relationship proposed by Halperin[22] is now perhaps more relevant since the cross-linked micelles could be viewed as star polymers having a number of arms equal to the association number. According to Halperin the micelle radius can be related to the degree of polymerisation of both blocks and the segment length by equation 4.2.

$$R \approx N_B^{4/25} N_A^{3/5} a \qquad \textbf{Equation 4.2}$$

where N_B is the degree of polymerisation of the core block, N_A is the degree of polymerisation of the shell block, and a is the segment length, the value of which was given in chapter three (4.01Å)[23]

Table 4.2 details the values expected from equation 4.2, and the experimentally determined values for the micelles both before and after cross-linking.

Copolymer	R_h/Å	R/Å	R_h:R
10k hPB-hPEO ($B_{14}E_{89}$) - micelles	135.8	92.4	1.470
5k hPB-hPEO ($B_{27}E_{164}$) - micelles	168.2	146.6	1.147
10k hPB-hPEO ($B_{14}E_{89}$) - xl micelles	93.8	92.4	1.015
5k hPB-hPEO ($B_{27}E_{164}$) -xl micelles	156.1	146.6	1.065

Table 4.2 - *Hydrodynamic radii determined by QELS, and theoretical radii determined using Halperin's star model (equation 4.2),R, with R_h:R being the ratio of the experimental and theoretical radii.*

It is evident from table 4.2 that the correlation between the experimentally determined value and the theoretically expected value is better for the micelles after they have been cross-linked. This is likely to be due to the origins of the model being in the description of star polymers, and as the cross-linked micelles behave more like star polymers due to their fixed core than the micelles, better agreement would be expected.

4.3.2. Concentration effects

In common with the micelles, the effect of concentration upon the size distribution of the cross-linked micelles was investigated at concentrations as high as 100 mg mL^{-1} for both molecular weights. Figures 4.2 and 4.3 show the size distributions, obtained from CONTIN[24] analysis, for 10k hPB-hPEO and 5k hPB-hPEO respectively.

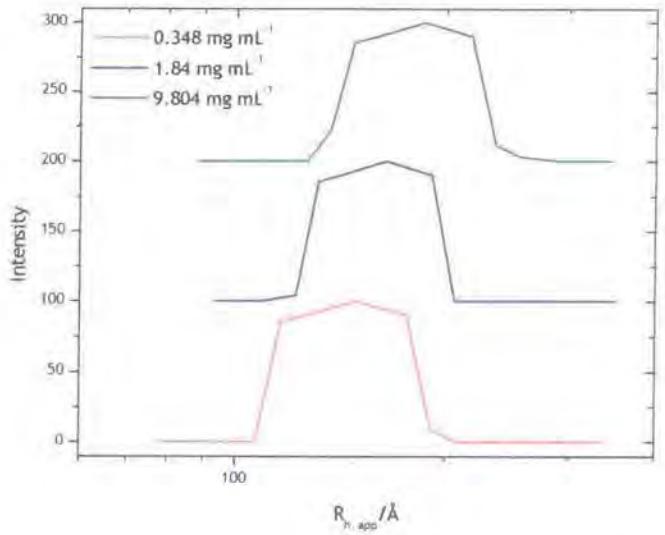

Figure 4.2 - *Size distribution for 10k hPB-hPEO in dilute solutions. The distributions are shifted successively by 100 for clarity.*

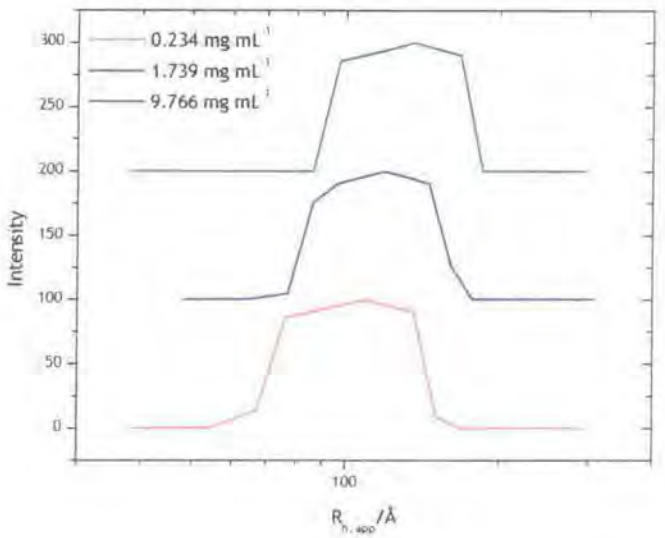

Figure 4.3 - *Size distribution for 5k hPB-hPEO in dilute solutions. The distributions are shifted successively by 100 for clarity.*

What is immediately apparent from figures 4.2 and 4.3 is that the distributions are monomodal, and relatively wide in comparison to those of the virgin micelles. The cross-linking reactions were carried out at concentrations of ca. 10%, and the size distributions for such concentrations presented in chapter three showed bimodal populations. The fact that the cross-linked micelles exhibit monomodal distributions in dilute solution

suggests that the reaction has been confined to the core of the micelle, and that no intermicellar reactions have taken place. SANS data for micellar dispersions at this concentration also presented in chapter three suggested a higher polydispersity in the micelle size with respect to more dilute solutions, and this fact could likely explain the increased width of the size distributions. Figures 4.4 and 4.5 show size distributions of the cross-linked micelles at higher concentrations.

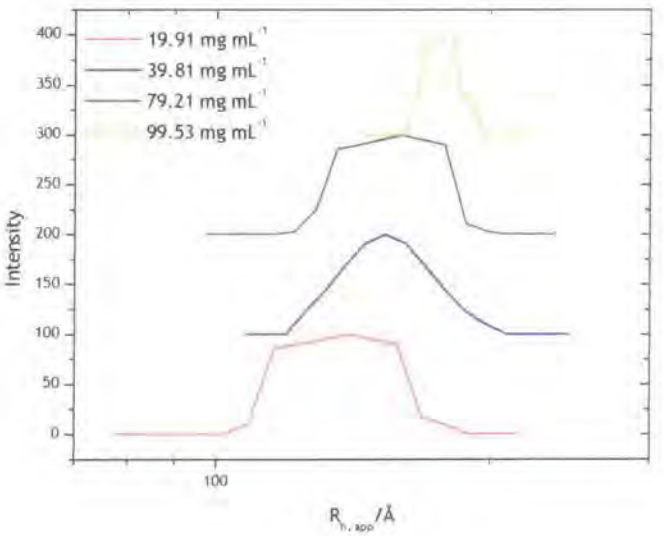

Figure 4.4 - *Size distribution for 10k hPB-hPEO at higher concentrations. The distributions are shifted successively by 100 for clarity.*

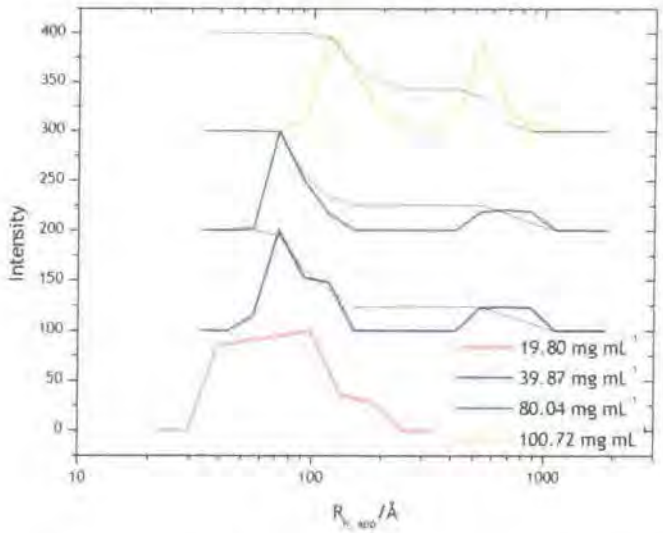

Figure 4.5 - *Size distribution for 5k hPB-hPEO at higher concentrations showing the development of dual populations at c>2%. The black lines on the cumulative distributions represent the relative amounts of each present. The distributions are shifted successively by 100 for clarity*

Interestingly, the 10k cross-linked micelles do not show any evidence of dual populations, in contrast to the virgin micelles and its lower molecular weight counterpart. There does not appear to be any rational reason for this as it is a departure from the behaviour observed thus far for these copolymers. Bimodal populations are not always observed for block copolymer micelle dispersions at high concentrations,[25] indeed the Booth group rarely report this phenomenon for the PBO-PEO systems they have studied.[26, 27] The 5k cross-linked micelles exhibit the same pattern as their virgin counterparts, namely the appearance of bimodal distributions at c>2%, with the larger particles having radii of ca. six to seven times that of the micelles and constituting less than a quarter of the population.

4.3.3. Conclusions

For clarity, the important facts that have been concluded from the QELS data are presented here.

- The micelles of both molecular weights have decreased in size following the cross-linking reaction, with the 10k having a hydrodynamic radius of 156Å, and the 5k of 94Å.

- The micelle size distributions are wider after the cross-linking reaction.
- The 10k cross-linked micelles do not show any evidence of bimodal distributions at higher concentrations, in contrast to their lower molecular weight counterparts.

4.4. Static light scattering

The procedure utilised for analysis of the cross-linked micelles was the same as that employed for the characterisation of the of block copolymer micelles detailed in chapter three, namely the Zimm plot methods.

4.4.1. Zimm plot determination

The Zimm plots constructed use equation 2.23 as their theoretical basis, *viz.*

$$\frac{K(c-cmc)}{R_\theta} = \left|_{\substack{c\to 0\\ \theta\to 0}} \frac{1}{M}\left[1+\frac{16\pi^2}{3\lambda^2}\left\langle R_g^2\right\rangle \sin^2(\theta/2)\right] + 2A_2(c-cmc)\right. \qquad \text{Equation 4.3}$$

It was assumed that the dn/dc value for the micelles had not changed upon cross-linking, and so was still 0.137ml g^{-1}.

Figures 4.6 and 4.7 show Zimm plots for 10k hPB-hPEOxl and 5k hPB-hPEOxl respectively.

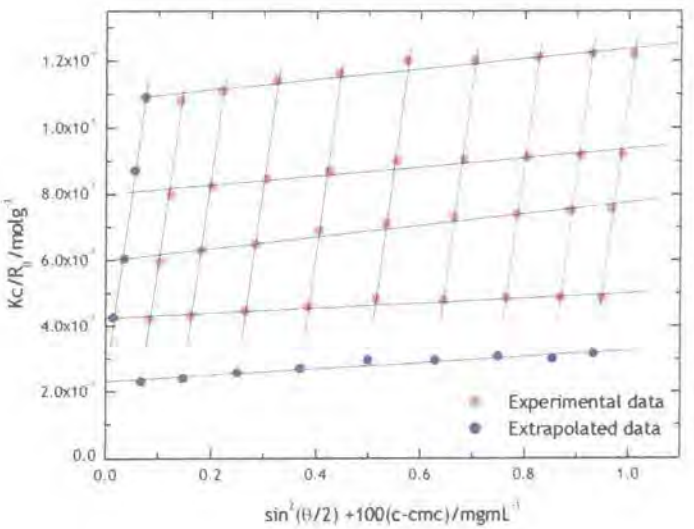

Figure 4.6 - *Zimm plot for 10k hPB-hPEOxl in water generated using equation 4.3. Vertical lines are fits through concentration series at a given angle and the horizontal lines are fits through angular series at a given concentration.*

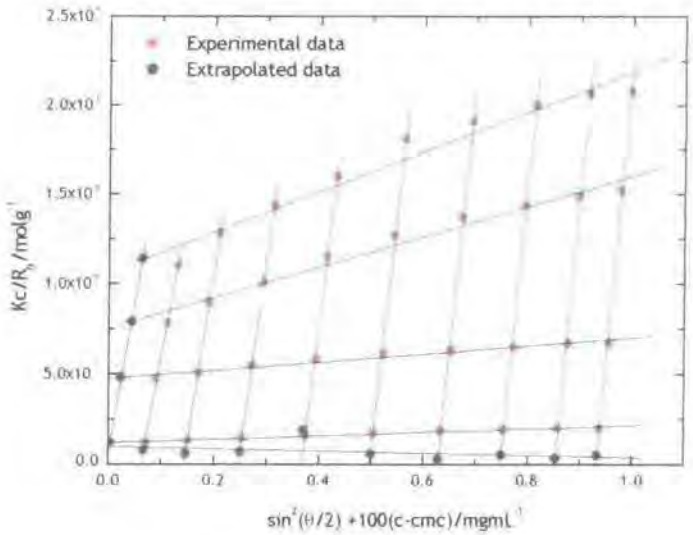

Figure 4.7 - *Zimm plot for 5k hPB-hPEOxl in water generated using equation 4.3. Vertical lines are fits through concentration series at a given angle and the horizontal lines are fits through angular series at a given concentration.*

The parameters determined from the extrapolations to zero angle and zero concentration are listed in table 4.3.

Polymer	M_{app}/g mol^{-1}	A_2/cm^3 mol g^{-1}	$R_{g,\,app}$/Å
10k hPB-hPEOxl	$4.275\times10^6 \pm 4.5\times10^4$	5.083×10^{-4}	470
5k hPB-hPEOxl	$1.195\times10^7 \pm 1.85\times10^5$	8.393×10^{-4}	undefined

Table 4.3 - *Molecular weights, second virial diffusion coefficients (A_2) and radii of gyration calculated from extrapolated data in figures 4.6 and 4.7.*

What is immediately apparent from table 4.3 are the differences in the molecular weight of the two species of cross-linked micelles. Similar to the virgin micelles, the lower molecular weight copolymer micelles display a higher molecular weight. Again, perhaps the only rational explanation is that of experimental error, with the quality of the data being quite poor. In this respect the observation of a negative radius of gyration for the 5k cross-linked micelles clearly indicates other factors at work. This may result from the unusual solvent conditions imparted from the presence of the inorganic slats in the dispersions. The radius of gyration determined for the 10k cross-linked

micelles is not that expected for micelles behaving as hard spheres then R_g:R_h =0.77 should apply.[28] The observed value is ca. 3, more in line with the value expected for cylindrical morphology. SAXS and SANS data presented later in this chapter suggest micelles are spherical in nature, calling into question the validity of the SLS data.

Using equation 3.16, and the dn/dc values calculated for the individual blocks, along with their respective molecular weights the true value of the micelle molecular weight can be calculated.[29] These values are listed in table 4.4.

Polymer	M_{app}/g mol^{-1}	M_w/g mol^{-1}
10k hPB-hPEOxl	$4.275\times10^6 \pm 4.5\times10^4$	$3.168\times10^6 \pm 3.518\times10^4$
5k hPB-hPEOxl	$1.195\times10^7 \pm 1.85\times10^5$	$8.851\times10^6 \pm 1.379\times10^5$

Table 4.4 - *True molecular weights of 10k hPB-hPEOxl and 5k hPB-hPEOxl calculated using equation 3.16.*

4.4.3. Conclusions

As was the case with the virgin micelles, interpretation of the SLS data is open to question. The molecular weights and radii obtained from the data do not make a great deal of sense with respect to the QELS data and theoretical predictions. One can only assume that the dubious quality of the data is either a phenomenon of the particular system or due to experimental error. The presence of the inorganic salts is likely to complicate the behaviour of the micelles due to the changes in the solvent properties for the coronal brush.

4.5. Small-angle X-ray scattering

4.5.1. Introduction

The SAXS experiments were carried out under the same conditions reported earlier, with the exception of D_2O being the solvent as opposed to H_2O, due to the solutions being obtained by direct dilution from the reaction mixture. As

the contrast-determining factor in SAXS is the electron density of a molecule, the replacement of H with D in the solvent has no effect.

4.5.2. Dilute solutions

The scattering from dispersions with c<1% was too weak to obtain acceptable data. Indeed scattering from the 1% dispersions was also quite weak, making interpretation of any parameters obtained from it quite difficult, and leading to a degree of uncertainty.

4.5.2.1. Preliminary analysis

Following correction of the scattering data for solvent and instrument effects, a plot of log(I(Q)) *vs.* log(Q) (figure 4.8) for the 1% dispersion of 10k hPB-hPEOxl was constructed to determine the presence of cylindrical micelles.

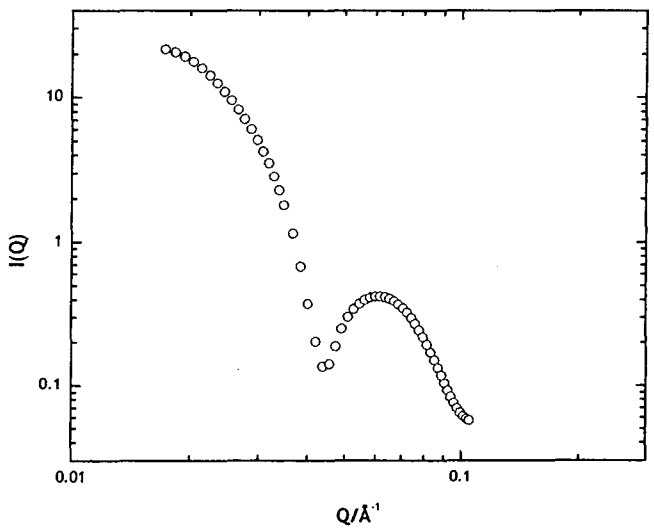

Figure 4.8 - *Log-Log plot for 10k hPB-hPEOxl after correcting for solvent and instrument effects*

It was impossible to to apply this procedure to the 5k micelles since the scattering was too weak.

Using a Guinier approximation:[30]

$$I(Q) \approx NV^2(\Delta\rho)^2 \exp\left(-\frac{(QR)^2}{5}\right) \approx NV^2(\Delta\rho)^2 \exp\left(-\frac{(QR_g)^2}{3}\right) \qquad \textbf{Equation 4.4}$$

both the radius of gyration and the radius of a sphere can be determined from the scattering data. A plot of $\ln(I(Q))$ vs. Q^2 gives a gradient of $-R^2/5$ or $-R_g^2/3$. Figure 4.9 shows a Guinier approximation for the 10k cross-linked micelles.

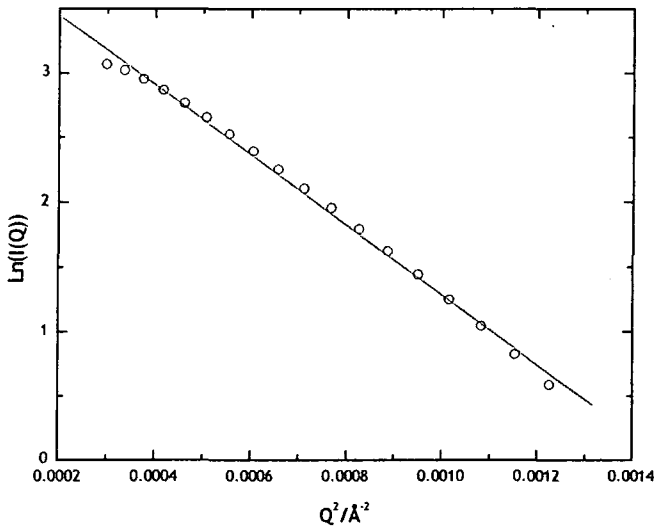

Figure 4.9 - *Guinier approximation for 10k hPB-hPEOxl constructed using equation 4.6. Sphere radius determined from linear fit is 116 Å.*

The radius determined from a linear fit to the data is 116Å. This is smaller than the hydrodynamic radius of 156Å determined from the QELS experiments. It is larger than the value of 70Å obtained from SAXS experiments on the virgin micelles however, in contrast to the observations made in the QELS experiments where the micelles contracted in size following cross-linking. As was stated earlier, the scattering from the dilute dispersions before and after cross-linking was relatively weak and so values obtained from them should be treated with caution.

4.5.2.2. Fitting to a core-shell model

The spherical core-shell model employed to fit the micelle data was also utilised here.[31] The model was described in some detail in section 3.4.2.2, and so will not be discussed. Dr Richard Heenan's FISH2 analysis software was used to fit the data; with the same strategy used earlier.[32]

Figure 4.10 shows the fit obtained for 10k hPB-hPEOxl using the core-shell model in both linear and semi-logarithmic form, with the parameters extracted from the fit given in table 4.5.

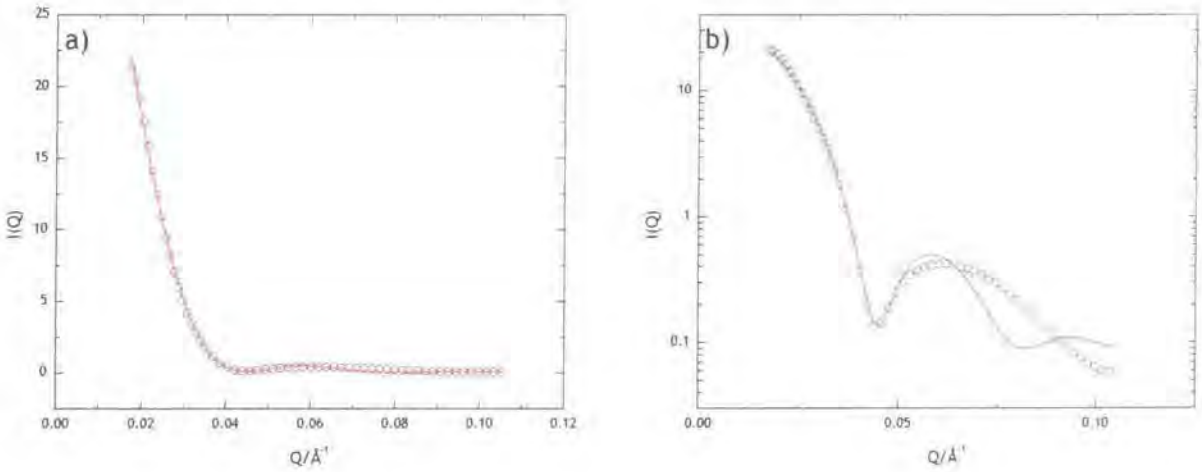

Figure 4.10 - *Fits obtained to 1% dispersion data for 10k hPB-hPEOxl using the FISH2 software program. a) shows a linear intensity scale, and b) shows a logarithmic intensity scale. Red lines are fits to the data*

Parameter	10k hPB-hPEOxl
R_c/Å	23
R_{cs}/Å	98
R_s/Å	75
σ/R	0.17

Table 4.5 - *Parameters obtained from fits to 10k hPB-hPEOxl, shown in figure 4.14, using the core-shell model*

It is evident from figure 4.10, that the model does not really fit the data, and so the dimensions obtained from it should not be taken as absolute.

The micelle dimensions obtained from the core-shell fit to the data are larger than those of the virgin micelles, which was also seen from the Guinier approximation. Again this contradicts the QELS data, but as the scattering observed in the SAXS experiments was relatively weak, and the fit to the data not exact, it is perhaps more prudent to trust the QELS data.

4.5.3. Higher concentration dispersions

Section 3.4.3 detailed two of the possible methods that could be used to model the structure factor peak evident at higher concentrations, namely the hard-sphere potential, and the mean spherical approximation of Hayter and Penfold.[33] It was also noted that whilst the hard-sphere potential did not satisfactorily model S(Q), the mean spherical approximation reproduced many of the features quite well. For this reason it was decided to pursue the latter to model the current SAXS data.

The model used was the same as for the micelles i.e. a spherical core-shell form factor coupled with the mean spherical approximation.

Typical fits to the data from both the 5k and 10k cross-linked micelles can be seen in figures 4.11 to 4.13, with the associated parameters given in tables 4.6 and 4.7 respectively.

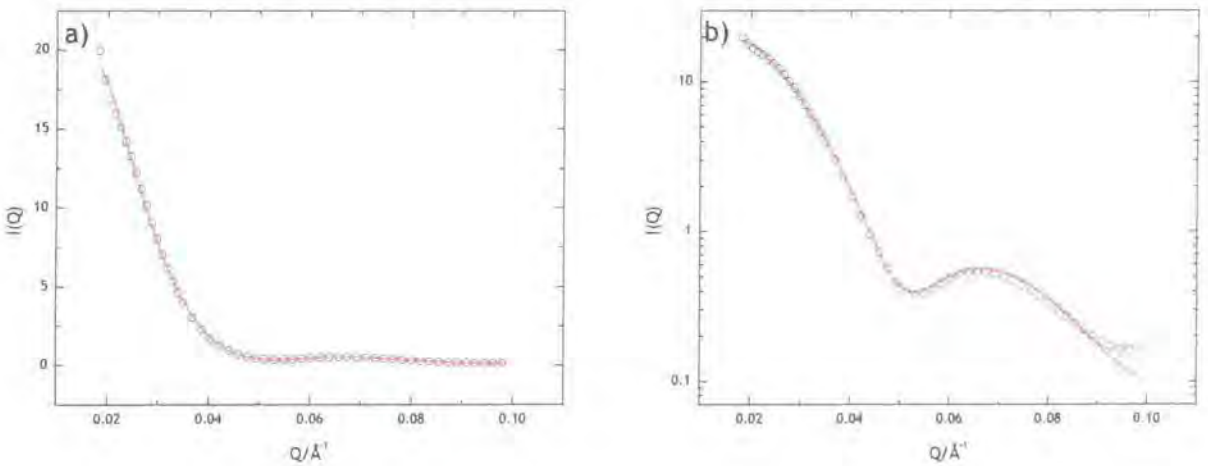

Figure 4.11 - *SAXS from a 2% dispersion of 10k hPB-hPEO. a) shows a linear cross-section and b) a logarithmic scale. Red lines are fits to the data.*

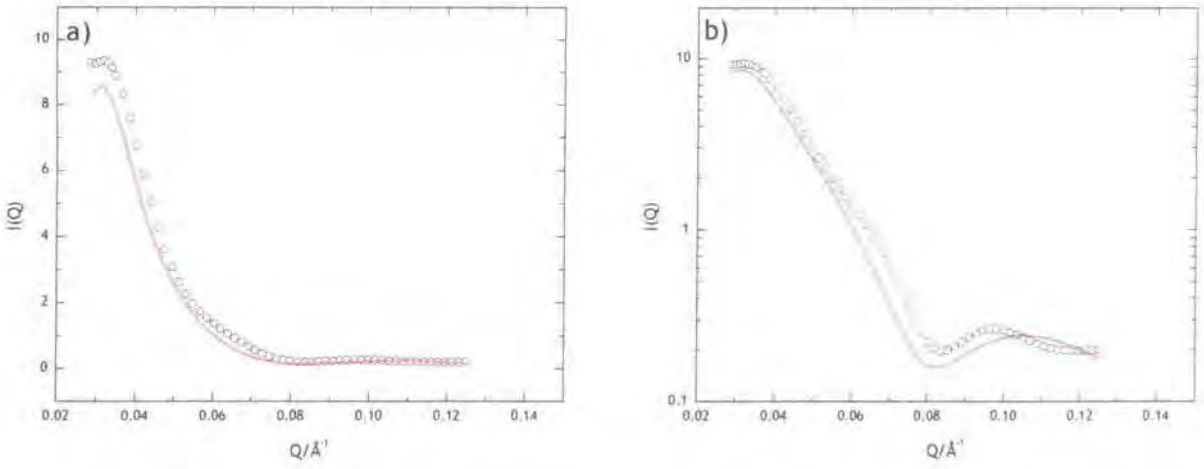

Figure 4.12 - *SAXS from a 4% dispersion of 5k hPB-hPEO. a) shows a linear cross-section and b) a logarithmic scale. Red lines are fits to the data.*

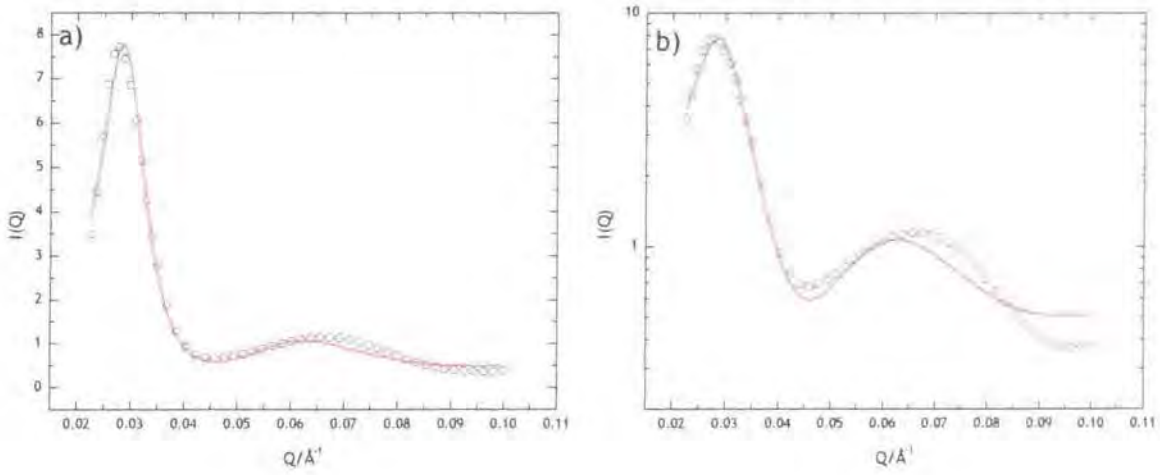

Figure 4.13 - *SAXS from a 10% dispersion of 10k hPB-hPEO. a) shows a linear cross-section and b) a logarithmic scale. Red lines are fits to the data.*

Parameter	10%	8%	4%	2%
R_c/Å	8	8	8	8
R_s/Å	47	47	46	46
σ/R	0.45	0.44	0.42	0.41
H-P S(Q) R/Å	50.95	50.02	45.62	41.11
Charge	5.71	9.012	17.00	19.66
κ/Å^{-1}	5.931×10^{-3}	7.931×10^{-3}	9.931×10^{-3}	1.751×10^{-2}
γ	2.466	6.580	26.515	47.836
$\gamma\exp(-k)$	1.347	2.977	10.716	11.347

Table 4.6 - *Parameters from fits to dispersions of 5k hPB-hPEOxl using a core-shell model with the mean spherical approximation to model the structure factor*

Parameter	10%	8%	4%	2%
R_c/Å	26	25	26	27
R_s /Å	52	52	55	52
σ/R	0.34	0.31	0.32	0.30
H-P S(Q) R/Å	65.71	64.93	67.31	73.29
Charge	32.73	13.00	15.62	17.56
κ/Å^{-1}	9.490×10^{-3}	4.196×10^{-2}	5.665×10^{-2}	7.351×10^{-2}
γ	76.879	5470.059	1146.340	17609.906
$\gamma\exp(-k)$	22.089	0.118	0.559	0.368

Table 4.7 - *Parameters from fits to dispersions of 10k hPB-hPEOxl using a core-shell model with the mean spherical approximation to model the structure factor*

The model generated fits for the higher concentration dispersions match the features of the data more closely than that seen for the dilute dispersion, but still don't reproduce all of the features observed in the data. However, in

common with the virgin micelles, the low SAXS contrast hinders any quantitative treatment of the data.

4.5.4. Comparison between virgin and cross-linked micelles

Comparisons between the SAXS data for the micelles before and after cross-linking is not one that can be done quantitatively due to the nature of the fits generated using the core shell model, as the fits do not reproduce all the features in the data. It is however, a useful exercise to show changes in the behaviour of the micelles before and after cross-linking.

Figures 4.14-4.17 show the SAXS data from the virgin and cross-linked micelles plotted on the same axes. Representative samples of the concentration and molecular weight effects have been given. Table 4.8 details the dimensions determined from the fits before and after cross-linking.

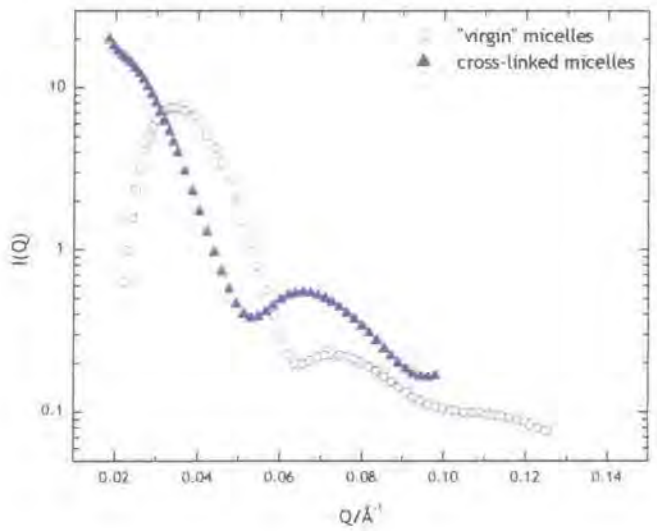

Figure 4.14 - *SAXS data from 10k 2% hPB-hPEO before and after cross-linking. Lines are fits to the data.*

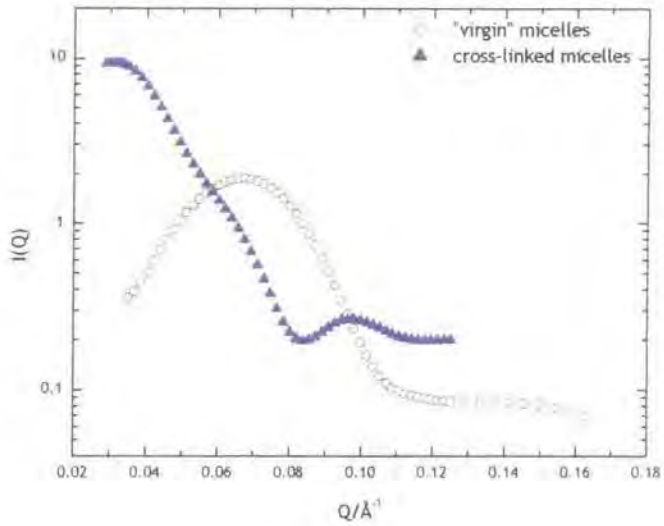

Figure 4.15 - *SAXS data from 5k 4% hPB-hPEO before and after cross-linking. Lines are fits to the data.*

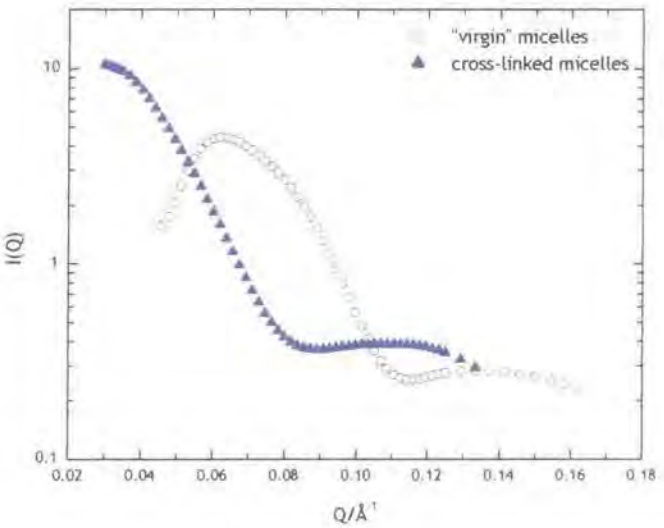

Figure 4.16 - *SAXS data from 5k 8% hPB-hPEO before and after cross-linking. Lines are fits to the data.*

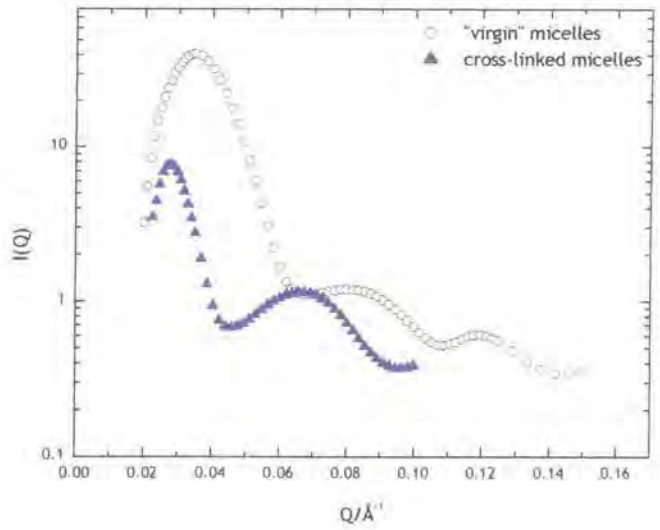

Figure 4.17 - *SAXS data from 10k 10% hPB-hPEO before and after cross-linking. Lines are fits to the data.*

Conc/%	Parameter	10k hPB-hPEO		5k hPB-hPEO	
		Virgin micelles	xl micelles	Virgin micelles	xl micelles
10	R_c/Å	15	26	6	8
	R_s /Å	43	52	32	47
	γexp(-k)	23.083	22.089	13.901	1.347
8	R_c/Å	16	25	6	8
	R_s /Å	43	52	30	47
	γexp(-k)	23.465	0.118	20.477	2.977
4	R_c/Å	13	26	6	8
	R_s /Å	48	55	30	46
	γexp(-k)	29.057	0.559	21.294	10.716
2	R_c/Å	11	27	6	8
	R_s /Å	59	52	25	46
	γexp(-k)	62.594	0.368	27.194	11.347

Table 4.8 - *Micelle dimensions determined from fits to SAXS data before and after cross-linking reaction.*

What is immediately apparent from figures 4.14-4.17 is the change in the shape of the structure factor peak. In all of the samples characterised, with the exception of the 10k 10% dispersion, the peak has largely disappeared, with it no longer showing a clearly pronounced maximum as it does in the virgin micelles. This appears to be caused by the shift in the entire data to lower Q values, which one could associate with an increase in dimensions of the micelles, a fact supported by the parameters from fits to the data shown in table 4.8. However, the change in shape could also be due to decreased interactions between the micelles, reducing the degree of ordering in the system, and thus the intermicellar interference that gives rise to the structure factor peak. As stated in chapter three, $\gamma\exp(-k)$ is the contact potential between a macroion pair, which for uncharged species such as those encountered here, can serve as an indication as to the strength of interaction between the micelles. For any given concentration at either of the two molecular weights the value of $\gamma\exp(-k)$ is smaller for the micelles after cross-linking than before, supporting the notion of decreased interaction between them. However, as the model does not reproduce the features of the scattering data to an acceptable degree, values obtained from fitting the data should be treated with caution. The safest conclusion is that the contact potential suggests reduced interaction on cross-linking.

The interpretation of the scattering data from the cross-linked micelles is made troublesome by the residual inorganic salts from the cross-linking reaction. These effect the properties of the solvent, in terms of its thermodynamic quality, and serve to increase the SAXS contrast by virtue of their large numbers of electrons. Thus quantitative comparisons between the two sets of scattering data are impossible.

4.5.5. Conclusions

In common with the virgin micelles, the low SAXS contrast hindered attempts to produce a quantitative picture of the micelles in terms of their dimensions and interactions. Scattering from the dilute regime was even less pronounced than for the virgin micelles, consequently obtaining quantitative of sufficient quality was difficult if not impossible. For clarity the main conclusions that can be inferred from the data are presented below.

- Fits to the dilute dispersion data for 10k hPB-hPEOxl, using a spherical core shell model, suggest the micelles have a core radius of 23Å surrounded by a shell that is 75Å thick, giving a total micelle radius of 98Å, larger than from the micelles prior to cross-linking. These values should be treated with caution since the fit does not match the data exactly.
- The scattering from 5k hPB-hPEOxl at 1% was too weak to fit.
- The mean spherical approximation due to Hayter and Penfold was used to model the scattering from the higher concentration data, but with limited success.
- Fits to the higher concentration data suggest 10k hPB-hPEOxl micelles have a core radius of 26Å and a shell thickness of 52Å, whilst their 5k counterparts have a core of 8Å and a shell of 46Å, both of which are larger than for the virgin micelles.
- The structure factor peak due to intermicellar interactions is not as pronounced for the cross-linked micelle dispersions. There is support from interpretations of fits to the data that this is due to a decrease in intermicellar interactions.
- A detailed comparison of the data with that of the virgin micelles was impossible due to the different solvent conditions under which the scattering experiments were carried out.

4.6. Small-angle Neutron scattering

4.6.1. Introduction

The protocol for the SANS experiments on the cross-linked micelles was the same as that employed for the virgin micelles, the same range of concentrations and contrasts were explored, except for the fully hydrogenous micelles where the maximum concentration probed was 10%.

4.6.2. Dilute dispersions

4.6.2.1. Preliminary treatment

Double logarithmic plots showed no Q^{-1} dependencies indicative of cylindrical micelles.[34] Typical plots for 1% dispersions of both molecular weights for all contrasts are shown in figure 4.18. The reader is referred to pg 139 for the equivalent plots for the virgin micelles.

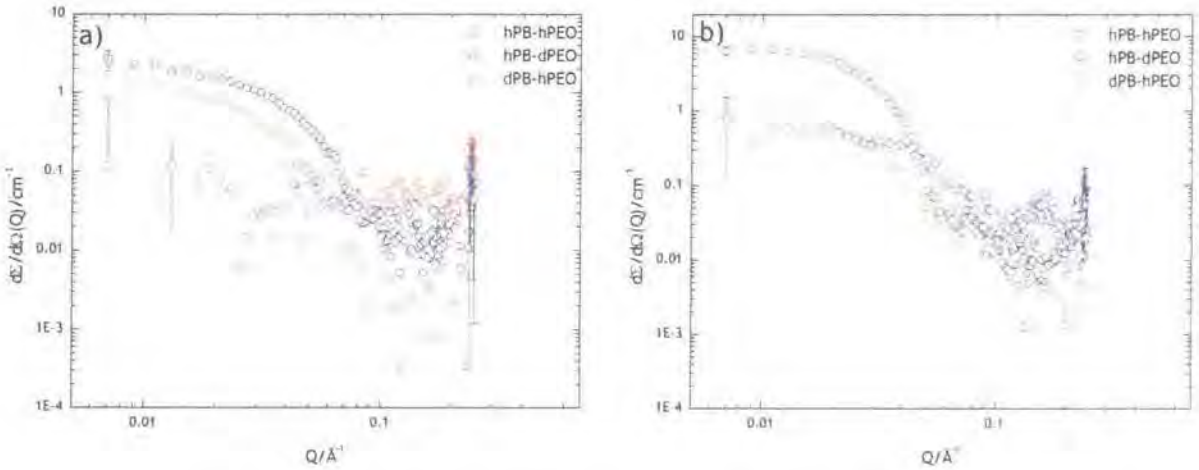

Figure 4.18 - *Double logarithmic plots for a)5k and b) 10k dispersion of cross-linked micelles. Representative error bars are shown for clarity.*

The Guinier approximation was applied to the dilute solution data. Typical plots are shown in figure 4.19 again for both copolymers and all three contrasts, with the respective results obtained detailed in table 4.9.

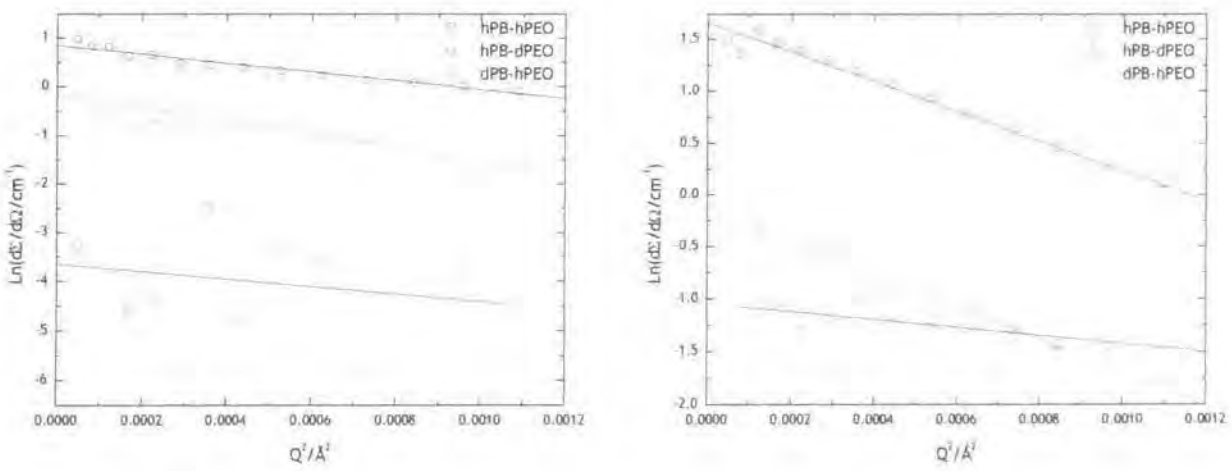

Figure 4.19 - *Guinier plots for 1% dispersions of a) 5k and b) 10k cross-linked micelles generated using equation 4.6. Lines are linear fits to the data*

Isotopic variation		Conc/%	Sphere Radius/Å 0.2	0.4	0.6	1
hPB-hPEO	**5k**	**micelles**	76	74	77	74
		xl micelles	n/a	64	67	69
	10k	**micelles**	132	131	130	130
		xl micelles	82	88	84	85
hPB-dPEO	**5k**	**micelles**	126	125	120	123
		xl micelles	n/a	99	66	85
	10k	**micelles**	161	173	168	169
		xl micelles	100	88	88	87
dPB-hPEO	**5k**	**micelles**	n/a	n/a	48	61
		xl micelles	n/a	n/a	n/a	n/a
	10k	**micelles**	56	65	60	66
		xl micelles	n/a	n/a	44	52

Table 4.9 - *Sphere radii determined using Guinier approximation for micelles both before and after cross-linking for both molecular weight series and all contrasts. Isotopic variant in bold is the part of the molecule scattering the radiation. n/a indicates scattering was too weak to give acceptable values.*

It is evident from table 4.9 that in all cases the size of the micelles has decreased following cross-linking. This is consistent with the observations of the QELS experiments, and in line with the result expected.

4.6.2.2. Fitting to a core-shell model

The model used to fit the data from the cross-linked micelles was that employed for the virgin micelles described in chapter three, i.e. a spherical core-shell form factor, with uniform core density and a parabolic volume fraction profile in the shell.

The FISH2 analysis software was used to fit the data, fixing the volume fraction of water in the innermost sub-shell of the corona.

Figures 4.20 to 4.22 show representative fits for the different contrasts and concentrations explored for the two molecular weights, with the parameters from all of the fits for the dilute dispersions given in tables 4.10 and 4.11.

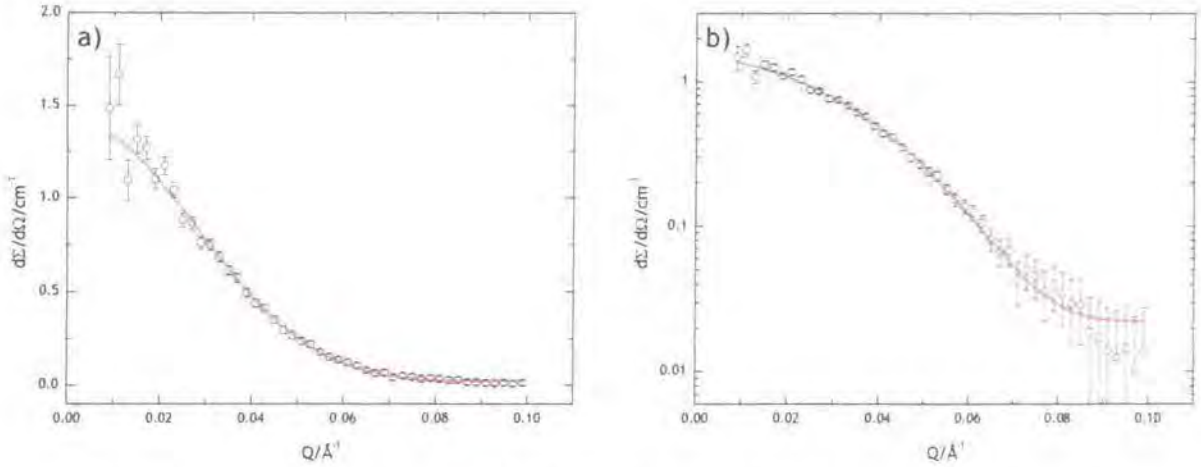

Figure 4.20 - *0.4% dispersion of 5k hPB-hPEO in D_2O. a) linear scale, b) semi-logarithmic. Red lines are fits to the data.*

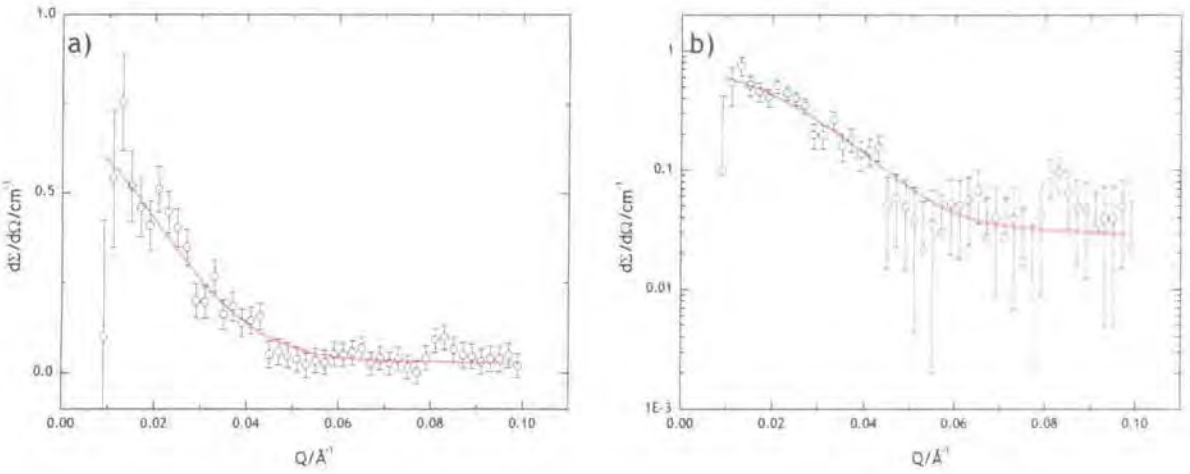

Figure 4.21 - *0.6% dispersion of 5k hPB-dPEO in hPB contrast match H_2O. a) linear scale, b) semi-logarithmic. Red lines are fits to the data.*

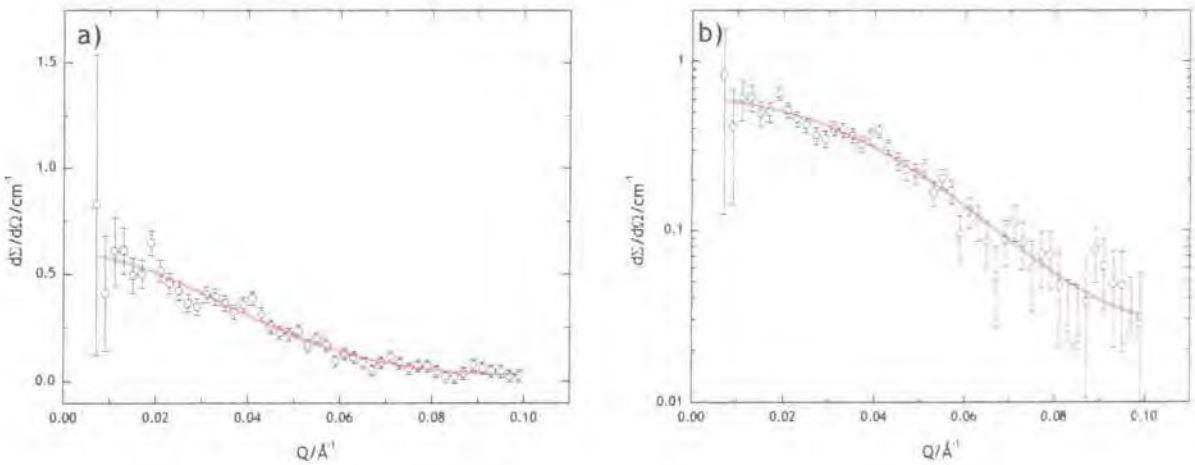

Figure 4.22 - *1% dispersion of 10k dPB-hPEO in hPEO contrast match H_2O. a) linear scale, b) semi-logarithmic. Red lines are fits to the data.*

Copolymer	Conc/%	R_cÅ	R_sÅ	$\Delta\rho_c/10^{10}cm^{-2}$	$\Delta\rho_s/10^{10}cm^{-2}$	σ/R	ϕ_w
hPB-hPEO	0.2			Scattering too weak to fit			
	0.4	14	53	-4.877	-1.033	0.20	0.82
	0.6	14	53	-4.762	-1.148	0.20	0.8
	1.0	14	52	-4.590	-1.320	0.20	0.77
hPB-dPEO	0.2			Scattering too weak to fit			
	0.4	19	53	-1.078	1.078	0.67	0.82
	0.6	19	55	-1.198	1.198	0.54	0.80
	1.0	21	54	-1.198	1.198	0.64	0.80
dPB-hPEO	0.2						
	0.4			Scattering too weak to fit			
	0.6						
	1.0	19	-	6.180	0	0.27	-

Table 4.10 - *Parameters obtained from 5k cross-linked micellar dispersions fitted to the core-shell model shown using FISH 2.*

Copolymer	Conc/%	R_cÅ	R_sÅ	$\Delta\rho_c/10^{10}cm^{-2}$	$\Delta\rho_s/10^{10}cm^{-2}$	σ/R	ϕ_w
hPB-hPEO	0.2	29	79	-5.049	-0.861	0.25	0.85
	0.4	29	76	-4.877	-1.033	0.15	0.82
	0.6	24	74	-4.475	-1.435	0.15	0.80
	1.0	25	74	-4.647	-1.263	0.15	0.78
hPB-dPEO	0.2	29	61	-0.899	0.899	0.41	0.85
	0.4	29	61	-1.078	1.078	0.37	0.82
	0.6	30	59	-1.198	1.198	0.28	0.80
	1.0	30	58	-1.318	1.318	0.20	0.78
dPB-hPEO	0.2						
	0.4			Scattering too weak to fit			
	0.6	37	-	6.180	-	0.20	-
	1.0	37	-	6.180	-	0.20	-

Table 4.11 - *Parameters obtained from 10k cross-linked micellar dispersions fitted to the core-shell model shown using FISH 2.*

From tables 4.10 and 4.11 it is evident that the total micelle radius for the 5k series is of the order of 80Å, with the core radius being circa 17Å. The 10k series shows a micelle radius of 100Å, with a core radius of circa 30Å.
These values are smaller than those observed for the virgin micelles, supporting both the observations of the QELS measurements and the Guinier approximation.
One interesting point to note, is that not only has the core contracted upon cross-linking, but the shell thickness has also decreased. The likely explanation for this is the presence of inorganic salts in the dispersions that were not removed following the cross-linking reactions. Salts reduce the solvent quality for the PEO brush, changing it from a good solvent possibly to a theta solvent, resulting in the partial collapse of the corona as the chains seek to maximise the more favourable interactions with one another as opposed to the less favourable interactions with the solvent. Beaudoin and co-workers have reported similar results for micelles formed from hydrophobically end-capped PEO.[35] They noted that the addition of monovalent ions such as potassium resulted in reduced swelling of the shell of the micelles as observed by QELS and SANS.

Table 4.12 sets out the micelle dimensions after cross-linking and relates these to the dimensions of virgin micelles in terms of the percentage decrease.

Copolymer	Conc/%	5k series				10k series			
		R_c/Å	%-	R_s/Å	%-	R_c/Å	%-	R_s/Å	%-
hPB-hPEO	0.2	Scattering too weak				29	17	79	31
	0.4	14	26	53	15	29	28	76	30
	0.6	14	26	53	10	24	38	74	34
	1.0	14	30	52	10	25	34	74	35
hPB-dPEO	0.2	Scattering too weak				29	28	61	48
	0.4	19	21	53	45	29	34	61	45
	0.6	21	16	55	41	30	29	59	48
	1.0	19	24	54	41	30	33	58	46
dPB-hPEO	0.2	Scattering too weak to fit				Scattering too weak to fit			
	0.4								
	0.6					37	21	-	-
	1.0	19	30	-	-	37	18	-	-

Table 4.12 - *Change in radii relative to the virgin micelles. %-calculated by 1-(xl micelle/virgin)*

Table 4.12 demonstrates that there is a finite change in the micelle dimensions, ranging from 16-38% for the core radius, and 10-48% for the shell thickness. These are a larger relative change than the 13% decrease in core radius reported by Won *et al.* for cylindrical micelles of PB-PEO.[3]

In chapter three, the association numbers for the micelles were calculated on the basis of the core radius and the volume of the poly(butadiene) block. This is not possible for the cross-linked micelles since the core no longer consists of chains that are independent of one another, but of chains that are covalently bonded to each other. Under these circumstances perhaps a realistic assumption to make is that the association number of the micelles remains unchanged from the value obtained prior to cross-linking, i.e. the value determined at 10%. This can be justified on the basis that once the micelle has been cross-linked, just one covalent bond per chain is sufficient to prevent the chain leaving the micelle. On this assumption, it is possible to calculate the distance of separation between the PEO chains on the surface of the core, and relate this to the unperturbed radius of gyration of the PEO

block. Tables 4.13 and 4.14 provide the values of the association numbers calculated for the 10% dispersions of the micelles, the respective radii of gyration of the PEO blocks, the separation distance between the PEO blocks on the surface of the core, and the degree of stretching in the corona relative to the unperturbed radii of gyration of the respective PEO blocks. The reader is referred to section 3.5.2.2 for details of the calculations.

Copolymer	Conc/%	p	R_g PEO/Å	D_{PEO}/Å	R_s:R_g
hPB-hPEO	0.4	27	23	9.55	2.27
	0.6	27		9.55	2.27
	1.0	27		9.55	2.23
hPB-dPEO	0.4	20	26	15.06	2.05
	0.6	20		15.06	2.13
	1.0	20		16.65	2.09
dPB-hPEO	1.0	59	30	-	-

Table 4.13 - *Values of association number, p, distance between PEO chains on the core surface D_{PEO}, and the ratio of the shell thickness to the unperturbed radius of gyration R_s:R_g for dilute dispersions of the 5k cross-linked micelles.*

Copolymer	Conc/%	p	R_g PEO/Å	D_{PEO}/Å	R_s:R_g
hPB-hPEO	0.2	106	36	9.99	2.18
	0.4	106		9.99	2.10
	0.6	106		8.26	2.04
	1.0	106		8.61	2.04
hPB-dPEO	0.2	197	26	7.32	2.32
	0.4	197		7.32	2.32
	0.6	197		7.58	2.24
	1.0	197		7.58	2.20
dPB-hPEO	0.2	140	40	-	-
	0.6	140		-	-
	1.0	140		-	-

Table 4.14 - *Values of association number, p, distance between PEO chains on the core surface D_{PEO}, and the ratio of the shell thickness to the unperturbed radius of gyration R_s:R_g for dilute dispersions of the 10k cross-linked micelles.*

The two molecular weight series cross-linked micelles show some similarities in their behaviour following cross-linking. With the exception of the 5k hPB-dPEO cross-linked micelles, they all show a reduction in the separation distance between PEO chains on the core surface. One explanation for the unusual behaviour of the 5k hPB-dPEO species is the association number used in the calculations. All of the values of p were based upon the core dimensions determined from fits to the data at the concentration the reactions were carried out, i.e. 10%. The 5k hPB-dPEO micelles gave a slightly smaller core radius, and therefore association number, than the more dilute dispersions. This gives rise to a larger separation distance than that observed for the dilute dispersions, a result that is quite unexpected. Because the association numbers determined for the 5k micelles were modest in size (<50), any small change in the core radius affects the association number greatly. Consequently the real association number may be larger than quoted, and thus the PEO chain separation distance may have decreased along with the others.

4.6.2.3. Comparison with theory

Scaling relationships due to Daoud and Cotton,[36] Halperin,[22] and Zuhlina and Birshtein[37] were used in chapter three to compare the micelle dimensions obtained through fits to the data with those expected from theory. The scaling relationships were given in table 3.25 in chapter three. Those due to Halperin were used to calculate the expected micelle dimensions that are given in table 4.15.

Parameter	Model	5k xl micelles			10k xl micelles		
		h-h	h-d	d-h	h-h	h-d	d-h
N_A		89	106	140	164	90	164
N_B		16	16	12	29	24	26
R_cÅ	*Experiment*	*14.00*	*19.67*	*19.00*	*26.75*	*29.50*	*36.00*
	Halperin	24.02	23.61	20.11	34.32	30.64	31.92
	E:Hal	0.58	0.83	0.94	0.78	0.96	1.13
R_sÅ	*Experiment*	*52.67*	*54.00*	-	*75.75*	*59.75*	-
	Halperin	68.38	78.77	-	112.33	68.51	-
	E:Hal	0.77	0.69	-	0.67	0.87	-
R_{cs}Å	*Experiment*	*66.67*	*73.67*	-	*102.50*	*89.25*	-
	Halperin	92.41	102.38	115.76	146.66	99.15	143.07
	E:Hal	0.72	0.72	-	0.70	0.90	-
p	*Experiment*	*27.00*	*20.00*	*59.00*	*106.00*	*197.00*	*140.00*
	Halperin	9.19	8.98	7.25	14.79	12.71	13.42
	E:Hal	2.94	2.23	8.14	7.17	15.50	10.43

Table 4.15 - *Comparison between experimentally determined and model predicted values*

Figure 4.23 shows a plot of experimentally determined values *vs.* model predicted values, with both the virgin and cross-linked micelles data shown.

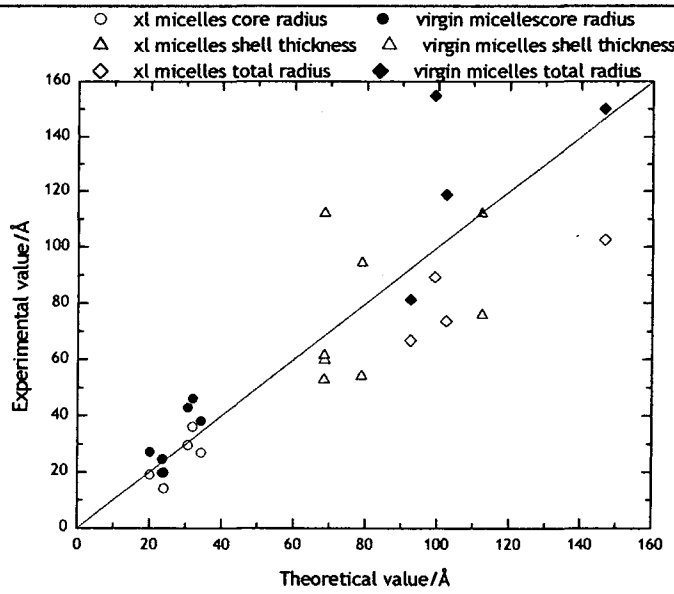

Figure 4.23 - *Plot of experimentally determined radii vs. theoretical values for virgin and cross-linked micelles. Open symbols represent xl micelles, filled symbols represent virgin micelles. The line is the y=x condition, i.e. perfect match between theory and experiment.*

Figure 4.23 demonstrates that there is a reasonable correlation between the experimentally determined dimensions and those predicted by theory for both the virgin and cross-linked micelles. The graph also shows the decrease in the micelle dimensions upon cross-linking. Taking a vertical line from any theoretical value, the dimensions of the cross-linked micelles are always lower than the equivalent virgin micelles.

Theories relating to polymer brush-like layers were discussed in chapter one, and applied to the SANS results from the micelles in chapter three. The same theories applied to the earlier results were also utilised here.

Table 4.16 details the values predicted using from theory using the models of Alexander,[38] de Gennes,[39] Milner *et al.*[40] and Dan and Tirrell[41] and compares these to values of the corona thickness obtained experimentally.

Parameter	Model	5k series		10k series	
		hPB-hPEO xl	hPB-dPEO xl	hPB-hPEO xl	hPB-dPEO xl
N_A		89	106	164	90
D/Å		9.55	15.59	9.21	7.45
σ		0.177	0.066	0.190	0.290
Experiment/Å		*52.67*	*54.00*	*75.75*	*59.75*
h/Å	Alexander	200.33	172.75	378.17	238.59
	E:Alex	0.263	0.313	0.200	0.250
h/Å	de Gennes	41.83	36.07	78.96	49.81
	E:dG	1.259	1.497	0.959	1.199
h/Å	Milner	44.64	38.50	84.27	53.17
	E:Milner	1.180	1.403	0.899	1.124
h/Å	D&T	69.11	72.19	131.54	103.48
	E:D&T	0.762	0.748	0.576	0.577

Table 4.16 - *Comparison between experimental data and theoretically predicted values for the corona thickness based on polymer brush theory*

Figure 4.24 shows a plot of the ratio between experimental and theoretical data *vs.* the degree of polymerisation for the corona block for the micelles before and after the cross-linking reaction.

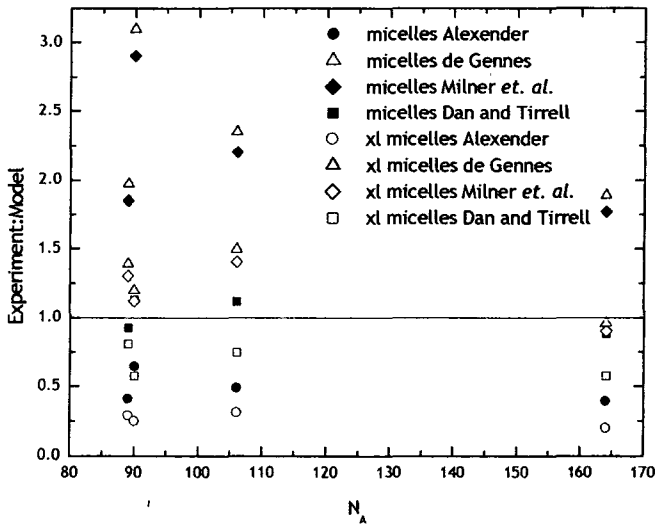

Figure 4.24 - *Ratio of experimentally determined values:model predicted values vs. degree of polymerisation of the corona forming block, N_A for micelles before and after cross-linking. Horizontal line is Experiment:theory=1, i.e. perfect match.*

Figure 4.24 suggests a reasonable correlation between the experimentally determined corona thickness and the value predicted from brush theory. However, the relationships of de Gennes[39] and Milner *et al.*[40] incorporate the excluded volume parameter, which is determined by the quality of the solvent. The models assume that the brush is in a good solvent, and thus ν=0.588; indeed this value was used in the calculation of the brush heights. Earlier observations with respect to the corona thickness, suggest that the micelles are no longer in a good solvent, so $\nu \neq 0.588$, and may be closer to the theta value of 0.5. It is possible to calculate the brush height that would be expected under such conditions, the results of which are given in table 4.17.

Parameter	Model	5k series		10k series	
		hPB-hPEO xl	hPB-dPEO xl	hPB-hPEO xl	hPB-dPEO xl
N_A		89	106	164	90
D/Å		11.10	15.59	9.21	7.45
σ		0.131	0.066	0.190	0.290
Experiment/Å		*52.67*	*54.00*	*75.75*	*59.75*
h/Å	de Gennes	37.84	36.07	78.96	49.81
	θ solvent	39.63	34.17	74.81	47.19
	E:dG (θ)	1.329	1.580	1.013	1.266
h/Å	Milner	44.64	38.50	84.27	53.17
	θ solvent	42.29	36.47	79.84	50.37
	E:Milner (θ)	1.245	1.481	0.949	1.186

Table 4.17 - *Comparison between experimental data and theoretically predicted values for the corona thickness based on polymer brush theory in both a good and a theta solvent.*

Table 4.17 shows that the values for the brush height expected in a theta solvent are less than those expected for a good solvent. Figure 4.25 shows a comparison between the brush heights calculated for both theta and good solvents with respect to the experimentally determined corona thickness.

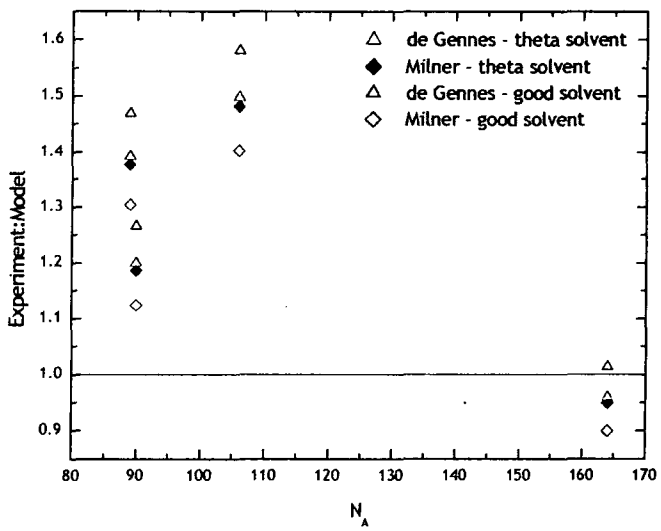

Figure 4.25 - *Ratio of experimental brush height to theoretical brush height for cross-linked micelles in both a theta and a good solvent. The horizontal line represents a perfect match between theory and experiment, i.e. Experiment:theory=1.*

Figure 4.25 shows that the brushes formed from the lower molecular weight polymers do not conform as well to the theoretical predictions as those formed from higher molecular weight polymers. This result is not entirely unexpected since the theories were postulated for high molecular weight polymers. The agreement with theory is also improved when considering the solvent as a theta solvent as opposed to a good solvent.

4.6.3. Higher concentration dispersions

In common with the virgin micelles, when c≥2% a structure factor peak was present at low Q. Although less pronounced than in the virgin micelles, it was still present. Consequently, the mean spherical approximation utilised for the virgin micelle data was applied when fitting the data.[33]

4.6.3.1. Results and discussion

Figures 4.26 to 4.29 show typical examples of fits to the data for both molecular weights and all three contrasts, with the results obtained from the fits detailed in tables 4.18 to 4.23.

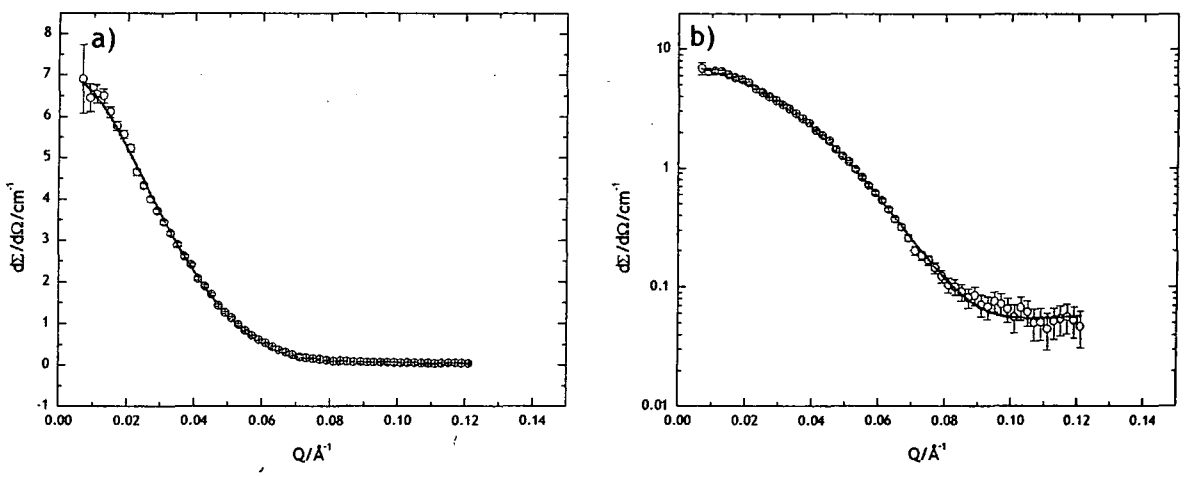

Figure 4.26 - *2% dispersion of 5k hPB-hPEOxl in D_2O. a) linear b)semi-logarithmic. Red lines are fits to the data*

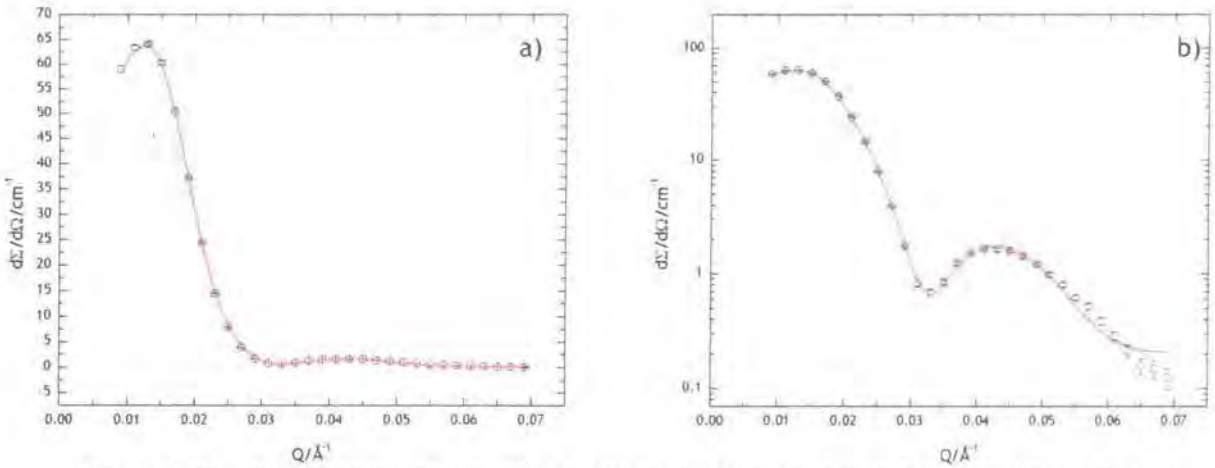

Figure 4.27 - *4% dispersion of 10k dPB-hPEOxl in hPEO contrast match H_2O. a) linear b)semi-logarithmic. Red lines are fits to the data*

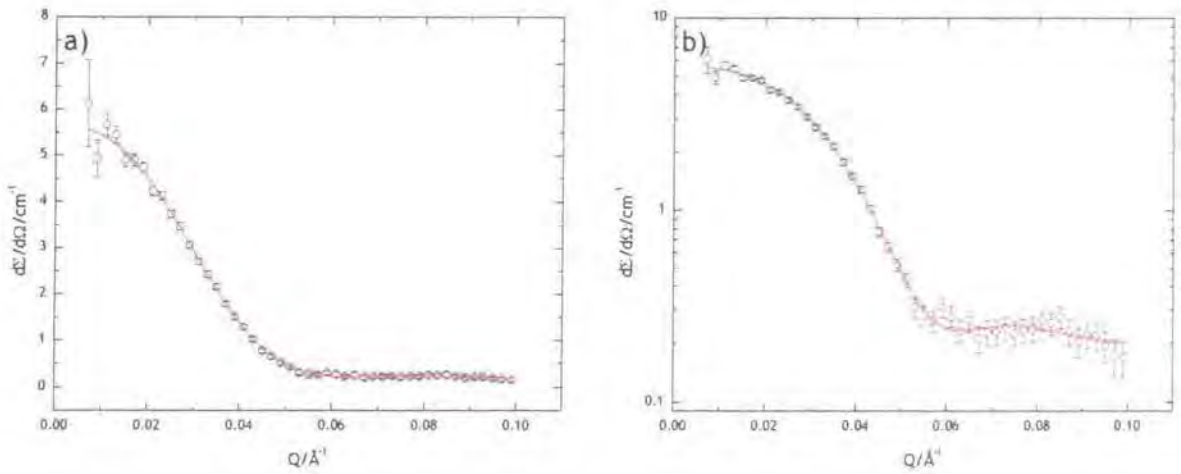

Figure 4.28 - *8% dispersion of 5k hPB-dPEOxl in hPB contrast match H_2O. a) linear b)semi-logarithmic. Red lines are fits to the data*

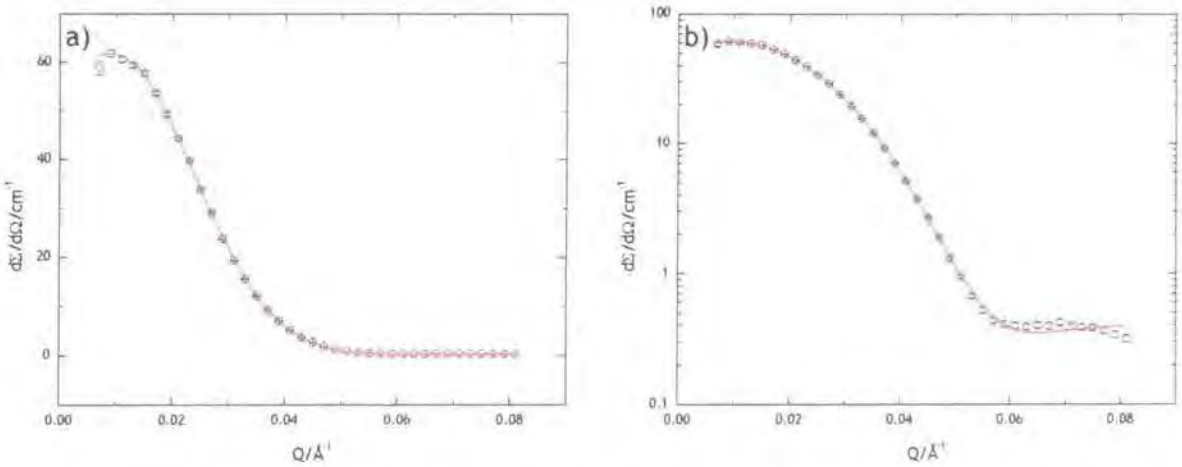

Figure 4.29 - *10% dispersion of 5k hPB-hPEOxl in D_2O. a) linear b)semi-logarithmic. Red lines are fits to the data*

Parameter	10%	8%	4%	2%
R_c/Å	14	14	13	12
R_s/Å	41	42	44	44
σ/R	0.747	0.745	0.722	0.723
ϕ_w	0.50	0.55	0.60	0.65
D_{PEO}/Å	11.10	11.10	10.30	9.51
R_s:R_g	1.76	1.80	1.89	1.89
H-P S(Q) R/Å	48.09	45.36	50.98	50.98
Charge	6.65	6.87	2.25	1.50
κ/Å^{-1}	3.732×10^{-3}	9.877×10^{-3}	1.129×10^{-2}	2.752×10^{-2}
γ	3.375	4.347	0.453	0.452
$\gamma\exp(-k)$	2.358	1.774	0.143	0.027

Table 4.18 - *Parameters from fits to 5k hPB-hPEO in D_2O 2%≤c≤10%*

In common with the virgin micelle data, (cf pg 158) the distinct steps in the value of ϕ_w result from the fitting procedure employed; namely fixing the scattering length densities at values corresponding to a given value of ϕ_w and investigating different values of ϕ_w until an acceptable fit was found.

Parameter	10%	8%	4%	2%
R_c/Å	13	13	12	12
R_s/Å	71	71	69	68
σ/R	0.614	0.472	0.641	0.801
ϕ_w	0.60	0.65	0.70	0.75
D_{PEO}/Å	10.3	10.3	9.51	9.51
R_s:R_g	2.75	2.75	2.67	2.63
H-P S(Q) R/Å	43.20	40.37	30.69	27.76
Charge	4.93	4.96	3.50	2.23
κ/Å^{-1}	1.372×10^{-2}	2.482×10^{-2}	2.431×10^{-2}	2.407×10^{-2}
γ	2.592	4.025	2.075	0.875
$\gamma\exp(-k)$	0.792	0.543	0.467	0.230

Table 4.19 - *Parameters from fits to 5k hPB-dPEO in hPB contrast match H_2O 2%≤c≤10%*

Parameter	10%	8%	4%	2%
R_c/Å	16	13	15	14
σ/R	0.523	0.508	0.403	0.342
H-P S(Q) R/Å	38.05	32.30	26.21	15.62
Charge	28.34	23.32	22.62	10.18
κ/Å^{-1}	2.674×10^{-2}	6.358×10^{-2}	1.011×10^{-1}	1.156×10^{-1}
γ	141.724	388.264	1148.305	111.418
$\gamma\exp(-k)$	18.522	6.405	4.855	3.017

Table 4.20 - *Parameters from fits to 5k dPB-hPEO in hPEO contrast match H_2O 2%≤c≤10%*

Parameter	10%	8%	4%	2%
R_c/Å	24	25	24	24
R_s/Å	69	71	71	71
σ/R	0.603	0.579	0.502	0.399
ϕ_w	0.5	0.55	0.60	0.65
D_{PEO}/Å	6.06	6.31	6.06	6.06
R_s:R_g	1.90	1.96	1.96	1.96
H-P S(Q) R/Å	68.33	58.68	51.69	37.69
Charge	6.30	5.78	4.40	3.09
κ/Å^{-1}	2.267×10^{-3}	3.373×10^{-3}	9.254×10^{-3}	1.637×10^{-2}
γ	2.122	2.104	1.592	1.190
$\gamma\exp(-k)$	1.557	1.416	0.611	0.347

Table 4.21 - *Parameters from fits to 10k hPB-hPEO in D_2O 2%≤c≤10%*

Parameter	10%	8%	4%	2%
R_c/Å	23	21	22	24
R_s/Å	56	56	51	50
σ/R	0.68	0.60	0.60	0.65
ϕ_w	6.06	5.56	5.3	5.81
D_{PEO}/Å	5.81	5.3	5.56	6.06
R_s:R_g	2.13	2.13	1.94	1.90
H-P S(Q) R/Å	49.30	40.98	35.12	35.12
Charge	6.68	7.82	9.22	7.25
κ/Å^{-1}	1.064×10^{-2}	3.064×10^{-2}	6.064×10^{-2}	9.064×10^{-2}
γ	3.971	12.893	62.809	177.400
$\gamma\exp(-k)$	1.391	1.046	0.890	0.306

Table 4.22 - *Parameters from fits to 10k hPB-dPEO in hPB contrast match H_2O 2%≤c≤10%*

Parameter	10%	8%	4%	2%
R_c/Å	32	31	31	28
σ/R	0.32	0.33	0.32	0.33
H-P S(Q) R/Å	46.84	39.87	52.14	47.84
Charge	4.50	5.25	5.83	5.83
κ/Å^{-1}	1.976×10^{-3}	1.060×10^{-2}	1.086×10^{-2}	3.000×10^{-2}
γ	1.558	2.845	2.942	7.542
$\gamma\exp(-k)$	1.295	1.222	0.948	0.427

Table 4.23 - *Parameters from fits to 10k dPB-hPEO in hPEO contrast match H_2O 2%≤c≤10%*

Figures 4.30 and 4.31 plot the variation of core radius and corona thickness respectively as a function of concentration for the contrasts explored.

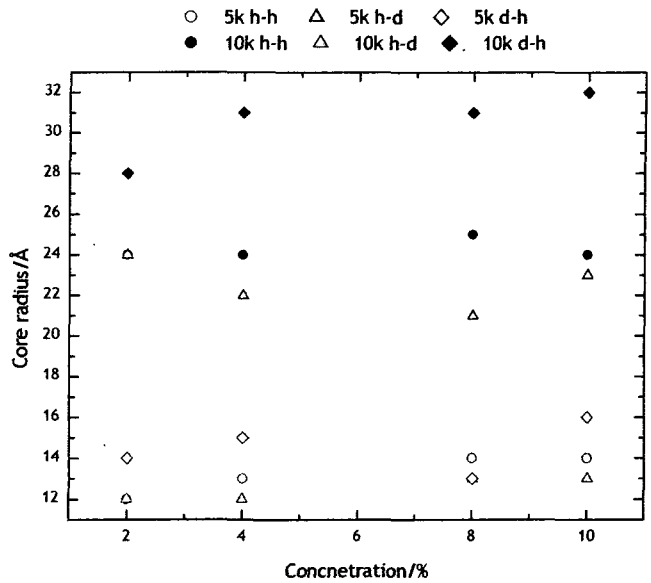

Figure 4.30 - *Variation of cross-linked micelle core radius with concentration for the different molecular weights and contrasts investigated.*

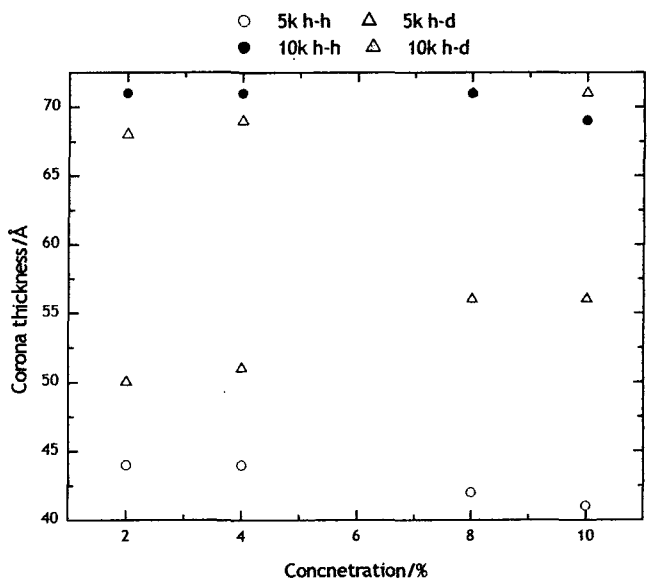

Figure 4.31 - *Variation of cross-linked micelle corona thickness with concentration for the different molecular weights and contrasts investigated*

From the data presented in tables 4.18-4.23, and figures 4.30 and 4.31 the following trends in the dimensions of cross-linked micelles can be observed.

i.) The core radius increases with concentration for all contrasts of the 5k series.

ii.) The 10k series show core radii that are approximately constant with concentration, with the exception of the dPB-hPEO case where an increase with concentration is observed.

iii.) The shell thickness decreases with concentration for the fully hydrogenous polymers of both molecular weights, whilst a slight increase is observed for the hPB-dPEO dispersions.

The changes in the micelle dimensions with concentration are quite small and so it is difficult to ascertain whether they are real trends or slight errors due to the fitting process.

In common with the virgin micellar dispersions the dimensionless interaction potential between micelles was calculated using equation 3.38. Figures 4.32 and 4.33 show plots of the interaction potential as a function of the micelle centre-to-centre distance.

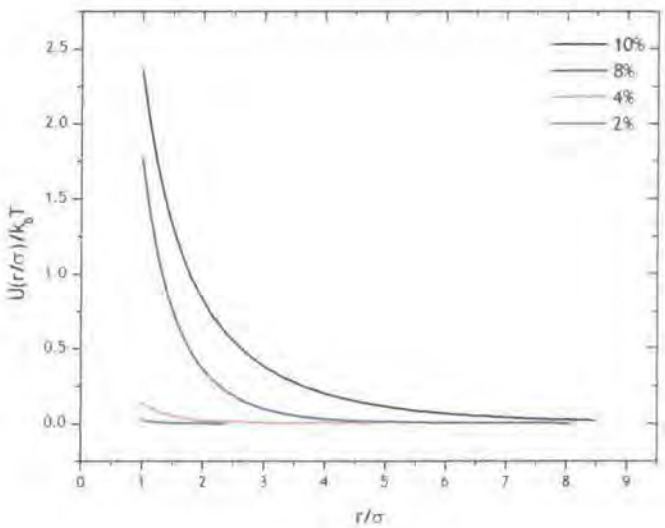

Figure 4.32 - *Dimensionless interaction potential for 5k hPB-hPEO xl calculated using equation 3.38.*

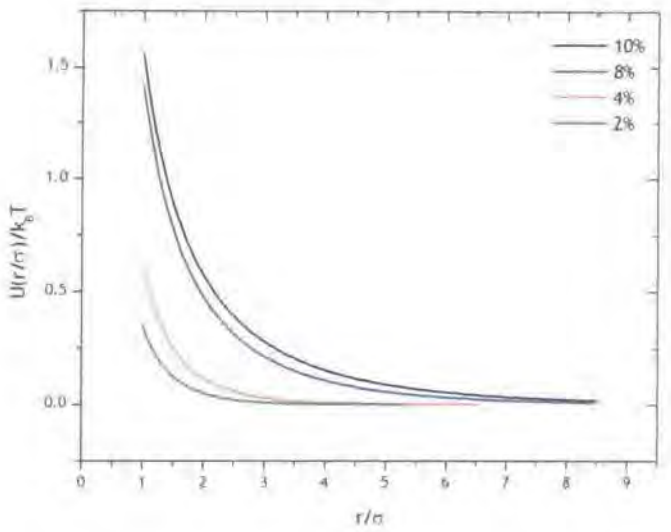

Figure 4.33 - *Dimensionless interaction potential for 10k hPB-hPEO xl calculated using equation 3.38.*

Figures 4.32 and 4.33 show that as the concentration increases so does the distance at which repulsion between the micelles is observed.

$\gamma\exp(-k)$ is the contact potential between a macroion pair, which for the neutrally charged system here can provide some indication as to the strength of interaction between micelles. Figure 4.34 plots the contact potential *vs.* concentration for the hPB-hPEO micelles of both molecular weights before and after cross-linking.

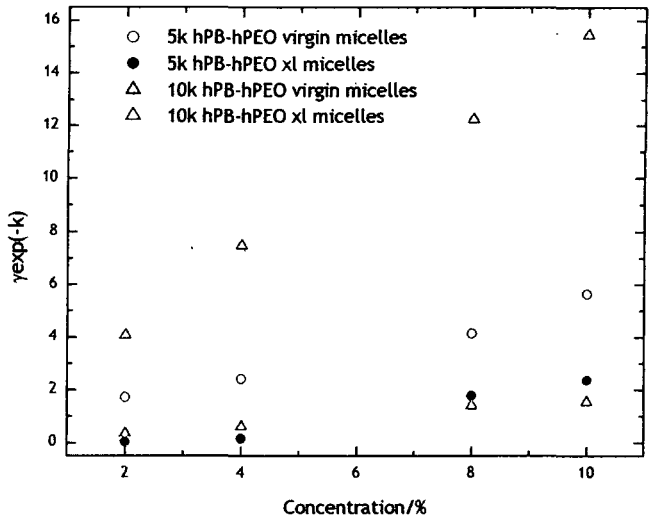

Figure 4.34 - *Comparison of contact potentials between hPB-hPEO micelles before and after cross-linking*

The contact potential between micelles follows the same trend both before and after cross-linking, namely that it increases with concentration. For a given molecular weight and concentration however, the contact potential decreases upon cross-linking. This is a pattern noted earlier from the SAXS data, and one used to explain the change in the scattering data following cross-linking. The reduction in the contact potential also suggests changes in the micelle properties. The interaction between 10k hPB-hPEO micelles was quite "hard" before the cross-linking reaction was carried out due to the high degree of stretching of the coronal chains as they were in a good solvent. The 5k hPB-hPEO micelles displayed considerably less "hard" interactions than the 10k micelles due to the smaller degree of stretching. Following the cross-linking reaction, both micelle sets have considerably softer interactions, and indeed show similar compressibility's from the contact potentials. This may be due to the reduction in quality of the solvent discussed earlier caused by the presence of inorganic salts following the cross-linking reaction. The chains in the corona now overlap more with one another, as this is more favourable than stretching out in the solvent. Consequently, the chains would be more prone to deformation due to the lower degree of stretching, and hence the micelles would be softer.

Similarly to the virgin micelles it is possible to construct reduced force-distance profiles from the interaction potentials,[42] shown in figures 4.35 and 4.36 for the 5k hPB-hPEO and the 10k hPB-hPEO respectively. The plots have been calculated using the excluded volume exponent for a theta solvent.

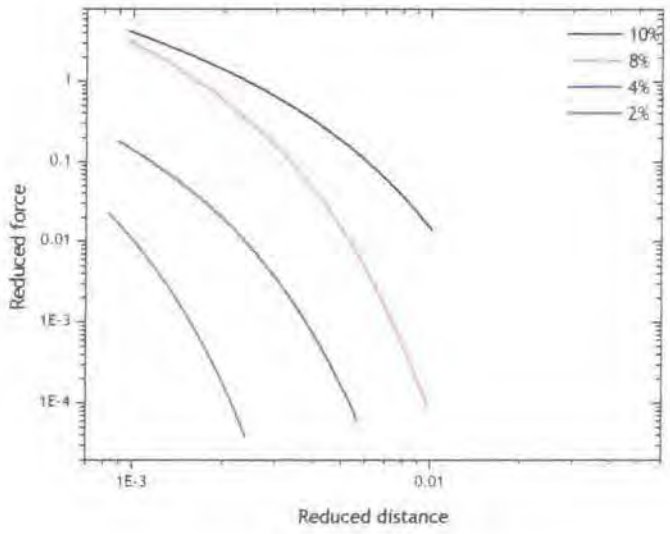

Figure 4.35 - *Reduced force as a function of reduced separation of micelle cores for 5k hPB-hPEO.*

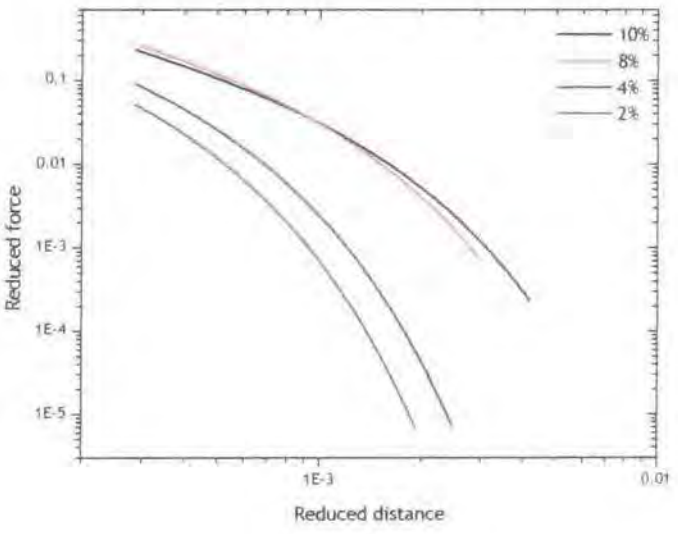

Figure 4.36 - *Reduced force as a function of reduced separation of micelle cores for 10k hPB-hPEO.*

The profiles in figures 4.35 and 4.36 are similar in nature to those determined for the virgin micelles, with the magnitude of the reduced force being smaller

for the cross-linked micelles compared to the virgin micelles. This reduction in the interactive force between the coronal brushes is consistent with the observations of the SAXS experiments and the interaction profiles shown earlier for the SANS experiments.

The SAXS data showed a marked reduction in the prominence of the S(Q) peak following cross-linking, a feature that is also evident in the SANS data (figures 4.37-4.40), and one that can be attributed to reduced intermicellar interactions.

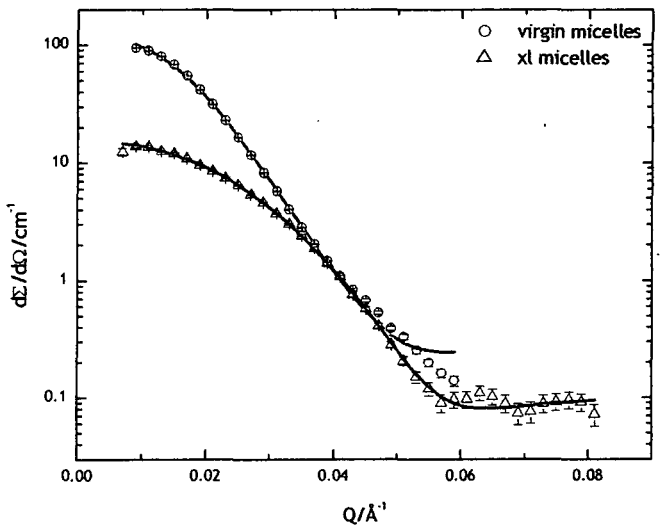

Figure 4.37 - *Comparison between 10k 2% hPB-hPEO micelles before and after cross-linking. Lines are fits to the data generated using core-shell model with modified mean spherical approximation for S(Q)*

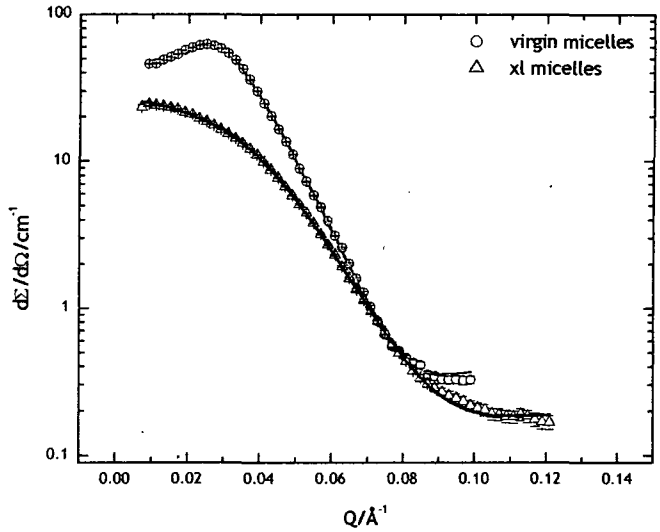

Figure 4.40 - *Comparison between 5k 10% hPB-hPEO micelles before and after cross-linking. Lines are fits to the data generated using core-shell model with modified mean spherical approximation for S(Q)*

4.6.4. Conclusions

The main conclusions that can be inferred from the SANS data are presented here for clarity.

- The micelle dimensions of all the contrasts and both molecular series decrease upon cross-linking.
- The contraction of the core radius is attributed to a reduction in volume of the core associated with the polymerisation reaction.
- Because of the reduction in the core size, the distance between the junction points of the PEO coronal chains on the core surface is reduced, with the exception of the 5k hPB-dPEO dispersions.
- The reduction in the corona thickness can be attributed to the presence of inorganic salts in the dispersion following cross-linking, which reduces the quality of the solvent, and thus the extent of chain stretching is also reduced.
- The repulsive interactions between the micelles at higher concentrations are reduced, as seen by the contact potentials determined from fits to the data.

- The reduction in repulsion between the micelles arises due to a change in the nature of the coronal brush. Residual salts from the cross-linking reaction change the brush from a highly stretched incompressible layer, to one that is quite soft and less stretched.

4.7. Final discussion

It was possible to cross-link the double bonds of the PB core of PB-PEO micelles in aqueous solution using a redox couple, to generate free radicals at room temperature. The success of the reaction was determined by the disappearance of vinyl protons in the ^{1}H NMR spectra. In common with a similar procedure employed by Won, Davis and Bates,[3] the reaction was confined to the core of the micelles as confirmed by the monomodal size distributions seen in QELS experiments. QELS revealed the micelle size was reduced by 7-30% upon cross-linking, which could be attributed to the contraction of the micelle core upon polymerisation. Several authors including Won *et al.*,[3] Wilson and Reiss,[43] and Guo *et al.*[17] have observed the same phenomenon.

The concentration dependence of the apparent diffusion coefficient was found to be negative for both molecular weights, in contrast to the virgin micelles where the 5k micelles exhibited a positive dependence. Hydrodynamic radii determined from this concentration dependence were 156Å and 94Å for the 10k and 5k respectively. The negative dependence of the apparent diffusion coefficient may be a result of the presence of inorganic ions remaining in solution from the cross-linking reaction. Such ions could cause bridging effects between the micelles and result in interaction of an attractive rather than a repulsive nature. In addition, the presence of such ions reduces the thermodynamic quality of the solvent for the PEO corona, resulting in interactions between the micelles being more favourable than those with the solvent.

The radii of cross-linked micelles determined by QELS showed closer agreement with Halperin's[22] star model than for their virgin counterparts. This is a little surprising, since although the model has its basis in the description of star polymers (which is what the cross-linked micelles could be considered as) it was formulated for a selectively good solvent for the corona-forming block. As already mentioned, the cross-linked micelle size

distributions were monomodal in dilute solution. They were however wider than those of the virgin micelles. This can be attributed to a higher degree of micelle polydispersity observed from both the QELS and SANS experiments on the virgin micelles at the concentration the cross-linking reactions were carried out (10%).

As observed for the virgin micelles, the quality of the SLS data was not good enough to enable determination of the micelle size or molecular weight. The cause of the poor quality data was discussed in chapter three, but may additionally be in some part due to the inorganic salts modifying the properties of both the micelles and the solvent.

Interpretation of the SAXS data with respect to the virgin micelles was complicated by the enhanced SAXS contrast in the cross-linked dispersions, due to the presence of electron-rich inorganic ions. Fits to the dilute dispersion data were only possible for the higher molecular weight species, and these did not fully reproduce the data. The results suggested increased micelle dimensions after cross-linking, contradicting the observations of the QELS experiments. A possible explanation for this increase in dimensions is the increased contrast between the scattering centres in the sample, caused by the residual inorganic ions from the cross-linking reaction. These contain large numbers of electrons and are likely to be associated with solvent water molecules both inside the corona of the micelles and in the surrounding medium. This would result in a greater electron density of both the corona and the solvent, making it easier to "see" the scattering from the polymer chains. Consequently, the conditions differ greatly from those of the virgin micelles, and thus quantitative comparisons of the micelles dimensions are impossible. A second possible explanation for the increase in micelle dimensions could be that the residual inorganic salts cause the unimers present in solution to associate with the micelles, resulting in their increased size.

Fits to the SANS data show a reduction in the core radius of the micelles of between 16 and 38%, with the corona thickness being 10-48% smaller in the cross-linked micelles compared to the virgin case. These two observations

support those from the QELS experiments of decreased micelle size upon cross-linking, with the magnitude of the reduction being comparable. The reduction in core radius was expected, due to the anticipated reduction in core volume associated with the polymerisation. Won *et al.*[3] observed a similar reduction in the core radius of their PB-PEO micelles, although the magnitude observed was ca 11%. It is noteworthy that the authors did not determine the corona thickness in the cross-linked micelles. They too used the same redox couple applied here, and so one might anticipate they would observe the same effect on the corona thickness seen here.

The reduction in the shell thickness of the micelles upon cross-linking is a little surprising. One would expect that upon contraction of the core, the distance between the grafting points of the PEO chains on the surface of the core would be reduced (this was indeed the case). With such a reduction, one would be expect an increase in the shell thickness as the chains stretch further into the solvent in order to minimise the unfavourable contact with each other and maximise favourable contacts with the thermodynamically good solvent. However, considering the conditions under which the investigations were carried out an explanation for this unusual behaviour becomes apparent. The dispersions used in the QELS, SAXS and SANS studies were prepared directly from the cross-linking reaction mixture by dilution with the appropriate solvent. Consequently, the inorganic salts added to generate the free-radicals required for the cross-linking reaction remained in the dispersions. The presence of such ions reduces the thermodynamic quality of the solvent for PEO, resulting in it no longer being a good solvent. Therefore it is no longer favourable for the chains to stretch away from the core surface to interact with the solvent; instead, interactions with neighbouring chains become more favourable, and thus a partial collapse of the coronal brush is observed. Support for this hypothesis is found in the work of Beaudoin and co-workers.[35]

Upon cross-linking the core of the micelles perhaps a reasonable assumption to make is the association number remains unchanged. Such an assumption can be justified by the fact that only one cross-link per copolymer chain would be sufficient to prevent the chain leaving the micelle. Using this assumption the distance between the PEO chains on the core surface was calculated. In all instances except the 5k hPB-dPEO micelles a reduction in

the distance between grafting points was observed. The likely explanation for this anomalous result lies in the value used for the association number. The 10% dispersion of the 5k HPB-dPEO micelles had a small association number of 20, with some of the more dilute dispersions exhibiting higher values. As the association numbers for the 5k micelles were low to moderate, any slight change in the core radius resulted in a dramatic change in the association number.

Calculation of the expected micelle radii based upon Halperin's star model produced better agreement that could have been anticipated as the model was formulated for a highly selective good solvent, which was no longer the case for these dispersions.

Comparison of the corona thickness to the theoretically predicted brush height using the models applied to the virgin micelles revealed better agreement for the cross-linked as opposed to the virgin micelles. The relationships of de Gennes[39] and Milner *et al.*[40] produced the best agreement, when good solvent conditions were applied but even better when theta solvent relations were used. The agreement was also better for the longest forming corona chain. Perhaps the reason for the improved agreement of these models over that of Dan and Tirrell[41] is that the former two relationships allow incorporation of the solvent quality, whereas the latter relationship assumes instead the brush is in a good solvent, which as eluded to earlier is not the case here.

Fitting of the SAXS data from the higher concentration dispersions and subsequent comparison to the virgin micelle case was complicated by the presence of the contrast enhancing inorganic ions. The mean spherical approximation[33] produced fits that matched the features of the data more closely than for the virgin micelles, but the different solvent conditions between the two sets of dispersions made quantitative comparisons impossible. The structure factor peak was much less pronounced in the cross-linked micelles compared to the virgin micelles suggesting reduced intermicellar interactions.

Comparison of the contact potential between the micelles both before and after cross-linking revealed that for any given molecular weight/concentration

combination the contact potential was lower for the cross-linked micelles. Such a comparison, although not quantitative could be taken as indicative of a reduction in the micelle interactions following cross-linking.

Fits to the data suggested increased micelle dimensions for both molecular weights after cross-linking, contradicting both the QELS and the SANS data discussed earlier. As with the SAXS from dilute dispersions such an increase can be attributed to the enhanced contrast resulting in more of the micelle being "seen".

In common with the SAXS data the SANS data from the higher concentration dispersions shows a greatly reduced structure factor peak when compared to the virgin micelles. The mean spherical approximation provided excellent reproduction of the features of the data in the same manner that was observed for the virgin micelles. Again comparison of the contact potentials reveals that those of the cross-linked micelles are smaller for a given molecular weight/concentration combination, suggesting reduced micelle interactions.

The nature of the interaction potentials appears to have changed upon cross-linking. The lower concentration dispersions (where the structure factor peak is still evident) show softer tails at low separations when compared to their virgin counterparts, which were approaching hard sphere-like interactions. As the concentration increases the tails become softer, and extend to marginally longer separations than observed for the virgin micelles (ca. eight times the diameter as opposed to seven). This suggests the micelle interactions have become softer, likely due to the reduced degree of stretching discussed earlier. The reduced force-distance profiles are similar to those of the virgin micelles and indeed those reported in the literature,[42, 44, 45] with the magnitude of the force smaller than that of the former.

4.8. Glossary of symbols

The symbols used in the body of the text and the equations are defined here in the order in which they appear in the text.

4.8.1. Quasi-Elastic Light Scattering

D_{app}	apparent diffusion coefficient
cmc	critical micelle concentration
D_0	diffusion coefficient at infinite dilute
k_d	diffusion second virial coefficient
c	concentration
$R_{h,app}$	apparent hydrodynamic radius
R	micelle radius
N_B	degree of polymerisation of core forming B block
N_A	degree of polymerisation of corona forming A block
a	segment length

4.8.3. Static Light Scattering

K	optical constant
c	dispersion concentration
cmc	critical micelle concentration
R_θ	Rayleigh ratio at angle θ
M	molecular weight
R_g	radius of gyration
λ	incident wavelength
θ	scattering angle
A_2	second virial coefficient

4.8.3. Small-angle X-ray scattering

I(Q)	scattering intensity
N	number of scattering particles
V	particle volume
Q	scattering vector
R	radius of a sphere

$(\Delta\rho)^2$	contrast (electron density difference)
R_g	radius of gyration
R_c	core radius
R_s	shell thickness
R_{cs}	micelle radius
σ/R	width of Schultz distribution
κ	Debye-Huckel inverse screening length

4.8.4. Small-angle neutron scattering

Q	scattering vector
$(d\Sigma/d\Omega)(Q)$	differential scattering cross-section
ϕ_w	volume fraction of water in inner most sub-shell of corona
σ/R	width of Schultz distribution
R_g	radius of gyration
p	micelle association number
ρ_{PB}	density of poly(butadiene) block
N_A	degree of polymerisation of corona forming A block
N_B	degree of polymerisation of corona forming B block
ν	excluded volume parameter
h	brush height
N	degree of polymerisation of brush forming polymer
σ	grafting density
R	radius of curvature (core radius)
κ	Debye-Huckel inverse screening length
$U(r/\sigma)$	dimensionless interaction potential
r/σ	dimensionless separation
f	reduced force
σ	reduced distance
D (same as σ for S(Q))	macroion diameter

4.9. Bibliography

1 M. Muthukumar, C. K. Ober, and E. L. Thomas, *Science*, 1997, **277**, 1225.

2 Y. Y. Won, *et al.*, *J. Phys. Chem. B*, 2001, **105**, 8302.

3 Y. Y. Won, H. T. Davis, and F. S. Bates, *Science*, 1999, **283**, 960.

4 K. B. Thurmond II, T. Kowalewski, and K. L. Wooley, *J. Am. Chem. Soc.*, 1997, **119**, 6656.

5 R. Saito, *et al.*, *Colloid. Surf. A: Physiochem. Eng. Aspects*, 1999, **153**, 305.

6 R. Saito, Y. Akiyama, and K. Ishizu, *Polymer*, 1999, **40**, 655.

7 R. Saito, S. Yoshida, and K. Ishizu, *J. Appl. Polym. Sci.*, 1997, **63**, 849.

8 R. Saito and K. Ishizu, *Polymer*, 1997, **38**, 225.

9 R. Saito, K. Ishizu, and T. Fukutomi, *Polymer*, 1992, **33**, 1712.

10 R. Saito, K. Ishizu, and T. Fukutomi, *Polymer*, 1991, **32**, 531.

11 R. Saito, K. Ishizu, and T. Fukutomi, *Polymer*, 1991, **32**, 2258.

12 R. Saito, K. Ishizu, and T. Fukutomi, *Polymer*, 1990, **31**, 679.

13 O. Rheingans, *et al.*, *Macromolecules*, 2000, **33**, 4780.

14 M. Iijima, *et al.*, *Macromolecules*, 1999, **32**, 1140.

15 F. Henselwood and G. Liu, *Macromolecules*, 1997, **30**, 488.

16 H. Huang, *et al.*, *J. Am. Chem. Soc.*, 1997, **119**, 11653.

17 A. Guo, G. Liu, and J. Tao, *Macromolecules*, 1996, **29**, 2487.

18 C. Konak, *et al.*, *Progr. Colloid Polym. Sci.*, 1985, **71**, 15.

19 J. Selser, in '*Dynamic Light Scattering - The method and some applications*', ed. W. Brown,Clarendon Press, Oxford, 1993.

20 Z. Zhou, B. Chu, and V. M. Nace, *Langmuir*, 1996, **12**, 5016.

21 Z. K. Zhou, *et al.*, *Macromolecules*, 1996, **29**, 8357.

22 A. Halperin, *Macromolecules*, 1987, **20**, 2943.

23 R. Nagarajan and K. Ganesh, *J. Chem. Phys.*, 1989, **90**, 5843.

24 S. W. Provencher, *Makromol. Chem.*, 1979, **180**, 201.

25 P. F. Dewhurst, *et al.*, *Macromolecules*, 1998, **31**, 7851.

26 C. Booth and D. Attwood, *Macromol. Rapid Commun.*, 2000, **21**, 501.

27 C. Booth, G. E. Yu, and V. M. Nace, in '*Amphiphilic block copolymers: Self assembly and applications*', ed. P. Alexandridis and B. Lindman,Elsevier, Amsterdam, 2000.

[28] W. Burchard, M. Schmidt, and W. H. Stockmayer, *Macromolecules*, 1980, **13**, 580.

[29] H. Benoit and D. Froelich, in '*Light Scattering from Polymer Solutions*', ed. M. B. Huglin,Academic Press, London, 1972.

[30] in '*Small Angle X-ray Scattering*', ed. O. Glatter and O. Kratky,Academic Press, 1982.

[31] R. H. Ottewill, in '*Colloidal Dispersions*', ed. J. W. Goodwin,Royal Society of Chemistry, London, 1982.

[32] R. K. Heenan, 'The "Fish" Reference Manual', RAL-TR-89-129, Rutherford Appleton Laboratory, Didcot, 2000.

[33] J. B. Hayter and J. Penfold, *Molec. Phys.*, 1981, **42**, 109.

[34] I. W. Hamley, *et al.*, *Langmuir*, 2001, **17**, 6386.

[35] E. Beaudoin, *et al.*, *J. Colloid Interace Sci.*, 2002, **251**, 398.

[36] M. Daoud and J. P. Cotton, *J. Physique*, 1982, **43**, 531.

[37] E. B. Zhulina and T. M. Birshtein, *Polymer Science USSR*, 1986, **27**, 570.

[38] S. Alexander, *J. Physique*, 1977, **38**, 983.

[39] P. G. de Gennes, *J. Physique*, 1976, **37**, 1445.

[40] S. T. Milner, T. A. Witten, and M. E. Cates, *Macromolecules*, 1988, **21**, 2610.

[41] N. Dan and M. Tirrell, *Macromolecules*, 1992, **25**, 2890.

[42] G. J. Bown, R. W. Richards, and R. K. Heenan, *Polymer*, 2001, **42**, 7663.

[43] D. J. Wilson and G. Reiss, *European Polymer Journal*, 1988, **24**, 617.

[44] G. A. McConnell, *et al.*, *Faraday Discuss.*, 1994, **98**, 121.

[45] S. Patel, M. Tirrell, and G. Hadziioannou, *Colloids Surf.*, 1988, **31**, 157.

5. Conclusions and Future work

Using a two-step anionic polymerisation procedure based on the methods of Hillmyer and Bates[1] and Jialenalla *et al.*[2] (scheme 5.1) two different molecular weight series of poly(butadiene)-poly(ethylene oxide) block copolymers have been synthesised. One of approximately 5,000 g mol^{-1}, the other ca. 10,000 g mol^{-1}. Each series had the same composition of ca. 15wt% poly(butadiene), and all possible H and D variants of the two blocks were synthesised. The polybutadiene block had approximately 90% 1,2 microstructure to facilitate post-polymerisation cross-linking.

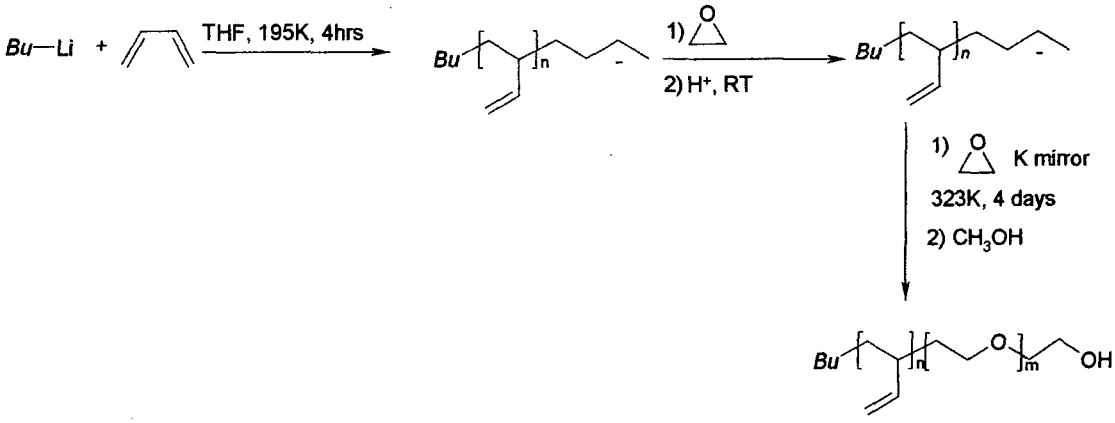

Scheme 5.1 - *Two step anionic polymerisation procedure employed to synthesise PB-PEO block copolymers.*

Because of their amphiphilic nature, the copolymers formed micelles *via.* a closed process when dispersed in water, a selective solvent for the PEO block. QELS was used to determine the critical micelle concentration (cmc) of the two fully hydrogenous copolymers with values of 0.148 mg mL^{-1} and 0.268 mg mL^{-1} obtained for the 10k and 5k copolymers respectively. Comparison of the cmc values with those of other PEO containing block copolymers enabled of the hydrophobic character of the PB block to be estimated. Within the limited data set available the hydrophobic character was intermediate of that seen for poly(butylene oxide) (PBO) and poly(propylene oxide) (PPO) with the former being the most hydrophobic. Such an observation was supported by a hydrophile-lipophile balance calculation[3, 4] for the three hydrophobes, with PB and PBO having identical values, whilst PPO had a higher value suggesting a less hydrophobic character.

Size determination from QELS experiments revealed hydrodynamic radii of 168Å and 136Å for the 10k and 5k copolymer micelles respectively, which showed reasonable agreement with Halperin's star model.[5]

The quality of the data from SLS and SAXS did not allow size determination of the micelles, with the lack of contrast and weak scattering intensity from dilute dispersions in the latter hindering efforts to fit the data.

SANS data from dilute dispersions were successfully fitted to a spherical core-shell model with a parabolic volume fraction profile (as one would expect in a polymer brush)[6] across the micelle corona. The lower molecular weight micelles had core radii of ca 22Å surrounded by a shell thickness of ca 80Å, whilst their higher molecular weight counterparts had core radii of ca 40Å and a shell thickness of ca 110Å. The two molecular weights exhibited contrasting association behaviour, with the 5k series having low to moderate association numbers whilst the 10k series had high association numbers.

In common with the QELS data, reasonable agreement was noted between the micelle dimensions and Halperin's star model of micelle formation, but experimental dimensions were generally larger than those predicted by theory.

The distance between the PEO junction points on the surface of the core was less than the calculated unperturbed radius of gyration in all instances, with the corona chains exhibiting a degree of stretching ca 2.5-4.5 times that of their unperturbed radius of gyration. These two observations supported the use of a brush like profile for the corona volume fraction, since they give rise to the conditions commonly associated with a polymer brush.[7, 8]

The volume fraction of water in the corona was used to determine the number of water molecules associated with each ethylene oxide segment. This revealed that a minimum of six water molecules were associated with each segment at the core-corona boundary (the driest part of the corona), with this number increasing with distance from the interface. The number of water molecules exceeded that associated with hydrated PEO in aqueous solution, suggesting the conditions inside the polymer brush were highly dilute.[9]

Comparison of the corona thickness to theoretical models predicting brush height showed mixed agreement. The models of Alexander,[7] de Gennes[8] and Milner *et al.*[6] for planar grafting interfaces provided reasonable agreement

with the experimental values. The model of Dan and Tirrell[10] for curved grafting surfaces provided excellent agreement with the experimental values.

As the concentration of the dispersions was increased, intermicellar interactions became more prominent. QELS experiments suggested the presence of particles with dimensions greater than that of the individual micelles. These larger particles have been attributed to micellar clusters by others.[11] The 10k micelles formed clusters that were 3-4 times the size of the micelles whilst the 5k micelles formed clusters that were 6-7 times larger than the micelles. The difference in the relative dimensions of these clusters was attributed to the nature of the interactions that appeared to be operating.

In both SAXS and SANS the presence of a structure factor peak at low Q was systematic of intermicellar interactions. A hard-sphere potential[12-14] could not describe adequately the observed structure factor and so the mean spherical approximation of Hayter and Penfold[15] was applied. This reproduced most, but not all, of the features in the SAXS data. In common with the dilute dispersions, the lack of SAXS contrast made quantitative determination of interactions difficult. Excellent reproduction of the structure in the SANS data was however achieved with this model in situations where the dispersions were still liquid-like in their properties. As the concentrations were increased to the point where gel formation was observed, the shape of the scattering changed, with the structure factor peak moving to higher Q. Under these conditions the MSA could no longer fully reproduce the features of the data, but reasonable agreement was observed. The nature of the interactions between the micelles determined from the MSA agreed well with those determined by M^{c}Connell[16] and co-workers using self-consistent field theory. The interaction potentials at low concentrations were almost hard sphere like in their nature, with a steep rise in potential at low separations although this was coupled with a slightly softer tail extending to short separation distances of two to three times the micelle diameter. At higher concentrations but where the dispersions remained liquid-like, the interaction potentials rose less steeply at shorter separations, and were accompanied by a soft tail extending out to relatively long separations of six

to seven times the diameter. The separation distance at which interactions was observed increased with concentration. Once the dispersions reached the point where they formed solid gels, the interactions between the micelles returned to the hard-sphere like potentials observed for the lower concentrations, but with the rise being steeper and the tail shorter, only extending to ca 1.5 times the micelle diameter.

Using a redox couple to generate free radicals at room temperature[17, 18] it was possible to cross-link the double bonds of the poly(butadiene) forming the core of the micelles. The absence of vinyl protons in the NMR spectra was used to confirm cross-linking. Cross-linked samples of the same isotopic variants investigated for the virgin micelles were produced.

The use of inorganic salts as a redox couple, and their presence in the subsequent dispersions complicated the behaviour of the cross-linked micelles compared to the virgin micelles, due to the reduction in quality of the solvent for the PEO brush.[19] QELS experiments showed a decrease in the micelle size upon cross-linking, an observation anticipated both from the expected core contraction and from published results. The 10k micelles exhibited a decrease in hydrodynamic radii of ca 7% whilst their 5k counterparts showed a reduction of ca 30%. Monomodal size distributions in dilute dispersions confirmed the reaction had been confined to the core of the micelles. Both molecular weight species exhibited attractive interactions towards one another, a phenomenon due to remaining inorganic ions after the cross-linking reaction. Such ions caused a reduction in the thermodynamic quality of the solvent for the PEO corona resulting in interactions between chains being more favourable than those between chains and the solvent. As for the virgin micelles the SLS data was not of sufficient quality for determination of micelle molecular weight or size with confidence.

SAXS data suggested the micelles had increased in size following the cross-linking reaction, contradicting the observations of the QELS experiments. However, the inorganic ions are electron rich and as a result increase the contrast between the different scattering components of the sample. Consequently, comparison of the micelle dimensions before and after cross-

linking is a fruitless exercise due to the vastly different contrast conditions, which result in more of the micelle being "seen" in the cross-linked dispersions.

The SANS data from dilute dispersions were successfully fitted using the same spherical core shell model as for the virgin micelles, suggesting that the morphology of the micelle remained unchanged upon cross-linking. Dimensions obtained from these fits showed that both the core radius and corona thickness had decreased upon cross-linking. The former is due to the reduction in volume associated with polymerisation of the core, and the latter is due to the reduced thermodynamic quality of the solvent for the PEO corona causing the brush to collapse. With one exception, the distance between the PEO grafting points on the core surface was reduced upon cross-linking. In a good solvent, the fact that the coronal chains come closer together would be expected to give rise to a thicker corona as the chains stretch further away from the interface to minimise unfavourable interactions with one another and maximise favourable interactions with the solvent. However, in the case here where the solvent may be approaching the theta condition, interactions between the chains are more favourable than those with the solvent.

Surprisingly there was still reasonable agreement between the experimentally determined micelle dimensions and those predicted by the star model of Halperin,[5] even though this was proposed for good solvent conditions. The model of Dan and Tirrell[10] still showed the best agreement for the predicted brush height, although the relationships of de Gennes[8] and Milner *et al.*[6] showed improved agreement compared to the virgin micelles. This latter observation is probably a result of the densification of the core upon polymerisation making the interface between the core and the corona more rigid and less prone to deformation than in the virgin micelles.

Higher concentration dispersions studied by SAXS exhibited a structure factor peak that was less pronounced than in the virgin micelles. The mean spherical approximation was again applied to the data, with more features of the data captured for the cross-linked micelles than was the case in the virgin micelles, with the contact potentials between the micelles suggesting a

reduced level of interaction in the cross-linked micelles. As with the dilute dispersions quantitative comparisons with the virgin micelles was not possible due to the different contrast conditions between the two sets of dispersions.

In common with the SAXS experiments, the SANS investigations of higher concentration dispersions also revealed a far less pronounced structure factor peak. The mean spherical approximation provided excellent fits to the data, with the contact potentials between micelles also being reduced for a given molecular weight/concentration combination.

With respect to future work, there are several avenues of research that would be interesting to explore in the wake of the results presented here.

i.) The micellisation behaviour of PB-PEO block copolymers remains poorly understood with respect to other PEO containing copolymers. It would be interesting to expand the data set of copolymers in terms of the molecular weights and compositions explored, in order to elucidate the effect of these variables upon the cmc, micelle dimensions and interactions. The group of Frank Bates have recently explored PB-PEO block copolymers of varying composition and molecular weight but only in terms of the morphology of the micelles formed.[20, 21]

ii.) It would likely prove possible to remove the inorganic salts from the dispersions using a dialysis method, which would enable the cross-linked micelles to be studied under good solvent conditions, in common with the virgin micelles.

iii.) The method used to cross-link the micelles could be developed further such that the micelles can be isolated, separated from the inorganic ions, and redispersed. This may mean approaching the problem with an entirely new technique such as photo-initiation with UV light and an appropriate initiator. Alternatively, a redox couple wherein fewer free radicals are generated could be used.

iv.) If the cross-linking chemistry could be developed such that the micelles were redispersible, it would be interesting to study them both in a good solvent, water, and in a range of solvents with differing affinities for the PEO, perhaps water at different temperatures, such that the effect of solvent on the coronal brush could be elucidated.

5.1. Bibliography

1 M. A. Hillmyer and F. S. Bates, *Macromolecules*, 1996, **29**, 6994.

2 G. L. Jialanella, E. M. Firer, and I. Piirma, *J Polym Sci, A, Polym Chem.*, 1992, **30**, 1925.

3 J. T. Davies and E. K. Rideal, 'Interfacial Phenomena', 2nd, ed., Academic Press, New York, 1963.

4 R. J. Hunter, 'Foundations of Colloid Science Vol 2', Oxford University Press, New York, 1989.

5 A. Halperin, *Macromolecules*, 1987, **20**, 2943.

6 S. T. Milner, T. A. Witten, and M. E. Cates, *Macromolecules*, 1988, **21**, 2610.

7 S. Alexander, *J. Physique*, 1977, **38**, 983.

8 P. G. de Gennes, *J. Physique*, 1976, **37**, 1445.

9 K. Taskai, *J. Am. Chem. Soc.*, 1996, **118**, 8459.

10 N. Dan and M. Tirrell, *Macromolecules*, 1992, **25**, 2890.

11 R. L. Xu, *et al.*, *Macromolecules*, 1991, **24**, 87.

12 N. W. Ashcroft and J. Lekner, *Phys. Rev*, 1966, **145**, 83.

13 J. K. Perkus and G. J. Yevick, *Phys. Rev*, 1958, **110**, 1.

14 R. H. Ottewill, in 'Coloidal Dispersions', ed. J. W. Goodwin, Royal Society of Chemistry, London, 1982.

15 J. B. Hayter and J. Penfold, *Molec. Phys.*, 1981, **42**, 109.

16 G. A. McConnell, *et al.*, *Faraday Discuss.*, 1994, **98**, 121.

17 Y. Y. Won, H. T. Davis, and F. S. Bates, *Science*, 1999, **283**, 960.

18 Y. Y. Won, *et al.*, *J. Phys. Chem. B*, 2001, **105**, 8302.

19 E. Beaudoin, *et al.*, *J. Colloid Interace Sci.*, 2002, **251**, 398.

20 S. Jain and F. S. Bates, *Science*, 2003, **300**, 460.

21 Y.Y. Won, *et al.*, *J. Phys. Chem. B*, 2002, **106**, 3354.

Appendix A

An analytic structure factor for macroion solutions

$$S(K) = \frac{1}{1 - 24\eta a(K)} \qquad \text{where } K = Q\sigma$$

The macroion volume fraction, η, is expressed in terms of the number density, n, and the macroion diameter, σ, as:

$$n = \frac{\pi n \sigma^3}{6}$$

$$a(K) = A(\sin K - K\cos K)/K^3 + B[(2/K^2 - 1)K\cos K + 2\sin K - 2/K]/K^3$$
$$+ \eta A[24/K^3 + 4(1 - 6/K^2)\sin K - (1 - 12/K^2 + 24/K^4)K\cos K]/2K^3$$
$$+ C(k\cosh k\sin K - K\sinh k\cos K)/K)/K(K^2 + k^2)$$
$$+ F[k\sinh k\sin K - K(\cosh k\cos K - 1]/K(K^2 - k^2)$$
$$+ F(\cos K - 1)/K^2 - \gamma\exp(-k)(k\sin K + K\cos K)/K(K^2 + k^2)$$

where k is the dimensionless screening constant and γ is the dimensionless coupling constant. γexp(-k) is the contact potential for a macroion pair (expressed in units of K_BT).

The coefficients A, B, C and F are expressed in terms of several further sets of coefficients. For further details the reader is referred to

J.B. Hayter and J. Penfold, *Molec. Phys.*, 1981, **42**, 109